



Developing an electrospun membrane to promote regeneration of periodontal ligament

Nouf Hamad Aljamel

*A thesis submitted to the University of Sheffield in fulfilment of the
requirements for the degree of
Doctor of Philosophy*

SCHOOL OF CLINICAL DENTISTRY
UNIVERSITY OF SHEFFIELD
UNITED KINGDOM

May 2023

Covid-19 statement

I joined the University of Sheffield in November 2018 to begin my PhD which involved working in the Dental School and Engineering Materials Department. Unfortunately, in March 2020 in my second year, the UK went into a National lockdown due to the COVID-19 pandemic and all the Universities were closed so I could not access any laboratory facilities. Therefore, all my practical work was stopped. The Kuwaiti embassy here in the UK arranged flights for evacuation of Kuwaiti UK University students back to Kuwait and I had to leave the UK in May 2020 not knowing when I would be back. By that time, Kuwait Airport was closed and did not re-open for international flights until mid-May 2021 for only those who had to travel with approval. In August 2020 I got married and while on Honeymoon my husband and I suffered a serious road traffic accident. Unfortunately, I broke my wrist/hand and my husband broke both his legs. We both had to undergo emergency surgeries and I had screws fit into my hand and wrist, my husband was in a wheelchair for almost 3 months, and I was also taking care of him during this period. Post-surgery I had scheduled physiotherapy sessions at the Government Hospital in Kuwait until May 2021 when I was cleared to start using my wrist gradually at work. Living through this pandemic and especially after the serious accident I had, I could not help but feel overwhelmed with anxiety due to very real, imminent health concerns.

The pandemic situation has had a significant effect on my own personal resilience. As well as keeping up with my PhD research, I have had to face uncertainty about how I will support myself financially in the immediate term. I had to leave my flat and belongings in the UK for more than a year and was paying a huge amount of money for rent without being in the country or staying

in the flat. I was unaware when I would be back to the UK at that point of time, and everything seemed so confusing and worrying.

When I returned to the UK in June 2021 after these incidents, the laboratory facilities were running but at a much reduced occupancy to ensure compliance with UK COVID-19 guidance on safe distancing between people. Therefore, there was limited access to the laboratories to ensure all lab users could book some essential laboratory time. Reduced laboratory occupancy and access to maintain safe distancing was a university-wide policy. This limited lab access hindered my work and delayed my progress significantly as I was unable to achieve my results as per the previous timeline. My Sponsor and the University of Sheffield kindly granted me a year extension to enable me to complete my research project.

In September 2022, I had to undergo my second surgery for my wrist to remove the metal screws that were placed during the first surgery in 2020. This took place at a hospital in London, after which I then had to undergo physiotherapy sessions again to gain full working of my wrist. All I can say about my PhD journey is that it was not an easy one, however, I managed to work really hard despite the circumstances and obstacles to be able to achieve these results and submit my thesis. I was very lucky indeed to have a very supportive supervisor who was available throughout and supported me in every possible way to help me complete my PhD.

Acknowledgements

foremost, praises and thanks to **Allah the Almighty**, the most Merciful and Gracious, for his blessing given to me throughout my PhD journey to complete this thesis successfully.

The completion of this thesis could not have been possible without the expertise of my lead supervisor **Dr Aileen Crawford**. Although, I would like to express my deepest appreciation to my second supervisor **Dr Ilida Ortega Asencio** for her continuous support and motivation during my PhD. It was a great privilege and honour to work under their guidance.

My gratitude goes to all the laboratory Staff in the dental school for their invaluable assistance, guidance and training during my PhD journey. My special thanks go to all of my colleagues and friends for their cooperation and support. I am extending my heartfelt thanks to my friend **Mariam Murad** for her friendship, empathy and great sense of humour. I also would like to thank my funder, The Ministry of Health in Kuwait, for their financial support in making this PhD happen.

Last but not least, I am extremely grateful to my Husband, **Abdullatief**, for his absolute love, care and patience. Thank you for your encouragement, uplifting support and your appreciated sacrifices throughout this journey. Special thanks to my family, this is as much my achievement as it is yours. Even being far away from home, I have always felt loved and supported by all of you.

الحمد لله

Abstract

Periodontal disease is an inflammatory condition, which can lead to tooth loss. The Clinical treatment and management of periodontal disease is focussed on the regeneration of the periodontal tissues to achieve a good alveolar bone mass and to maximise re-attachment of the periodontal ligament. Guided tissue regeneration (GTR) using a biomaterial membrane is currently the method of choice in more severe tissue loss. The clinical regeneration treatments can give varied results in patients, however, the reasons for this are still unknown.

The overall aim of this study was to use electrospinning and surface modification techniques to fabricate a biodegradable GTR membrane/scaffold composed of aligned fibres with enhanced regenerative and biomimetic (biologically responsive) properties. Model systems using random-fibre and aligned-fibre Poly-L-lactic acid (PLLA) and poly (ϵ -caprolactone) (PCL) scaffolds were prepared via electrospinning. However, commercial aligned-fibre PCL scaffolds had to be ordered. The morphology and the size of the fibres was determined by scanning electron microscopy (SEM). The surfaces of the scaffold fibres were modified by the addition of amine groups by using cold plasma deposition of allylamine. 6mm diameter scaffolds were then incubated with heparin. The heparin-bound scaffolds were then incubated for 24 hours with growth factors (10 μ g of TGF- β 1, TGF- β 3 or FGF2 in PBS/ 1 mg/ml BSA). Human periodontal ligament cells were seeded onto the functionalised and control membranes and incubated at 37°C. Cell viability was checked using PrestoBlue™ on days 7, 14 and 21 and investigated using Live-Dead staining using 5-chloromethylflourescein diacetate (CMFDA) and Propidium iodide (PI) dyes. On day 35, the cell/scaffold constructs were taken to measure the

amount of DNA using PicoGreen, total protein using bicinchoninic acid (BCA) and total collagen by measuring the amount of hydroxyproline using a Total Collagen assay kit.

Random-fibre scaffolds of PCL or PLLA were successfully fabricated by electrospinning and commercial aligned fibre PCL scaffolds were used. A smaller range of fibre diameters was observed by SEM in the PCL scaffolds compared to PLLA scaffolds. On day 7, 14 and 21 - the cells were fully viable as determined using PrestoBlue™. Moreover, live-dead staining showed mainly green (live) cells on both PLLA and PCL membranes with few dead cells (stained red). DNA determination indicated a lower cell number on the PLLA random membrane than PCL random membrane. Cold plasma functionalisation of the random and aligned fibre scaffolds with allylamine was carried out and XPS analysis of the amine-functionalised scaffolds showed the presence of nitrogen groups on the surface. All the growth factors tested (TGF β 1, TGF β 3 and FGF-2) bound to the heparin-functionalised membranes and eluted from the scaffolds for a minimum period of 14 days. On biofunctionalization with the growth factors, the aligned TGF- β 3 bio-functionalised scaffolds constructs produced significantly more DNA, total protein and collagen ($P \leq 0.01$) than control and plasma treated cell/scaffolds constructs.

Table of Contents

Abstract	iv
List of Figures	ix
List of Tables	xiv
Abbreviations	xv
1. Introduction	1
2. Literature review	3
2.1. Periodontium	3
2.1.1. Cementum.....	3
2.1.2. Periodontal ligament	6
2.1.3. Alveolar bone	7
2.2. Periodontal ligament function and composition	8
2.2.1. Fibres of the periodontal ligament.....	8
2.2.2. Cells	9
2.3. Periodontal disease	10
2.3.1. Classification of periodontal disease.....	11
2.3.2. Pathology of periodontal disease.....	11
2.4. Periodontal treatment	14
2.4.1. Options for periodontal treatment	14
2.4.2. Control of infection.....	15
2.4.3. Open flap surgery.....	16
2.4.4. Regeneration of the periodontal ligament and supporting alveolar bone	17
2.5. The healing process	17
2.6. Guided tissue regeneration (GTR)	18
2.6.1. GTR membrane types	19
2.6.2. The mechanism of the GTR membrane in mouth	20
2.7. Cell and scaffold selection for periodontal tissue engineering	21
2.7.1. Potential cells for periodontal tissue engineering	22
2.7.2. Types of scaffolds.....	22
2.7.3. Scaffold properties.....	26
2.8. Cells for regenerative approaches to repair periodontal ligament	27
2.8.1. Periodontal ligament fibroblasts.....	27
2.8.2. In situ regeneration of the periodontal ligament	28
2.9. Polymers used in regenerative medicine and tissue engineering	29
2.9.1. PLLA	29
2.9.2. PCL.....	30
2.9.3. Breakdown of PLLA and PCL in the human body	30
2.10. Electrospinning	31
2.10.1. Fabrication of PLLA and PCL fibre scaffolds using electrospinning.....	33
2.11. Scaffold surface modification and biofunctionalization	38

2.11.1.	Plasma polymerisation of PLLA and PCL scaffolds	40
2.11.2.	Glycosaminoglycans (GAGs) with PLLA and PCL scaffolds	44
2.11.3.	The effect of growth factors on HPDL seeded scaffolds	47
2.12.	Hypothesis, Aim and Objectives	57
2.12.1.	Hypothesis.....	Error! Bookmark not defined.
2.12.2.	Aim	57
2.12.3.	Objectives.....	57
3.	<i>Materials and methods</i>	59
3.1.	Materials.....	59
3.1.1.	Polymers.....	59
3.1.2.	Cells	59
3.1.3.	Media for cell culture.....	59
3.1.4.	Reagent	60
3.1.5.	Instruments and machines	61
3.1.6.	Assay Kits and ELISA's	63
3.1.7.	Miscellaneous	63
3.1.8.	Software.....	64
3.2.	Methods.....	65
3.2.1.	Viscosity measurement of electrospinning solution.....	65
3.2.2.	Scaffold fabrication.....	65
3.2.3.	Scaffolds characterisation.....	67
3.2.4.	Cell culture and biological testing	68
3.2.5.	Surface modification and biofunctionalization of the scaffold's mat	74
3.2.6.	Mechanical testing.....	76
3.2.7.	Porosity testing	76
3.2.8.	Evaluation of hydrophobicity via measurement of water contact angle.....	77
3.2.9.	Binding of growth factors to heparin immobilised on pAMM-PCL aligned scaffolds	77
3.2.10.	Binding of growth factors to glycosaminoglycans (GAGs) immobilised in 96-well plates	78
3.2.11.	ELISA.....	79
3.2.12.	Biological testing of biofunctionalised HPDLs seeded PLLA and PCL scaffolds	80
3.2.13.	Quantitative PCR.....	86
3.2.14.	Statistical analysis	89
4.	<i>Results</i>	90
4.1.	Optimisation and characterization study for initial polymer selection: PLA Vs PCL	90
4.1.1.	Fabrication of electrospun scaffolds	90
4.2.	Surface modification and biofunctionalization of the scaffold's mats.....	109
4.2.1.	X-ray photoelectron spectroscopy (XPS).....	109
4.2.2.	Stiffness testing.....	113
4.2.3.	Scaffolds porosity and pore size distribution.....	117
4.2.4.	Scaffold hydrophobicity (Contact angle measurement).....	119

4.2.5. Heparin binding to the allylamine-functionalised membranes (binding of fluorescein-labelled Heparin)	121
4.2.6. Binding of growth factors (TGF β 1, TGF β 3 and FGF-2) to heparin-functionalised membranes	124
4.2.7. Measurement of binding of the growth factors to plasma treated aligned PCL scaffolds and the elution of the growth factors from the scaffolds.....	126
4.3. In vitro cell culture	129
4.3.1. DNA PicoGreen assay.....	130
4.3.2. Total protein assay (BCA).....	133
4.3.3. Alkaline phosphatase assay.....	136
4.3.4. Total collagen assay	138
4.3.5. Hematoxylin and Eosin staining	140
4.3.6. Picro Sirius Red staining (Collagen type I & III)	145
4.3.7. Quantitative PCR.....	150
5. Discussion and conclusion	151
5.1. Discussion	151
5.1.1. Initial random fibres scaffold selection: PLLA Vs PCL	151
5.1.2. Aligned fibre PCL scaffold Vs random fibre PCL scaffold	154
5.1.3. Effect of surface modification and biofunctionalization of scaffold's mats...	155
5.2. Conclusion.....	170
6. Future work	173
7. References	174

List of Figures

<i>Figure 2.1 The macroscopic tooth structure for incisor tooth</i>	3
<i>Figure 2.2 The acellular fibrillar cementum of incisor tooth (arrow)</i>	5
<i>Figure 2.3 The principal fibres of the periodontal ligament allow three-dimensional support and protection against multidirectional forces</i>	7
<i>Figure 2.4 Schematic illustration of using GTR membrane in the regeneration of infected periodontal tissue</i>	19
<i>Figure 2.5 Schematic diagram of a basic horizontal electrospinning process</i>	35
<i>Figure 2.6 Representation of using the bio-functionalised membrane to promote the periodontal ligament regeneration</i>	58
<i>Figure 4.1: Effect of electrospinning conditions on the macroscopic appearance and fibre density of PLLA scaffolds. Scaffold (A) was electrospun with 3ml of the polymer solution while scaffold (B) was electrospun using 9ml of the same solution</i>	90
<i>Figure 4.2: Image of a PCL scaffold electrospun using 10 ml of PCL solution with setting of 23 kV, flow rate of 2ml/hr with a distance of 20cm between the polymer jet and collecting plate</i>	91
<i>Figure 4.3: Comparison of the fibre diameters of PLLA random, PCL random. The diameter of the scaffold fibres was obtained using imageJ software. This data was then analysed using Graphpad prism v9.1</i>	92
<i>Figure 4.4: SEM images showing the fibre morphology of electrospun PLLA scaffolds (images A and B) and electrospun PCL scaffolds (images C and D). At a magnification of x500, (images A and C, scale bar= 100 µm) and x100, (images B and D, scale bar= 50 µm).</i>	93
<i>Figure 4.5: Effect of varying speeds on the collecting mandrel of aligned PCL scaffolds. Image A the electrospun fibres were obtained with a rotation speed of 500 r.p.m, image B 1000 r.p.m, image C 1500 r.p.m and image D 2000 r.p.m</i>	95
<i>Figure 4.6: SEM of aligned PCL scaffold fabrication on the Bioinicia electrospinning machine. Images were taken at x500 magnification, scale bar =100 µm for image A and x1000 magnification, scale bar =50 µm for image B. The micrographs show partial alignment of PCL</i>	96
<i>Figure 4.7: Photographs showing the problems caused by the vibration of the collector during the drum rotation. The air flow during the rotation allow the fibre to stick in the floor of the machine rather than on the collector</i>	97

Figure 4.8: SEM images was taken at x500 magnification, scale bar =100 μm . SEM shows the effect of the electrospinning voltage on the alignment of the PCL fibres. Image (A) shows PCL scaffold electrospun with voltage of 21 kV and image (B) shows PCL scaffold electrospun with voltage of 15 kV..... 98

Figure 4.9: Comparison of the mean fibre diameters of PLLA random, PCL random and PCL aligned. The diameter of the scaffold fibres was obtained using imageJ software. This data was then analysed using Graphpad prism v9.1 100

Figure 4.10: SEM images was taken at x2500 & x1000 magnification by the electrospinning company. scale bar A & B = 50 μm and C = 150 μm . SEM shows the Tri-layer of the PCL scaffolds mat. Image (A) shows top PCL aligned layer, (B) shows PCL random layer (middle layer). (C) shows bottom PCL aligned layer 102

Figure 4.11: SEM images was taken at x500 and x1000 magnifications, scale bar =100 μm and 50 μm . SEM shows the alignment of the scaffold mat that been ordered from the electrospinning company 103

Figure 4.12: SEM images was taken at x500 magnifications, scale bar =100 μm , to show the comparison of cells bound to PLLA and PCL scaffold in different regions of the scaffold..... 104

Figure 4.13: Fluorescence microscopy images on day 21 shows live cells in green (CMFOA) and dead cells in red (PI). PLLA control scaffold (image A) and PCL control scaffold (image B) shows that the scaffolds themselves do not fluoresce. On the other images (B,E C and F) the green staining represents the living cells on the scaffolds. Images (B and C) are PLLA seeded scaffold B is the edge and C is the middle of the seeded scaffolds. Furthermore, images (E and F) is PCL seeded scaffold. Where image E is the edge and image F is the middle of the seeded scaffold. Scale bar = 200 μm 106

Figure 4.14: Cellular activity of PLLA and PCL cell-scaffold constructs on days 7,14 and 21 determined using prestoBlue dye. The values are the means SDs..... 107

Figure 4.15: Graph shows the cellular activity on day 21 normalised to DNA of the random electrospun PLLA and PCL scaffolds. The values are the means SDs. 108

Figure 4.16: XPS analysis spectra. Showing (A) non treated PLLA random scaffold and (B) PLLA random scaffold after allylamine polymerisation which shows the appearance of a Nitrogen peak. Survey scans were collected between 1200 to 0 eV binding energy, at 160 eV pass energy and 1 eV intervals. High-resolution O 1s, C 1s, N 1s and Si 2p spectra were collected over an appropriate energy range at 20 eV pass energy and 0.1 eV intervals. The binding energy scale was calibrated to fix the C 1s peak for C-C/C-H type carbons at 285.0 eV 110

Figure 4.17: XPS analysis spectra. Showing (A) non treated PCL random scaffold and (B) PLLA random scaffold after allylamine polymerisation which shows the appearance of a Nitrogen peak. Survey scans were collected between 1200 to 0 eV binding energy, at 160 eV pass energy and 1 eV intervals. High-resolution O 1s, C 1s, N 1s and Si 2p spectra were collected

over an appropriate energy range at 20 eV pass energy and 0.1 eV intervals. The binding energy scale was calibrated to fix the C 1s peak for C-C/C-H type carbons at 285.0 eV 111

Figure 4.18: XPS analysis spectra. Showing (A) non treated PCL aligned scaffold and (B) PLLA random scaffold after allylamine polymerisation which shows the appearance of a Nitrogen peak. Survey scans were collected between 1200 to 0 eV binding energy, at 160 eV pass energy and 1 eV intervals. High-resolution O 1s, C 1s, N 1s and Si 2p spectra were collected over an appropriate energy range at 20 eV pass energy and 0.1 eV intervals. The binding energy scale was calibrated to fix the C 1s peak for C-C/C-H type carbons at 285.0 eV 112

Figure 4.19: images of aligned fibre PCL scaffolds. Image A; during the mechanical testing by the tensile tester machine using 10N and the aligned fibre PCL scaffold keep stretching without tearing during the test. Image B: a picture of the aligned fibre PCL scaffold before and after stretching 114

Figure 4.20: stress/strain curve of fabricated random and aligned scaffold, plasma and non-plasma scaffolds. A PLLA random scaffolds, B PCL random scaffold and C aligned PCL scaffold tested under dry condition for tensile properties 115

Figure 4.21: Mercury intrusion porosimetry results are plotted as the log differential of intrusion vs. pore size of each scaffold type. During the test, the samples were placed inside an evacuated chamber and the pressure was increased up to a maximum of 414 MPa. The mercury is compressed to penetrate the pores of the scaffold and the results were recorded using a MicroActive AutoPore. Each peach representing the different average pore size of the scaffolds. A: PLLA random scaffold, B: PCL random scaffolds and C: PCL aligned scaffolds. 117

Figure 4.22: Contact angle results of PLLA and PCL random and PCL aligned scaffolds, plasma treated and non-treated scaffolds. The measurement was obtained using DSA instruments. Graph A: bar chart of three types of scaffolds the contact angle of the three scaffold types. This graph shows the reduced water contact angle indicating a significant higher hydrophilic characteristics for all the scaffold types after the plasma treatment. B images of water contact angle of the three types of scaffolds..... 120

Figure 4.23: diagram showed the coating layers of the biofunctionalized scaffolds which were plasma treated with allylamine and then coated with heparin followed by growth factors..... 121

Figure 4.24: different amounts of fluorescein-labelled heparin was added to the plasma-treated scaffolds and plotted against how much was bound out of the total amount added after a 24 hours incubation at 20 degree in the dark..... 122

Figure 4.25: different amounts of heparin were added to the plasma-treated scaffolds and plotted against how much was bound out of the total amount after 24 hours at 20 degree C incubation in the dark..... 123

Figure 4.26: different growth factors binding to several example sulphated glycosaminoglycan immobilised on an allylamine functionalised surface. Binding of A: TGF-Beta 1, B; TGF-Beta 3

and FGF-2 growth factors. The values are the mean SD of 3 experiments, each is performed in triplicate 125

Figure 4.27: sample calibration curve for ELISA A: TGF-Beta-1, B: TGF-Beta-3 and C: FGF-2. The standard curve in between optical density and the different growth factors concentration was linearized by applying lodarithmic transformation..... 127

Figure 4.28: shows the release of A: bound TGF-Beta 1, B: bound TGF-beta 3 and C: bound FGF growth factors from the functionalised scaffolds over 14 days. Highest level of release was recorded in day 1 for TGF-Beta 3 and FGF, were for TGF-Beta 1 the highest level was in day 2. All activated membrane demonstrated a release of the growth factors until day 14 but in at deferent rates..... 129

Figure 4.29: shows the DNA quantification using PicoGreen dye 48 hours after seeding. A; Random PCL scaffolds with and without functionalisation and B: Aligned PCL scaffolds with and without functionalisation. The values are the mean SD of 3 experiments, each is performed in triplicate..... 131

Figure 4.30: shows the DNA quantification using PicoGreen DNA content assay on day 35. A: Random PLLA scaffolds with 5% serum, B: random PCL scaffolds with 5% serum and C: Aligned PCL scaffolds with 5% serum. The values are the mean SD of 3 experiments, each is performed in triplicate..... 132

Figure 4.31: shows the DNA quantification using PicoGreen DNA content assay on day 35 without serum. A: Random PCL scaffolds, B: Aligned PCL scaffolds. The values are the mean SD of 3 experiments, each is performed in triplicate 133

Figure 4.32: shows the total protein of Human Periodontal ligament cells seeded to A: random PLLA scaffolds, B: Random PCL scaffolda and C: Aligned PCL scaffolds all with 5% of serum for 35 days. P values were established using ANOVA. Data is presented as mean SDs of 3experiments, each is performed in triplicate 135

Figure 4.33: shows the total protein of Human Periodontal Ligament cells seeded onto A: Random fibre scaffolds and B: Aligned fibre PCL scaffolds both without serum for 35 days. P valued were established using ANOVA. Data is presented as mean SDs of 3experiments, each is performed in triplicate 136

Figure 4.34: shows ALPA expression on the seesds A: Random PLLA scaffolds, B: Random PCL scaffolds and C: Aligned scaffolds all with 5 % of serum cultured for 35 days. The ALPA amount in all type of scaffolds are nearly the same which indicated the ALPA activity is very law after 35 days of HPDLs cultured. Data is presented as mean SDs of 3experiments, each is performed in triplicate..... 137

Figure 4.35: shows the total Collagen of HPDL cells seeded to A: Randm fibre PCL , B: Aligned fibre PCL incubated in medium with serum and C: Random fibre PCL, D: Aligned fibre PCL without serum all experiment for 35 days. P values were established using ANOVA. Data is presented as mean SDs of 3experiments, each is performed in triplicate 139

Figure 4.36: shows a light microscope image of H&E stained section of a seeded aligned PCL with 5% serum cultured for 35 days in tissue engineering medium. A: Control, B: plasma treated, C: Heparin, D: TGF-Beta 1 growth factor, E: TGF-Beta 3 growth factor & F: FGF growth factor. Scale bars = 100 μm 141

Figure 4.37: shows a light microscope image of H&E stained section of a seeded random PCL with 5% serum cultured for 35 days in tissue engineering medium. A: Control, B: plasma treated, C: Heparin, D: TGF-Beta 1 growth factor, E: TGF-Beta 3 growth factor & F: FGF growth factor. Scale bars = 100 μm 142

Figure 4.38: shows a light microscope image of H&E stained section of a seeded aligned PCL without serum cultured for 35 days in tissue engineering medium. A: Control, B: plasma treated, C: Heparin, D: TGF-Beta 1 growth factor, E: TGF-Beta 3 growth factor & F: FGF growth factor. Scale bars = 100 μm 143

Figure 4.39: shows a light microscope image of H&E stained section of a seeded random PCL without serum cultured for 35 days in tissue engineering medium. A: Control, B: plasma treated, C: Heparin, D: TGF-Beta 1 growth factor, E: TGF-Beta 3 growth factor & F: FGF growth factor. Scale bars = 100 μm 144

Figure 4.40: shows a light microscope image of Picro Sirius Red stained section of a seeded aligned PCL with 5% serum cultured for 35 days in tissue engineering medium. A: Control, B: plasma treated, C: Heparin, D: TGF-Beta 1 growth factor, E: TGF-Beta 3 growth factor & F: FGF growth factor. Scale bars = 100 μm 146

Figure 4.41: shows a light microscope image of Picro Sirius Red stained section of a seeded random PCL with 5% serum cultured for 35 days in tissue engineering medium. A: Control, B: plasma treated, C: Heparin, D: TGF-Beta 1 growth factor, E: TGF-Beta 3 growth factor & F: FGF growth factor. Scale bars = 100 μm 147

Figure 4.42: shows a light microscope image of Picro Sirius Red stained section of a seeded aligned PCL without serum cultured for 35 days in tissue engineering medium. A: Control, B: plasma treated, C: Heparin, D: TGF-Beta 1 growth factor, E: TGF-Beta 3 growth factor & F: FGF growth factor. Scale bars = 100 μm 148

Figure 4.43: shows a light microscope image of Picro Sirius Red stained section of a seeded random PCL without serum cultured for 35 days in tissue engineering medium. A: Control, B: plasma treated, C: Heparin, D: TGF-Beta 1 growth factor, E: TGF-Beta 3 growth factor & F: FGF growth factor. Scale bars = 100 μm 149

Figure 4.44: Fold change in mRNA expression of COL1A1 gene with time in culture for aligned PCL scaffolds seeded with HPDL cells. Culture for deferent periods of time points. Data was normalised to the endogenous control (B2M). P values were calculated using ANOVA. N =3 separate experiments, each performed in triplicate 150

List of Tables

<i>Table 2.1 Scaffold materials used for periodontal tissue engineering</i>	<i>25</i>
<i>Table 3.1 the polymers that been used in the electrospinning for scaffold fabrication.....</i>	<i>59</i>
<i>Table 3.2 ligament cells used in this study</i>	<i>59</i>
<i>Table 3.3 list of media used for tissue cultural</i>	<i>60</i>
<i>Table 3.4 list of reagents used in this study</i>	<i>61</i>
<i>Table 3.5 list of instruments and machines used in this study</i>	<i>63</i>
<i>Table 3.6 list of kits used in this study</i>	<i>63</i>
<i>Table 3.7 list of miscellaneous used in this study</i>	<i>64</i>
<i>Table 3.8 list of software used in this study.....</i>	<i>64</i>
<i>Table 4.1: fibre diameters and scaffold thickness of the commercial aligned fibre PCL scaffolds</i>	<i>100</i>
<i>Table 4.2: Tensile strength, elongation at break and Young's modulus of PLLA and PCL random fibre scaffolds and commercial PCL aligned fibre scaffold</i>	<i>116</i>
<i>Table 4.3: The main output data of mercury intrusion porosimetry analysis</i>	<i>117</i>
<i>Table 4.4: The percentage of how much heparin bound to the plasma scaffolds</i>	<i>123</i>

Abbreviations

3D	3 Dimensional
CMFDA	5-ChloroMethylFluorescein Diacetate
ALP	Alkaline phosphatase
Beta-TCP	Beta-Tricalcium Phosphate
BCP	Biphasic Calcium Phosphate
BMP2	Bone Morphogenetic Protein 2
CaP	Calcium Phosphate
COL1A1	Collagen type I alpha 1
DCM	Dichloromethane
DMF	Dimethylformamide
DMEM	Dulbecco's Modified Eagle's Medium
ECM	Extracellular Matrix
FGF	Fibroblast Growth Factors
FCS	Foetal calf serum
FDM	Fused Deposition Modelling
Gal	Galactosamine
Glc	Glucosamine
GAGs	Glycosaminoglycans
GDFs	Growth Differentiation Factors
GTR	Guided Tissue Regeneration
GTRM	Guided Tissue Regeneration Membrane

GDNFs	Glial-Derived Neurotrophic Factors
HS	Heparan Sulphate
β 2M	Human beta-2-microglobulin
HPDLs	Human Periodontal Ligament cells
HA	Hydroxyapatite
PDL	Periodontal ligament
PLLA	Poly-L-Lactic acid
PCL	Poly(ϵ -caprolactone)
PLGA	Poly(lactic-co-glycolic) acid
PDLSCs	Periodontal ligament stem cells
PDLSCs	periodontal ligament stem cells
MIP	Mercury Intrusion Porosimetry
MSCs	Mesenchymal Stem Cells
μ g	Micro gram
μ l	Micro litre
μ m	Micro metre
MIS	Müllerian Inhibiting Substance
NEAA	Non-Essential Amino Acids
pNPP	p-NitroPhenol Phosphate
PBS	Phosphate Buffer Saline
PDGF	Platelet Derived Growth Factor
PLGA	Poly (Lactic-co-Glycolic) Acid
ePTFE	PolyTetraFluoroEthylene

pH	Potential of Hydrogen
PI	Propidium Iodide dye
qRT-PCR	Quantitative Real Time Polymerase Chain Reaction
SEM	Scanning Electron Microscopy
TGF β	Transforming Growth Factor- β
TGF- β 1	Transforming Growth Factor β 1
TGF- β 3	Transforming Growth Factor β 3
vol/vol	Volume per unit volume
Wt %	Weight percent
wt/vol	Weight per unit volume
XPS	X-ray Photoelectron Spectroscopy

1. Introduction

Periodontal disease, the infection-related loss of essential bone and ligaments supporting teeth, is usually treated by addressing underlying health issues as well as good plaque control (Hughes, 2015). Nearly 50% of UK adults reported the same level of irreversible periodontitis (Chapter 5: Periodontal Diseases, 2022). However, globally about 10% of the world's population has evidence of a serious periodontal disease symptom. The ages between 60 to 64 are at the high-frequency level (Bernabe et al., 2020). Periodontal tissue regeneration is often needed to facilitate periodontal healing and regenerate all the lost tissues (Siailli et al., 2018). Currently, guided tissue regeneration (GTR) is a therapy to regenerate the periodontal ligament and alveolar bone. GTR uses barrier membranes which facilitate lost tissue regeneration by providing a mechanical barrier which prevents the faster proliferating long junctional epithelium and gingival tissues from migrating along the tooth surface and preventing the attachment of the periodontal ligament to the tooth surface. The mechanical properties of the scaffold provide stability during implementation and allow the scaffold to maintain good resistance against the oral load (Tran et al., 2018). The GTR membrane encourages periodontal ligament and bone formation by acting as a mechanical support to 'guide' the regeneration of these cells (Scantlebury, 1993; Shimauchi et al., 2013). There are various scaffold materials available for GTR such as poly-L-Lactic acid (PLLA) which has long-term stability and is ideal for the development of aligned-fibre scaffolds (Dabra et al., 2012). However, poly (ϵ -caprolactone) (PCL) has optimal biocompatibility, excellent structural and mechanical properties and can mimic physiological growth factor delivery (Patrício et al., 2013). These scaffolds are usually prepared via

electrospinning, which allows the tailored creation of nanofibrous 3D structures with the needed patterning, pore characteristics and cell signalling properties (Seo et al., 2016).

2. Literature review

2.1. Periodontium

The periodontium is a group of specialised tissues, which surround the teeth and function to hold the teeth in position within the bone sockets during mastication. It comprises the cementum, periodontal ligament and the alveolar bone (Figure 2.1) which all have unique components and characteristics, which enable the periodontium to perform its function.

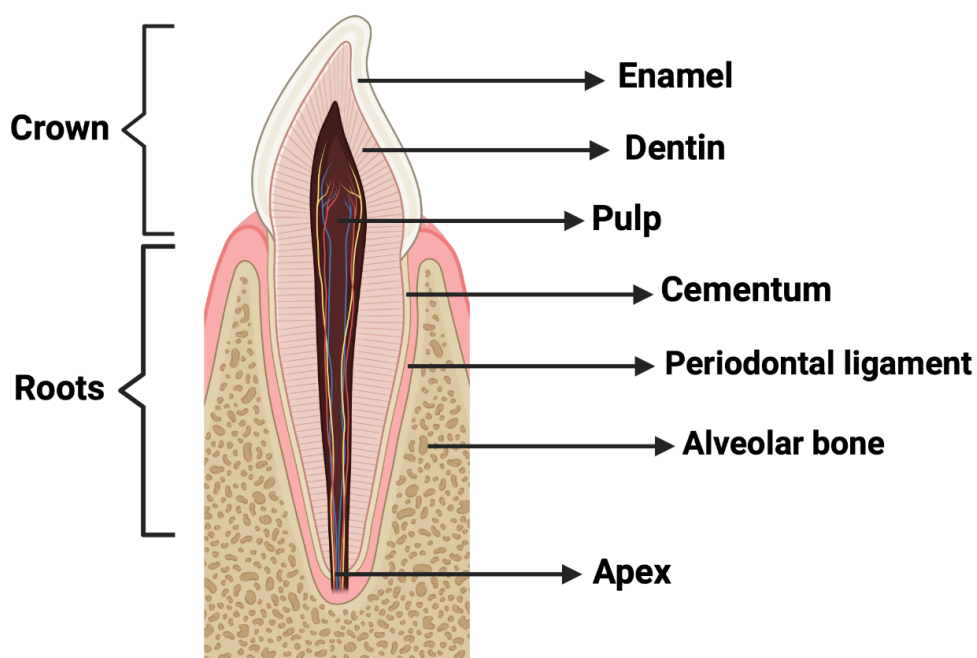


Figure 2.1 The macroscopic tooth structure for incisor tooth.

2.1.1. Cementum

This is the avascular, neural, mineralised tissue that covers the root surface (Figure 2.1) forming an intermediary layer between the root dentine and the periodontal ligament (Nanci, 2008). Although the cementum is classified as a component of the tooth, it functionally belongs to the dental attachment apparatus - the periodontium.

The thickness of the cementum grows over the lifespan of the individual, but in contrast to the bone, it does not undergo tissue remodelling (Gonclaves et al., 2005). The main structural role of the centum is to anchor the periodontal ligaments to the root; however, it has additional adaptive and reparative functions to maintain the root integrity (Gonclaves et al., 2005; Bosshardt and Nanci, 2004). It is thought that the cementum is essential for the maturation of the periodontium during the organism's development and also, during periodontal tissue regeneration (Saygin et al., 2000).

In-man, there are three different types of cementum:

- A-cellular, fibrillar cementum covers a few small areas of the enamel. The cemento-enamel junction is the most common position, but this varies from tooth to tooth (Figure 2.2). The functional importance of this cementum is still unknown. It has no collagen fibrils, which implies that it does not contribute to the attachment of the tooth. However, it is mainly made up of glycoproteins and proteoglycans (Yamamoto et al., 2016).

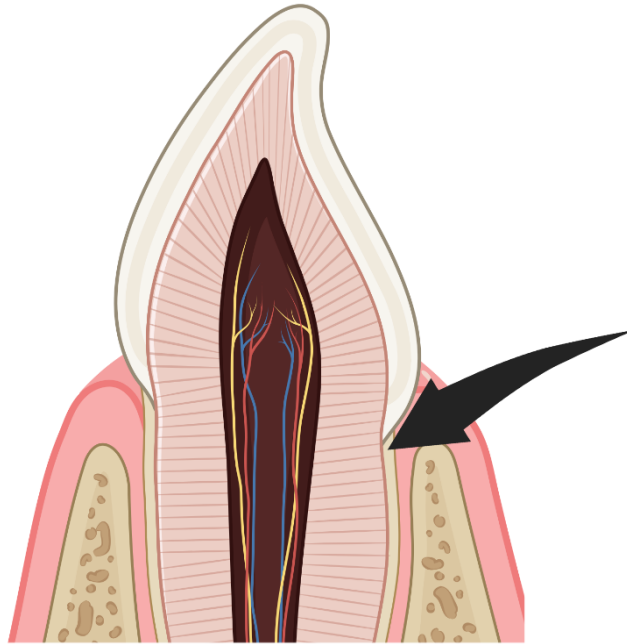


Figure 2.2 The acellular fibrillar cementum of incisor tooth (arrow).

- Cellular intrinsic fibre cementum is made up of cementocytes embedded within a collagenous matrix of collagen fibres which lie parallel to the root surface and circular around the root (Yamamoto et al., 2016). The role of the cementocytes is to provide rapid matrix deposition between the epithelial cells of Hertwig's root sheath and the dentinal surface (Bosshardt and Schroeder, 1991). Cellular intrinsic fibre cementum acts as an adaptive tissue that keeps the tooth in the right position in response to minor movements (Bosshardt and Selvig, 1997). However, it does not contribute to tooth attachment (Yamamoto et al., 2016).
- Acellular extrinsic fibre cementum covers 40-70% of the tooth surface and is found on the cervical and middle root regions. Its apical extension increases from posterior to anterior teeth and so can even be found on the apical root portion of anterior teeth (Gonclaves et al., 2005). This acellular extrinsic fibre cementum is continuously produced and is made up of short collagenous fibres and proteoglycans, which are oriented perpendicularly to the root surface (Yamamoto et al., 2016).

2.1.2. Periodontal ligament

The periodontal ligament is a fibrous tissue that acts as the interface between the root cementum and the alveolar bone, thereby attaching the tooth to the jawbone. It functions as a shock absorber during mastication and so prevents damage to the tooth or the bone (De Jong et al., 2017). The orientation of these fibres is complex, but they allow the 3-dimensional support function (Figure 2.3). The periodontal ligament does not only provide mechanical stability, it also protects the oral cavity from pathogens and contributes to the function of the mastication system (De Jong et al., 2017). This tissue is heterogenous and has a good blood supply, neural network and various cell types (Nanci and Bosshardt, 2006) including bone cells, cementum cells, epithelial rests of Masez, endothelial cells, and neural cells (De Jong et al., 2017). However, the most numerous cell type is the fibroblast that produces the extracellular matrix of the periodontal ligament; mainly type I collagen, (Lekic and McCulloch, 1996). The collagen fibres of the periodontal ligament are remodelled by the ligament fibroblasts. This remodelling process occurs at a higher rate on the bone side than on the cementum side (Lindhe et al., 2003).

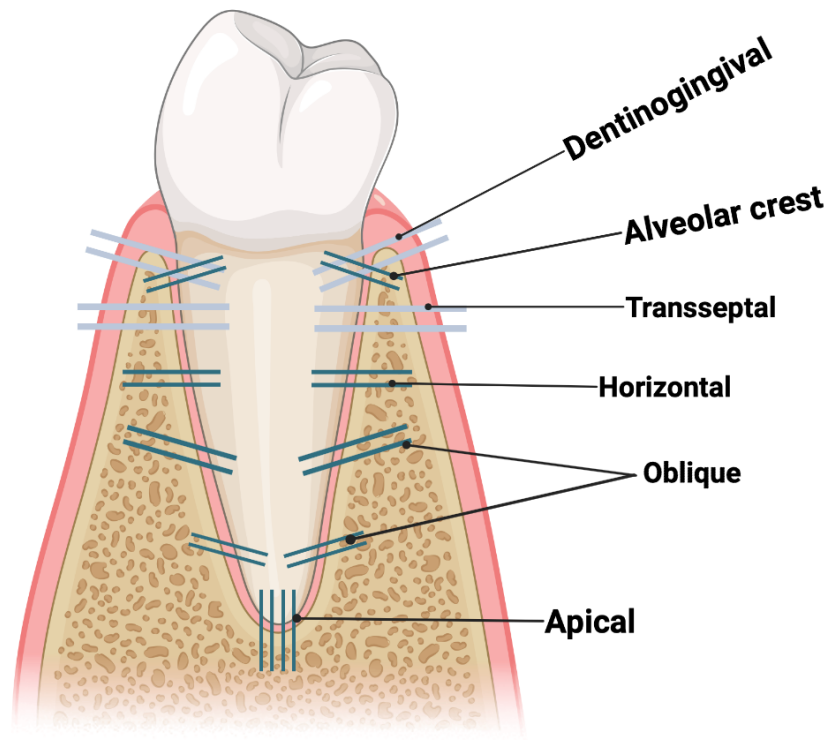


Figure 2.3 The principal fibres of the periodontal ligament allow three-dimensional support and protection against multidirectional forces.

2.1.3. Alveolar bone

In the mandible, the alveolar bone has a thicker cortical and denser trabecular bone compared to the maxilla. This difference is very important for dental implant surgery (Hughes, 2015). The anatomical structure of alveolar bone is complex and is made up of bundle bone, Sharpey's fibres, and the thicker outer layer of spongy cancellous bone (Sodek and McKee, 2000; Nanci, 2008). The cancellous bone has marrow spaces with smaller endosteal spaces that extend into the periodontal ligament (Sodek and McKee, 2000; Newman et al., 2011). The main cellular components of the alveolar bone are osteoblasts that produce the bone, osteocytes which maintain communication flow throughout the bone, bone-lining cells that cover the regions of the bone, and osteoclasts that play a vital role in bone resorption that goes hand-in-hand with bone formation by the osteoblasts (Sodek and McKee, 2000).

2.2. Periodontal ligament function and composition

The main role of the periodontal ligaments is to enable the transfer and distribution of force during mastication. It has recently been found that blood vessels within the ligaments confer the 'shock absorber' function of this layer by acting as a cushion spreading the occlusal load; thereby protecting the underlying alveolar bone from the occlusal load. The ligament shows this specialised behaviour due to the fluid within the ligament which is resistant to the mechanical demands (Dean, 2017). Therefore, the cells, vasculature, and extracellular matrix consisting of proteins and proteoglycans enable the teeth some degree of movement while remaining attached to their bony socket (Retrouvey et al., 2012).

The periodontal ligaments are usually about 0.2mm in width, but when the occlusal load is reduced, such as when the opposing teeth are missing, this can lead to a narrowing of the periodontal ligament and less bone deposition (Hughes, 2015). However, normal loading of the tooth can restore the original periodontal ligament and bone thickness. The periodontal ligaments also respond to overloading and unidirectional force whereby a pressure and a tension side occur. On the tension side, the stretched periodontal ligament fibres are remodelled, and bone deposition occurs. However, on the pressure side, bone resorption by osteoclasts occurs and the periodontal ligaments are remodelled. This function of the periodontal ligaments allows the teeth to move through the alveolar bone and respond to the different pressures and forces they are exposed to.

2.2.1. Fibres of the periodontal ligament

Periodontal tissues are equipped with various stress and strain relieving components, including the fibrillar proteins collagen, fibronectin, and elastin, as well as minerals, and globular proteins (Lin et al., 2013; Newman et al., 2011). These globular proteins interact with

the fibrillar proteins and the interstitial fluid from the blood capillaries and can respond combinatorically or individually depending on the load rate (Lin et al., 2013). Nerve bundles also enter the periodontal ligament, where they branch and end in small rounded bodies near the cementum. The nerves provide the sensitive function of the masticatory system (Walmsley et al., 2007).

The fibres of the periodontal ligament are divided into two types - interstitial fibres, and principal fibres. Interstitial fibres are randomly arranged throughout the periodontal ligament and provide the supporting function of the ligament for the blood vessels and the nerves. The denser principal fibres occur in fibre bundles running from the cementum to the alveolar bone and keep the tooth in its place (Walmsley et al., 2007). The principal fibres run in different directions and so they are named according to their location and orientation, i.e.: crest, horizontal, oblique, interradicular and apical (Walmsley et al., 2007; Newman et al., 2011). Where the principal fibres insert into the alveolar bone and the cementum they insert through small calcified fibres known as Sharpey's fibres.

2.2.2. Cells

The cellular component of the periodontal ligament consists mainly of fibroblasts in conjunction with mineralised tissues, as mentioned earlier. This fibroblastic cell population is heterogeneous which contains fibroblast cells, mesenchymal stem cells and transit-amplifying progenitor cells in the conjunction (Somerman 1988, Kuru 1998). The periodontal ligament also contain epithelial islands called the epithelial cell rests of Malassez, which form a network throughout the ligament. The nerves in the periodontal ligament are mainly mechanoreceptors, which are found in the apical third of the ligament (Hughes, 2015). The mechanoreceptors allow control during mastication. The blood supply to the tooth is

provided by a branch from the apical supply to the tooth which forms a vascular plexus throughout the ligament.

Not only does the periodontal ligament provide the tooth attachment, it also absorbs and dissipates occlusal loads. The strongly hydrophilic proteoglycans in the ligament enable the ligament to respond to compressive loading. Under occlusal loading hydrostatic pressure builds in the tissue and enables the load to be spread around the tooth so protecting the underlying alveolar bone. The tooth responds to loading in the form of hydraulic pressure and elastic recoil, but this property is not due to the collagen fibres which allow some degree of movement and load transfer to the surrounding bone. Therefore, regions where the bone is thin often experience higher degrees of mobility (Hughes, 2015).

2.3. Periodontal disease

Gingivitis and periodontitis are a signs and symptoms of having periodontal disease. Chronic gingivitis is defined as plaque which induces inflammation of the superficial gingival tissues. The clinical signs of gingivitis are bleeding, minor trauma, redness and swelling of the gingiva. However, good plaque control can help in these conditions (Hughes, 2015). If this inflammation is allowed to progress and infiltrate to the deeper periodontal tissue, it causes loss of attachment, destroying of the alveolar bone and loss of the periodontal ligament (Armitage, 2004).

Periodontitis is an inflammatory condition that causes destruction of the bone and the ligaments supporting the teeth. This is caused by the inflammatory response of the soft tissues to the bacteria on the surface of the teeth, which leads to tissue loss and eventually tooth loss. However, the bacteria infection alone is often not the main reason for

periodontitis and a defective inflammatory response is also required to develop the condition (Delima et al., 2002).

2.3.1. Classification of periodontal disease

Classification of the different periodontal diseases is based on their effects on the gingival and periodontal tissues as well as their presentation, progression and etiological factors.

Chronic periodontitis is characterised by slow destruction of periodontal tissues, while aggressive periodontitis is due to a rapid periodontal breakdown that does not correspond with the amount of plaque present. Periodontitis can also be associated with some systemic conditions like cardiovascular disease, osteoporosis and diabetes (Kim and Amar, 2006). Perio-endo lesions are due to inflammation in the periodontium and the pulpal tissues with varying severity and treatment strategies depending on the severity and involvement of the different tissues (Singh, 2011). Periodontal abscesses are often a chronic and refractory form of the disease with a localised accumulation of pus (Patel et al., 2011).

2.3.2. Pathology of periodontal disease

Periodontal disease is the condition of infection of the periodontium. It is a host-microbial interaction that considers both the microbial and host factors. A change in the balance between the factors results in health to disease. Periodontal pathology is more prevalent among the black populations, tobacco users, preterm birth, individuals with previous tooth disease, teeth developmental delays, retained third molars, and term births with elevated serum C reactive protein. The disease has adverse effects on individuals with long-term conditions and is likely to affect other body organs. Long-term conditions affected by the disease include kidney diseases, cancer, HIV/AIDS, and neural disorders such as Alzheimer's

and diabetes. The pathology indicates a pocket depth categorised as 5mm or more (Haug et al., 2009) and risk factors include gingival crevicular fluid inflammatory mediators at baseline and levels of periodontal pathogens.

Pathological processes in the periodontal tissues can be associated with vascular disorders and autonomic nervous system tone changes due to impairment in minerals, protein metabolism, parathyroid glands dysfunctions and endogenous hypovitaminosis (Nemesh et al., 2021). However, determining the aetiology for periodontal disease is complex. That is due to the many species of bacteria such as the gram-negative bacteria: *Tanerella forsythensis*, *Treponema denticola* and *Porphyromonas gingivalis* (Agerbæk et al., 2006). in the pockets, host response, difficulty in getting a representative species sample, and pathogen action, which present differently at various times.

Histopathology of periodontal disease can be divided into initial, early, established, and advanced lesions. The plaque biofilm is a bacterial deposit which is difficult to remove by simple tooth brushing. It develops on teeth, mucosa, or any other solid surfaces. The primary microbes are facultative anaerobes such as *Gram-positive cocci* and *anaerobic microorganisms* (Hasan and Palmer, 2014). There may be a later predominance of Gram-positive filaments. Established lesions are mostly controlled by leukocyte aggregation and B cells, which can be lymphocytes or plasma cells. These cells start the site's change by converting the junctional and sulcular epithelium into the pocket epithelium. It is usually marked with chronic and successful defence reactions, while advanced lesions result from destructive immunopathological mechanisms. The established lesion stays for many years, becoming periodontitis when it advances to advanced lesions. The factors facilitating the advancement are unknown, although scientists believe it is due to host immune response, bacterial plaque microorganisms, or virulence change in the plaque bacteria (Hasan and

Palmer, 2014). Advanced lesions are clinically identified as periodontitis featured by bone resorption, pocket formation, destruction of the collagenous periodontal ligament, and pocket epithelium ulceration.

Further, gram-negative anaerobic bacilli increase, resulting in bacterial flora shifts and more complex pathogenic plaque. The primary aetiological agent of periodontal disease is Gram-negative rods such as the *Porphyromonas gingivalis*, *Aggregatibacter actinomycetemcomitans*, *Prevotella intermedia*, *Fusobacterium nucleatum*, *Eikenella corrodens*, *Treponema denticola*, *Campylobacter rectus*, *Capnocytophaga* and *Tannerella forsythia* (Hasan and Palmer, 2014). These bacteria cause damage to the supporting tissue which then affects mobility and causes loss of the tooth. Apically and laterally presents inflammatory infiltrate extensions, collagen content reduction, and the dense collection of lymphocytes, macrophages, and plasma cells.

The inflammatory stage is suited for the emergence of inflamophilic anaerobic microorganisms like *P. gingivalis*, *Tannerella* and *Treponema* (Azizah, 2020). The heme in blood haemoglobin attracts *P. gingivalis*, which promotes its growth and provides an alkaline environment in the subgingival pockets, making them the dominant bacteria. At the same time, *Treponema* depends on the short-chain fatty acids excreted by other bacteria (Nyvad and Takahashi, 2020). Furthermore, co-colonisation of acid neutralising species such as *Prevotella* and *Fusobacterium* promotes the alkalinity of the periodontal pockets, which enhances the ecological benefits of *P. gingivalis*. Reparative fibrosis is present between the plaque and periodontal connective tissues at the periphery. Epithelial barrier breakdown can be linked with crucial changes in the immunity response and opens up direct access to the plaque metabolites and antigens (Hasan and Palmer, 2014). This stage presents irreversible

attachment loss and loss of periodontal ligament and bone with the advanced progression of the pocket formation.

2.4. Periodontal treatment

The management of periodontal disease is based on the treatment of etiological factors and plaque accumulation. Good plaque control usually can be performed by the patient and the clinician, and can be done by removing the plaque by tooth scaling. This strategy aims to eliminate plaque so decreasing inflammation to prevent tooth loss. In patients with periodontitis, the dental professional, who performs non-surgical root surface debridement (Deep cleaning) by using manual and ultrasonic instruments, can only remove the sub-gingival plaque. However, this non-surgical approach may not always be successful and so, surgical treatment of the pockets may be required (Hughes, 2015).

2.4.1. Options for periodontal treatment

Periodontal disease can be treated successfully. After periodontal cleaning, a dentist may recommend a healing medication such as antibiotics in the form of pills or mouth-wash (American Dental Association, 2005). After the cleaning, the next visits include preventive care for many patients, but when there is loss of the supporting bone and formation of deep gingival pockets, surgical removal of inflamed tissue and plaque are recommended to prevent tooth loss. Surgeries are essential for the better removal of inflamed tissues and decreasing damage to the alveolar bone supporting the teeth. During the enlargement of the gingival pockets, the enlarged pocket offers a better environment where bacteria can live while attacking the tissues and bones (Cionca et al., 2010).

Surgeries allow the dentist to reach under the gum areas and tooth roots where plaque and tartar have converged. Removal of the bacterial-infested areas and bone and tissue regeneration aid in pocket reduction and repairing damage caused by the disease (American Dental Association, 2005).

Bone surgery is utilised to rebuild or reshape bone destroyed by periodontal disease. Tissue stimulating proteins (enamel matrix proteins), bone grafts, guided tissue regeneration (GTR) membranes, and facilitate the body to regenerate the periodontal tissues including bone. Loose teeth can be stabilised by bite guards and splints and these can assist in tissue or bone regeneration during tissue healing. A soft-tissue graft is an option in case of excessive gum-tissue loss. In this case, the gum tissue is removed from the patient's palate or a donor during the procedure, and the exposed root is covered by them. It can be done for single or many teeth to align the gum line and reduce gum sensitivity. In addition, laser-assisted surgery has been used due to its excellent performance in homeostatic action, excision of oral tissues, and healing faster (Capodiferro et al.,2019). This technique has revolutionised gingival overgrowth management and promotes postsurgical periodontal good status in the patients.

2.4.2. Control of infection

The primary objective in treating periodontal disease is to develop substantial infection control. It aims to reduce the bacterial load below the patient's threshold disease level (Jönsson and Abrahamsson, 2020). Mechanical infection control is a significant procedure in treating non-surgical periodontal disease and scaling. The technique is most successful in its execution and completion (Milosavljevic, 2018). Instruments for removing plaque such as ultrasonic and hand descaling equipment complement each other resulting from cleaning teeth.

Self-performed supragingival plaque control that is effective alters the ecological environment of the subgingival by microbial biofilm disruption, suppressing inflammation, and decreasing bacterial number. Adequate oral hygiene is crucial in reducing the progression of periodontal disease infection (Jönsson and Abrahamsson, 2020). Daily tooth brushing and cleaning the interdental are essential in maintaining periodontal infection control. Further, educating the essence and impacts of the behaviours on patients is vital for the control of infection. Although changing a patient's habit is difficult, making them aware of the disease's repercussions results in their compliance with instructions and daily oral hygiene practice. Regular dental check-ups are essential for monitoring the dentition to detect and prevent infections.

2.4.3. Open flap surgery

Open flap surgery is among today's ways of treating and repairing periodontal pockets. Open flap surgeries are essential with deeper probing lengths of gingival pocket (Caffesse et al., 1986). The objective of the surgery is gingival pocket elimination and reduction of inflammation. A Flap -like insertion on the gum tissue is performed to access it, and dead tissues from the gingival pockets are removed. This procedure provides access to the roots of the teeth for a thorough cleaning that assists in removing plaque and calculus. The flap is then closed, and stitched in place. Furthermore, flap surgery assists with regenerating the bone and tissue that could have been lost from the periodontal disease. Although flap surgery has long been used as a standard practice, it poses a higher risk for disease progression. The gingival pockets can get deeper, which causes the progression of periodontal disease that result in tooth loss in the long term (Cortellini et al., 2017).

2.4.4. Regeneration of the periodontal ligament and supporting alveolar bone

To reconstruct the periodontal tissues, the recommended approach is to mimic the natural sequence that occurs during the healing process in the periodontal ligament (Siaili et al., 2018). The stem cells and immature progenitor cells within the periodontal ligaments are responsible for the tissue regeneration of the bone and the epithelial and the gingival connective tissues (Siaili et al., 2018). The early phase of the inflammatory response usually takes about 3 days, the late inflammation phase begins when the wound and tissue regeneration begin. After about 7 days, connective tissue may have formed at the root surface (Polimeni et al., 2006).

2.5. The healing process

For reconstructive therapy, primary closure of the wound site is essential to prevent exposure and contamination of the regenerative materials used. This is performed in addition to good plaque control (Siaili et al., 2018). Conventional surgical techniques, mentioned previously, are often more traumatic and cause severe tissue injury that can prevent periodontal regeneration. Therefore, the use of tissue flaps is recommended which prevent tension on the wound margins and support passive wound closure. This would allow healing with less re-epithelialisation, collagen formation and remodelling, wound contraction, and overall tissue remodelling (Bhavsar et al., 2018).

The success of periodontal regeneration relies greatly on wound stabilisation, which requires the maintenance of the integrity and stability of the blood clot. However, a thick blood clot attracts inflammatory cells and creates a dead space between the flap margin and the tooth surface, which prevents regeneration. Therefore, current recommendations are to maintain

a thin and stable blood clot that can be achieved by preventing occlusal trauma and tooth mobility (Bhavsar et al., 2018).

2.6. Guided tissue regeneration (GTR)

Guided Tissue Regeneration (GTR) is a procedure based on the use of barrier materials to aid the regeneration of the lost periodontal tissues and bone (Figure 2.4). These materials allow the cells to proliferate and the extracellular matrix of the periodontal ligament to be re-established. Therefore, GTR materials need to be biocompatible and allow tissue integration, cell closure, clinical handability and enable space-making for the periodontal and bone cells to rebuild within the defective site (Scantlenbury, 1993).

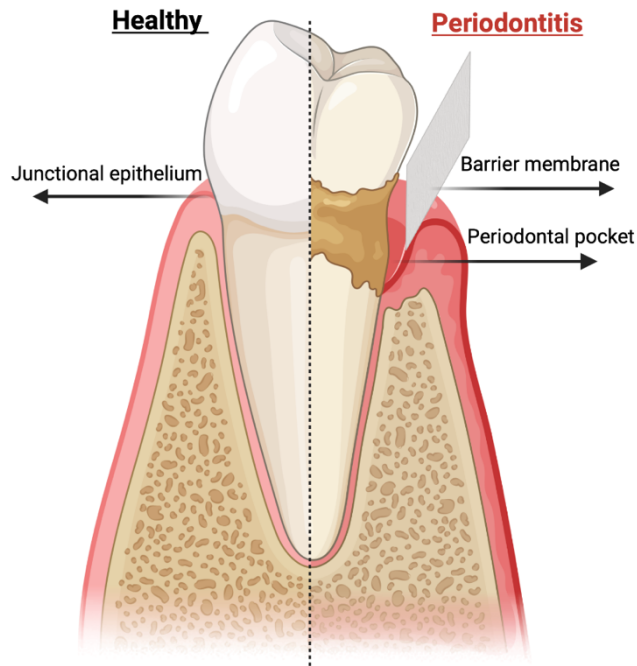


Figure 2.4 Schematic illustration of using GTR membrane in the regeneration of infected periodontal tissues

2.6.1. GTR membrane types

Currently, resorbable materials are being used for the GTR procedure. Some of these are outlined below:

Collagen barrier membranes have found wide application due to their suitable physical and biological properties. These are mainly comprised of type I collagen which mimics the major collagen of the natural periodontal ligament. However, these materials have been found to provide limited wound space maintenance and regeneration (Tatakis et al., 2000).

Synthetic materials such as poly alpha-hydroxy acid can be used; however, these materials have been found to inhibit osteogenesis and are only slowly degraded in the human body after four to six years, which can cause a late wound for the defect area (Tatakis et al., 2000). The degradation rate of the polymer can be affected by the molecular weight of the polymer itself. As thought, polymers with high molecular weight usually demonstrate slower

degradation due to the slower decrease in the properties loss of the hydrolysis (Speight, 2011).

Oxidised cellulose mesh barriers are resorbable and are suitable for GTR procedures. However, cell closure may become an issue as these materials provide limited wound space (Siaili et al., 2018).

Autogenous periosteal barrier membranes combine connective tissue and periosteum from the patient's palate with bone chips (Paloantoio et al., 2010) and have been found to provide promising results for GTR; however, further studies are still required before this can be used routinely.

Laminar bone allograft membranes contain demineralised freeze-dried bone allograft, but these materials need more studies for the use in GTR (Siaili et al., 2018).

2.6.2. The mechanism of the GTR membrane in mouth

Periodontal tissue regeneration has focussed on repairing the defect in tissues such as alveolar bone, periodontal ligament and cementum. Traditionally, non-resorbable materials such as expanded polytetrafluoroethylene (ePTFE) was used for GTR but this was faced with the disadvantage of requiring additional surgery to remove the membrane after tissue regeneration. This has led to the development of biodegradable synthetic and natural materials like collagen, Polylactic acid (PLA), Polycaprolactone (PCL) and Poly(lactic-co-glycolic acid) (PLGA). However, their biological and mechanical properties have been found to be unstable but can be controlled by different methods.

Electrospun nanofibers have been found to be ideal to mimic the collagen fibres of the extracellular matrix (ECM) which allow it to support ligament and bone regeneration due to their ability to resist loading and also able to hold and release growth factors (Seo et al., 2016).

This has been found to be beneficial in helping stem cell attachment and increasing the overall need for tissue regeneration (Seo et al., 2016). However, these materials have also found application in drug delivery to the root canals too. For example, during endodontic therapy (Zafar et al., 2016). Dental implants have also found application for these electrospun GTR membranes. Further research is required to determine the exact benefit of some approaches (Zafar et al., 2016). However, the success of the approaches is highly dependent on good mouth hygiene. Poor oral hygiene would lead to bacterial accumulation in the mouth and subsequent contamination of the tissue-implantation site. In addition, poor plaque control and residual periodontal infection can affect periodontal tissue regeneration (Bhvsaret al., 2018). Smoking is also a major factor for poor outcome of periodontal tissue regeneration, which is thought to be due to damaging the body immune responses (Bhvsaret al., 2018). Genetics can also influence cell reaction and tissue regeneration, while diabetes may affect the body's response to bacteria, which increases the risk of infection and causes a delay in wound healing that leads to treatment failure (Bhvsaret al., 2018).

2.7. Cell and scaffold selection for periodontal tissue engineering

Tissue engineering is a multi-disciplinary science, which uses a combination of suitable cells with a biocompatible support material/scaffold and biological signals to generate de novo tissue for regeneration of lost/damaged tissues. Tissue engineering is a relatively new field in periodontal therapy. This requires three components: cells, the essential signalling molecules, and suitable scaffolds (Chen and Jin, 2010). Stem cells are capable of self-renewal and multi-lineage differentiation that is controlled by their actual signalling pathways as well as by external stimuli and signalling molecules (Sialli et al., 2018). The third component needed for tissue engineering is a biomaterial support or scaffold.

2.7.1. Potential cells for periodontal tissue engineering

The regenerative cells' capacity limits the potential of periodontal regeneration. Periodontal cells promote the regeneration of damaged periodontal tissues, and the extracellular matrices regulate it by causing selective or nonselective responses in their precursors and different cell lineages (Benatti et al., 2007). Periodontal ligament (PDL) cells can create new connective tissue attachments, which is the basis of guided tissue regeneration. Cells in periodontal tissue engineering offer the machinery for new tissue growth and regeneration. Periodontal tissue engineering created delivering cell populations principle in enough numbers required for healing including the PDL cells, cementoblasts and osteoblast cells. PDL cells enhance root resorption, bone resorption and soft tissue regeneration. Alveolar bone cells covered roots and induce tissue formation that is cementum-like. Bone sialoproteins and osteopontin cells migrate to the new bone formed after transplantation, expressing phenotypic markers like PDL cells. PDL cells such as fibroblasts, osteoblasts, cementoblasts, macrophages, and undifferentiated ectomesenchymal cells maintain and regenerate periodontal tissue (Benatti et al., 2007). Stem cells in human PDL (PDLSCs) are responsible for partial periodontal regeneration from preliminary periodontal tissue regenerative approaches.

2.7.2. Types of scaffolds

Scaffolds are designed to retain and support cells to enable them to develop the appropriate tissue components. A scaffold retains the cells and so allows them to grow in the required site (Shimauchi et al., 2013). The function of the scaffold is to provide a suitable environment that maintains cell viability and supports their growth and formation of appropriate tissue to

regenerate and repair the injury site (Shimauchi et al., 2013). The scaffold can be polymeric and should be porous and in the majority of cases biodegradable. Scaffolds can be fabricated with natural and synthetic materials and can take the form of films, fibres, sheets, gels and sponges, among others (Martino et al., 2011).

- **Inorganic materials**

Inorganic materials used for periodontal regeneration include ceramics such as calcium hydroxyapatite (HA) and calcium phosphate (CaP) which have been successful in regenerating alveolar bone (Shimauchi et al., 2013). Materials made from CaP like beta-tricalcium phosphate (beta-TCP) are often the material of choice due to having a similar composition to the natural bone, and their ability to form bone-like material and to support osteoconductivity (Chai et al., 2012). HA is the natural form of calcium phosphate, which is found in bone. HA makes up 60% of dry weight of natural bone (Wagoner-Johnson and Helsheler, 2011). However, beta-TCP is an osteoconductive material which mean it allows the bone to grow onto the scaffold where this has found wide clinical application when combined with the growth factor and platelet-derived growth factor (Sarment et al., 2006).

- **Natural polymers**

Natural polymers include chitosan and collagen among others. Chitosan is a natural polymer of a carbohydrate that is biocompatible does not show or immunogenicity and has been used to support general wound healing and bone formation due to its ability to act as a bone substitute and good scaffold for cell attachment (Dabra et al., 2012). It is important to highlight that published studies have reported that some of chitosan it can be toxic.

Collagen can be found in various forms like foam/sponge, fibre and membranes. Collagen foam scaffolds can easily be moulded into the required 3-dimensional form and are relatively resistant to protease degradation. However, scaffolds fabricated from collagen fibres are more resistant to collagenase than foam scaffolds (Dabra et al., 2012).

Matrigel is widely used in basic science for the investigation of cell-matrix interactions and has found application in tissue engineering for nerves, adipose tissue and skeletal muscle (Salehi-nik et al., 2017). However, it has not been used widely for periodontal tissue engineering.

Fibronectin is a glycoprotein that easily associates with other extracellular matrix components like collagen and it is thought to support vascularisation in scaffolds (Salehi-nik et al., 2017).

- **Synthetic polymeric materials**

Synthetic polymers are often the material of choice for scaffold manufacture due to their biocompatibility, biodegradability and processability according to specific tissue requirements. For example, the biodegradability can be modified by changing the molecular design and the pore size, while the physical and chemical properties can be controlled by introducing surface modifications which can control the tissue's biological responses (Salehi-nik et al., 2017; Rasal et al., 2010).

Synthetic polymeric polyester materials for example, polyglycolic acid and polylactic acid can often be used to fabricate scaffolds. Polyglycolic acid, which is a polymer of glycolic acid, was the first polymeric scaffold to be used in periodontal tissue engineering. It is also a suture material and often used as an implant for bone fracture fixation. Another example is polylactic acid, which is a lactic acid-derived polymer and is more resistant to hydrolysis than the

polyglycolic acid. Both polylactic acid and polyglycolic acid are considered as biomaterials because they provide good biocompatibility, structural and mechanical properties and degradation rates (Dabra et al., 2012).

scaffold	Growth factor (combination)	reference
1- Natural Polymers Porous chitosan Collagen-chitosan Hydroxypropyl cellulose Hydroxyapatite modified collagen	PDGF or BMP-7gene Fibroblast FGF-2 bFGF	Zhang et al. (2007) Susanto et al. (2019) Kitamura et al. (2011) Wang et al. (2020)
2- Synthetic polymers PLA-PGLA copolymer Pluronic F127 Porous poly(L-lactic acid) PCL	rhBMP-2 TGF-Beta 1 MSCs BMP-7	Takahasho et al. (2007) Mohammed et al. (1998) Ito et al. (2017) Sophia et al. (2018)
3- Hydrogels Dex-GMA gelatin gel Bovine insoluble collagenous matrix Collagen gel Gelatinous carrir Injectable waven bone-like hydrogel	rhBMP-2 - FGF-2 FGF-2 BMSCs	Chen et al. (2005) Ripamonti et al. (1996) Sato et al. (2004) Takayama et al. (2001) Yang et al. (2020)
4- Bioactive ceramics Calcium phosphate cement b-Tricalcium phosphate Hydroxyapatite and b- b-Tricalcium phosphate b-Tricalcium phosphate Hydroxyapatite	- rhPDGF-BB hDPSCs FGF-2 mADSCs	Shirakata et al. (2002) Giannobile et al. (2006) Kang et al. (2017) Ogawa et al. (2016) Boeckel et al. (2019)
5- Bone grafts Bone allograft Injectable cartilaginous graft Platelet-rich fibrin and bovine bone	rhPDGF-BB BMSC -	Lynch et al. (2003) Feng et al. (2018) Brouwars et al. (2019)

Table 2.1 Scaffold materials used for periodontal tissue.

2.7.3. Scaffold properties

Ideally, scaffolds should mimic the native extracellular and native environments which may also include the environment where stem cells reside (i.e. the stem cell niche). Therefore, tissue engineering faces the challenge of using the right cells from a suitable origin to develop the desired organ while providing a scaffold that allows the tissue formation and its function (Levenberg and Langer, 2004). The scaffold of choice needs to support the essential cell-cell, cell-matrix and cell-extracellular matrix interactions.

Cell-cell interactions occur between cells e.g. stem cells, and between cells and supporting, stromal cells e.g. stem cells and supporting cells that enable stem cell retention within the niche and their regulation. Cell surface also plays an essential role in stem cell activation and retention (Shimauchi et al., 2013).

The cell-scaffold interaction is bi-directional since the cells can also cause the modification, degradation or deformation of the scaffold. Therefore, there is constant feedback between the cells and the scaffolds. Therefore, the topography, chemical and physical properties of the scaffolds are important for controlling and directing cell fate.

The extracellular matrix provides properties such as stiffness, topography and is usually composed of fibres like elastin and collagen (Muiznieks et al., 2012). These components of the extracellular matrix allow the stem cells to interact with their environment; for example via their adhesion molecules, which initiate intracellular signalling and so regulate stem cell behaviour, growth and differentiation (Shimauchi et al., 2013).

2.8. Cells for regenerative approaches to repair periodontal ligament

The periodontium has a well-arranged structure that consists of multiple tissue types and complex structures (Xu et al., 2019). Periodontal regeneration currently relies on guided tissue regeneration techniques to regenerate multiple periodontal tissues such as alveolar bone, cementum, and periodontal ligament.

2.8.1. Periodontal ligament fibroblasts

The ligament cells of the periodontal ligament have a fibroblastic phenotype. In in vitro experiments, cells isolated from the periodontal ligament are the most commonly used. The periodontal ligament also contains stem cells (PDLSCs) (Jönsson et al., 2011). PDLSCs have the potential to differentiate into multiple cell types but they can also undergo self-renewal (Tomokiyo et al., 2019). This is still an interesting field of research relying on the use of PDLSCs as there are different techniques for periodontitis treatments (Xu et al., 2019).

A study by Shi et al. (2018) found that cultured, osteogenically induced human periodontal ligament stem cells (PDLSCs) seeded onto the improved biphasic calcium phosphate (BCP), when transplanted into dogs achieved effective periodontal regeneration. This tissue regeneration included not only new bone formation, but also, periodontal ligament with correctly organised collagen fibres, which were inserted into the cementum and the bone at the correct angles. Therefore, scaffolds seeded with periodontal ligament stem cells are a promising option for periodontal regeneration. However, a disadvantage of using scaffolds is that they can induce inflammation, therefore, other approaches such as the use of cell sheet engineering are currently being explored (Xu et al., 2017). This is because the creation of a cell sheet contains cells connected via cell-cell interactions and extracellular matrix only (Li et al., 2017). This approach has been successful in transplanting PDLSCs and achieving

periodontal regeneration in animal models (Ishikawa et al., 2009). However, this is still not a well-established approach.

2.8.2. *In situ* regeneration of the periodontal ligament

Periodontal tissue regeneration is often essential to facilitate periodontal healing and periodontal ligament tissue attachment (Siailli et al., 2018; Scantlebury, 1993; Shimauchi et al., 2013). The biomaterials that are usually used consist of collagen, hydrogels or gelatine, which have well-known problems with transplantation. These problems include degrading very fast and at an uncontrolled rate, their uncertain interaction with cells and difficulties associated with their production (Hu et al., 2017). Moreover, these biological materials have poor mechanical properties which limits their regeneration for periodontal ligament tissue where load bearing properties are essential (Hu et al., 2017). Therefore, the use of electrospun synthetic scaffolds is recommended since they can be engineered to provide a 3D environment with the required mechanical properties. In addition, they are homogenous and reproducible which is not usually the case with biological scaffolds (O'Brien, 2011). Another benefit of using these electrospun synthetic scaffolds is that their composition can be tailored according to the degradation characteristics that are required (Oh et al., 2003). The use of electrospinning allows the membrane architecture to be engineered to provide additional desirable properties such as patterning (Ramos-Rodriguez et al., 2021; Paterson et al., 2017), pore characteristics and cell signalling properties (Seo et al., 2016). Examples of such electrospun scaffold materials are poly-L-Lactic acid (PLLA) (Dabra et al., 2012) and the more easily degradable co-polymer poly Lactic-co-Glycolic Acid (PLGA) (Chen et al., 2013). Therefore, it would be interesting to the field of dentistry to determine whether these electrospun synthetic scaffolds would be ideal for periodontal ligament tissue regeneration.

2.9. Polymers used in regenerative medicine and tissue engineering

Poly-L-lactic acid (PLLA) and poly (ϵ -caprolactone) (PCL) are two of the most commonly used electrospun nanofiber scaffolds for bone, nerve and vascular tissue engineering (Hu et al., 2010; Yang et al., 2004; Ahmadi et al., 2017) and have also found wide application for three-dimensional cell culture and transplants in dental research and surgery too. This is due to their biodegradability, easy availability and easy processing (Chen et al., 2013).

2.9.1. PLLA

A study done by Terjo et al. (1998) found that PLLA barrier membranes in 30 patients successfully managed intrabony defects after open flap surgery. However, PLLA is a hydrophobic material with high mechanical strength but does not support strong cell adhesion and tissue formation. The surface characteristics of this material do not provide an osteoinductive environment (Chen et al., 2013). Therefore, more recent research has focussed on coating PLLA with natural materials like collagen, HA, hyaluronic acid, sulphated glycosaminoglycans and growth factors which have been successful in supporting bone formation (Ahmadi et al., 2017); Richardson et al., 2006). Ahmadi et al. (2017) coated PLLA with Wharton's jelly, which surrounds the umbilical cord vessels and has high proportions of collagen and hyaluronic acid. PLLA with Wharton's jelly was found to be successful in promoting osteogenesis. PLLA has also been coated with chitosan, which improved the properties with regards to biocompatibility and the support of wound healing (Chen et al., 2013). On the other hand, animal research studies show that the use of PLLA can support bone formation (Holderegger et al., 2015) and this was reported with limited inflammatory

responses with no infection, which makes this a promising material for future applications in periodontal tissue engineering. A recent study found that coating PLLA with collagen and HA supported osteoconduction, the mineralisation of the extracellular matrix and the expression of bone differentiation markers (Gonclaves et al., 2016).

2.9.2. PCL

PCL can be degraded *in vivo*, but this occurs very slowly due to the synergistic action of hydrolytic and enzymatic mechanisms. It has low tensile strength and very high elongation at its breakage point and has very good elastic properties (Nobile et al., 2015). As well as a low *in vivo* degradation rate the above properties make PCL an ideal material for use in scaffolds (Conte et al., 2018).

Louvrier et al. (2017) used PCL to facilitate odontogenic differentiation of human dental pulp cells and form functional odontoblast-like cells that secrete extracellular matrix which has similar properties to mineralised dentine matrix which further supports their use in scaffolds. Another study done by Chuenjikuntaworn et al. (2016) found that a 3D-PCL/hydroxyapatite scaffold efficiently supported the growth, gene expression and osteogenetic differentiation of stem cells and also, encouraged calcium deposition. Moreover, scaffolds based on PCL allowed the incorporation of antibiotics which have been found to reduce the dental caries pathogenic load as well as support fibroblast growth which makes this a very promising material for dental engineering (Baranowska-Korczyn et al., 2016).

2.9.3. Breakdown of PLLA and PCL in the human body

PLLA is degraded naturally at the site of implantation with the main mechanism being the hydrolysis of the ester-bond backbone. However, the rate of degradation depends on the pH

and temperature in the tissue as well as the composition of the polymer and whether it is a component of a copolymer. Therefore, if there is inflammation or infection at the site of implantation, the rate of degradation will be higher. Besides, chirality affects degradation too with the L conformation having a lower rate of degradation than the D-conformation (Da Silva et al., 2018). Other influencing factors include crystallinity, degree of crosslinking, geometry and size can affect the biodegradability of PLLA (Da Silva et al., 2018). However, the absorption for PLLA ranges between 40 weeks and 6 years (Da Silva et al., 2018).

For PCL, similar factors influence its degradation in the body such as: temperature and whether it exists as a copolymer. However, its rate of degradation is still slower than for PLLA (Abedalwafa et al., 2013). The melting temperature for PCL is higher than body temperature, so it remains in its rubbery state, but it is still capable of hydrolytic degradation (Abedalwafa et al., 2013).

As highlighted above, polymers offer many processability opportunities depending on the application. Injection moulding and 3D-printing are common techniques used for the manufacture of polymeric biomaterial devices. However, the electrospinning technique for polymeric biomaterials is currently a very powerful approach to manufacture membranes

2.10. Electrospinning

Electrospinning is a fabrication method for producing polymer nanofibers from various materials. It involves the application of an electric field to a solution of the polymer to generate a fine, continuous nanofiber structure, and the technique is established for the fabrication of ultrafine fibres, making it ideal for the design of complex micro-structures (Forciniti, 2011; Barhoum et al., 2019; Mamidi et al., 2022).

A micro/nanostructured membrane has been suggested to improve dental restoration due to a three-dimensional structure, which mimics the size of fibres in natural extracellular matrices and improves the cell adhesion, growth and survival. In addition, these materials like electrospun nanofibrous scaffolds have demonstrated better mechanical stability (Seo et al., 2016). The polymers often used for these electrospun nanofibrous scaffolds are PLA, PCL and PLGA. The process of electrospinning provides the advantages of it being a relatively simple additive manufacturing procedure, which enables the control of fibre diameter and the fibre size (Seo et al., 2016). Electrospun scaffolds can be fabricated to more closely resemble the tissue extracellular collagen structure (aligned fibres). The fibres produced have a wide range of biomedical applications, including use in the guided tissue regeneration membrane (GTRM) for periodontal ligament regeneration. GTRMs are used to improve wound healing and periodontal tissue regeneration by offering a physical barrier to prevent the penetration of unwanted cells while allowing access to the desired cells. Therefore, these nanofibrous scaffolds formed by electrospinning have benefit in overcoming some of the challenges of the small size of the dental tissues and implant that is exposed to high tension and force and also, to bacteria within the oral cavity (Seo et al., 2016).

Electrospinning has achieved considerable attention among all methods to produce nanofibers with high porosity and surface area, excellent pore architecture, and various chemical compositions. The unique properties of nanofibers have brought about novel advances in nanomedicine to create innovative fibre-based developments for biomedical use and healthcare (Asadian et al., 2020). The electrospinning process is simple and cost-effective, making it an attractive option for GTRM fabrication. Further, guided tissue regeneration (GTR) systems are a trending topic in the treatment of periodontitis, and their benefits include inhibiting connective tissue from interfering in osteogenesis and cell growth, enhancing the

healing process of degenerated periodontal ligaments and tissues, and inhibiting inflammation and bacterial infection (Mirzaeei et al., 2022). GTRMs are fabricated with biocompatible and biodegradable materials that control tissue regeneration in periodontal tissues. They are composed of electrospun nanofibers produced from biodegradable polymers, such as poly-lactic-co-glycolic acid (PLGA) and polycaprolactone (PCL).

The electrospun nanofibers create a three-dimensional matrix that resists enzymatic degradation, offering a barrier between the periodontal wound and the surrounding tissue. The barrier promotes periodontal tissue regeneration, effectively restoring the periodontal tissues damaged due to periodontal disease (Zhao et al., 2022). Nanofibers enhance protein absorption and foster specific gene expression. Additionally, they improve cell adhesion and inhibit fibroblasts from passing through the barrier membrane (Zhuang et al., 2019). Nanostructured-fibre scaffolds are more efficient for bone regeneration than macro- or micro-sized fibre scaffolds, as they sufficiently permit cell adhesion, proliferation, and chemical transformation. The use of electrospun nanofibers in developing GTRMs has been successful due to the ability of the nanofibers to provide an ideal environment for tissue regeneration (Anjum et al., 2022). Furthermore, nanofibers control the formation of new tissue by offering a scaffold for cell attachment, fostering cell proliferation, and facilitating the diffusion of nutrients and growth factors into the periodontal site. They offer mechanical support to the periodontal tissue, which is vital for proper healing (Sylvester et al., 2020). Electrospun fibres are suitable materials for GTRMs due to their unique properties.

2.10.1. Fabrication of PLLA and PCL fibre scaffolds using electrospinning

Electrospinning is a fabrication method for producing scaffolds from various materials. It involves the application of an electric field to a solution of the polymer to generate a fine,

continuous nanofiber/or microfibre structure, and the technique is established for the fabrication of ultrafine fibres, making it ideal for the design of complex micro-structures (Forciniti, 2011; Barhoum et al., 2019; Mamidi et al., 2022). The fibres produced have a wide range of biomedical applications, including use in the guided tissue regeneration membrane (GTRM) of the periodontal ligament. GTRMs are used to improve wound healing and periodontal tissue regeneration by offering a physical barrier to prevent the penetration of unwanted cells while allowing access to the desired cells.

The general set up of electrospinning consists of a power supply, injection pump which delivers the polymer solution (contained in a syringe) and a conducting collector to collect the electrospun fibres (Figure 2.5). The polymer solution is passed through the syringe to the nozzle and within an electrical field the surface tension of the solution in the nozzle becomes unstable, which results in sudden jet spinning (Shin et al., 2012). This leads to the formation of the scaffolds which can be microfibres or nanofibers in an aligned or random configuration. As this basic set up can be modified to ensure that, the nanofibers produced to comply with the requirements of the scaffold. A major advantage of this process is that it is simple, fast and cost-efficient while it produces scaffolds that can provide physical indication and guide cell growth.

The strategy has achieved considerable attention among all methods to produce nanofibers/ or microfibres with high porosity and surface area, excellent pore architecture, and various chemical compositions. The unique properties of nanofibers have brought about novel advances in nanomedicine to create innovative fibre-based developments for biomedical use and healthcare (Asadian et al., 2020). The electrospinning process is simple and cost-effective, making it an attractive option for GTRM fabrication. Further, guided tissue regeneration (GTR) systems are a trending topic in the treatment of periodontitis, and their benefits include

inhibiting connective tissue from interfering in osteogenesis and cell growth, enhancing the healing process of degenerated periodontal ligaments and tissues, and inhibiting inflammation and bacterial infection (Mirzaeei et al., 2022). GTRMs are biocompatible and biodegradable materials that control tissue regeneration in periodontal tissues. They are composed of electrospun nanofibers produced from biodegradable polymers, such as poly-lactic-co-glycolic acid (PLGA) and polycaprolactone (PCL).

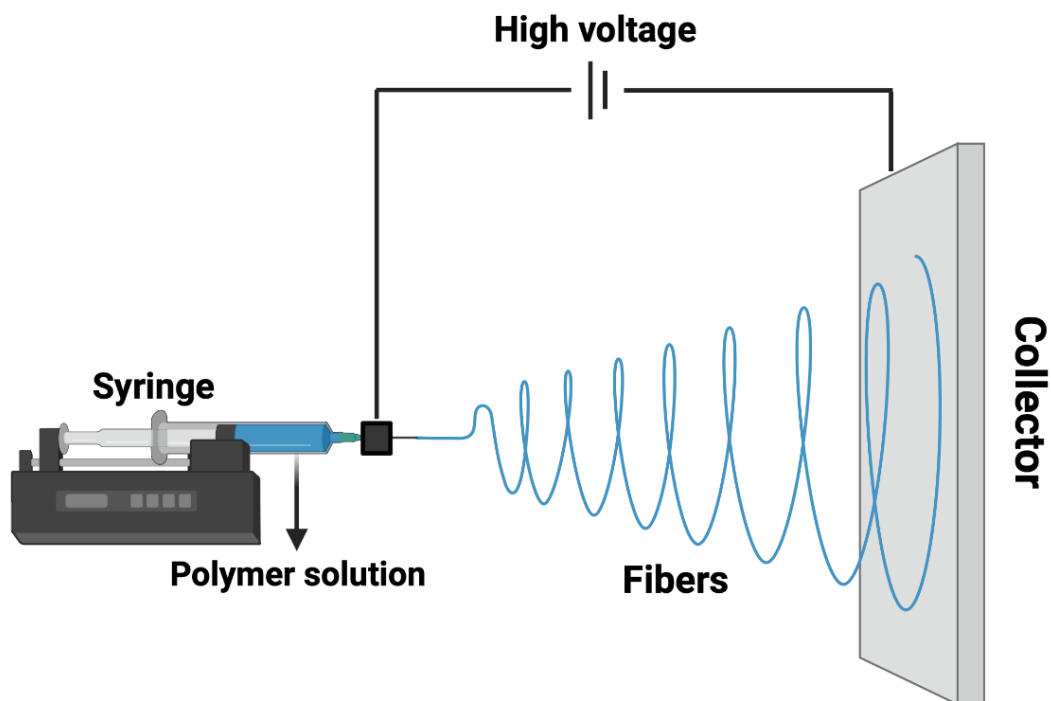


Figure 2.5 Schematic diagram of a basic horizontal electrospinning process.

Electrospun nanofibers are currently thought to be one of the best solutions for periodontal tissue engineering due to their similarities in size to the collagen fibres of the extracellular matrix (ECM) and the ability to control their nonporous structure, which can act like small blood vessels and would help support cell survival. The porosity of the electrospun nanofibers

scaffolds allows cells to exchange metabolites and nutrients while maintaining their original functionality, supporting tissue reconstruction and maintaining mechanical properties, preventing the wound bed from collapse and keeping the match between host tissues and scaffolds materials. The success of these nanofibers both in vitro and in vivo tests for the implantation of mesenchymal stem cells has been shown in animal studies (Kim et al., 2013). In addition, bone regeneration has also been supported by electrospun nanofibers of both synthetic and natural polymers (Seo et al., 2016).

Therefore, PLLA nanofibers scaffolds have been developed which have found applications in drug delivery, wound healing and in periodontics tissue engineering. A study by Woo et al. (2009) found that 3D PLLA nanofibers scaffolds were more effective than solid-walled PLLA scaffolds with equal porosity in promoting bone regeneration. This was thought to be due to the nanofiber scaffolds more closely mimicking the ECM and the morphology of type I collagen fibres. However, it has also been found that the mechanical stability of the nanofiber PLLA scaffolds decline with time and therefore, new bone formation is required to be produced rapidly to compensate for this (Schofer et al., 2011). Therefore, the osteogenic protein, BMP-2, has been incorporated in the PLLA nanofibers scaffolds to promote osteoblast differentiation and bone formation (Schofer et al., 2011).

Electrospinning of PCL has been used to create GTRM for periodontal ligament regeneration. They offer a 3D structure that supports and protects periodontal ligament stem cells, allowing them to differentiate into mature periodontal tissues (Safi et al., 2020; Yao et al., 2017). The electrospun PCL GTRM is biocompatible, biodegradable, and highly porous, allowing enhanced tissue ingrowth. Additionally, the micro- and nano-scale fibres of the PCL GTRM provide a high surface area for interactions between the periodontal ligament stem cells and the surrounding tissues, aiding in cell differentiation. The PCL GTRM prevents excessive

periodontal ligament scarring, impedes tissue regeneration, and effectively fosters damaged periodontal ligament regeneration in vivo.

Further, electrospinning of aligned PCL can be used to fabricate nanofibers to form the guided tissue regeneration membranes for the periodontal ligament (GTRMPL). The GTRMPL is a thin, flexible membrane that enables the regeneration and healing of periodontal tissue. The aligned PCL nanofiber membranes provide a scaffold for periodontal ligament cell growth and regeneration, allowing rapid healing of periodontal tissues (Bousnaki et al., 2022). They are highly porous, thus enabling the diffusion of nutrients and oxygen, and they provide a large surface area for cell adhesion, mechanical strength, and a 3-D structure for cell proliferation. The aligned PCL nanofiber membrane offers a favourable microenvironment for cell attachment, migration, and growth (Barhoum et al., 2019). That allows for faster tissue regeneration, resulting in better healing and sustainable outcomes. The alignment of the spun fibres is thought to guide the cells in forming tissues in defect directions. This is especially important for nerve and blood vessels development (Shin et al., 2012). For hard tissues like bone, this is also very important with the aligned fibres. As this shows, a higher tensile strength compared to the randomly aligned fibres (Subramanian et al., 2011).

Electrospinning creates a GTRM potentially for the periodontal ligament composed of electrospun nanofibers that provide a biocompatible and biodegradable matrix that allows tissue regeneration and mechanical support. The ability to customise the electrospun fibres to the desired specifications makes them highly versatile and essential for medical applications. Electrospun nanofibers have been used successfully to repair periodontal tissue damage.

2.11. Scaffold surface modification and biofunctionalization

Surface modification for electrospun scaffolds is essential to increase the biofunctionality of the membranes used for periodontal tissue regeneration. The surface of the electrospun scaffolds can further be biofunctionalised by technologies which modify their surfaces. Scaffolds biofunctionalisation have been shown to increase the cell attachment and wettability of the scaffolds. (Cipitrial et al., 2011).

There are different surface modification methods including protein adsorption, biomacromolecule immobilisation, mineral coating, functional group incorporation, and topographical modification (Richbourg et al., 2019). Their combination offers specific environments for targeted tissue development. Topographical modifications offer enhanced cell material interface, which increases tissue healing, cell anchorage improvements, and implant attachment (Metavarayuth et al., 2016). Protein adsorption is of great interest as it includes surface modification of implants either topographically or by surface chemistry (Roach et al., 2005). The mineral coating offers efficient and energy-saving separation for oil and water mixtures. It presents attractive applications for oil and water separation, and adding functional groups offers better composite files, which have improved barrier properties (Chen and Xu, 2013). The films exhibit enhanced antioxidant and antimicrobial activities.

Biomacromolecule immobilisation surface modifications stabilise enzyme molecules in applications (Tacias-Pascacio et al., 2019). The layer-by-layer assembly is significant for multi-layered nanocoating of scaffolds which offers alternating exposure of charged substrates (Rawtani and Agrawal, 2014). Heparin immobilisations are vital for improving surface modifications by enhancing vascular grafts from synthetic fibres to improve their bioactivity (Xu et al., 2020). Plasma treatments are vital for biomolecule immobilisations such as drugs

and proteins; for example, oxygen plasma is reproducible, bio-friendly, affordable, and does not affect the bulk chemical structure (Ghorban et al., 2020). The treatment presents enhanced biological characteristics and increased cell proliferation and attachment.

Plasma polymerization allows the introduction of different surface chemistries while leaving the surface topography of the scaffolds unchanged (Barry et al., 2005; Harding et al., 2012; Robinson et al., 2010). Therefore, modification of surfaces by plasma polymerisation of scaffolds with allylamine leaves the scaffold surfaces with an attached layer of charged amine groups. These surface amine groups can enhance cell adhesion (Barry et al., 2005). It has been shown that plasma deposition of allylamine throughout the 3D structure of PLLA scaffolds improves cell attachment and activity, thereby supporting the biofunctionality of the scaffold (Barry et al., 2005).

Glycosaminoglycans (GAGs), for example heparin, have also been bound to scaffolds to enhance cellular attachment, proliferation and differentiation (Harding et al., 2012). Heparin which has a similar structure to the sulphated regions of native heparan sulphate GAGs, is the most widely used due to its ability participate in various biological processes such as cellular proliferation, cell differentiation and tissue homeostasis as mentioned earlier (Mahoney et al., 2004). If scaffold surfaces are coated with bound amine groups, for example by plasma polymerization with allylamine, heparin can be bound to these surfaces via passive non-covalent absorption. Under these conditions the heparin still retains its functionality and ability to interact with heparin-binding proteins (Mahoney et al., 2004) such as various cytokines and growth factors. Therefore, heparin is proposed to be advantageous for use in periodontal tissue regeneration for its ability to bind growth factors and cytokines (Pomin and Mulloy, 2018). Therefore, coating allylamine-treated, electrospun scaffolds with heparin is a

potential way to make a biofunctionalised GTR membrane to improve the periodontal tissue regeneration properties of the scaffolds.

2.11.1. Plasma polymerisation of PLLA and PCL scaffolds

Regenerative medicine and tissue engineering rely on biomaterial scaffolds for cell adhesion, differentiation, and proliferation, chemically and physically, *in vitro* and *in vivo*. PLLA and PCL scaffold are aliphatic-based polyesters used commonly in tissue engineering.

Plasma polymerisation is a technique that makes it possible to deposit an ultra-thin cross-linked polymeric film on complex geometry surfaces whose chemical functions can be manipulated (Short et al., 2009). Plasma polymerisation is generally used in various applications to identify and characterise heparan sulphate (HS) proteins or heparin (Hp). The method facilitates analysing Hp-protein interactions using simple ELISA-like experiments and can be modified to be utilised in different methodologies. A suitable plasma (e.g. a plasma of allylamine) can be applied in various coatings in assay formats like plates, slides, materials such as polymers and glass, and beads (Mahoney et al., 2004). Further, it enhances the range of applications of biodegradable nanofibers when it is utilised to deposit stable thin films rich in amine (Manakhov et al., 2015).

The plasma polymerization processes involve ionizing the precursor molecules using high-energy electrons and ultraviolet radiation. The process leads to radicals that are very reactive and not stable which interact to develop bonds, deposit on substrates, and form surface coatings (Coad et al., 2022). Thus, the surface chemistry of the materials can be modified independently and not affect the treated material's bulk properties. Plasma may also break the substrate bonds, hence building the radicals that react with the precursor's radicals, acting as an anchor, improving the stability of the plasma polymerized coating. The method

encompasses major processes which are polymerization and ablation. Ablation removes the surface molecules, while polymerization entails the processes of monomer deposition on the surface. The two processes often compete; therefore, how they co-exist and interact in plasmas, is well documented but the technique is normally complex and versatile because different measurements, including the power discharge, the type of precursor, concentration, and the treatment time, affect the physical and chemical traits of the coating deposited. The dilution gas such as air, argon, nitrogen, and helium also determines the reactants formed, which equally affects the character of the coating (Aziz et al., 2018). When the pressure is reduced, a regime is obtained when the temperatures of the electrons are different from those of neutral atoms and ions and the plasma is known as cold or non-equilibrium. The environment results in much polymerisation among volatile organic compounds. Therefore, polymer contacting surfaces are coated and those downstream of discharge (Yasuda, 1985). The monomer is the organic molecule, and the deposit is the plasma polymer. Further, in low-power conditions, plasma polymers obtained retain a significant percentage of the original monomer chemistry. Decreasing the continuing power wave or performing pulse-like power off and off creates the low power concept (Fraser et al., 2002). During the plasma polymerisation processes, the species that are active fragments of monomer creating the radical may combine in the plasma and substrate's surface to create a cross-linked coating often known as the plasma polymer film.

Plasma films have been widely applied due to their vital qualities like good mechanical characteristics, nontoxic degradation substances, and manufacturing ease (Richbourg et al., 2019). For example, PLLA has been widely used in vivo for three-dimensional culture and dental surgery transplants due to its easy processing and biodegradable properties. There have been records of its use in open flap debridement as implants in intrabony defects, and

the treatments were successful (Chen et al., 2013). However, PLLA is hydrophobic and this property limits its use due to the difficulty of cell attaching to the scaffold. Since it is a good material for tissue regeneration, making it hydrophilic and improving its bioresponsivity is crucial.

The hydrophilic properties, however, are a hindrance to their applicability. PLC surface change with plasma polymerisation is a promising technique which makes it more successful in treatments. Plasma treatment refers to treating liquids with plasma transferred to cells or tissues (Weltmann and Von Woedtke, 2016). It is highly efficient in removing biological residues in implant surfaces (Yang et al., 2020) and very effective for long-lasting and high controlled surface modification like surface structuring to create antifouling surfaces, chemical functionalisation, coatings, and antimicrobial thin film depositions (Bazaka et al., 2011). Plasma deposition is also used in high surface nanostructures from various material sources, showing a high controlled level in cell and microorganisms attachment behaviour, hence offering a more selection tool (Bazaka et al., 2016).

According to Coad et al. (2022), the application of plasma polymerization requires cell attachment and adhesion to the synthetic material's surface, implant, or device to speed up metabolic activities without compromising the functionality of the cell. Critical examples are evident in laboratory glassware cell culture or in implants that need a tissue to be attached to the surface of the implant to attain bio-functional integration. Plasma polymer effectively supports the surface for attaching viable cells and tissues. A study exploring the improvement of internal cell colonization of porous scaffolds with chemical gradients produced by the plasma polymerization approach noted that plasma polymerization offers the perfect source for cell attachment (Sardella et al., 2017). Plasma polymerization using two component plasma has proven effective in forming hydrophilicity gradients and cell adhesion traits

outside through scaffolds capable of improving the quality and traits of colonization. In the biomedical field, polymers form compounds with heparin, which facilitates the calculation of concentration in the amino sites. Plasma treatment leads to heparin attachment that retards the coagulation of blood without preventing clot (Yasuda and Gazicki, 1982).

Further, in the study of Lanzalaco et al. (2020), plasma polymerisation resulted in more active chemical group surfaces, thus enabling cell adhesion. The features that prompted their conclusion were the cell adhesion to surfaces increasing when the mesh was heated at incubation temperatures of 37 °C and the availability of poly (N-isopropyl acrylamide) (PNIPAAm) chains on isotactic polypropylene iPP fibres, which enabled the adhesion of cells onto them. Asadian et al. (2019) found that a five-second exposure of plasma to the PCL structure, which deposited a thin coating of thiol-rich, significantly increased bone marrow stem cells' (BMSTs) adhesion. Thiol function inclusion by plasma polymerisation favours nanofibrous meshes response in cells resulting in a high potential for tissue engineering applications.

The study of Joseph et al. (2021) found that allylamine plasma-treated 3D printed PCL scaffolds improved hydrophilicity and mechanical properties, which suggest that the hydrophobicity of PCL, which inhibits their use in biological applications, can be overcome by the deposition of amine group. Furthermore, Kim et al. (2022) used amine plasma polymerisation modifications on 3D PCL scaffolds to investigate pre-osteoblast biological behaviours and surface characterisation. They were fabricated by fused deposition modelling (FDM) 3D printing, and the surfaces were modified by amine plasma-polymerisation using monomer allylamine (AA) and 1,2-diaminocyclohexane (DACH). That resulted in the improved proliferation and focal adhesion of pre-osteoblast and an increase in osteogenic differentiation.

Moreover, the technique can also impart chemical gradients in porous scaffolds such as PLLA to improve cell viability, unlike untreated surfaces (Wan et al., 2006). Plasma polymerisation of PLLA makes it an effective compatibilizing agent such as plasma poly (acrylic acid) (PAA) (Petisco-Ferrero et al., 2018). Park et al. (2021) experiment on plasma treatment of PCL showed that osteogenic differentiation and cell proliferation of the periodontal ligament stem cells were improved in the scaffolds coated with oxygen plasma and graphene oxide. Therefore, plasma treatment and graphene oxide coatings enhance cell proliferation and osteogenic differentiation.

2.11.2. Glycosaminoglycans (GAGs) with PLLA and PCL scaffolds

GAGs are the majority heteropolysaccharides in the body, also known as anionic mucopolysaccharides. They are polysaccharides which are long and unbranched with a disaccharide unit repeating. The unit contains modified sugars, glucosamine (Glc) or galactosamine (Gal) and a uranic acid like iduronate or glucuronate. GAGs are found in the side chains of proteoglycans and glycoproteins. The GAG side chains are covalently bonded to a protein core which is synthesised in the endoplasmic reticulum and modified post-translationally by the Golgi bodies. The GAG disaccharides are typically added as side chains to proteins to produce proteoglycans. They are a core component of the essential connective tissues. The GAG chains are formed through the covalent bonding of the relevant disaccharides. The GAGs are often categorized into two types that are homopolysaccharides and heteropolysaccharides. The homo portion is composed of a similar monosaccharide unit, while the heteropolysaccharide is made of several monosaccharide units. They have a molecular weight of 10- 100 kilodaltons (Mahoney et al., 2004). In the structure of GAGs is

the structural unit and linkage between the disaccharide's unit. The disaccharides unit can be categorized as non-sulphated GAGs such as hyaluronic acid. The second category are the sulphated GAGs, which include keratin sulphate, chondroitin sulphate, heparin sulphate, heparan sulphate and dermatan sulphate. These are molecules which are highly negatively charged with extended conformations, and which cause high viscosity to the solution containing them. They are located mainly on the extracellular matrix or the cell's surface. GAGs which are physiologically significant are heparin, heparan sulphate, hyaluronan, chondroitin sulphate, dermatan sulphate and keratan sulphate (Short et al., 2009).

GAGs' functions in the body are various and determined by their molecular structure. Historically their functions were only known to be as structural scaffolding and cell hydration (Casale and Crane, 2019). Raman et al. (2005) studies showed that GAGs play a central role in cell signalling, which modulates a huge number of biochemical processes like regulating cell proliferation and growth, wound repair, anticoagulation, and fostering cell adhesion. The GAG, heparin (Hp), is a well known immune mediator that is released from mast cells and has anticoagulant functions by activating serpins. Hp polysaccharide that is linear is a densely sulphated moiety of Heparan sulphate (HS) which is a GAG in the extracellular matrix that is ubiquitous and covalently bonded to proteoglycans and glycoproteins and contain disaccharides units that are repeating which contain L-iduronic acid or the epimer D-glucuronic acid and D-glucosamine either N-sulphated or N-acetylated (Mahoney et al., 2004). When bound with HS, chemokine growth factors enable hypotonic gradients to form, which drive leucocyte migration (Hub and Rot, 1998). The simplest form of GAG, the non-sulphated GAG, hyaluronan, has a different significance in the body, not limited to the signalling of activities during embryonic morphogenesis, wound healing, and healing the pulmonary and vascular diseases. Hyaluronic acid is also a lubricant in the synovial joint and essential for joint

movement, by reducing the friction that may affect the joints and musculoskeletal system in the body. Gandhi and Mancera (2008) noted that the hyaluronic acid (HA) influence on cancer progression had been documented, with evidence noting that the receptor HA, CD44, is presented on the surface of the cancer stem cells. The CD44/HA interaction aids leukocyte extravasation and rolling tissues. When the HA-binding membrane protein is applied, it induces focal adhesion and signals cytoskeletal changes that elevate cell mortality in the tumour progression.

The study of Liu et al. (2021) fabricated a novel hybrid bi-layer scaffold by utilising electrospun PCL nanofiber membrane and 3D printed PCL scaffolds. The study experiment was on manipulating their parameters and microstructures and conducting their biological assays in vivo and in vitro bone regeneration. Heparin-conjugated PCL membrane fostered L929 fibroblast proliferation and adhesion. In addition, Liu et al. (2020) prepared a novel bilayer fibrous membrane for guided tissue regeneration (GTR) by a two-stepped electrospinning process, surface conjugation with heparin, and subsequent crosslinking. The membrane bilayer had an upper layer PCL membrane for soft tissue regeneration and a lower layer PCL membrane for hard tissue regeneration. They found that the physical, chemical and biological characteristics were highly determined by heparin conjugation. The heparin-conjugated surface significantly improved the membrane's biological performance. Improved proliferation and adhesion of cells were discovered in fibrous membranes, which were heparin-conjugated. They also exhibited good histocompatibility and favoured degradability in vivo. Their study concluded that the bilayer scaffolds were promising in the regeneration of soft and hard tissues modulating cell response.

GAGs with PLLA are used efficiently for dental pulp tissue engineering (Goldberg, 2020). The biostability of natural polymers is improved by crosslinking them with GAGs and other

elements (Lin et al., 2019). GAGs on PLLA and PCL scaffolds up-regulate cell proliferation during tissue engineering. GAGs have cell recognisable moieties that offer microenvironments favourable for differentiation and cell proliferation (Zhou et al., 2020). Heparin is a core element of glycosaminoglycan that is crucial in the conjugation of PCL scaffolds. Cell adhesion is improved by heparin conjugation, allylamine for plasma deposition, and plasma polymerisation.

2.11.3. The effect of growth factors on HPDL seeded scaffolds

Growth factors are essential for regenerating the periodontal ligament, stimulating the healing process, and promoting the recruitment of cells. Mechanical force on HPDL cells induces the production of growth factors such as epidermal growth factor, which has been reported to increase the number of PDL cells (Ichioka et al., 2016). Thus, the growth factors may play a primary function in maintaining PDL homeostasis. Transforming growth factor-beta (TGF- β) prevents bone morphogenetic protein 2 (BMP2) from inducing early commitment into complex tissue-forming cells in PDL cells (Ko et al., 2020). Epidermal and nerve growth factors play primary functions in PDL maintenance (Yamawaki et al., 2010). TGF- β 3 has no adverse effects on the proliferation of HPDL and, in adequate proportions, promotes osteogenic differentiation and can be applied in alveolar bone repair (Li et al., 2019). TGF- β 1 induces inflammation in PDL stem cells.

2.11.3.1. TGF- β 1

Transforming Growth Factor Beta (TGF- β): TGF- β is a family of proteins involved in regulating cell growth and development. These proteins are involved in developing organs, tissue regeneration, and responses to injury. They also regulate the immune system and help fight

infections. TGF- β 1 increases gene expression in short-term treatments and upregulates methylation changes (Negreros et al., 2019). It fosters fibroblasts' transition into myofibroblasts, collagen synthesis acceleration, resulting in fibrosis. Thus, the growth factor and myofibroblasts are critical in fibrotic diseases, and myofibroblast suppression is an effective pharmacological treatment (Sano et al., 2020). It prevents skin fibrosis in human secondary lymphedema after cancer surgery, and TGF- β 1 is linked positively with triple negativity. TGF- β is primarily secreted by various cell types, including immune cells and fibroblasts, and it functions as both a paracrine and autocrine regulator. It plays a role in many biological processes, including cell differentiation, proliferation, migration, angiogenesis, and apoptosis. TGF- β binding requires two types of cell surface TGF- β receptors, type I and type II, both of which need to be present and to form an active dimer on binding TGF- β for the growth factor to have a biological action. Activation of the receptor dimer results in activating Smad proteins, a family of transcription factors regulating gene expression (Liu et al., 2022a). TGF- β is involved in various physiological processes, such as wound healing, inflammation, tissue remodelling, and cancer progression.

TGF- β 1 is a multifunction cytokine which belongs to a large family of growth and differentiation including TGF- β 2, TGF- β 3, Bone morphogenic proteins (BMPs), Growth Differentiation Factors (GDFs), Glial-derived neurotrophic factors (GDNFs), Activins, Inhibins, Nodal, Lefty, and Müllerian Inhibiting Substance (MIS). Members of this family are involved in diverse developmental and physiological processes. regulate the growth and differentiation of other cells; for example the development of organs, tissue regeneration, immune system regulation and responses to injury.

TG- β 1 has a role in angiogenesis, extracellular matrix synthesis, immune suppression, inhibiting cell growth, transformation, and apoptosis (Taipale and Keski-Oja, 1997). It

regulates the periodontal host response, which causes advanced progression of periodontal disease and causes exaggerated host response (Gürkan et al., 2006). TGF- β 1 has pleiotropic characteristics, which contain both inflammatory and anti-inflammatory properties in regulating inflammatory infiltrates. TGF- β 1 assists in the proliferation and early differentiation of Mesenchymal stem cells (MSCs) to tendon cells, osteoblasts, chondrocytes, and adipocytes (Li et al., 2019). TGF- β 1 stimulates tissue regeneration, which is abundant and extensive in the matrix and thus can be used in the fabrication and formation of complex tissues for clinical treatment use (Fan et al., 2019).

The effects of TGF- β 1 on cell behaviour is highly dependent on cell phenotype and cell differentiation.

The growth factor has been seen to promote a more ligamentous fibroblastic phenotype in PLLA scaffolds, and its impacts on the aligned fibres in HPDL provide an essential role in periodontal tissue engineering (Alotaibi, 2014). However, the study of Schander et al. (2010) shows a low expression of the growth factor in PLLA scaffolds than in others like poly(DL-lactide) which indicates that it works well in materials with large pore size. Evidence in PCL scaffolds suggests that TGF- β 1 contributes to osteogenic differentiation and secretion of other growth factors such as HIF-1 α , which promote bone regeneration and wound healing (Shi et al., 2021).

TGF- β 1 growth factor is used in conjunction with the GTRM to help speed up the process of healing and regeneration. MPDLSC treated with the growth factor show high amounts of mineral deposits in vitro and increased activity of ALP after osteogenic differentiation induction (Queiroz et al., 2023). It directs the cells to increase osteogenic differentiation and to mobilise stem cells from PDL. TGF- β -1 is critical in bone mineralisation and promotes osteoblast proliferation and differentiation (Koba et al., 2021). It increases RNA and bone

sialoprotein expression but does not impact cell proliferation. However, it significantly fosters HCEM cells' mineralisation and cell differentiation. TGF- β 1 bound to heparin blocks signal pathways such as those of cancer, thus developing anti-cancer agents (Ma et al., 2020). By blocking TGF- β 1, heparin potentially inhibits the growth and metastasis of cancer cells. McCaffrey et al. (1992) found that the growth factor bound to sulphated polysaccharide heparin and heparan sulphate (HS) had strong interactions, which is significant at pH and physiological ionic strength. The sulphate groups on heparin and HS are thought to interact with essential amino acid residues on TGF- β 1, forming a stable complex. The interaction between TGF- β 1 and heparin/HS is important in regulating the activity of TGF- β 1 in vivo.

2.11.3.2. TGF- β 3

TGF- β 3 growth factor stimulates the growth and repair of cells and tissues and are naturally occurring in the body, produced by the cells of the immune system, skin, and other organs. Which promotes osteogenic differentiation in HPDL stem cells (Li et al., 2019). TGF- β 3 has the potential for application to repair alveolar bone defects that are incomplete by inducing the endochondral formation of bones and complete remodelling of the bones. The growth factor has been utilised in vivo for cartilage repair, wound healing, and tissue regeneration (Sasaki et al., 2018). It is a small protein that aids in cell communication, and promotes matrix formation, maintenance of stem cell properties, and immunity. TGF- β 3 recruits MSCs to begin bone regeneration. When the growth factor is released controllably and autologous MSCs, it assists in reducing surgical trauma because of the local osteotomy. TGF- β 3 growth factors stimulates the production of collagen, a protein that assists in forming skin, tendons, and ligament structures, is involved in tissue repair and regeneration, and prevents the growth and repair of damaged tissues (Voleti et al., 2012). In addition, TGF- β 3 promotes new blood

vessel formation, which is vital for wound healing. It is found in the body's cells and tissues, allowing cells to grow, divide, and differentiate, and in organs such as the heart, lungs, and kidneys. For instance, TGF- β 3 is found in mesenchymal stem cells, platelets, and the brain produced by the hypothalamus during late foetal development. However, TGF- β 3 in common with many growth factors and cytokines can be synthetically produced in the laboratory for medical research and applications. Studies have shown TGF- β 3 may have potential for arthritis, tendon injuries, and wound healing (Cetik et al., 2022). TGF- β 3 is has been used in bone tissue engineering loaded on PCL scaffold for improvements in bone formation and blood vessels (Diomedea et al., 2018). Additionally, TGF- β 3 is used in high levels in cranial tissues when the skull matures, and suture patency and PCL scaffolds are applied for sustained cytokines expression in the long term due to craniofacial development (Aswin et al., 2018). Delivery of the factor to cells enhances ECM cartilage secretion such as glycosaminoglycan and collagen II. For instance, Research shows that the presence of TGF- β 3 enhances hyaline cartilage production in tissues than in its absence (Gonzalez-Fernandez et al., 2016). Thus TGF- β 3 provides advancements in bone formation in tissue engineering. More research is needed to determine its effectiveness in slowing aging and improving skin appearance. TGF-B3 is promising because of its discovered endogenic benefits; it positively affects Achilles' tendon mid-substance healing, and its nanoparticles enhance the remodelling process (Cetik et al., 2022; Roth et al., 2019). It promotes tenogenic differentiation and regeneration of tendons in vivo, and scaffolds aligned with TGF- β 3 have improved bioactivity. The growth factor is vital for the regeneration and differentiation of tendons. Further, TGF- β 3 preserved scaffold bioactivity; hence, applying the growth factor through absorption in decellularised tendon scaffolds is feasible (Roth et al., 2019). It is effective in tendon healing which is critical for clinical applications.

TGF- β 3 significantly reduces tissue fibrosis, where there is a need for more studies to be done on the impacts of TGF-beta 3 and tissue fibrosis to enable more understanding of the effects as it is poorly understood (Xue et al., 2019). The upregulation of the growth factor was found to cause the proliferation, collagen expression, and migration of human cardiac fibroblasts, which are significant contributors to fibrosis. TGF- β 3 promotes collagen cross-linking and the phenotypical shift, which inhibits fibrosis attributed to smad7 regulation. The growth factor is a potential therapeutic target for myocardial fibrosis post-MI.

The combination of TGF- β 3 growth factor and the guided tissue regeneration membrane of the periodontal ligament effectively promotes the periodontal tissue's healing and regeneration. It promoted corneal wound healing and inhibits fibrotic markers (Karamichos et al., 2014). Their alignment reduces inflammation, improves blood flow, and promotes tissue growth. TGF- β 3 foster osteogenic differentiation of hPDLSCs, which may include activating significant signalling pathways (Li et al., 2019). It can be applied in repairing incomplete alveolar bone defects. TGF- β 3 contains synergetic effects and increases collagen II expressions, which promotes chondrogenic differentiation of PDLSCs (Choi et al., 2013). It modulates fibrosis with TGF- β 1 and TGF- β 2 better to control injury response (Wilson, 2021). TGF- β 3 produces an improved non-fibrotic matrix, decreases the expression of Smad7, and enhances thrombospondin-1 expression in stimulated HCF (Guo et al., 2016). For example, it has significant non-fibrotic impacts on HCFs and rescues cellular and fibrotic matrix components.

TGF- β 3 bound with heparin increases rabbits' chondrogenic differentiation of mesenchymal stem cells in the thermo-reversible hydrogel. Park et al. (2008) found that the binding of TGF- β 3 with heparin optimised cartilage tissue formation, which was observed by the production of SOX9, Type II collagen, aggrecan, and the oligomeric cartilage matrix protein gene

expression. The rate of proliferation and production of specific ECM cartilage is greater in heparin n-bound TGF- β 3 than in its absence. The binding showed a long release time and stability, increased GAG content, showcasing increased potent to differentiated MSCs. Thus, heparin-binding TGF β 3 can be applied in neocartilage formation reconstruction.

2.11.3.3. Fibroblast Growth factor (FGF)

Fibroblast Growth Factor (FGF) is a family of proteins in human body tissues that functions in biological processes, including cell growth, differentiation, and survival, and is involved in developing the nervous system, cardiovascular system, and other tissues (Ornitz and Marie, 2015) and cover a family of FGF-1 TO FGF-23 (Mitchell et al., 2016). They stimulate angiogenesis, aiding in the formation of new blood vessels by stimulating the growth of endothelial cells, and are used to treat ischemia and wound healing by stimulating the growth of new tissue and cells. FGF encourages cells to migrate to areas of injury or inflammation, where they aid in healing and stimulate cell differentiation, allowing them to perform specialised cell functions. They stimulate cell growth, allowing them to divide and reproduce more quickly, and they promote wound healing by stimulating cell and blood vessel growth in the area. They are also involved in wound healing, cancer, and inflammation. FGF functions in cell proliferation by stimulating their growth and division and is also involved in the differentiation of cells by regulating the expression of genes (Sun et al., 2022). FGF helps to repair damaged tissue by stimulating the growth of new cells and tissue, and it also helps to regulate the immune system by stimulating the growth of immune cells. They have roles in healing cancer and inhibiting the growth of some cancer cells by blocking their access to growth factors and inflammation. FGF binds to receptors on the surface of cells and can stimulate the production of other proteins and molecules necessary for cell growth and

differentiation (Laestander & Engström, 2014). In addition, FGF receptors (FGFRs) have critical functions developmentally in adult cells, and their dysregulation has been implicated in various cancers such as lung adenocarcinoma, ovarian cancer, urothelial carcinoma, and hepatocellular carcinoma (Dai et al., 2019). They are potential drug targets for cancer therapy, and there has been the development of multiple small molecules which are being tried clinically. Some have been approved by the FDA, such as the pan-FGFR inhibitor erdafitinib (JNJ-42756493), for treating unresectable urothelial carcinoma (mUC). FGFR therapies are covalent small molecule inhibitors, non-selective, selective, and monoclonal antibodies against the receptors. However, cancer progression may exist hence the need for novel studies to facilitate the development of second-generation FGFR inhibitors (Krook et al., 2021).

FGFs can also inhibit the growth of some cancer cells by blocking their access to growth factors. They perform vital roles in suprabasal keratinocytes' morphogenesis and keratinocytes' differentiation. Its increased secretion results in the proliferation of fibroblasts in gingival hyperplasia (Saito et al., 1996). In addition, FGF increases epithelial cell proliferation and vascular smooth muscle cells, migration of epithelial cells, and tube formation in vitro.

Fibroblast Growth Factor-2 (FGF-2): FGF-2 is a potent growth factor that aids cell proliferation and differentiation (Mariz et al., 2019). It plays a role in angiogenesis and wound healing, forming new blood vessels from existing ones. It promotes cell vascularisation when loaded in fibres as it expresses immunohistochemical and angiogenesis (Zhang et al., 2021). When loaded on a scaffold, FGF-2 is a functional GBR membrane that fosters extraosseous blood vessel formation in repairing periodontal. Further, it improves the formation of bones during periodontal defects, as presented when combined with CO3Ap (Nagayasu-Tanaka et al.,

2023). The new bone replacement was accelerated by FGF-2, making scaffold replacement easier. FGF-2 maintains existing bone near the periodontal defect region, as seen in the beagle dog model of the one-wall periodontal defect. It induces new periodontal tissues whose maturation is the same as spontaneous healing; hence, FGF-2 can effectively promote periodontal regeneration in periodontal patients with severe bony defects. In vivo, it demonstrates angiogenesis (Pomin and Mulloy, 2015). Improved bone and cartilage regeneration have been shown in the release of FGF-2 from a negatively charged gelatin hydrogel or positively charged BMP-2. Further, FGF-2 seeded in PCL-PLLA scaffolds supports osteoblast differentiation and adhesion (Aswin et al., 2018). They bind in heparin molecules which stimulate the synthesis of RNA and DNA and the division of chondrocytes. The FGF factor has been widely used as a stimulant for bone healing (Lee and Shin, 2007). They are widely used in vascular tissue for the delivery of drugs, and due to their elastic properties, they have been applied in vascular regeneration loaded on PCL scaffolds (Jeong et al., 2005).

In addition, Fibroblast Growth Factor-7 (FGF-7): FGF-7 aids in forming new blood vessels, developing the nervous system, and healing wounds (Jameson et al., 2004). It is involved in the development and growth of epithelial cells.

Heparan sulphate can bind FGF from 1 to 100nm kd values (Rapraeger et al., 1994). The specific binding affinity depends on factors, including the specific type of FGF and heparin sulphate and experimental conditions used to measure the binding affinity. It has a high affinity for FGF and can isolate growth factors (Macri et al., 2007). The binding of the FGF to heparan sulphate helps to protect FGF from degradation and increases its bioavailability in the extracellular environment. Heparin also binds with FGF, which increases FGF and FGFR interaction (Ibrahimi et al., 2004). the interaction between FGF and heparan sulphate is vital

for regulating various cellular processes, such as cell growth, differentiation, and migration. Heparin increases FGFR-FGF lifetime, heparan sulphate plays a significant role, and the complex activates the signalling cascade. The binding increases the FGF-FGFR complex's lifetime by reducing the complex's dissociation rate, and Heparitinase releases basic FGF bound in the pericellular matrix (Sahni et al., 1998). The release of bFGF (FGF-2) by heparinase is not specific to the pericellular matrix, as heparin sulphate is found in other tissues and organs. The Endothelial cells, which are not damaged, release bFGF which is localised in the basement membrane by heparin. Fibrin-bound bFGF (FGF-2) is isolated in the cell microenvironment after release and production have stopped. It activates endothelial angiogenesis, mitogenesis, and cell migration. FGF-1 is not able to bind to fibrinogen or fibrin compared to bFGF. It binds to heparan sulphate proteoglycans (HSPGs) on the surface of many cell types and in the ECM.

2.12. Aim and Objectives

2.12.1. Aim

The overall aim of this study was the development of a “smart” bio-resorbable GTR to actively promote regeneration of the periodontal ligament. This aim will be carried out using the following objectives.

2.12.2. Objectives

- Fabrication of electrospun random fibres and aligned –fibre scaffolds of (PCL) or PLLA to reflect the parallel arrangement of collagen fibres in the native ligament. Random-fibre scaffolds were fabricated as control scaffolds.
- Culture of periodontal ligament cells on the scaffolds to determine basic cell biocompatibility and proliferation on the scaffolds.
- Comparison of electrospun PLLA and PCL scaffolds for potential use in periodontal tissue regeneration.
- Investigate cold plasma deposition of allylamine on the electrospun membranes and confirm coating by XPS.

- Determine binding of members of the heparin interactome family (e.g. heparin and heparan sulphates).
- Investigate use of heparin-binding growth factors and peptides that could be useful for periodontal tissue regeneration (e.g. TGF β family and FGF family).
- Determine the biocompatibility of human periodontal ligament cells on the biofunctionalised membranes.
- Determine the functionality of human periodontal ligament cells on the biofunctionalised membranes.

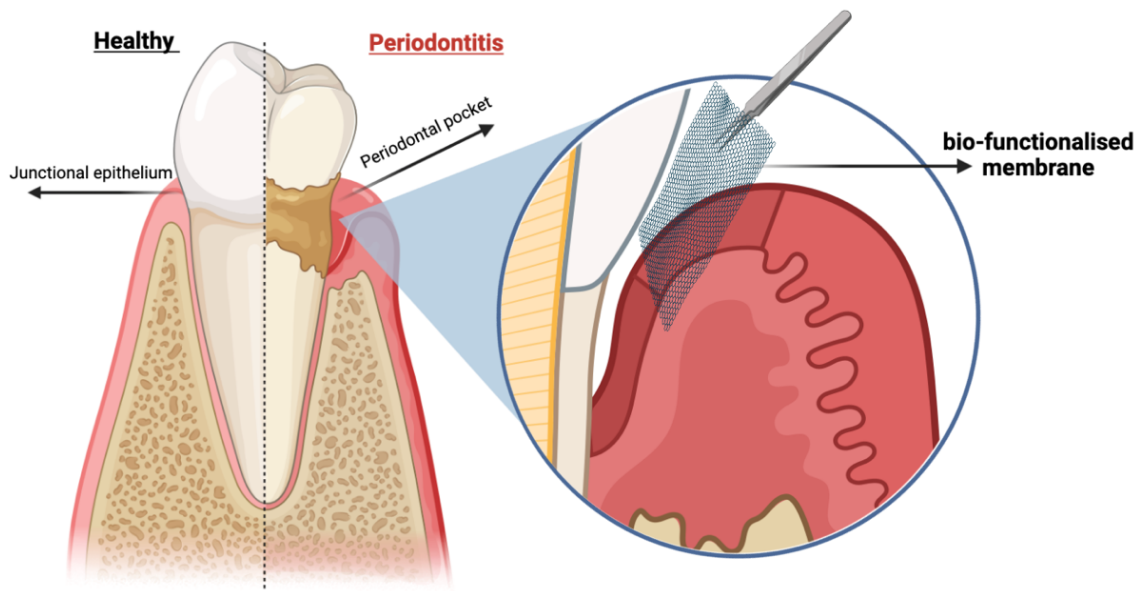


Figure 2.6 Representation of using the bio-functionalised membrane to promote the periodontal ligament regeneration.

3. Materials and methods

3.1. Materials

3.1.1. Polymers

Polymers	Lot number and Source
Poly (L-lactic acid) PLLA	Lot #BCBV6535, Sigma-Aldrich, Poole, UK
Poly (caprolactone) (PCL)	Lot #MKCB4025, Sigma-Aldrich, Poole, UK

Table 3.1 the polymers that been used in the electrospinning for scaffold fabrication.

3.1.2. Cells

Cells	Source/Supplier
Bovine ligament tissue	Isolated from the bovine tissues obtained from a local abattoir.
Human periodontal ligament cells	Sciencell Research Laboratories, USA

Table 3.2 ligament cells used in this study.

3.1.3. Media for cell culture

Media	Supplier
Dulbecco's Modified Eagle's Medium (DMEM) low glucose (1g/l) formula	Sigma-Aldrich, Poole, UK
Foetal calf serum (FCS)	Sigma-Aldrich, Poole, UK
0.025% Trypsin/ 0.02% EDTA in Hanks Balances Salt Solution with Phenol Red.	Sigma-Aldrich, Poole, UK

Ca ²⁺ /Mg ²⁺ free phosphate buffered saline (PBS)	Sigma-Aldrich, Poole, UK
L-Ascorbic acid powder.	Sigma-Aldrich, Poole, UK
Penicillin/ Streptomycin solution, (stabilised stock solution, with 50,000 U penicillin and 50,000 µg streptomycin/mL)	Sigma-Aldrich, Poole, UK
100x Non-essential amino acids (NEAA)	Sigma-Aldrich, Poole, UK
200mM L-Glutamine	Sigma-Aldrich, Poole, UK
ITS+3 Liquid Media Supplement (100x)	Sigma-Aldrich, Poole, UK

Table 3.3 list of media used for tissue cultural.

3.1.4. Reagent

Reagent	Supplier
Dichloromethane (DCM)	Fisher Scientific, Loughborough, UK
Dimethylformamide (DMF)	Fisher Scientific, Loughborough, UK
0.1 M sodium Cacodylate buffer, PH=7.4	Agar Scientific, Limited, Essex, UK
2% (vol/vol) aqueous osmium tetroxide	Agar Scientific, Limited, Essex, UK
2% (vol/vol) gluteraldehyde	Agar Scientific, Limited, Essex, UK
Hexamethyldisilazane (50%, 100% vol/vol)	Fisher Scientific, Loughborough, UK
PrestoBlue™ Cell Viability Reagent	ThermoFisher Scientific, UK, Loughborough, UK
Papain from papaya latex-lyophilised powder ≥ 10 units/mg protein	Sigma-Aldrich, Poole, UK
Ethylenediaminetetraacetic acid, EDTA	Sigma-Aldrich, Poole, UK

N-Acetyl-L-cysteine	Sigma-Aldrich, Poole, UK
Allylamine-98%	Sigma-Aldrich, Poole, UK
streptavidin-HRP for ELISA	R&D systems, Abingdon, UK
2N Sulfuric Acid	R&D systems, Abingdon, UK
Heparin, Fluorescein Conjugate	ThermoFisher Scientific UK.
Tris (hydroxymethyl) aminomethane	Sigma-Aldrich, Poole, UK
Hydrochloric acid 7.5 N	Fisher Scientific, UK
Magnesium chloride	UK Fisher Scientific, UK
Zinc chloride	UK Fisher Scientific, UK
Glycine	Fisher scientific, Loughborough, UK
Sodium Hydroxide	UK Fisher Scientific, UK
Harris Hematoxylin solution	(Shandon Scientific Limited, UK).
Eosin	(Shandon Scientific Limited, UK).
Nuclease-free water	ThermoFisher Scientific, Loughborough

Table 3.4 list of reagents used in this study.

3.1.5. Instruments and machines

Instruments and Machines	Manufactural details
Orbital shaker	Stuart, Scientific lab., UK
Electrospinning machine	Bioinicia SL, Valencia, Spain
Class II laminar flow cabinet	Walker Safety Cabinets Ltd, Glossep, UK
Centrifuge	Sanyo, Harrier 18/80
Sterile Pipettes (5ml, 10ml, 25ml)	Costar, USA

Incubator (Galaxy R plus CO2 incubator, 37 C)	Scientific laboratory Supplies, Nottingham
Cell strainers with 70 um pore size	BD Biosciences, Erembodegem, Belgium
Sterile syringe filters with 0.2 um pore size	Starsted, Germany
Adhesive carbon tabs and aluminium stubs	Agar Scientific Limited, Essex, UK
Gold Sputter Coater	Edwards S150B, UK
Infinite M200 PRO Series platereader	Tecan (UK), Reading, UK
Sterile syringe filters with 0.2 um pore size	Starsted, Germany
Heat block	Jencons-PLS, UK
vacuum pump	Edwards, Burgess hill, UK
AXIS Supra XPS	Kratos Analytical Ltd, UK
Dissection Scissors	SLS (Ireland) Ltd
Tweezers	SLS (Ireland) Ltd
Mini Mitutoyo micrometer	Mitutoyo, Aurora, IL, USA
Tensile testing machine Z3 X500	AML instrument, Lincoln, UK
Vice clamps	AML instrument, Lincoln, UK
KRUSS DSA100	Kruss, Germany
Biopsy Punch	Kai Europe GmbH, Germany
AutoPore IV 9500	Micromeritics Ltd, Bedfordshire, UK
Culture plates for cell culture (6-well, 12-well, 48-well and 96-well plates)	Greiner Bio-One GmbH, Austria
Cell Culture Flasks (T25 and T75 sizes)	Greiner Bio-One GmbH, Austria
Sterile syringe filters 0.2 um pore size	Starsted, Germany
infinite M200 PRO Series platereader	Tecan UK Ltd, Reading, UK

Microprocessor pH meter	Hanna Instruments, Inc, USA
Automated Leica TP1020 tissue processor	Leica Microsystems Nussloch GmbH, Germany
Microtome RM2145	Leica Microsystems Nussloch GmbH, Germany
Polysine®-coated glass slides	Thermo Fisher Scientific Loughborough, UK

Table 3.5 list of instruments and machines used in this study.

3.1.6. Assay Kits and ELISA's

Kits	Manufactural details
DNA Quantitation Kit, Fluorescence Assay	Sigma-Aldrich, Poole, UK
Human TGF-beta 1 DuoSet ELISA	R&D systems, Abingdon, UK
Human TGF-beta 3 DuoSet ELISA	R&D systems, Abingdon, UK
Human FGF basic/FGF2/bFGF DuoSet ELISA	R&D systems, Abingdon, UK
Quant-iT™ PicoGreen™ ds Assay Kit	ThermoFisher Scientific, UK
BCA Protein Assay Kit	Sigma-Aldrich, Poole, UK
Total collagen assay kit	Abcam, UK
Picro Sirius Red Stain Kit	Abcam, UK
Direct-zol™ RNA miniprep kit	Zymo Research Europe, Germany

Table 3.6 list of kits used in this study.

3.1.7. Miscellaneous

miscellaneous	Manufactural details
Isopropanol	Fisher scientific Loughborough, UK
Ethanol (50%,75%, 95%, 100% vol)	Fisher Scientific, Loughborough, UK

Agarose	Sigma-Aldrich, Poole, UK
Heparin	Iduron, Alderly Edge, UK
Low Molecular weight heparin	Iduron, Alderly eDge
Heparan sulphate	Iduron
Bovine Serum Albumin (BSA)	Sigma-Aldrich, Poole, UK
Recombinant Human TGF- β 1	Peprtech EC, Ltd, UK
Recombinant Human TGF- β 3	Peprtech EC, Ltd, UK
Recombinant human FGF-basic	Peprtech EC, Ltd, UK
Ethanol (50%, 75%, 95%, 100% vol/vol)	Agar Scientific Limited, Essex, UK
Agarose	Sigma-Aldrich, Poole, UK
Xylene	Fisher Scientific Loughborough, UK
p-Nitrophenyl phosphate	Sigma-aldrich, Poole, UK

Table 3.7 list of miscellaneous used in this study.

3.1.8. Software

Software	Programs
GraphPad Prism version (9.1)	Graph Software, CA, USA
Magellan TM Data Analysis Software	Tecan UK Ltd, Reading, UK
CasaXPS	Karatos Ultra, Kratos Analytical Ltd, UK
Drop Shape Analysis software	Kruss, Germany
Rotor-Gene Q Software	Qiagen, Germany
Biorender	Toronto, Canada

Table 3.8 list of software used in this study.

3.2. Methods

3.2.1. Viscosity measurement of electrospinning solution

The viscosity of PLA and PCL polymer solutions was measured by a rotational viscometer. An oscillation sweep method was applied using 25 mm parallel plate geometry at 25 °C. The tests were conducted with an angular frequency increased from 1 to 100 rad/s while maintaining a constant load of 1 Pa.

3.2.2. Scaffold fabrication

3.2.2.1. Electrospinning of random fibre PLLA scaffolds

Random PLLA fibres scaffolds were fabricated by electrospinning. A solution of 8% (wt/vol) poly (L-lactic acid) in dichloromethane was used. This solution was produced by mixing 0.4g of poly (L-lactic acid) in 4.6 g of dichloromethane (DCM) and stirring over 24 hours at room temperature. In a fume hood A 10 ml plastic syringe was used to draw up the polymer solution, which was nearly 2 ml. The syringe was placed in the pump of the Bioinicia electrospinning machine and attached so that the polymer in the syringe could be transferred to the needle. A solid metal collector covered with aluminium foil was used to collect the fibres and prevent damage to the electrospun scaffold when it was removed from the fibre-collecting plate. The distance between the tip of the needle and the collector was 20 cm

The parameters of the electrospinning were optimised to obtain the most appropriate electrospinning conditions. The polymer flow rate is dependent on the voltage rate. In these experiments, the electrical potential was 23 kV and the polymer flow rate was 2 ml/h. After fabrication, the PLLA scaffolds were air-dried in a fume hood overnight followed by wrapping in aluminium foil and storage with sachets of silica gel at 4°C in a refrigerator.

3.2.2.2. Electrospinning of random fibre PCL scaffolds

Random PCL fibre scaffolds were fabricated in the same manner as for the PLLA fibre scaffolds. The Bioinicia electrospinning rig was used. A co-solvent system of 90 wt% of DCM and 10 wt% of DMF was used. The solvent was prepared by mixing 13.9 g of DCM with 1.1 of DMF. A 10 wt % PCL solution was prepared by dissolving 1.5 g of PCL in 13.5 g of the mixing solvent. After stirring the polymer solution overnight, it placed in a 10 ml plastic syringe and placed in the pump of the electrospinning machine. The distance between the metal needle tip and the collector was set at 20 cm, which were the same conditions as those for electrospinning the PLLA scaffolds. The electrical potential and the polymer flow rate were 21kV and 3 ml/h respectively. After fabrication, the PCL electrospun scaffolds were air-dried in a fume hood overnight then wrapped in aluminium foil and stored with sachets of silica gel and stored at 4 °C in a refrigerator.

3.2.2.3. Electrospinning of aligned fibre PCL scaffold

The same concentration of PCL and solvent (8% in 90% DCM and 10% DMF) that was used for fabricating PCL random scaffolds was used for preparing aligned scaffolds. The same parameters of 21kV and 3 ml/h of polymer flow were used in the Bionicia electrospinning machine. To obtain aligned scaffolds the fibres were collected on a rotating drum. However, the Bionicia electrospinning broke down and had to be returned to the manufacturer for essential repairs. Therefore, electrospinning equipment in the Department of Engineering, University of Sheffield, had to be used to fabricate PCL aligned scaffolds initially using the same distance 20 cm of the collector from the needle tip and a flow rate 2 ml/h of the PCL polymer as were used for the Bionicia machine. However, a voltage of 15 kV was needed. At this point the practical work was first stopped completely and then seriously disrupted due

to COVID-19. This was due to National Lockdowns measures including University Closures. When the University of Sheffield re-opened the necessary COVID Regulations on safe, working practices meant much reduced laboratory occupancies and very limited access to the electrospinning machines in the Department of Engineering.

3.2.2.4. Commercial aligned fibre scaffolds

Due to the impact of COVID, an aligned fibre scaffold was commissioned from the Electrospinning Company. The scaffold fabrication was performed with the same solvent (90 wt% of DCM and 10 wt% of DMF) used in the random PCL scaffold. A tri-layer scaffold mat of aligned PCL was ordered from the Electrospinning Company. These layers provide stability to the scaffold during cutting and preparing. The morphology and the diameter of the fibres were examined the same way as the random fibre PLLA and PCL. Moreover, the thickness of the tri-layer scaffold mat was $393 \pm 18.5 \mu\text{m}$.

3.2.3. Scaffolds characterisation

3.2.3.1. Scanning electron microscopy (SEM) for scaffold only

For use in experiments, the scaffolds were removed from the refrigerator and allowed to reach room temperature. Samples of the scaffolds were cut out and stuck onto steel stubs using carbon tabs. An automatic sputter coater was used to gold-coat the scaffold. This process coated the surface of the scaffolds with a conductive layer of around 200 nm. Scanning electron microscopy imaging was taken for PLLA and PCL nanofibers scaffolds at 20 kV with a magnification of (x500, x1000) to examine the morphology of the scaffolds. The fibre diameters of the scaffold fibres were analysed using ImageJ software.

3.2.4. Cell culture and biological testing

3.2.4.1. Isolation and cell culture of bovine ligament cells

Initial experiments were done using ligament cells isolated from bovine ligaments as a substitute for the periodontal ligament. Isolation of cells for cell culture requires the acquisition of sterile ligament tissue which can be difficult to obtain from animal sources due to the bacterial loads of their oral environment. Previously, research by Dr. Dalal Alotaibi (Alotaibi et al., 2013) has shown that extraction of periodontal ligament from rat or porcine teeth yielded a high level of infected tissue.

Ligament tissue was isolated from the metacarpophalangeal joints of healthy bovines obtained from a commercial abattoir within 4h of slaughter for the human food chain. The joints were first cleaned with 1% Virkon followed by skinning. The skinned joints were disinfected with 1% Virkon followed by 70% ethanol and transferred into a laminar flow culture hood. All further steps were performed under sterile conditions. The joints were dissected and ligament tissue taken from the medial ligament and placed in PBS containing The ligament tissue was minced and digested overnight at 37 °C with 15 ml of 2 mg/ml of collagenase in DMEM containing 10% FCS. The digested tissue was passed through a 70 µm strainer into a new tube. The isolated ligament cells were pelleted by centrifugation (1000 rpm, 192 g for 10 min). The supernatant was removed and the cell pellet washed with PBS and the cells re-pelleted by centrifugation. This washing procedure was repeated and the final cell pellet was re-suspended in DMEM containing 10% FCS and the cell suspension transferred to a 25 cm flask. The culture flask of ligament cells was incubated at 37 °C in a humidified atmosphere of 95% air/5% CO₂. The culture medium was replaced every 3 days until the cells reached 90% confluence. The cell cultures were then passaged as described below in section (3.2.4.2).

3.2.4.2. Passaging of cultured bovine ligament cells

The culture medium was removed from the culture flasks and the cell layers were washed with PBS. 3 mL of 0.25% trypsin/0.02% EDTA was added to the flasks to detach the cells from the culture surface. The flask was incubated for 5 minutes at 37 °C and the degree of cell detachment checked using an inverted light microscope. The resultant cell suspension was transferred to a centrifuge tube and FBS added to give a 1-3% final concentration to inhibit the trypsin activity. The cell suspension was collected and the PDL cells were pelleted by centrifuged at 1000 rpm (192 g) for 10 minutes. The supernatant was removed and the cells were resuspended in DMEM containing 10% FBS. The cell suspension was then added to fresh culture flask with a seeding density of 1×10^6 cells/75cm². The flasks were labelled and placed in an incubator at 37 °C -in a humidified atmosphere of 95% air/5% CO₂.

3.2.4.3. Seeding bovine ligament cells onto scaffolds

6 mm diameter scaffolds were cut from the PLLA and PCL sheets using a biopsy punch. The scaffold discs were placed in a 6-well-plate (one scaffold/well). The scaffolds were sterilised by the addition 3 ml of isopropanol to each well and the scaffolds incubated in the isopropanol for 15 minutes in a class II culture hood. The isopropanol was then removed and each scaffolds washed twice with 5 ml of sterile distilled water for 5 minutes. The scaffolds were then washed 3 times with 5 ml of PBS. Next, fresh DMEM containing 10% serum (FBS) was added to each well and the scaffolds were transferred to an incubator.

A fresh 6 well-culture plate was coated with 1.5 ml of warm, sterile 2% agarose in PBS/well and allowed cool in a culture hood so that the agarose would gel. 4 ml of DMEM with 10% of serum was added to the agarose. Cultured ligament cells were harvested from culture plates and 1.30×10^6 cells added to each well containing a scaffold (5ml total volume/well). The 6-

well plates were incubated for 48h at 37°C on an orbital shaker (set at 60 rpm) to allow the cells to bind to the scaffold. After seeding, the seeded scaffolds were transferred to fresh agarose-coated wells and incubated at 37°C in the incubator for 3 weeks to enable an extracellular matrix to be deposited on the scaffolds. The cell-seeded scaffolds were cultured on an orbital shaker throughout the culture period.

3.2.4.4. Culture of human periodontal ligament cells (HPDLs) in monolayer culture

Human periodontal ligament cells (HPDLs) were purchased from Sciencell, USA. A vial containing 0.5×10^6 cells (1ml volume) was removed from liquid nitrogen storage and thawed in a water bath at 37°C. Once thawed DMEM containing 10% FBS was immediately added to the thawed cells. After mixing the cells were centrifuged at 1000, rpm (192 xg) for 5 min to pellet the HPDLs. After centrifugation, the supernatant was removed and the cell pellet gently resuspended in 6ml of culture medium. The cell suspension was then transferred to a culture flask (25 cm² growth area) which was placed in an incubator at 37 °C -in an atmosphere of 95% air/5% CO₂. The cells were grown to confluence with culture media changes every 3 days. When the cultures reached confluency of 80–90%, the HDPLs were passaged as described above and plated into T75 culture flasks.

3.2.4.5. Seeding human periodontal ligament cells (HPDLs) onto biofunctionalised scaffolds

Gently heated up the bottle of 2% agarose in the microwave and pipetted out the agarose into a fresh 6-well plate as described in section (3.2.4.3). Once the plates are ready, HPDL cells are removed from the cultured flasks by trypsinisation and pelleted using centrifuging for 5 minutes at 190 xg. Re-suspended in medium Dulbecco's Modified Eagle's Medium (1,000 mg/l

glucose), 100 units/ml penicillin, 100 µg/ml streptomycin, MEM nonessential amino acid and 5% FCS. Following, the cells are counted and $\approx 5 \times 10^5$ - 1×10^6 HPDL cells are added per each scaffold in a total volume of 2 ml of culture medium. The seeded scaffolds were then incubated for 48h at 37 °C on an orbital shaker at 65 rpm speed. After 48h, the seeded membranes were to a 12-well plate (scaffold/well) and cultured in the same medium used for seeding containing 1 mg/ml BSA, ITS (10 µg/ml, insulin 5.5 µg/ml transferrin, 0.5 µg/ml selenium and 4.7 µg/ml linoleic and oleic acids), 25 µg/ml L-ascorbic acid and one experiment without FCS and another one with 5% FCS. The plates are incubated at 37 °C on an orbital shaker at 40 rpm speed for 5 weeks with changing of the cultured medium every 3-4 days.

3.2.4.6. Cell termination

The scaffolds were prepared and seeded as described above in section (3.2.4.5). After seeding in 48 hours when the cells reach the confluency, they are terminated by washing them with PBS and then freezing them in the -20 °C freezer.

3.2.4.7. Measurement of cell viability of bovine ligament cells and human periodontal ligament cells (HPDLs) seeded on electrospun PLLA and PCL scaffolds using PrestoBlue™

The viability of the cell was measured using PrestoBlue™. It is a non-fluorescent blue dye, which is nontoxic. The active cells are reducing the resazurin dye during the experiment to fluorescent resorufin form and by measuring the fluorescence it can be detected.

The cell-seeded scaffolds were transferred to 24 well-plates with a total well volume of 1500 µl (150 µl PrestoBlue™ dye + 1350 µl of DMEM with 10% serum). The culture -plates were then incubated on the shaker for 1 hour at 37 °C then 150 µl samples were taken from each

well and transferred to 96 well-plates (twice to each well to give a total volume of 300 μ l). The 24 well-plates were placed again in the incubator and samples of the medium again transferred to 96-well plates after another hour. After all the scaffolds washed with PBS to remove the remaining PrestoBlue™ dye and the scaffolds moved back to the agarose coated 6 well-plates and culture medium was added. The amount of reduced dye was determined by measuring the fluorescence of the dye samples in a Tecan plate reader set at 560 nm excitation wavelength and 590 nm emission wavelength. Measurement of cell viability was repeated weekly for 3 weeks period with the bovine ligament cells and for 5 weeks with the (HPDLs) cells to monitor the viability of the seeded scaffolds and to determine rate of PrestoBlue™ conversion with time to determine if cell proliferation was occurring.

3.2.4.8. SEM imaging of cells

PLLA and PCL scaffolds were seeded with ligament cells and cultured for a week as described in section (3.2.4.3). After one week (day 7) the seeded scaffolds were soaked in 0.1M sodium cacodylate buffer and fixed in 2.5% glutaraldehyde buffer for 30 minutes. Later they washed with 0.1M buffer twice with 10 minutes intervals. The specimens then fixed in 2% aqueous osmium tetroxide for 30 minutes at room temperature. They were washed again in 0.1 M buffer, twice with 10-minute intervals. The scaffolds then dehydrated over a graded series of ethanol at room temperature (50, 75, 95, 100% vol/vol) each for 5 minutes. After they were placed in a 50/50 mixture of 100% ethanol 100% hexamethyldisilazane for 5 minutes and removed then followed by 5 minutes in 100% hexamethyldisilazane. The specimens then air-dried in the fume hood for 30 minutes. After drying, the scaffolds then mounted on aluminium stubs and attached with Carbon Sticky tabs and analysed by SEM as described in section (3.2.3.1).

3.2.4.9. Confocal imaging

The Live-Dead dyes were prepared as follows. 23 μL of DMSO was added to 50 μg of 5-chloromethylfluorescein diacetate (CMFDA) dye and shaken to ensure that the dye had dissolved completely. The dissolved CMFDA was added to a new tube and 23 ml of protein-free DMEM was added. A 79 μL of propidium iodide (PI) dye was then added the diluted CMFDA dye. This gave a final dye concentration of 10 μM CMFDA and 10 μM propidium iodide. Then the tube was shaken gently and wrapped with aluminium foil. The scaffolds were placed in 24 well-plates and washed with PBS. Then 2 ml of the diluted dye mixture was added to each scaffold. The scaffolds were incubated with the CMFDA and propidium dye for 1 hour at room temperature. After this incubation the dye was removed and the scaffolds were washed with PBS and each scaffold placed in a 5 ml tube and 2 ml of 10% neutral buffered formalin solution was added to each scaffold. The scaffolds in the buffered formalin were stored at 4°C for imaging by confocal microscopy.

3.2.4.10. DNA quantification assay using Hoescht reagent

After 21 days of culture the scaffold/cell constructs were taken and gently blotted with tissue to remove any excess culture medium, cut into 2 pieces and each piece transferred to a separate pre-weighed eppendorf tube. The samples were weighed and stored at -20 °C for assay. Before assay the scaffolds were incubated in 500 μl /sample of papain and n-acetyl cysteine in 20mM phosphate buffer containing 1mM EDTA (pH6.8) overnight in a heat block set at 60°C. After incubation, the samples were centrifuged to pellet scaffold debris. The papain solution was transferred to a new tube and stored at -20°C for assay. Measurement of DNA in the sample supernatants was carried out using a commercial DNA quantification kit (fluorescence assay) according to the manufacturer's instructions. 20 μL of the samples was

added to 200 μl of 0.1 $\mu\text{g}/\text{ml}$ bisBenzimide solution in a 96 well-plate. Using a Tecan plate reader, the amount of fluorescence of each sample was measured using an excitation wavelength of wavelength of 356 nm and an emission wavelength of 470 nm. Standard concentrations of DNA standard solutions were also determined to enable a standard curve to be calculated using the Excel program (Microsoft). The standard curve was used to calculate the DNA concentrations of the samples.

3.2.5. Surface modification and biofunctionalization of the scaffold mat

3.2.5.1. Cold plasma deposition of allylamine on the surface of scaffolds

Surface coating of both PLLA and PCL random fibre scaffolds by plasma polymerisation was carried out in a vacuum reactor chamber. Allylamine monomer was used for plasma deposition to generate thin films rich in amine on the scaffold surfaces. Samples of the electrospun scaffolds were placed inside the vessel. The flow of allylamine monomer was adjusted and the reactor chamber was evacuated to 8×10^{-3} mbar using a vacuum pump. The plasma was ignited using a radiofrequency generator and the plasma treatment was performed at a power of 30 W for 20 minutes.

3.2.5.2. Heparin coating

A heparin stock solution was prepared of 1 mg of heparin per ml PBS. The stock solution was stored at -20°C . To coat the pAAMscaffolds, a 20-fold dilution of the stock was made in PBS to give a heparin concentration of 50 $\mu\text{g}/\text{ml}$. 6mm diameter Control and pAAM scaffolds were sterilised as described in section (4.2.4.3) the sterilised scaffolds were transferred to a 48-well culture plate (one scaffold /well) and 200 μl of 50 $\mu\text{g}/\text{ml}$ of heparin in PBS was added to each pAAM scaffold. and added 200 $\mu\text{l}/\text{well}$ of PBS was added to each control scaffold (i.e., those

are not treated with allylamine). The lid was replaced on the culture plate of scaffolds and the plate with the lid was wrapped with aluminium foil and incubated overnight at 4 °C. After 24 hours, the PBS in the wells containing control scaffolds and the PBS containing the unbound heparin was removed. All scaffolds were then washed x3 with PBS.

3.2.5.3. X-ray photoelectron spectroscopy (XPS)

The detect allylamine bound to the pAAM-scaffold. 6 mm diameter scaffolds were cut from the PLLA and PCL random control sheets and allylamine coated random sheets using a punch. The samples were placed in 6 well-plate and labelled. Then they were sent to the Surface Analyses Centre in the Chemistry Department for XPS analysis. Kratos Ultra instrument with a monochromate aluminium source was used to carry out the analyses. Two areas per sample were analysed, each over an area of 700 by 300 microns. Survey scans were collected at 160 eV pass energy and 1 eV intervals between 1200 to 0 eV binding energy. Allylamine was detected by the presence of a nitrogen signal and heparin by a sulphur signal.

3.2.5.4. Heparin detection assay

The aligned plasma-treated scaffold was moved out of the fridge to cool down at room temperature. 6 mm membranes were punched out of control and plasma treated. They were sterilised with isopropanol for 15 minutes then it was removed and membranes were washed twice with sterile distilled water. Lastly, the membranes were washed 3 times with PBS. In a 48 well-plate, 200 µl of PBS or fluorescein-labelled heparin solutions in PBS containing (2.5, 5, 10, 20, 40) µg of the heparin were added to each scaffold. The plate was incubated overnight at 20 °C in the dark. After 24 hours, the unbound PBS and fluorescein-labelled heparin solution were removed from each well and transferred to a 96-well plate. The plate

was read in the plate reader to measure the fluorescence of unbound fluorescein-labelled heparin using excitation wavelength 490 nm and emission wavelength 486 nm. The scaffolds were washed 3 times with PBS and the PBS was removed. The fluorescein-heparin scaffolds were then photographed (using a camera phone).

3.2.6. Mechanical testing

The control group scaffolds and plasma-treated ones were removed from the fridge to cool down and reach room temperature. Samples were cut out to 40 mm x 6 mm length with scissors and peeled off the aluminium foil using tweezers. The thickness measured was checked for each sample using a mini Mitutoyo micrometre. Mechanical properties were obtained on a tensile testing machine (Z3 X500, AML Instruments, UK) with two load capacities (5N and 10N). Each sample was clamped using small vice clamps (TH140k, AML Instruments, UK) and pulled longitudinally at a rate of 4mm/min extension speed and 30 mm separation distance. The slope of the stress-strain curve was measured. The average of three samples of each group was used to calculate the tensile strength, elongation at break and young's modulus (stiffness).

3.2.7. Porosity testing

About 0.5 g of each scaffold type was prepared as requested by the engineering and has been sent to them. The Mercury Intrusion Porosimetry (MIP) technique was carried out to measure the pore size of the random PLLA and PCL scaffolds and the aligned PCL scaffolds.

Micromeritics AutoPore V 9620 porosimeter was used which has a maximum pressure output of 60000 psi and can estimate a theoretical pore width by assuming a contact angle of 130 and a mercury surface tension of 48510-3 N/m. The samples should be dry to be weighted

and then attached to the holders. The evacuation was turned on and the mercury was applied into the holder of the sample until it surrounds the sample. At first, the pressure applied to the mercury steadily increased from roughly 0.1 to 25 psi. 25 psi of pressure was then increased to 60000 psi. To provide the fundamental information for the investigation of pore structure, the mercury intrusion volumes and the accompanying applied pressures over four hours were collected at each pressure step. A mercury stem volume between 25% and 90% was sought after in all experiments to meet the manufacturer's suggestion.

3.2.8. Evaluation of hydrophobicity via measurement of water contact angle

A rectangular sample (1cm width and 3cm length) of each scaffold group (PLLA random, PCL random and PCL aligned) control and plasma-treated was cut out. The sessile drop technique was used to measure the WCA using an optical goniometer and a fine needle. The samples were mounted onto the holder. Each sample's surface had a 5 μ L drop of distilled water in 3 different areas.

3.2.9. Binding of growth factors to heparin immobilised on pAMM-PCL aligned scaffolds

Solutions containing 250 ng/ml of each growth factor (TGF- β 1, TGF- β 3 or FGF-2) were prepared in in PBS containing 1mg/ml BSA. 200 μ L of the 250 ng/ml of TGF- β 1, TGF- β 2 or FGF-2 was added to individual sterile, 6 mm diameter, heparin-functionalised scaffold. 200 μ l of PBS containing 1 mg/ml BSA was to the control samples (non-functionalised scaffolds) and to control pAAM samples (without heparin). The culture plate containing the scaffolds was sealed, covered with aluminium foil and incubated overnight at 4°C. After incubation, the PBS/BSA or the unbound growth factor solutions were removed from the samples and

washed 3 times with PBS containing 1mg/ml BSA. At this point, the membranes are ready for seeding.

3.2.10. Binding of growth factors to glycosaminoglycans (GAGs) immobilised in 96-well plates

The binding of the growth factors to the immobilised GAGs was carried out using an ELISA-based method. The detection antibodies and buffers and Strep-avidin solutions came from the R&D ELISA assays purchased from R&D Systems.

200 μ l of 50 μ g/ml solutions of heparin, or low molecular weight (LMW) heparin or heparan sulphate in PBS were added/well of a commercial, allylamine functionalised 96-well plate which was and the incubated overnight at room temperature. Each well contained 10 μ g of either heparin, LMW heparin or heparan sulphate. The next day, the unbound GAGs were removed and the wells were washed 3 times with PBS. The assay plate was then blocked to prevent non-specific binding by adding 300 μ l of PBS containing 5 mg/ml ELISA grade BSA to each well and incubating the plate at room temperature for 1.75 hours. The blocking buffer was removed and the wells washed 3 times with PBS containing 0.05% Tween 20. After the final PBS wash the assay plates were again drained of their contents and 200 μ l of each growth factor was added per well to give 50ng/well each of (TGF- β 1, or TGF- β 3 or FGF-2). The plate was incubated at room temperature for 4 hours. After which, it was drained of the growth factors and washed another 3 times in 400 μ l of PBS/0.05% Tween 20. A 200 μ l of a detection antibody specific to each individual growth factor was added and the assay plate was sealed and incubated overnight at 4 °C. After incubation, the assay plate contents were aspirated and the plate washed 3 times with PBS/0.05% Tween 20. Streptavidin-HRP from the ELISA kits for the individual growth factors were diluted according to the manufacturer's instructions

for the relevant ELISA assays. 200 μ l of the pertinent streptavidin-HRP was added in each well for each growth factor. The assay plate was then sealed and incubated in the dark for 20 minutes at room temperature. When the incubation time had lapsed, the assay plates were again washed 3 times with PBS/0.05% Tween 20. After the final wash, 200 μ l of the HRP substrate solution was added to each well. The assay plate was again sealed and incubated in dark avoiding any direct contact with light for 20 minutes; after which, 50 μ l of 2N Sulfuric Acid was added to each well. The optical density was measured immediately by a TECAN Infinite M200 plate reader at 405 nm.

3.2.11. Sandwich ELISA to measure the binding of growth factors to plasma treated aligned PCL scaffold and the elution of the growth factors from the scaffold

The aligned scaffolds were taken out of the fridge and allowed to warm up at room temperature. They have been cut to 6 mm diameter using a biopsy punch and then sterilised and coated with heparin and one of the growth factors (TGF- β 1, TGF- β 3 and FGF-2) as described in section (3.2.5.2 and 3.2.9). The unbound growth factor, the three washes of them and added PBS/BSA were collected daily and stored in a -80 freezer until day 14. ELISA analysis was carried out using commercial DuoSet ELISA (Human TGF- β 1, Human TGF- β 3 and Human FGF basic/FGF2/bFGF) kits. The capture antibody was diluted to the working concentration by PBS of each growth factor and coat a 96-well plate coated with 100 μ l per well. The plate was then sealed with a sealer and incubated at room temperature overnight. The next day, each well in the plate was aspirated and washed using 400 μ l of wash buffer 3 times. 300 μ l of Reagent Diluent was added to each well to block the plate. The plate is sealed and incubated at room temperature for 90 minutes. while incubating the plate, the samples were thawed and placed on ice.

The Reagent Diluent was used to dilute the samples to make sure they would fit within the sensitivity of the calibration curve. The standard curve samples were prepared as described in the kit. Following 90 minutes, the aspirated and washed steps were repeated 3 times. A 100 µl of each sample and standard curve samples were pipetted into the wells in duplicate. The plate was sealed with an adhesive strip and incubated for 2 hours at room temperature. Repeated the aspirated and washed step 3 times as before. The detection antibody was diluted in Reagent Diluent to the working concentration and a 100 µl was added to each well. Plate sealed and incubated at room temperature for 2 hours. The plate was aspirated and washed 3 times as mentioned before. A working dilution of streptavidin-HRP was added to each well in a volume of 100 µl. Covered the plate and incubated, avoiding direct light for 20 minutes at room temperature. A last aspirated and washed was applied in this step, followed by adding 100 µl in each well of substrate solution. Again, avoiding direct light, the plate was incubated for another 20 minutes at room temperature. Lastly, a 50 µl of stop solution was added to the plate. Carefully tap the plate from the side to make sure it has been a mix. The optical density of the plate was determined using a Tecan plate reader set to absorbance at 450 nm and wavelength correction set to 540 nm. Absorbance log readings of the standard curve were plotted on Graphpad prism 9.1 and a final concentration of the growth factor release was achieved by interpolated absorbance sample readings using a four-parameter logistic (4-PL) curve-fit.

3.2.12. Biological testing of biofunctionalised HPDLs seeded PLLA and PCL scaffolds

3.2.12.1. Biofunctionalised scaffolds digestion

At the beginning preparing an x20 stock of lysis Buffer (i.e. 200ml of 200 mM Tris-HCL buffer pH 7.5 containing 20 mM EDTA):

Weigh out 4.844g Tris Base [Tris(hydroxymethyl)aminomethane] and 1.6648 g of EDTA. They were placed in a glass beaker with 120ml of distilled water. The glass beaker was placed on a stirrer with a stirrer bar and gently stir the solution until the Tris and EDTA are dissolved. After mixing, added 1M HCL using a pipette to bring the pH down to 7.5. While adding the HCL I monitored the pH with the pH meter. When a pH of 7.5 is reached, the buffer is poured into a measuring cylinder and added distilled water until the total volume of the buffer is 200ml. Closed the cylinder tightly and stored it in the fridge at 40 °C.

At each time point, the stock lysis buffer is diluted to the required dilution. The samples were taken out of the freezer and transferred to an Eppendorf tube individually with 800 µl of TE lysis buffer. The samples then freeze and thaw with the lysis buffer in three cycles. Each cycle consisted of 2 hours in a -80 °C freezer followed by thawing at room temperature for about 30 minutes. The lysed cell solution was removed from each sample and transferred to a 1.5 ml new Eppendorf tube. At this point, samples for an alkaline phosphatase assay should be taken and assessed directly. The rest samples were centrifuged at 10.000 g for 5 minutes. The supernatants were removed from the new Eppendorfs tube and stored at -80 °C. The samples are ready at this stage for DNA, protein and collagen assay.

3.2.12.2. DNA PicoGreen assay

This assay measured the DNA quantity within each sample by specific binding of the dye to double standard DNA in the sample. When bound the dye can fluoresce and measurement of the fluorescence is a measure of the amount of double stranded DNA. The -80 °C lysate of the samples was thawed. Then prepared the appropriate amount of Tris –HCL/EDTA, (T/E) solution was prepared by diluting down the kit 20x TE buffer (200 mM Tris-HCl, 20 mM EDTA, pH 7.5) at 1:20 with distilled water. Made up the DNA standard curve using the table below

and kept it in ice during the assay. Added 50 μ l of distilled water in each well with 50 μ l of each sample to 96 well plates in triplicate. Placed 100 μ l of DNA standard curve solutions that were made in separate wells in triplicate. At this point, the PicoGreen dye solution was diluted 1:200 with TE solution and wrapped in foil. 100 μ l of PG dye reagent was added to each well (the tested samples and standard curve samples) using a multi-pipette. The plate was wrapped in foil and incubated at room temperature for 5 minutes. The fluorescence of the plate was measured by the Tecan plate reader at an excitation wavelength of 485 nm and an emission wavelength of 528. The standard curve reading was plotted against their known concentrations to convert the fluorescence units into DNA content.

3.2.12.3. Total protein assay (BCA)

Total protein was measured in the cell lysates of cell/scaffold constructs stored at 80°C after completion of their incubation times. The lysed cell/scaffold construct extracts were taken out of the -80 °C freezer and thawed at room temperature. Bichinoic acid (BCA) protein assay kit was used (Smith et al., 1985) to measure protein concentration of the cell/scaffold extracts. The working reagent was prepared by mixing reagent A with reagent B in a 1:50 ratio. 10 μ l of the lysed cell solution of each sample was aliquoted in triplicate in 96 well plates. A standard curve was also prepared with known concentrations as suggested in the kit at 0, 0.125, 0.25, 0.5, 1 and 2 mg/ml. 200 μ l of working reagent was then added to each well in the plate including the standard curve. The assay plate was wrapped with foil and incubated it 37 °C or 30 minutes. After incubation, a Tecan plate reader was used to measure the optical density of each sample at a wavelength of 570 nm. The absorbance of each sample was applied in the standard curve equation and the outcome was multiplied by the dilution factor. This gave the protein concentration of the samples. A reference standard curve was made by

plotting the absorbance of diluted six serially protein standards for known concentrations (0, 0.125, 0.25, 0.5, 1 and 2 mg/ml). The absorbance of the samples was used to generate the standard curve's equation, which was then multiplied by the dilution factor to determine the protein concentration in the samples.

3.2.12.4. Alkaline phosphatase assay

A 50 mM glycine -NaOH buffer at pH 9.5 containing 1 mM magnesium chloride and 1 mM zinc chloride was prepared.

Standard curve of known concentrations of p-nitrophenol standard was made. Diluted down the standard solution of pNP (10 mM) 1:10 in the glycine -NaOH buffer to get a concentration of 1 mM. The stock standard of 1 mM pNP equals 1 μ mole/ml. Serial dilutions in glycine - NaOH buffers were made to produce a range of concentrations: 0, 0.25, 0.5, 1, 2.5, 5, 10, 25, 50, and 100 nmole/ml. A 140 μ l of each standard was added in 96 well plates in triplicate. P-nitrophenol phosphate (pNPP) substrate was prepared by dissolving 25.9 mg in 2.327 μ l of glycine -NaOH buffer. This will give us 30 mM of substrate solution. This was diluted down 1:10 in glycine -NaOH buffer to get a substrate concentration of 3 mM. This was wrapped in foil and prepared fresh each time. At this point, the lysed samples are taken out of the freezer to thaw at room temperature and then store in ice. Placed 40 μ l of each sample in the same 96 well plates of the standard curve in triplicate. Followed, added 100 μ l of 3 mM substrate solution to each sample well using a multi pipette and wrapped in foil. The 96 well plate was incubated at 37°C in an incubator for about 1.30 hours and monitored for any colour change. After 1.30 hours, a 60 μ l of the stop solution (NaOH) was added to stop the reaction. The

absorbance was measured at 405 nm on the Tecan plate reader. The standard curve was plotted to convert the optical density (OD) into the PnP concentration.

3.2.12.5. Measurement of total collagen

The assay is based on measuring the cell/scaffold construct were transferred to pressure-tight, screw-capped polypropylene vials. A 100 μ l of 10 N concentrated NaOH was added to each vial and tightened the cap securely. Prepared the standard stock by transferring 50 μ l of Collagen 1 standard stock provided with the kit to a pressure-tight, screw-capped polypropylene vial. A 50 μ l of 10 N concentrated NaOH was added to the standard stock and the tightened the cap securely. Then placed all the scaffold samples vials and the standard stock vial in the heat block to alkaline hydrolyzed at 120 °C for 1 hour. Followed hydrolysed and moved all the vials into ice to allow them to cool down briefly before opening. When the vials cooled, the caps were opened to add 100 μ l of 10 N concentrated HCL to the scaffold samples. This is to make sure the residual NaOH is neutralized. While for the standard stock vial was neutralized by adding 50 μ l of 10 N concentrated HCL. All the vials were then centrifuged at 10.000 xg for 5 minutes. Using a pipette to collect supernatant and transfer it to a new propylene tube. Whilst, the final total volume of the standard will be~ 150 μ l with a final concentration of 1 mg/ml hydrolyzed collagen. Prepared the standard curve dilutions as described in the kit to get the final concentrations: 0, 2, 4, 6, 8, and 10 μ g of collagen 1. Added 10 μ l of each standard in 96 well plates in duplicate and 10 μ l of each experimental sample in duplicate as well. Placed the 96 well plates on the heat block at 65 c to evaporate them. During this time the Oxidation master mix is prepared as described in the kit. Following the evaporation, 100 μ l of the Oxidation mix was added to all the wells and gently shaken on the plate to make sure that the crystals have been dissolved then incubate on the plate for 20 minutes at room temperature. After 20 minutes, added 50 μ l of the developer to each

standard and sample well and incubate for 5 minutes at 37 c. Lastly, added 50 µl of DMAB concentrate solution was to each well again and ensure it had been mixed well. The plate was then sealed with microplate sealer film and incubated for 45 minutes on a heat block at 65 °C. When the plate is ready, the film is removed and the plate is placed in the Tecan reader to measure the absorbance at OD 560 nm.

3.2.12.6. Histological analysis of tissue engineered

After 5 weeks of seeding, one-half of the samples were fixed in 10% formalin and stored in the fridge ready for histological evaluation. Each fixed scaffold was placed inside a labelled plastic cassette which is then placed in a basket. The basket is then placed in the tissue processor and the appropriate program is then selected. After pressing start the machine will move the basket into each bath, where the samples are submerged in different baths of ethanol to dehydrate then xylene and lastly immersed in melted wax. The procedure is carried out using an automated Leica TP1020 tissue processor, where the cycle takes up to 18 hours. Once the cycle of the tissue processor is completed, the samples were transferred and emptied into the tissue embedder. The suitable metal mould size is selected, the scaffold is placed vertically into the mould and molten paraffin wax is then added to the mould. The labelled cassette is then placed on top of the wax and all of the samples are left on a cool surface, which allows the molten wax to cool down and solidify. After a while, the blocks of the samples are ready for sectioning. A 5 µm thickness specimen was sectioned using a microtome RM2145 (Leica, UK) and mounted on Polysine® glass slides (Thermo Scientific, UK). Dried out in the 60c oven for around 45 minutes before staining.

-Staining with hematoxylin and eosin (H&E):

Since the slides are completely dry, an automatic analysis staining machine was used. First, samples are dewaxed in xylene for 5 minutes followed by hydration gradually in different percentages in ethanol for 3 minutes each. Then samples were washed with distilled water for 1 minute followed by 3 washes of 2 minutes each in Harris Hematoxylin solution. Then another 3 washes of 2 min stain with Eosin Y. A dehydration procedure pursued by 3 washes of 1 minute of ethanol and 2 washes of 2 minutes xylene. Once the staining is done, the slides are left to air dry inside a fume hood for nearly 1 minute and then mounted using DPX. Lastly, covered with glass coverslips. The samples were then examined under a light microscope (Motic DM-B1) at different magnifications by the live imaging module software (Motic 2.0).

3.2.12.7. Picro Sirius red imaging

Once the samples completely dry after being in the oven, they were collected and placed in the slides staining rack. Staining the slides following the Picro Sirius Red Stain Kit protocol. Starting with the same dewaxing and hydration steps of the H&E staining, then lined up the slides on a flat surface. Applied the Picro Sirius Red Solution using a pipette and make sure to cover the tissue section completely and incubate the slides for an hour. Later, wash the slides quickly in 2 changes of (0.5%) Acetic Acid solution. Followed by the same dehydration steps of the H&E staining and mounting.

3.2.13. Quantitative PCR

- Scaffolds seeded with HPDL cells protocol:

When the cells were ready for seeding three groups of scaffolds were prepared as mentioned in section (3.2.4.5). 12 control PCL-aligned scaffolds, 12 Plasma treated PCL-aligned scaffolds

and 12 plasma/heparin /TGF-beta 3 treated PCL-aligned scaffolds. After centrifuging the cells, the supernatant was discarded and the pellet was resuspended in fresh medium and then counted using a haemocytometer. Following, about $\approx 8 \times 10^5$ HPDL cells were seeded in each scaffold in agarose-coated 6 well plates. The same cell number was seeded on each scaffold added in three polypropylene Eppendorf tubes and centrifuged to pellet the cells. The supernatants were removed from the tubes and the cell pellets were snap-frozen in liquid nitrogen for a couple of minutes then immediately transferred and stored in a -80°C freezer. This will give the time 0-time point to check if the 2D cells produce any collagen 1 mRNA. The scaffolds will be seeded as normal for 48 hours and then transformed into 12 well plates for 8 days.

- RNA extraction.

The RNA was isolated from the HPDL cells on the scaffolds on day 0, immediately after seeding, one day after seeding, 4 days after seeding and 7 days after seeding. This is done in three repeats at each time point. The scaffolds were grouped for each scaffold group to increase the RNA yield.

Direct-zol™ RNA miniprep kit (Zymo Research, USA) was used to extract the RNA. The scaffolds were washed with PBS and dried gently with tissue from the side for a total medium removal which could prevent cell lysis. A 450 μl of TRI Reagent® was used to dissolve three grouped scaffolds and lyse the cells in a polypropylene Eppendorf tube. An exact amount of 100% ethanol was then added to the TRI Reagent® and mixed well. Transferred the samples to a Zymo-Spin™ IICR Column and gently closed the lid. The columns were centrifuged at 16,000 x g for 30 seconds with the flow-through discarded. The tube was then filled with RNA wash buffer and centrifuged as before and the flow-through again was discarded. 75 μl of

DNA digestion buffer mixed with 5 μl of DNase 1 (6 U/ μl) and added to the tube. incubated the samples at room temperature for 15 minutes and washed them using 400 μl of Direct-Zol™ RNA Prewash twice. Lastly, a 700 μl of RNA wash buffer was added and re-centrifuged for 1-minute. A 10 μl of DNase/RNase-Free water was added finally to elute the mRNA and re-centrifuged for 1-minute again.

The mRNA concentration and purity were determined using Nanodrop Spectrophotometer (Thermo Scientific, USA). The quantities of mRNA were established. The samples were labelled properly and carefully then stored at $-80\text{ }^{\circ}\text{C}$ freezer until required.

- cDNA conversion:

A 236 ng/ μl RNA concentration was used for cDNA conversion with nuclease-free water (Invitrogen, UK). The cDNA conversion was carried out using 10 μl of RNA sample added to 2 μl random primers, 2 μl RT buffer, 1 μl multiscribe enzyme, 0.8 μl of dNTPs and 4.2 μl of nuclease-free water. Make sure all the reagents are mixed probably in the PCR tube (VWR, USA) then the tubes are placed into a thermal cycle AB 2720 program (Applied Biosystems, UK) for 10:00 at $25\text{ }^{\circ}\text{C}$, 120:00 at $37\text{ }^{\circ}\text{C}$, 5:00 at $85\text{ }^{\circ}\text{C}$. Once the cDNA was acquired it can be used straight away for qPCR or stored at $-80\text{ }^{\circ}\text{C}$ until required.

- qPCR:

Col1A1 extracellular matrix coding gene mRNA expression levels were measured using TaqMan® gene expression assays (Thermo Fischer Scientific, USA). Each experimental strip tube for the qPCR contains 5 μl of the qPCRBIO probe blue mix, 0.5 μl B2M control mix, 0.5 μl TaqMan® target gene probe, and 3 μl nuclease-free water. The profile cycling was applied for the real-time PCR (qPCR) was the two-step cycling. It started at $95\text{ }^{\circ}\text{C}$ with a 10-minute hold then dropped down to $60\text{ }^{\circ}\text{C}$ with 40 Cycles of 45 seconds each. Followed by 10 seconds at 95

°C. The Green cycle excitation was 470 nm \pm 10 and detection was 510 nm \pm 5. While the Yellow cycle excitation was 530 nm \pm 5 and detection was 557 nm \pm 5. A Rotor-Gene Q Software was used to detect the fluorescence with a gain of 5.

3.2.14. Statistical analysis

Data were plotted as the mean \pm standard deviation (SD) from three separate experiments runs in triplicate. One-way and two-way analyses of variance ANOVA were performed followed by a comparison of Tukey's multiple tests. Student's t-test was utilized for pair-wise comparisons. GraphPad Prism software (version 9.1) was used to utilise the statistical analyses where the p-value is considered to be significant if it is <0.05 .

4. Results

4.1. Optimisation and characterization study for initial polymer selection: PLA Vs PCL

4.1.1. Fabrication of electrospun scaffolds

4.1.1.1. Electrospun random fibre scaffolds

It was found that using 3 ml of the PLLA solution gave a really thin mat which made it too difficult to handle. A minimum volume of 9 ml of the 8% (wt vol) PLLA solution was needed to electrospin a PLLA mat that was handleable.

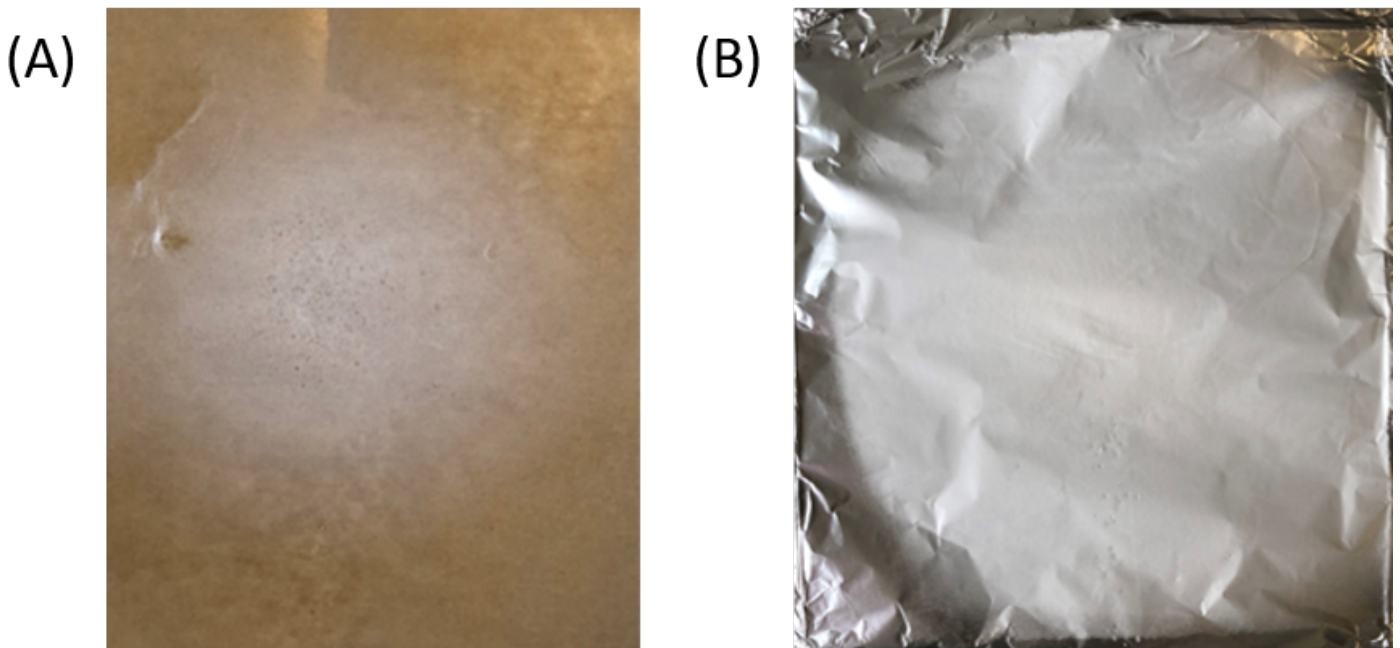


Figure 4.1: Effect of electrospinning conditions on the macroscopic appearance and fibre density of PLLA scaffolds. Scaffold (A) was electrospun with 3ml of the polymer solution while scaffold (B) was electrospun using 9ml of the same solution.

The electrospinning conditions to fabricate PLLA scaffolds were determined. The effect of changing the voltage, the distance of the needle from the collector, and flow rate of the polymer through the needle on the diameter of the electrospun scaffold was then

investigated. Settings of 23 kV, with a distance from the collector of 20 cm and flow rate of 2 ml/h appeared to give the best scaffold morphology macroscopically. Scaffold morphology and fibre diameters of the electrospun scaffolds were studied using SEM.

For fabricating PCL random-fibre scaffolds, the same electrospinning conditions described above were used; initially and found out that it was a good condition to produce a handleable (e.g. that can be detached easily without curling and can be picked up with forceps without tearing apart), scaffold with good features macroscopically and a dense fibre mat of thickness as shown in Figure 4.2. SEM was used to determine the fibre diameters and morphology of the electrospun fibres.

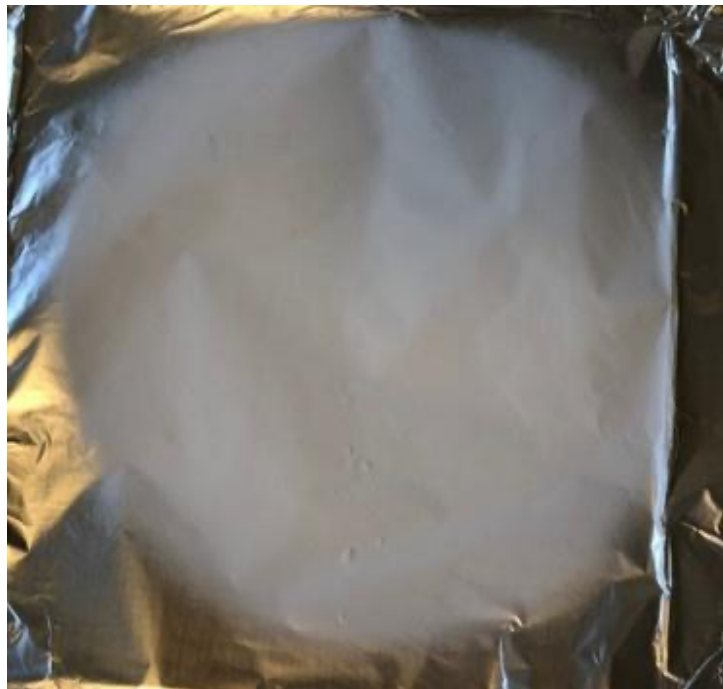


Figure 4.2: Image of a PCL scaffold electrospun using 10 ml of PCL solution with settings of 23 kV, flow rate of 2ml/hr with a distance of 20cm between the polymer jet and collecting plate.

4.1.1.2. Determination of scaffold morphology and fibre diameter

SEM was used to determine the fibre morphology and diameter. Figure 4.4 shows SEM micrographs for the PLLA and PCL random-fibre scaffolds. Two scaffolds per polymer group were used to determine fibre diameter and morphology for each scaffold sample, and the diameters of 15 fibres were measured randomly all around each scaffold from the same image. ImageJ software was used to measure the average diameter of the fibres. Results are shown in Figure 4.3. For the PLLA scaffolds a range of fibre diameters of 1-3 μm was observed with a mean fibre diameter of 2.69 μm , \pm 1.54. In contrast, the PCL scaffolds showed nearly the same fibre diameters with less variation in the fibre diameter. The PCL fibres ranged from 1-3 μm in diameter with a mean diameter of 2.44 μm , \pm 0.45.

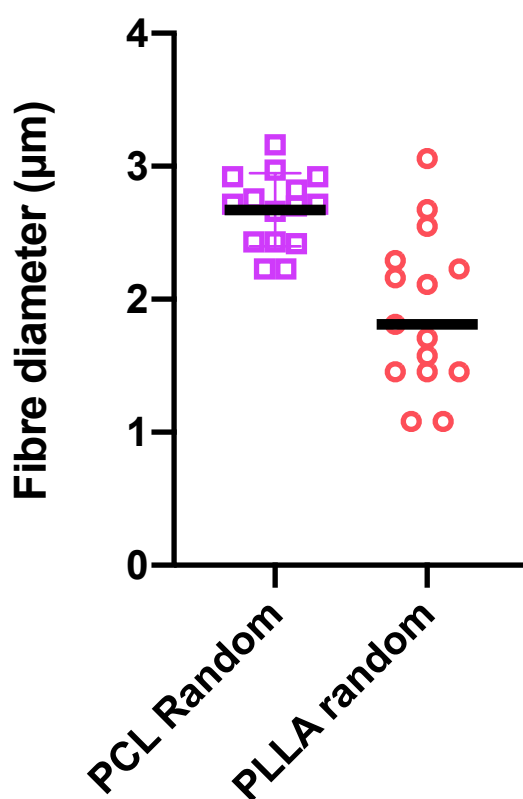


Figure 4.3: Comparison of the fibre diameters of PLLA random, PCL random. The diameter of the scaffold fibres was obtained using ImageJ software. This data was then analysed using Graphpad prism v9.1.

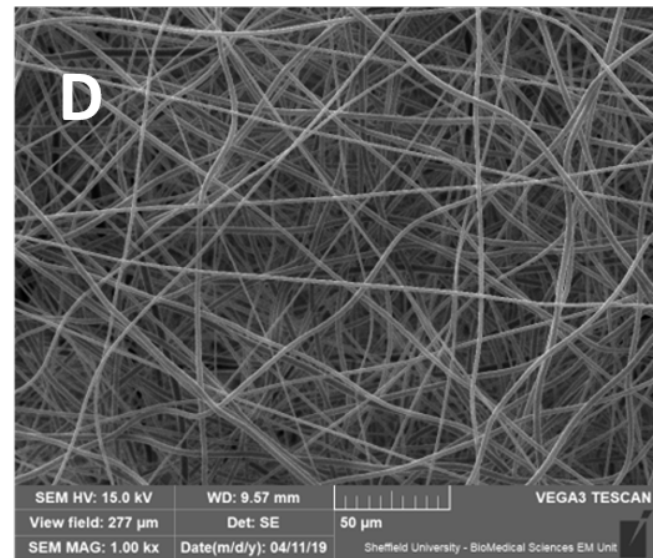
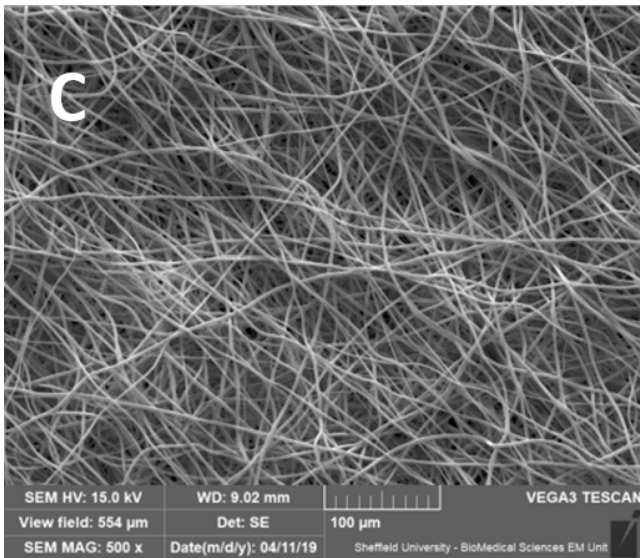
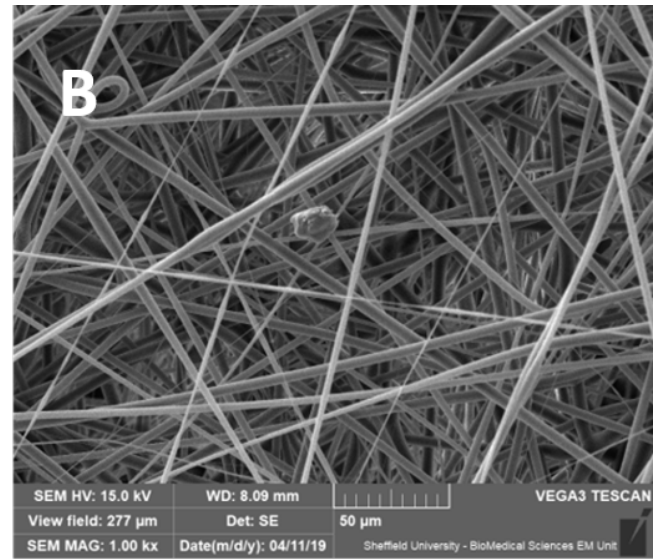
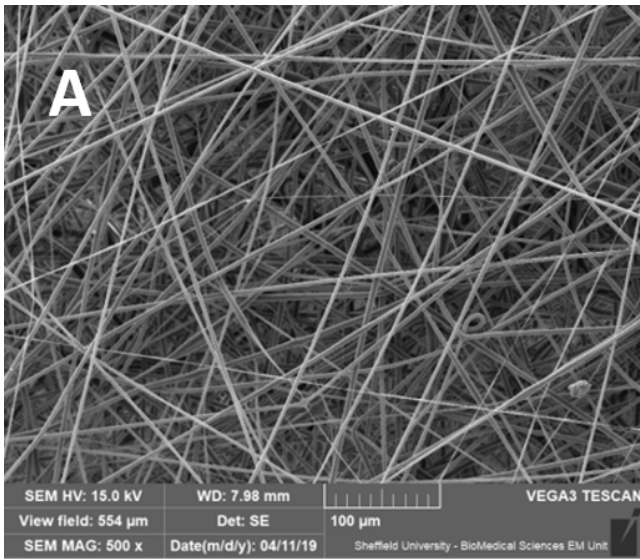


Figure 4.4: SEM images showing the fibre morphology of electrospun PLLA scaffolds (images A and B) and electrospun PCL scaffolds (images C and D). At a magnification of x500, (images A and C, scale bar = 100 μm) and x1000, (images B and D, scale bars=50 μm).

4.1.1.3. Fabrication of aligned fibre electrospun scaffolds

As discussed previously (3.2.2.3), aligned-fibre scaffolds were electrospun to fabricate a scaffold which better reflected the aligned structure of collagen fibres in the native periodontal ligament. Therefore, to enable collection of aligned fibres a rotating drum collector was used in the Bioinicia Electrospinning machine. The effect of the speed of rotation of the collector on fibre alignment and deposition was investigated. Speeds of 500, 1000, 1500 and 2000 r.p.m. were used while the flow rate of the polymer and the voltage were kept constant.

Our observation was, as shown in Figure 4.5, that a rotating speed of 1000 rev/min was found to be the best speed for depositing a fibre scaffold with some apparent alignment of the fibres. The actual degree of alignment of the fibre mat was determined by SEM. Although four rotating speeds were tested only the scaffold fabricated at a rotating collector speed of 1000 r.p.m. was easy to handle and was therefore used for SEM imaging.

Figure 4.6 shows that the fibres were not perfectly aligned; this may have occurred because of an eccentric rotation movement and vibration of the rotating drum collector during the electrospinning experiment. During the electrospinning experiments problems with a heavy vibration of the collector were observed and it also appeared to have an eccentric rotation. Additionally, there was a heavy deposition of electrospun fibres on the floor of the machine and immediately below the rotating collector and not on the collector itself as shown in Figure 4.7. This may have been caused by the vibrating collector altering the air flow inside the electrospinning machine.

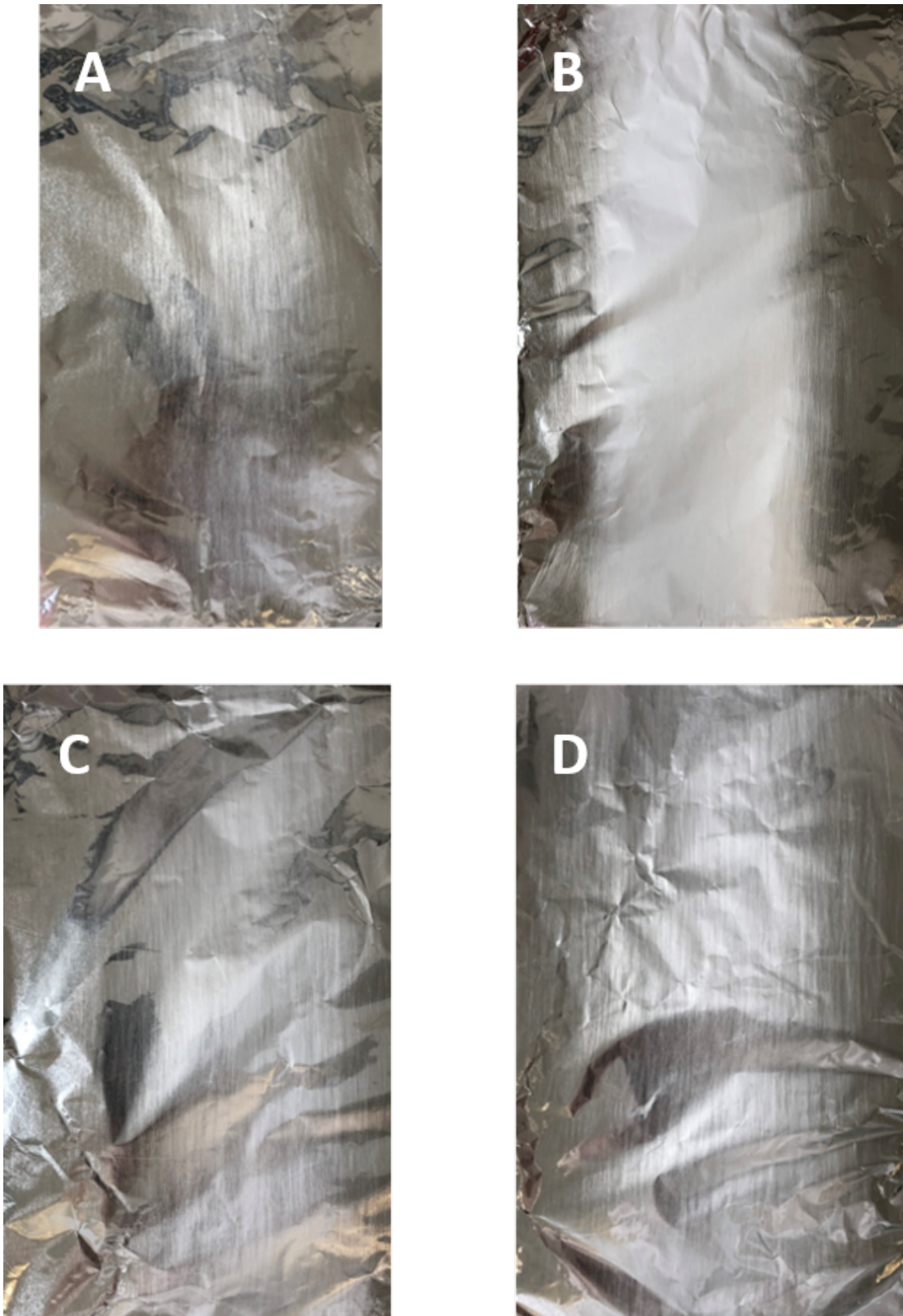
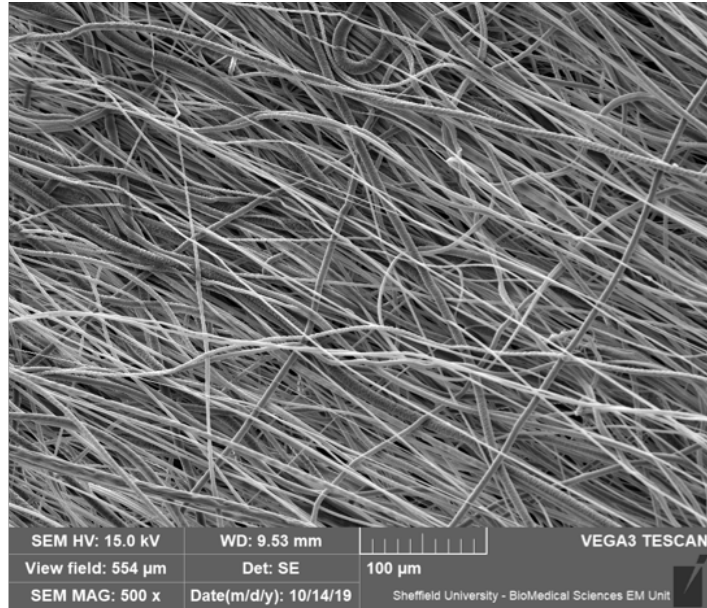


Figure 4.5: Effect of varying speeds on the collecting mandrel of aligned PCL scaffolds. Image A the electrospun fibres were obtained with a rotation speed of speed of 500 r.p.m, image B 1000 r.p.m, image C 1500 r.p.m and image D 2000 r.p.m.

(A)



(B)

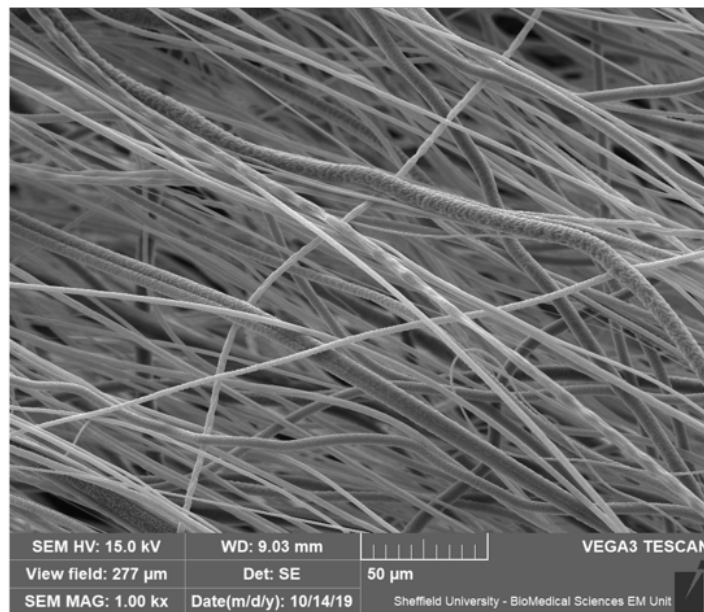


Figure 4.6: SEM of aligned PCL scaffold fabricated on the Bioinicia electrospinning machine. Images were taken at x500 magnification, scale bar =100 μm for image A and x1000, magnification, scale bar =50 μm for image B. The micrographs show partial alignment of PCL.

It was found the vibration of the drum collector was due to damage of the collector itself, which required repair by the manufacturer. Therefore, the electrospinning machine had to be sent back to the Spanish manufacturer (Bioinicia) for repair which took 6-8 months.

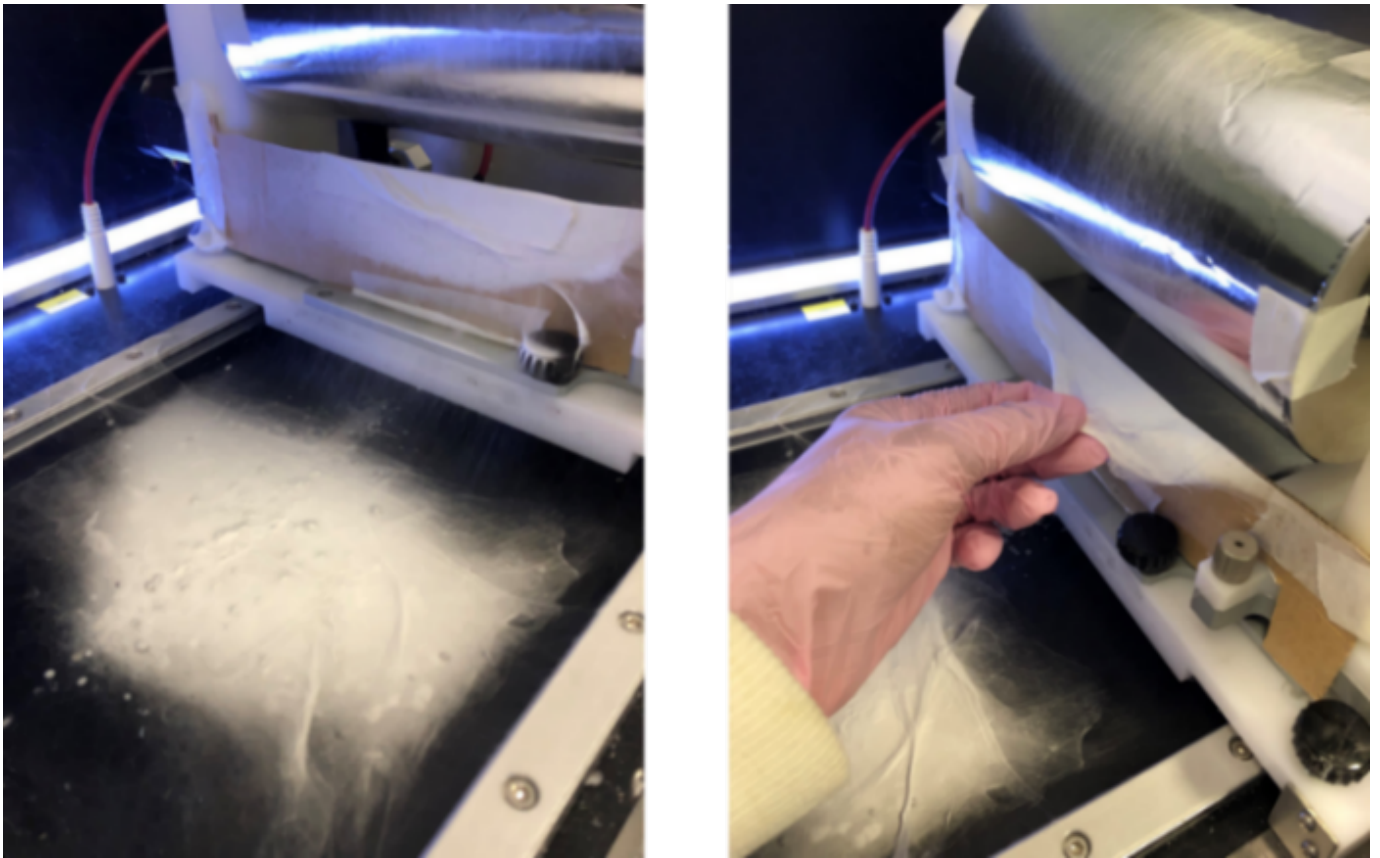


Figure 4.7: Photographs showing the problems caused by the vibration of the collector during the drum rotation. The air-flow during the rotation allow the fibre to stick in the floor of the machine rather than on the collector.

To try to avoid a delay in fabricating aligned fibre scaffolds, electrospinning equipment was located in the Department of Engineering, and this was used to fabricate aligned fibre scaffolds. Initially the same parameters as used on the Bioinicia equipment were applied, and the change in voltage was studied. SEM imaging was used to check the alignment of the fibres on both scaffolds. Figure 4.8 shows that the lower voltage (15 kv) gave the better alignment of the fibres. Further electrospinning experiments were performed to investigate the effect of using lower voltages to obtain great aligned fibre scaffolds.

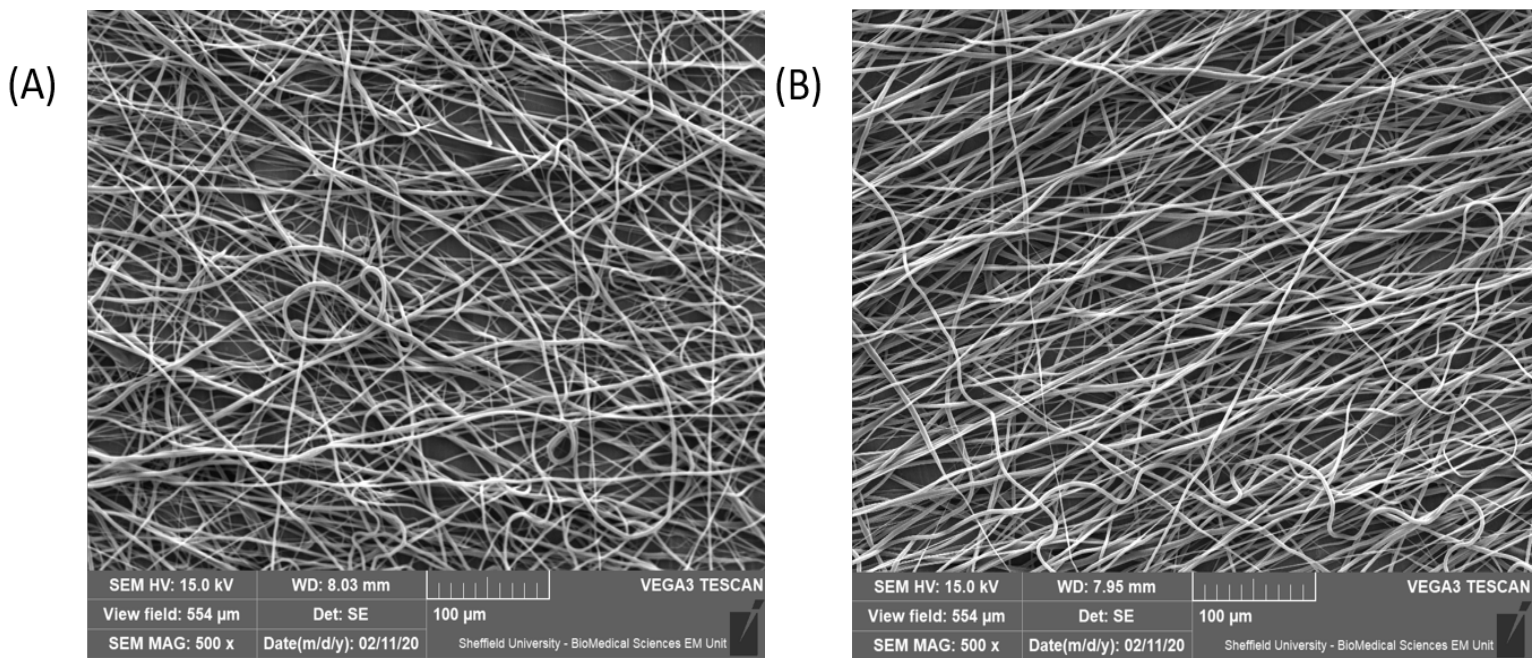


Figure 4.8: SEM images were taken at x500 magnification, scale bar = 100 μm. SEM shows the effect of electrospinning voltage on the alignment of the PCL fibres. Image (A) shows PCL scaffold electrospun with voltage of 21 kv and image (B) shows PCL scaffold electrospun with voltage of 15 kv.

At this point the COVID-19 pandemic occurred. After a UK National Lockdown, the University COVID 19 Policies for safe working meant that the maximum number of people allowed to use the laboratory at the same time was greatly reduced to maintain safe working distances in accordance with the National guidance. Because of the restrictions due to Covid, I could not use the electrospinning machines outside of the Department of Clinical Dentistry. Therefore, I could not use the electrospinning machines in the Department of Engineering and the electrospinning machine in the school had not been repaired therefore the decision was taken to order an aligned fibre scaffold had to be purchased from the Electrospinning Company to avoid any more delay in the project.

An aligned fibre scaffold was ordered from the Electrospinning Company due to the impact of COVID 19 as described above. The commercially aligned scaffolds had a tri-layer structure of PCL fibres to give the aligned fibre scaffold mat more stability during handling and the experiments. The overall thickness of the scaffold was $393 \pm 18.5 \mu\text{m}$. The table below shows the analysis results of the commercially aligned PCL scaffold from the Electrospinning Company. The fibre diameter and morphology of the commercial PCL aligned scaffolds was established in the same way as the random PLLA and PCL scaffolds. The commercial PCL aligned scaffolds showed higher range of fibre diameters 3.5-5 μm with a mean fibre diameter of 4.49 μm , ± 0.43 compared to the random PLLA and PCL scaffolds.

Table 4.1: fibre diameters and scaffold thickness of the commercial aligned fibre PCL scaffolds.

	Batch	Top
Fibre diameter & standard deviation	01399(01).03 – top aligned layer	3.30 ± 1.23 µm
	01399(01).03 – random fibres	3.20 ± 0.59 µm
	01399(01).03 – bottom aligned layer	4.47 ± 0.41 µm
Thickness profile	Tri-layer	393 ± 18.5 µm

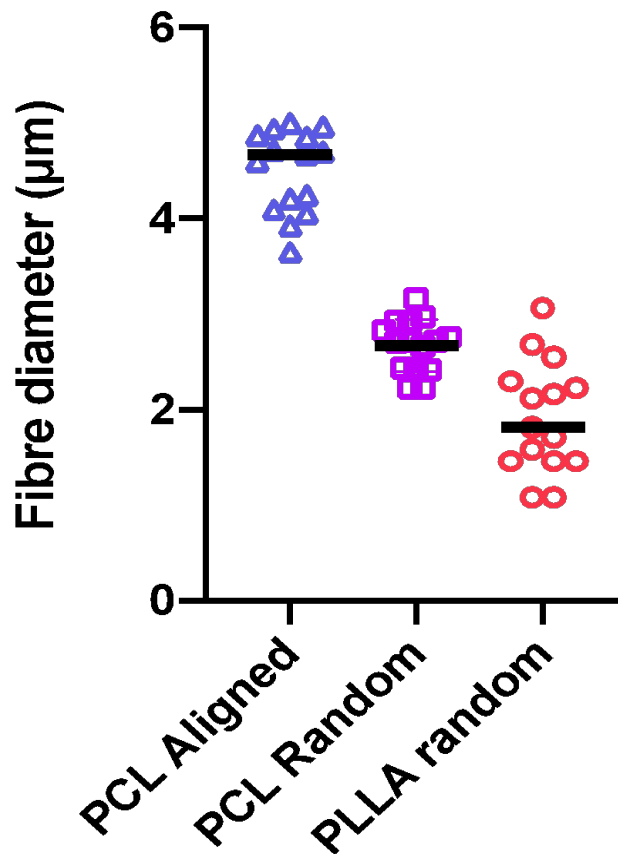
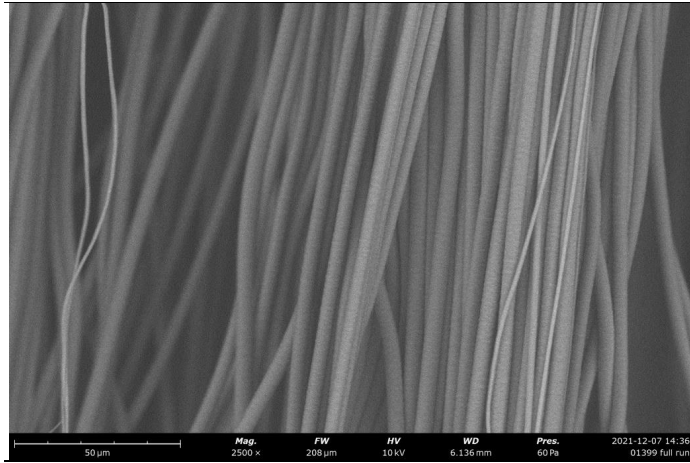


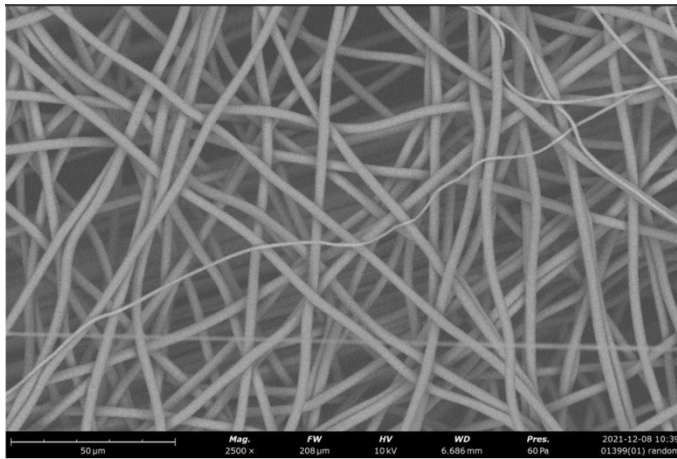
Figure 4.9: Comparison of the mean fibre diameters of PLLA random, PCL random and PCL aligned. The diameter of the scaffold fibres was obtained using ImageJ software. This data was then analysed using Graphpad prism v9.1.

Figure 4.10 shows the SEM images of each layer in the aligned PCL scaffold mat which were provided by the company. The random layer in the middle of both aligned layers are there to provide more stability to the scaffold mat. Furthermore, the random layer will prevent the aligned fibres from tearing apart during the cutting. Figure 4.11 shows the in-house SEM images taken of the aligned PCL scaffold mat to check the alignment of the fibres. All the images indicate the perfectly aligned fibres in the ordered PCL scaffold mat.

A



B



C

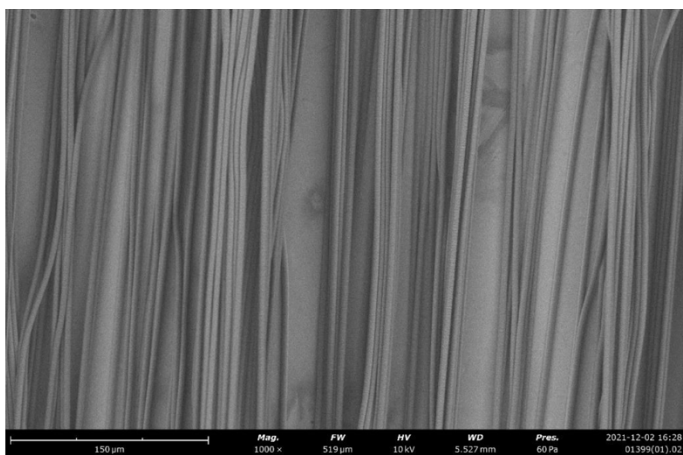
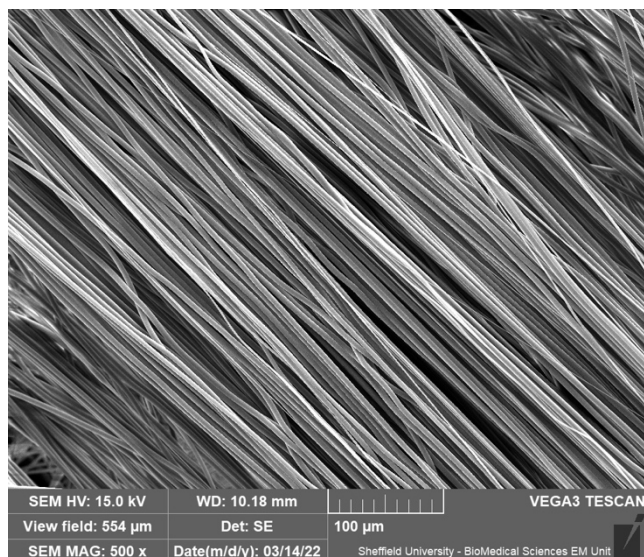


Figure 4.10: SEM images were taken at $\times 2500$ & $\times 1000$ magnifications by the electrospinning company. scale bar A & B = $50\ \mu\text{m}$ and C = $150\ \mu\text{m}$. SEM shows the Tri-layer of the PCL scaffold mat. Image (A) shows top PCL aligned layer, (B) shows PCL random layer (middle layer). (C) shows bottom PCL aligned layer.

A



B

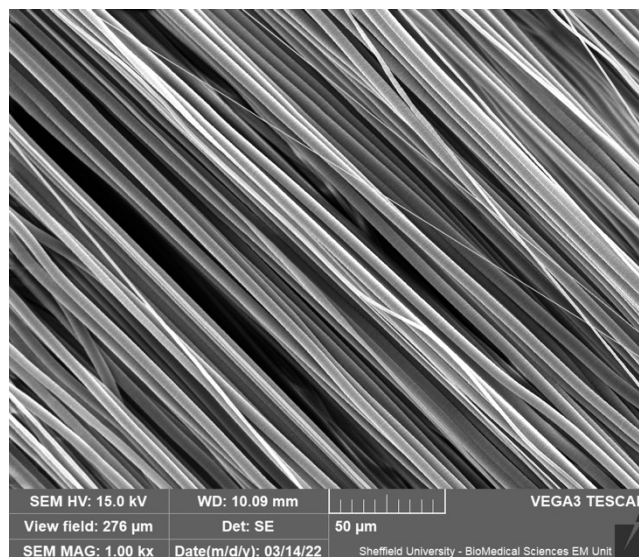
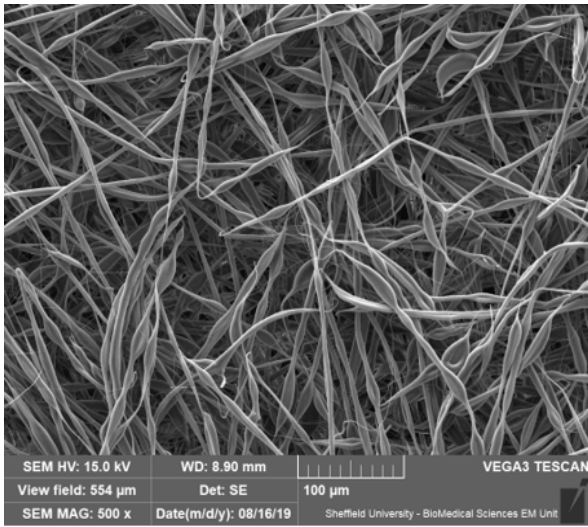


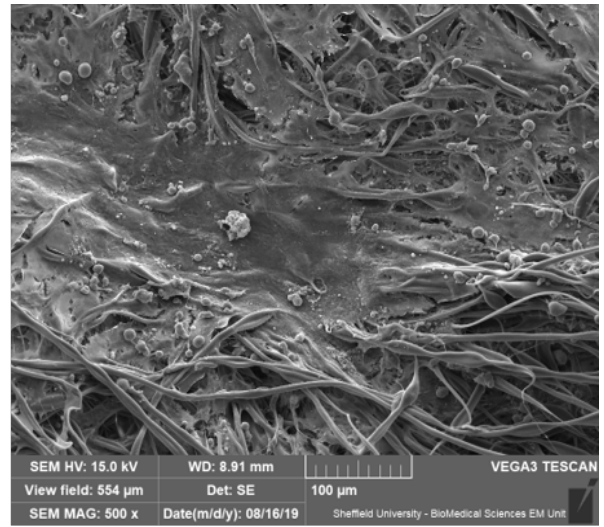
Figure 4.11: SEM images was taken at x500 and x1000 magnifications, scale bar =100 μm and 50 μm . SEM shows the alignment of the scaffold mat that been ordered from the electrospinning company.

4.1.1.4. Cell viability and cell proliferation on the electrospun PLLA and PCL mats

6 mm diameter samples of random-fibre PLLA and PCL scaffolds were sterilised with 70% isopropanol for 15 minutes then washed with sterile distilled water twice and lastly washed 3 times with PBS. Then the sterilised membranes were seeded with bovine ligament cells according to the method given in section (3.2.4.3). After incubating the scaffolds for 7 days, SEM imaging was used to observe binding of the cells with the scaffolds. Figure 4.12 shows the scanning electron micrographs of seeded random-fibre PLLA and PCL scaffolds. In the micrographs it can be observed that the cells were spread on the fibres on both the outer and middle regions and the random-fibre PCL scaffolds but in contrast, in the random-fibre PLLA, scaffolds few cells appeared bound on the edges of the scaffolds but appeared concentrated in the middle region of the scaffold. This is maybe because of the PLLA scaffolds curled up during the culture period. This curling behaviour made the PLLA scaffolds more difficult to handle and work with.



PLLA Edge



PLLA Middle

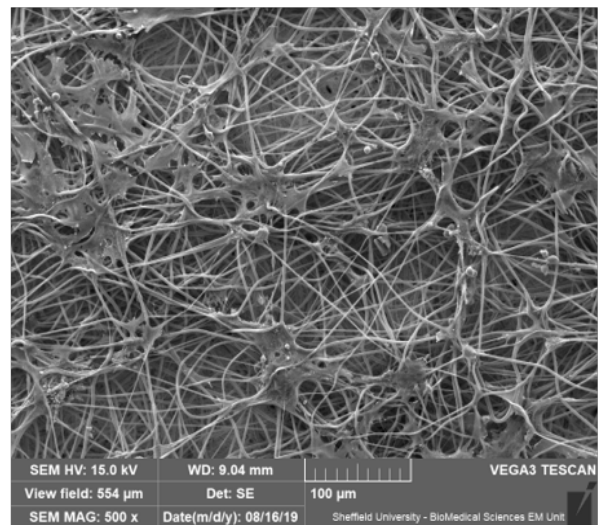
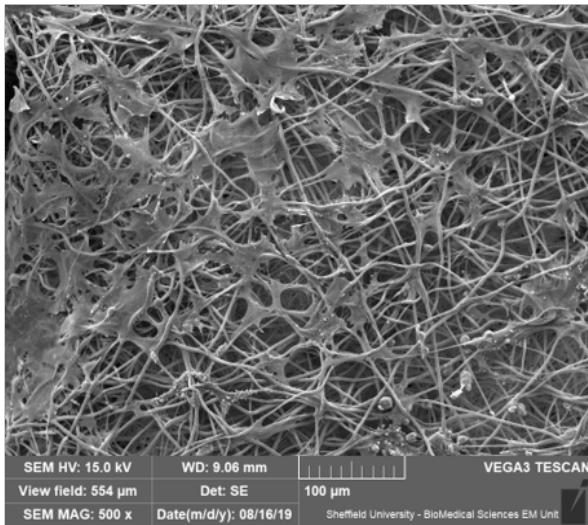


Figure 4.12: SEM images was taken at x500 magnifications, scale bar =100 μm, to show the comparison of cells bound to PLLA and PCL scaffold in different regions of the scaffold.

Cell distribution of live and dead cells on the scaffolds was also established by imaging of the scaffolds using confocal microscopy after labelling the cells with a live-dead stain (as described on section (3.2.4.9)). Control scaffolds (i.e. scaffolds that had not been seeded with cells) were also stained with the live-dead stain to check for any fluorescence, due to the dyes binding to the scaffold fibres themselves. Figure 4.13 showed that there appeared to be more cells on the PLLA random scaffold than on the PCL random scaffold. Live-dead images also showed scaffolds had a high population of live cells and very few dead cells with no significant fluorescence by cell-free scaffolds. PLLA random scaffold appears to have more cells than PCL random scaffold.

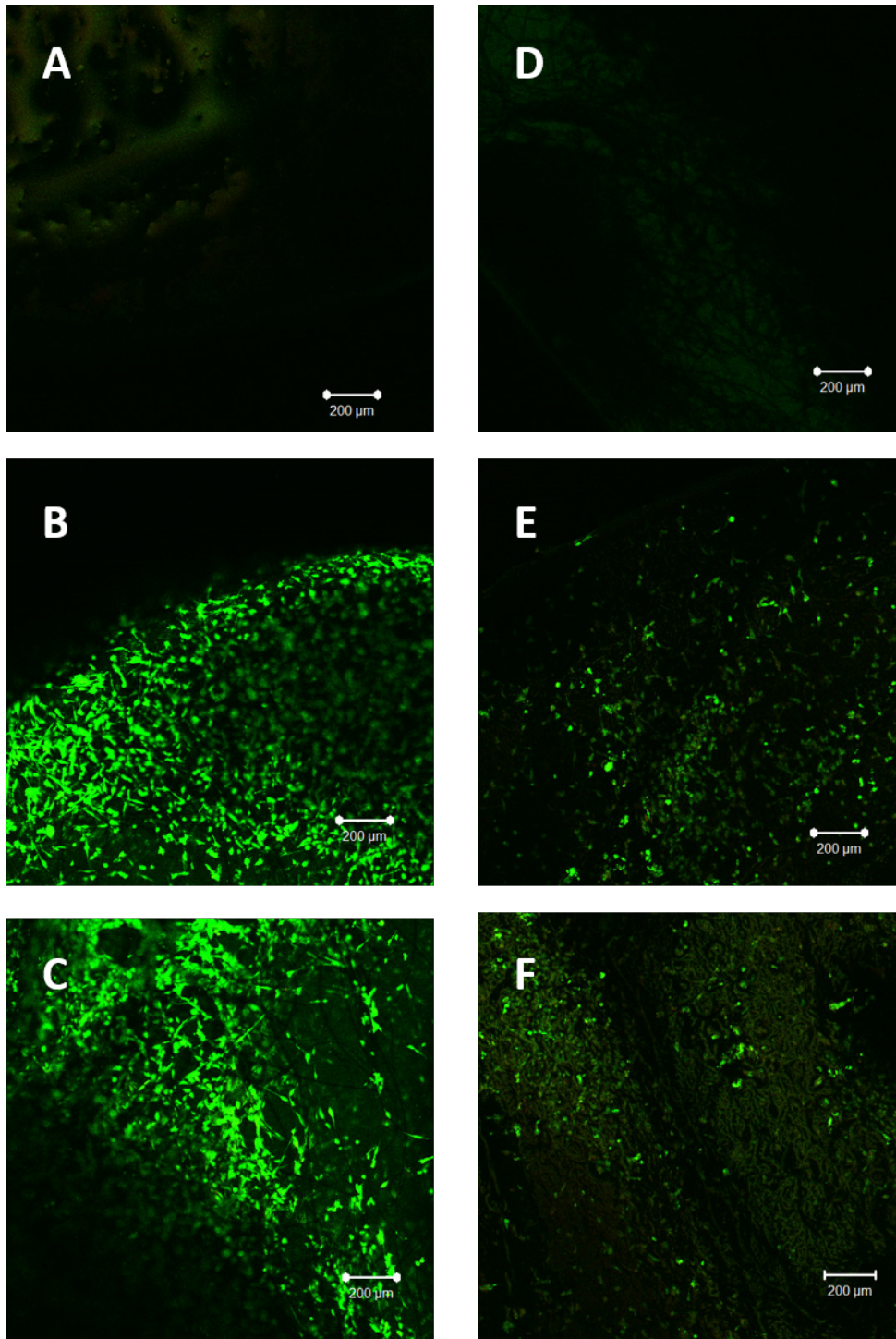


Figure 4.13: Fluorescence microscopy images on day 21 shows live cells in green (CMFOA) and dead cells in red (PI). PLLA control scaffold (image A) and PCL control scaffold (image D) shows that the scaffolds themselves do not fluoresce. On the other images (B, E, C and F) the green staining represents the living cells on the scaffolds. Images (B and C) are PLLA seeded scaffold B is the edge and C is the middle of the seeded scaffolds. Furthermore, image (E and F) is PCL seeded scaffold. Where image E is the edge and image F is the middle of the seeded scaffold. Scale bar = 200 μm.

The viability of the ligament cells over a 21-day culture period was determined by measuring the reduction of resazurin to resorufin using PrestoBlue™ dye on days 7, 14 and 21. Figure 4.14 shows the activity of the cells on seeded random PLLA and random PCL scaffolds. Random PCL cell/scaffold constructs had a higher metabolic activity than PLLA/cell scaffold constructs at all-time points.

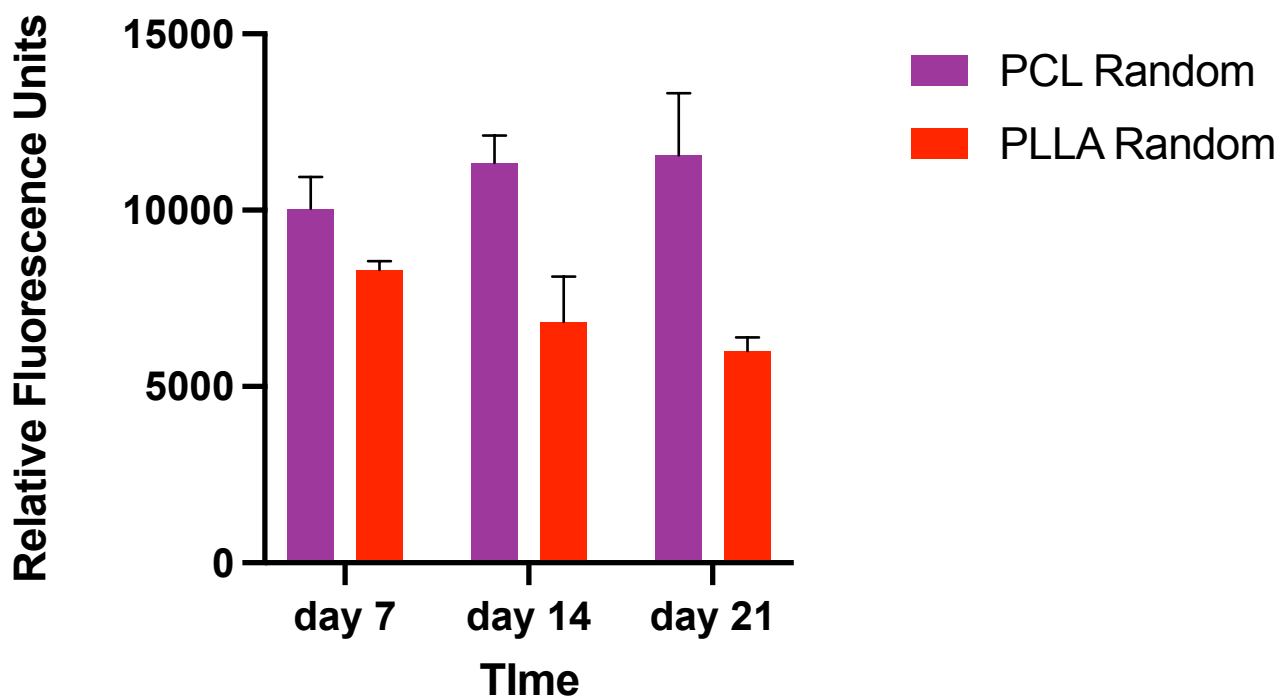


Figure 4.14: Cellular activity of PLLA and PCL cell-scaffold constructs on days 7,14 and 21 determined using PrestoBlue™ dye. The values are the means \pm SDs.

The degree of cells binding to the scaffolds was determined by measuring the level of cellular DNA on the cell-scaffold constructs. This was determined on day 21 using a commercial DNA quantification assay kit as described in section incorrect section number. DNA measurements showed that the amount of DNA in the PCL random scaffolds was greater than that on the

PLLA random scaffolds (DNA on PCL scaffolds was 10971.4, \pm 1756.7 ng/scaffold and DNA on the PLLA scaffolds was 5760.3, \pm 390.4 ng/scaffold).

Figure 4.15 shows the cellular activity of the ligament cells after 21 days of culture. The values were normalised per nanogram of DNA. These results show that cell activity was greater on the PCL random fibre scaffolds than that on the PLLA random fibre scaffolds. This difference was due to the higher number of ligament cells on the PCL scaffolds.

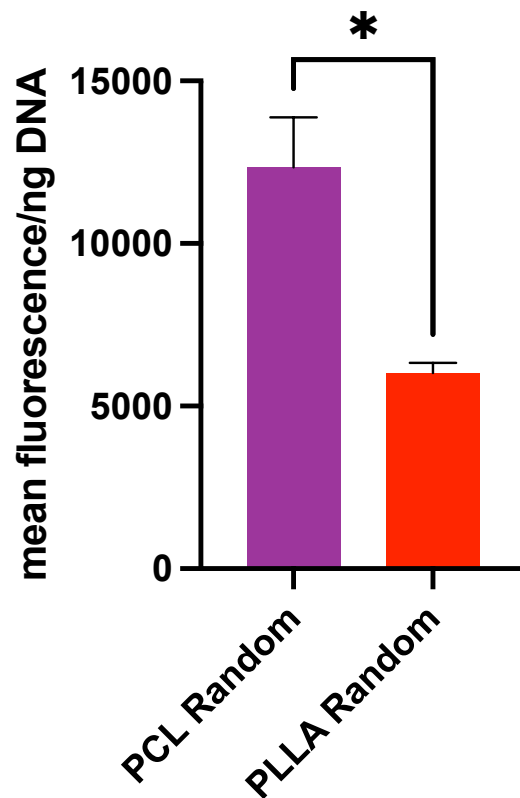


Figure 4.15: Graph shows the cellular activity on day 21 normalised to DNA of the random electrospun PLLA and PCL scaffolds. The values are the means \pm SDs.

4.2. Surface modification and biofunctionalization of the scaffold mats

4.2.1. X-ray photoelectron spectroscopy (XPS)

As mentioned earlier in section (3.2.5.1), PLLA and PCL random fibre scaffolds and PCL aligned fibre scaffolds were surface coated with allylamine using cold plasma polymerisation. The change in the scaffold surface charge due to the amine addition during the allylamine plasma treatment, increased the attachment and the activities of the cell. XPS analysis was used on the controlled and plasma treated scaffolds to confirm the amine content on the surface of the plasma treated scaffolds. After XPS analyses of PLLA plasma coated and controlled scaffolds, the results showed that there was an appearance of a nitrogen peak, which was caused by the deposition of allylamine. on the scaffold surfaces the oxygen to carbon ratio did not change (figure 4.16). However, the PCL random allylamine coated scaffold showed a substantial peak nitrogen at the surface of the scaffolds, which was greater than the nitrogen peak seen with the PLLA random allylamine coated scaffold. Moreover, with the PCL aligned scaffolds there was an increase in the nitrogen peak after the allylamine deposition. The deposition of allylamine in PCL random scaffold results in an increase of the oxygen concentration.

However, there was a small silica contamination noticed in both PLLA and PCL random scaffolds and PCL aligned scaffold. This is maybe a result of keeping the scaffold with sachets of silica gel to keep the scaffolds dry.

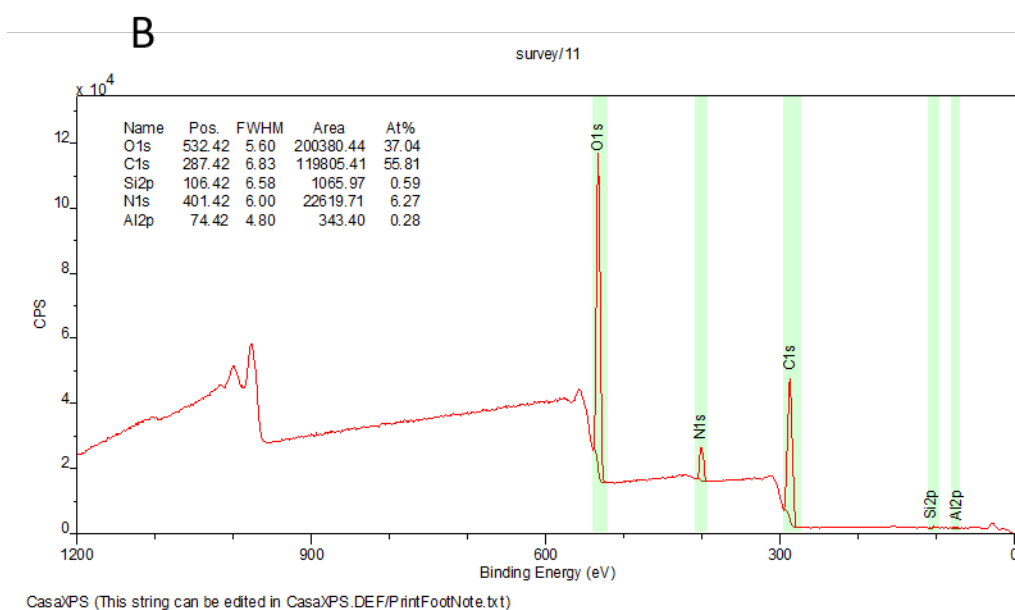
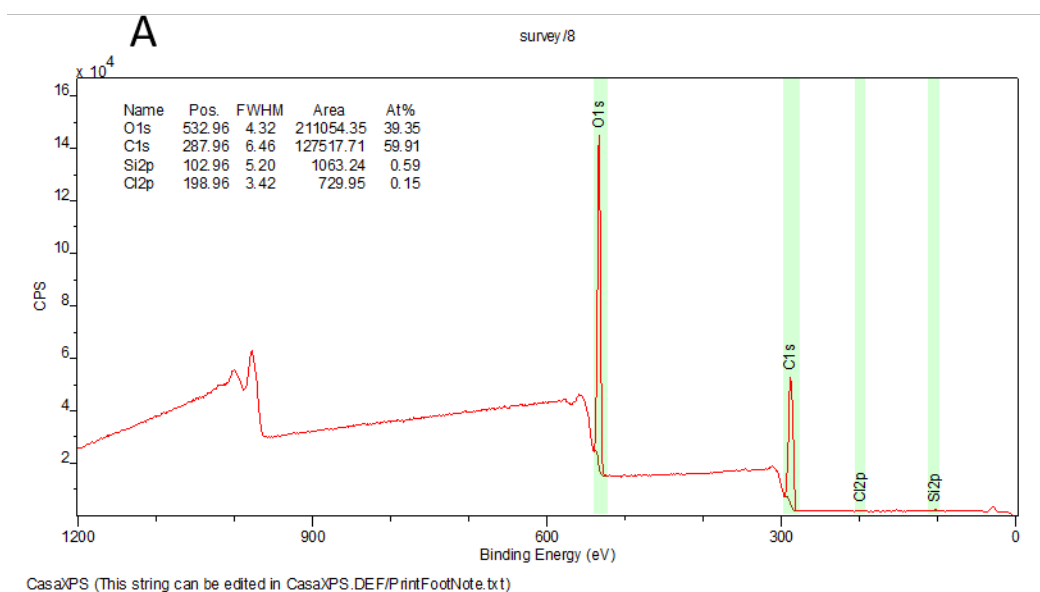


Figure 4.16: XPS analysis spectra. Showing (A) non treated PLLA random scaffold and (B) PLLA random scaffold after allylamine polymerisation which shows the appearance of a Nitrogen peak. Survey scans were collected between 1200 to 0 eV binding energy, at 160 eV pass energy and 1 eV intervals. High-resolution O 1s, C 1s, N 1s and Si 2p spectra were collected over an appropriate energy range at 20 eV pass energy and 0.1 eV intervals. The binding energy scale was calibrated to fix the C 1s peak for C-C/C-H type carbons at 285.0 eV.

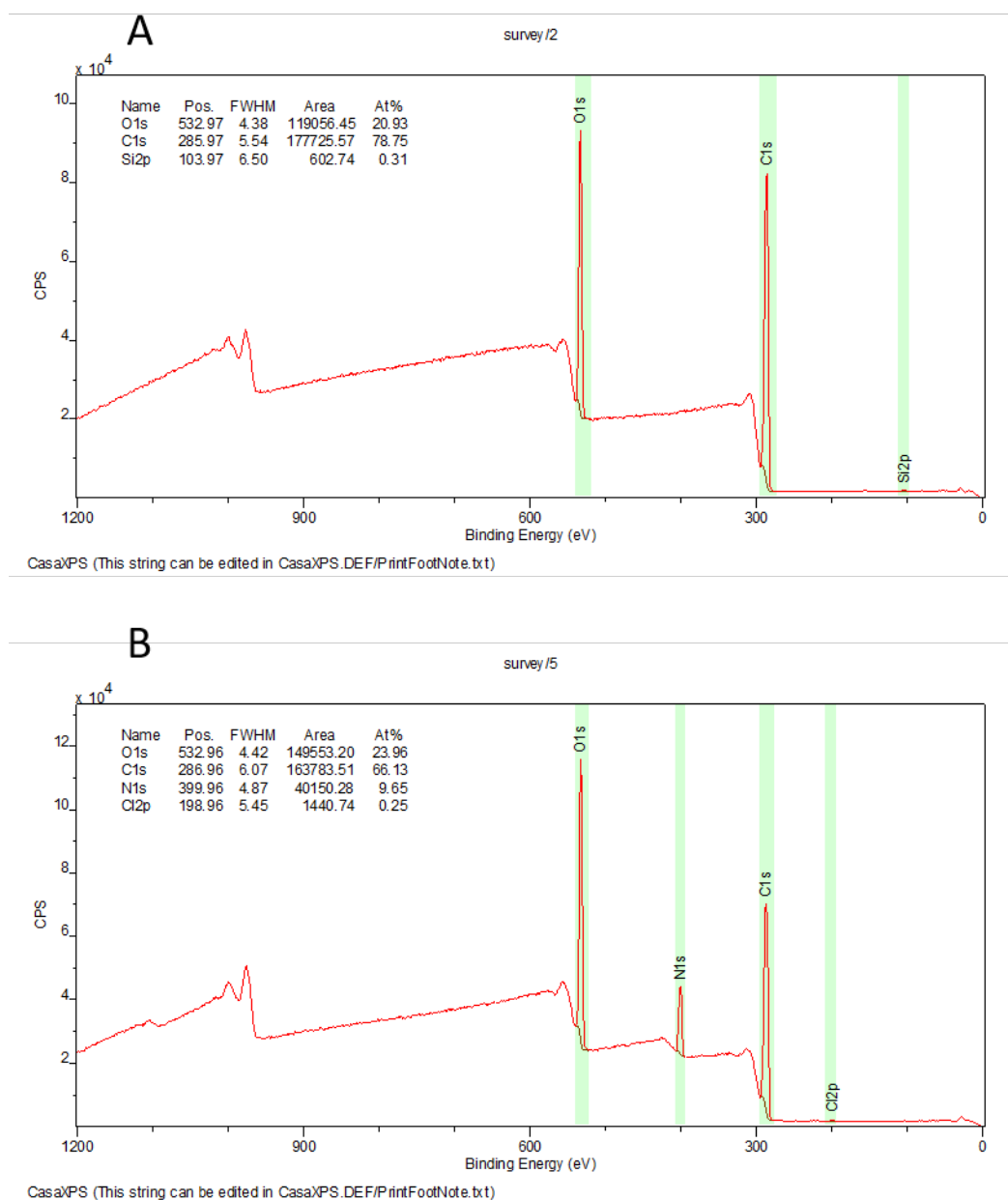
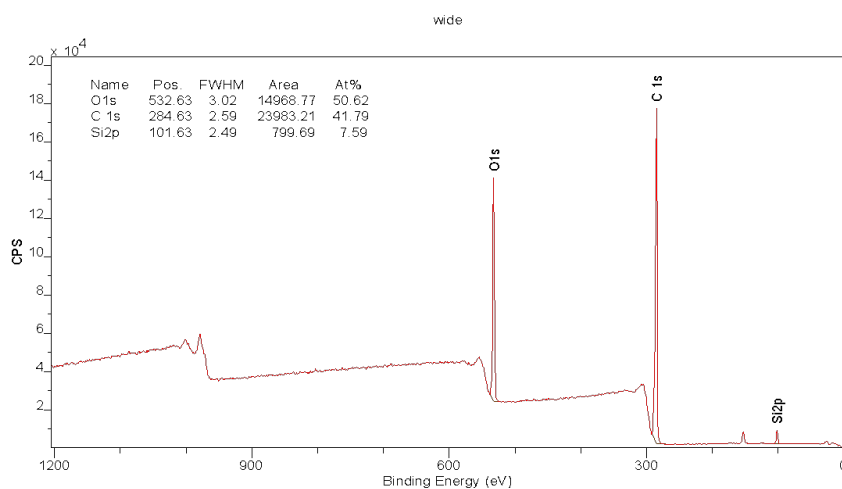


Figure 4.17: XPS analysis spectra. Showing (A) non treated PCL random scaffold and (B) PCL random scaffold after allylamine polymerisation which shows the appearance of a Nitrogen peak. Survey scans were collected between 1200 to 0 eV binding energy, at 160 eV pass energy and 1 eV intervals. High-resolution O 1s, C 1s, N 1s and Si 2p spectra were collected over an appropriate energy range at 20 eV pass energy and 0.1 eV intervals. The binding energy scale was calibrated to fix the C 1s peak for C-C/C-H type carbons at 285.0 eV.

A



D

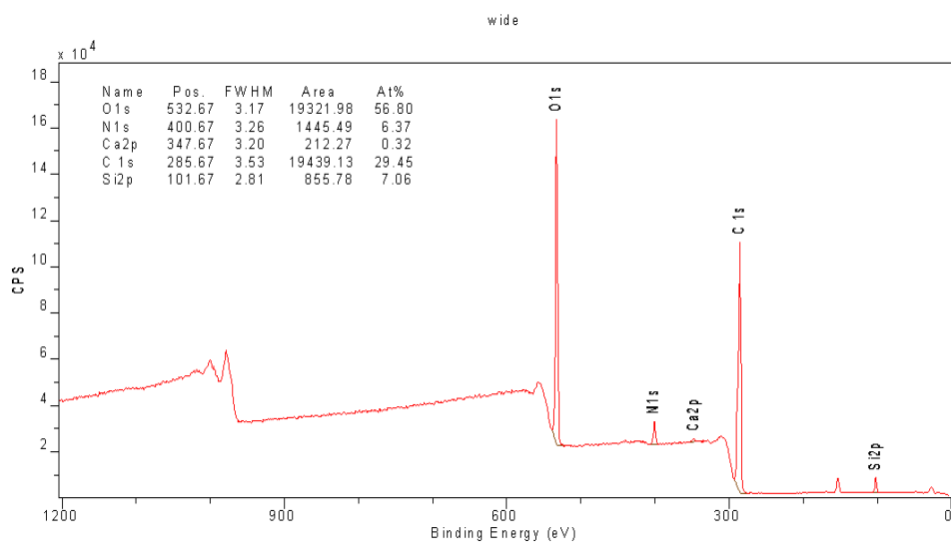


Figure 4.18: XPS analysis spectra. Showing (A) non treated PCL aligned scaffold and (B) PCL aligned scaffold after allylamine polymerisation which shows the appearance of a Nitrogen peak. Survey scans were collected between 1200 to 0 eV binding energy, at 160 eV pass energy and 1 eV intervals. High-resolution O 1s, C 1s, N 1s and Si 2p spectra were collected over an appropriate energy range at 20 eV pass energy and 0.1 eV intervals. The binding energy scale was calibrated to fix the C 1s peak for C-C/C-H type carbons at 285.0 eV.

The data in Figures 4.17 shows that after deposition of amine groups on the scaffolds by plasma polymerisation with allylamine, the nitrogen content on the surface of the PCL random scaffolds was higher (9.7 %) than that on the surface of PLLA random scaffolds (6.3 %). These results indicated that the plasma-treated PCL scaffold should function better than the plasma-treated PLLA scaffolds to promote increased cell binding, viability and cell proliferation. While comparing the XPS data of the PCL random scaffold with that of the PCL aligned scaffold, showed that the PCL random scaffold has higher nitrogen peak than the PCL aligned scaffolds (6.4 %).

4.2.2. Stiffness testing

The mechanical properties of the scaffolds were determined in the Department of Automatic Control and Systems Engineering (ACSE) in the university of Sheffield, Trained and supervised by Dr. Thomas Paterson.

The slope of stress and strain curves for each scaffold group was calculated using the average of three scaffold samples of size 40 mm x 6 mm in length to achieve statistically reliable results. The mechanical properties were measured using Z3 X500 AML, UK Instruments. The load capacity for PLLA random and PCL random was 5N, while that of the PCL aligned utilised 10N as it was stiffer and continued stretching without a tear. Every sample clamp in the machine was pulled at the rate of 4mm/min extension speed and a 30 mm separation distance at room temperature.

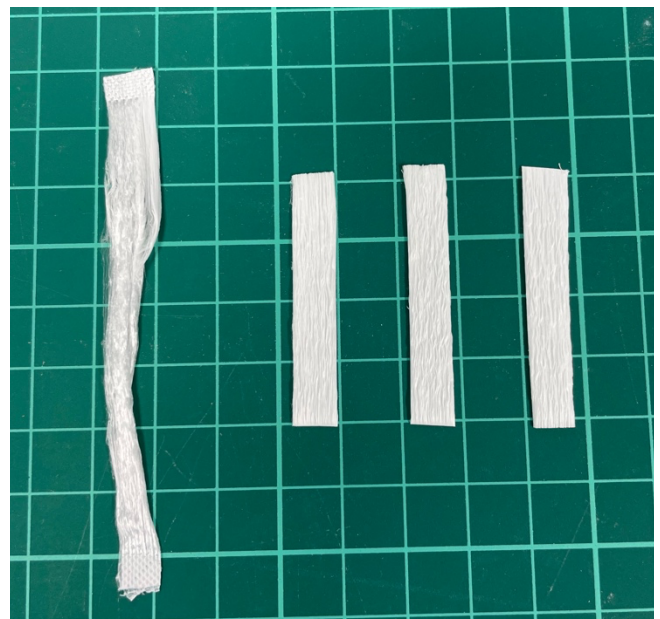
The thickness of the samples was measured using micrometre (Mitutoyo 293-816 digital micrometre) with a resolution of 0.001 mm. Figure 4.20 showed, the PCL and PLLA stress-strain curves showed standard non-linear curves, as shown in the figures A, B and C. The PLLA

random plasma, PCL random plasma, and the PCL aligned plasma showed a reduction in mechanical strength after allylamine plasma deposition.

However, PCL aligned fibres scaffolds need more load than the random fibres scaffolds for breaking down. The aligned fibres had a different profile to the random, they were stretchy, and they are acting like a ligament. This is because of the alignment of the fibres which needs more force to stretch the scaffold mat more. Aligned PCL scaffolds did not tear at all as it kept stretching along the time during the test.



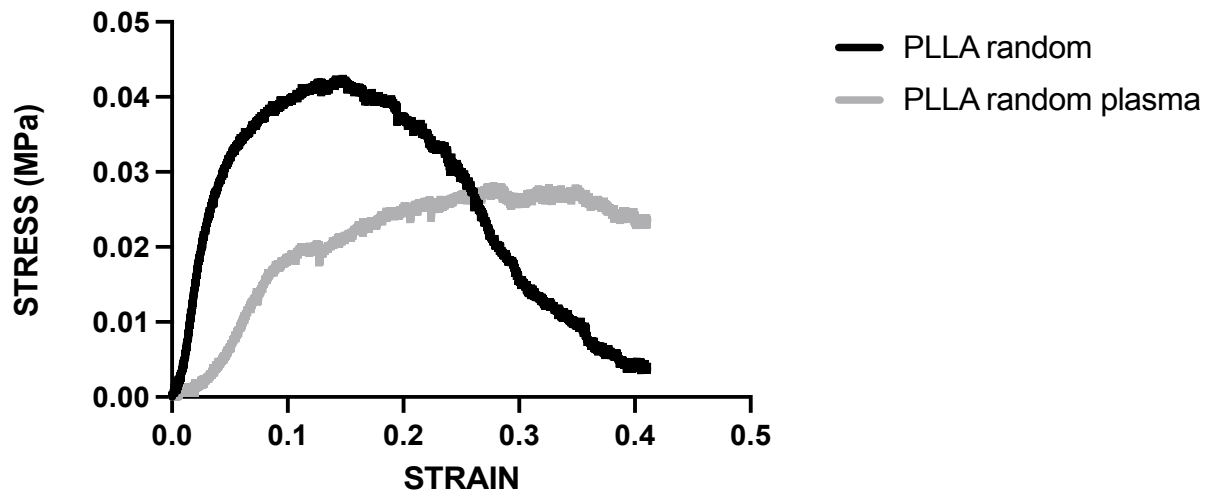
A



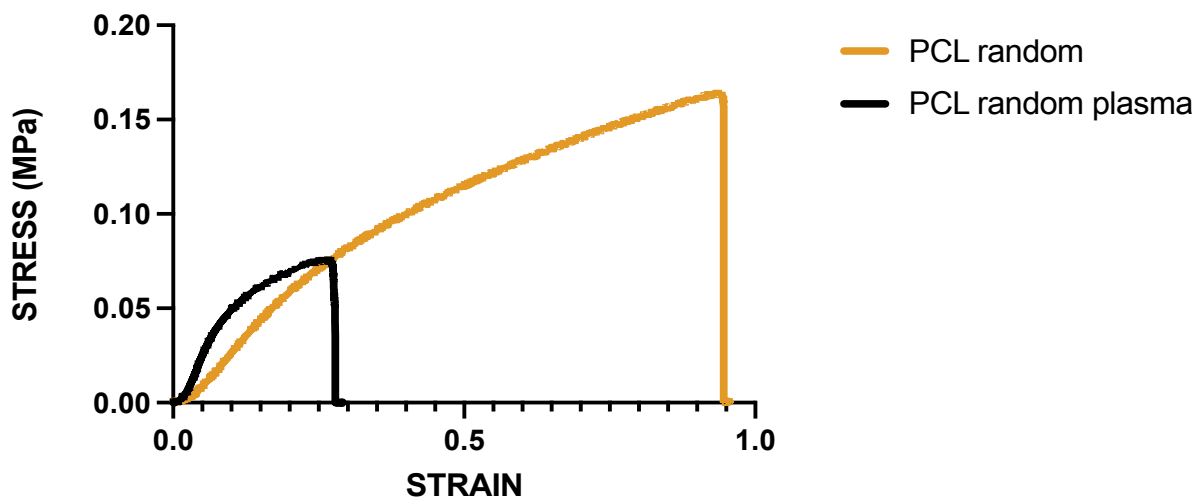
B

Figure 4.19: images of aligned fibre PCL scaffolds. Image A: during the mechanical testing by the tensile tester machine using 10N and the aligned fibre PCL scaffold keep stretching without tearing during the test. Image B: a picture of the aligned fibre PCL scaffold before and after stretching.

A



B



C

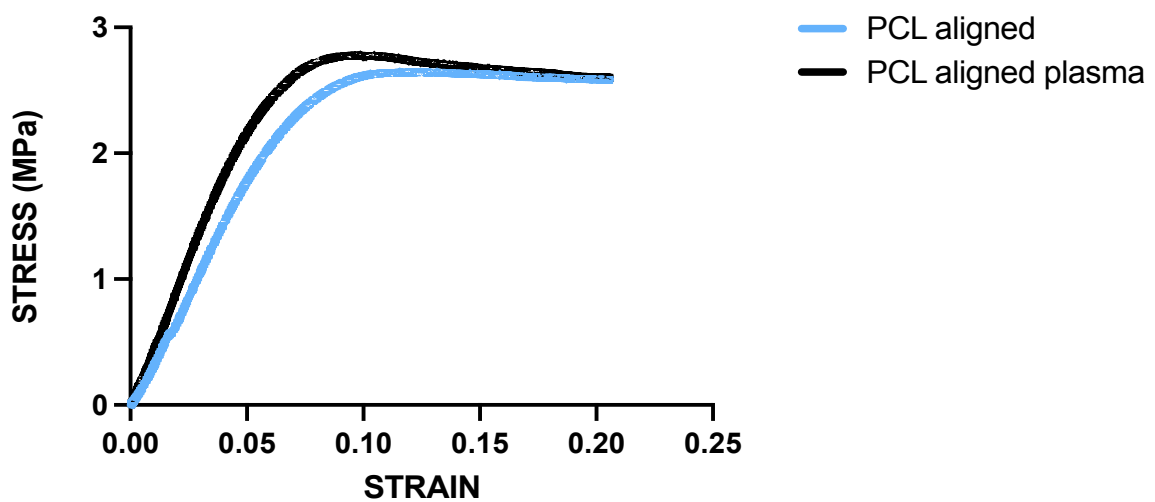


Figure 4.20: stress/strain curve of fabricated random and aligned scaffolds, plasma and non-plasma scaffolds. A: PLLA random scaffolds, B PCL random scaffold and C aligned PCL scaffold tested under dry condition for tensile properties.

Table 4.2: Tensile strength, elongation at break and Young's modulus of PLLA and PCL random fibre scaffold and commercial PCL aligned fibre scaffold.

	PLLA random	PLLA random Plasma	PCL random	PCL random plasma	PCL aligned	PCL aligned plasma
Tensile strength (σ) (MPa)	0.04 \pm 0.00	0.02 \pm 0.00	0.15 \pm 0.01	0.08 \pm 0.00	2.59 \pm 0.32	2.93 \pm 0.32
Elongation at break (% strain)	40.7 \pm 1.08	55.8 \pm 13.1	107 \pm 13.2	30.2 \pm 2.41	20.9 \pm 0.53	20.8 \pm 0.41
Young's modulus (E) (MPa)	0.86 \pm 0.24	0.34 \pm 0.28	0.32 \pm 0.04	0.78 \pm 0.03	41.58 \pm 7.04	47.21 \pm 3.81

After establishing stress-strain curves, the tensile strength, and the Young's modulus of each sample was calculated. The table above showed the Young's modulus, tensile strength and the elongation at break for each group. The applied load at failure (F) was divided by the initial cross-sectional area (A_0) to get the tensile strength of the samples ($\sigma = F/A_0$). The gauge length change (Δl) and the sample's initial length (l_0) are related by the unitary deformation (strain $\epsilon = \Delta l/l_0$). As a result, it is possible to determine the young's modulus modulus ($E = \sigma/\epsilon$).

The PCL aligned fibre scaffolds have a greater Young's modulus compared to the PLLA random fibre and PCL random fibre scaffolds. As mentioned above, this is due to the fibre alignment of the scaffolds which makes it harder to tear, the fibres keep stretching as the strain increased during the test. The plasma treatment in the aligned scaffolds caused a small increase with significant difference in the Young's modulus of the scaffolds (41.58 \pm 7.04 MPa To 47.21 \pm 3.81 MPa). Comparing the PLLA random fibre scaffolds to the PCL random fibre scaffold, the non-treated PLLA random scaffolds had a higher Young's modulus than the non-

treated PCL random scaffolds (0.86 ± 0.24 MPa vs 0.32 ± 0.04 MPa). However, after the plasma treatment with allylamine, the Young's modulus of the PLLA random fibre scaffolds was decreased (0.34 ± 0.28 MPa). Where in the PCL random fibre scaffolds Young's modulus increased after the plasma treatment (0.78 ± 0.03 MPa).

4.2.3. Scaffolds porosity and pore size distribution

Porosity is calculated usually by dividing the total size of pores in the scaffold via the total area of the membrane. The Mercury Intrusion method was used to establish the pore size of the scaffolds under applied pressure as mentioned in section (3.2.7).

Figure 4.21 below shows the PCL and PLLA intrusion porosimeter results which were plotted as the log differential intrusion (ml/g) versus pore size diameter (μm), and every curve peak represents the average pore size of the scaffolds. The graph displays the total cumulative pore area and total cumulative intrusion plotted against pressure.

The results in the table below showed that PCL aligned has the highest percent porosity (90.26%). Where the PLLA random has the highest intrusion volume pore area (8.52 ml/g). However, PCL random fibres have least porosity (80.27%) as well as intrusion volume (6.85 ml/g) and pore area ($43.68 \text{ m}^2/\text{g}$) compared to others. The values shown in table 4.3 are calculated from the graphs in figure 4.21.

Table 4.3: The main output data of mercury intrusion porosimetry analysis.

Content	Total intrusion Volume mL/g	Total pore Area m^2/g	Porosity %
PLLA random	8.52	63.16	89.48
PCL random	6.85	43.68	80.27
PCL aligned	7.27	49.13	90.26

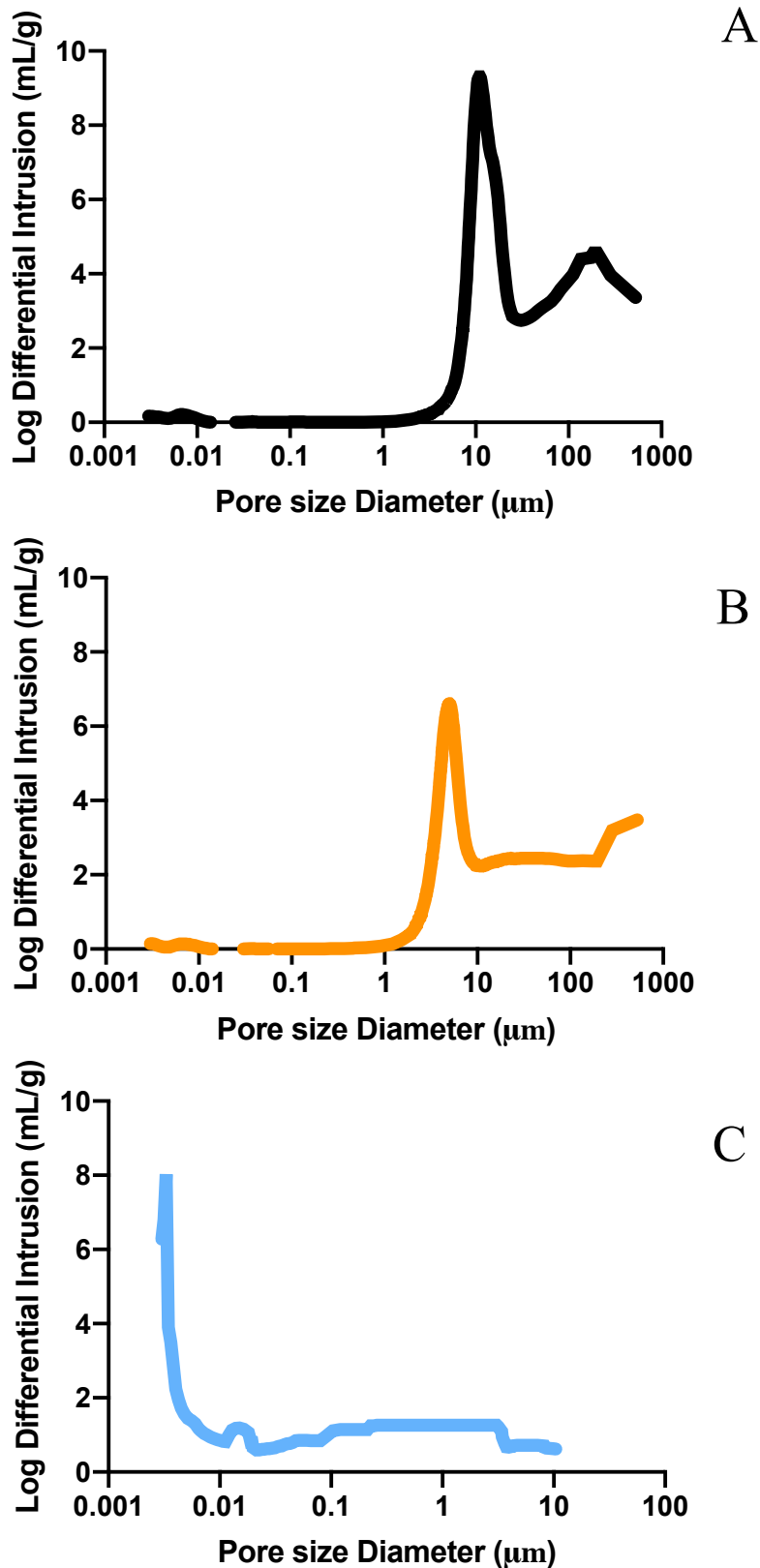


Figure 4.21: Mercury intrusion porosimetry results are plotted as the log differential of intrusion vs. pore size of each scaffold type. During the test, the samples were placed inside an evacuated chamber and the pressure was increased up to a maximum of 414 MPa. The mercury is compressed to penetrate the pores of the scaffold and the results were recorded using a MicroActive AutoPore. Each peak representing the different average pore size of the scaffolds. A: PLLA random scaffolds, B: PCL random scaffolds and C: PCL aligned scaffolds.

4.2.4. Contact angle measurement

Contact angle methodology was used to measure the change in hydrophilicity of the scaffolds after plasma treatment. Rectangular samples of size 1cm width and 3 cm length of each scaffold group, PLLA random, PCL random, PCL aligned, controls, and plasma treated were tested. The water contact angle (WCA) was measured by the sessile drop technique with a drop of 5 μ L of distilled water.

WCA experiment on the scaffolds obtained their surface hydrophobic aspects. WCA for aligned PCL was the highest recorded ($157.6^{\circ} \pm 17$) and followed by random PCL ($132.2^{\circ} \pm 14$) and random PLLA ($126.6^{\circ} \pm 3.5$), which showed that the materials were highly hydrophobic and non-absorbent to water. However, the plasma-treated scaffolds recorded a great increase in hydrophilicity which showed 100% wettability by the water droplets, affirming the presence of hydrophilic groups on the scaffolds' surfaces (see Figure 4.22). This data indicates that plasma treatment increases the hydrophilicity of the scaffolds, which would improve the cell attachment and proliferation.

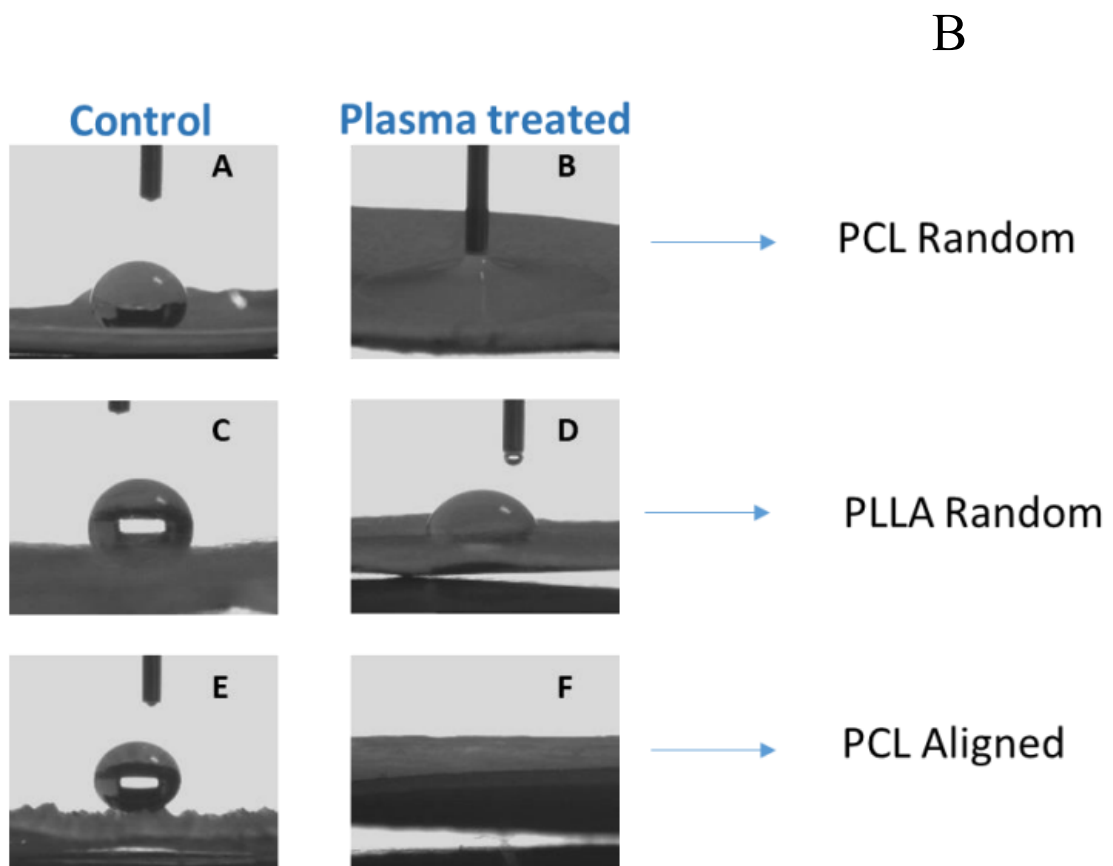
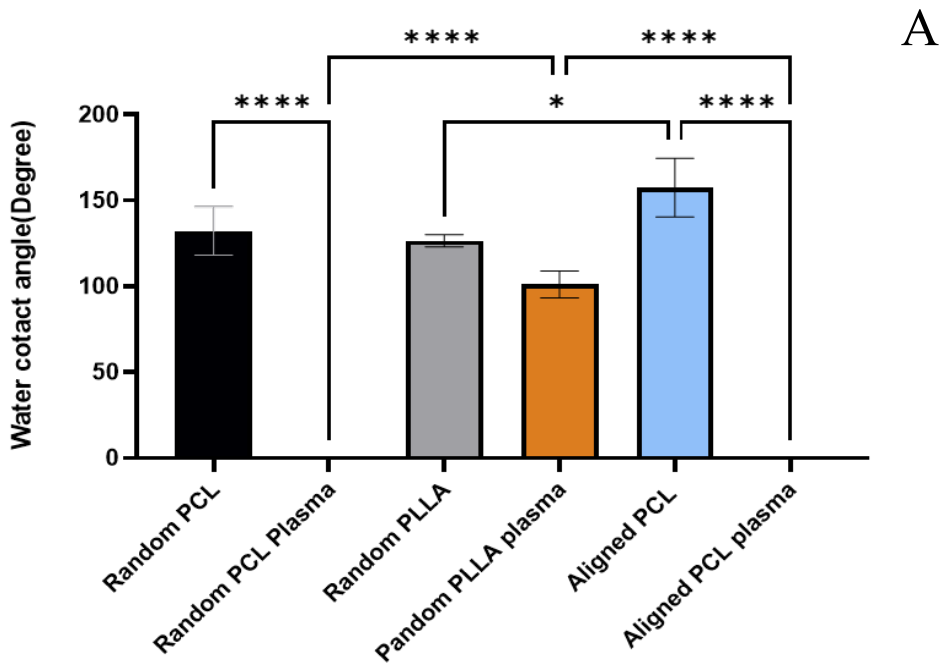


Figure 4.22: Contact angle results of PLLA and PCL random and PCL aligned scaffolds, Plasma treated and non-treated scaffolds. The measurement was obtained using DSA instruments. Graph A: bar chart of three types of scaffolds the contact angle of the three scaffold types. This graph shows the reduced water contact angle indicating a significantly higher hydrophilic characteristics for all the scaffold types after the plasma treatment. 3 B: images of water contact angle of the three types of scaffolds.

4.2.5. Heparin binding to the allylamine-functionalised membranes (binding of fluorescein-labelled Heparin)

To bind the growth factors to the membrane, a heparin coat needs to be done to the plasma-treated scaffolds as mentioned earlier in the section (3.2.5.2). This method mimics and reflects what happens in our bodies regarding the binding between the heparin and growth factors. In our body, in the extracellular matrix, there are proteins they got heparan sulphate and the growth factors have a binding side which will bind to the heparan sulphate. Without this binding side, the growth factors will not be able to bind to heparin. Furthermore, we coated the plasma-treated scaffolds with heparin to mimic this bind as the growth factors will not bind very well to the plasma-treated scaffolds without the heparin-binding existence.

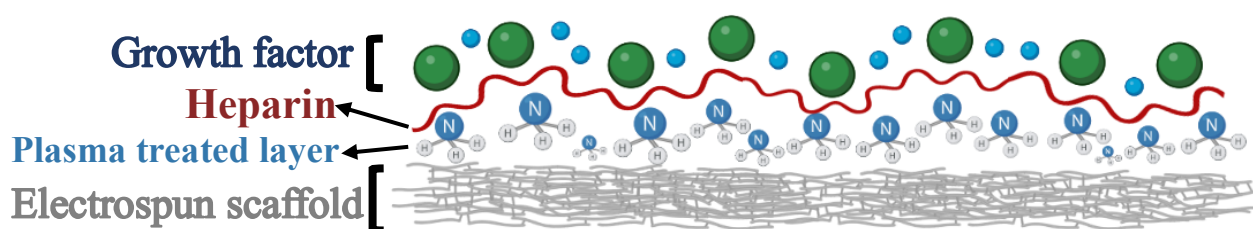


Figure 4.23: diagram showed the coating layers of the biofunctionalized scaffolds which were plasma treated with allylamine and then coated with heparin followed by growth factors.

To confirm the binding of heparin to the plasma-treated membranes and assess the heparin-binding to plasma-treated electrospun scaffolds a fluorescein labelled heparin was used. By measuring the fluorescence fluorescent heparin solution, the amount of the heparin will be known. As the fluorescent heparin contains 1 molecule of fluorescein for each molecule of heparin.

The plasma-treated scaffold samples were coated with 200 μl of fluorescent heparin solution containing 2.5, 5, 10, 20, and 40 μg of the heparin each. The fluorescein-labelled heparin

contained 1 mole of dye per mole of protein. After 24 hours the unbound heparin solution was transferred to the 96-well plat. The plate was taken to the plate reader, to measure the fluorescence of unbound fluorescein-labelled heparin.

Figure 4.24 shows the relationship between the fluorescence of the fluorescein molecules and molecules of heparin. When the fluorescein-labelled heparin diluted down, the fluorescent decreased. This results in straight line, which shows the amount of fluorescence from the fluorescein label is directly proportional to the amount of heparin. The results validated that the fluorescein-labelled heparin can be used to investigate the binding of heparin to the plasma treated membranes more in depth.

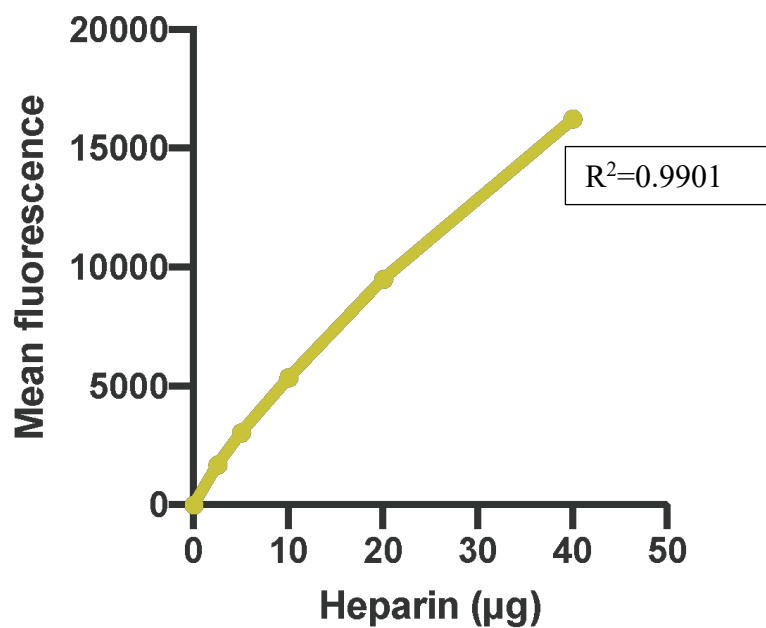


Figure 4.24: different amounts of fluorescein-labelled heparin was added to the plasma-treated scaffolds and plotted against how much was bound out of the total amount added after a 24-hour incubation at 20 degree in the dark.

Figure 4.25 showed that the heparin bound to the plasma-treated scaffolds. The results displays that the more heparin was added to the scaffold, the more heparin binding will accrue. Moreover, the table below shows the percentage of the bounded heparin of each amount added to the heparin.

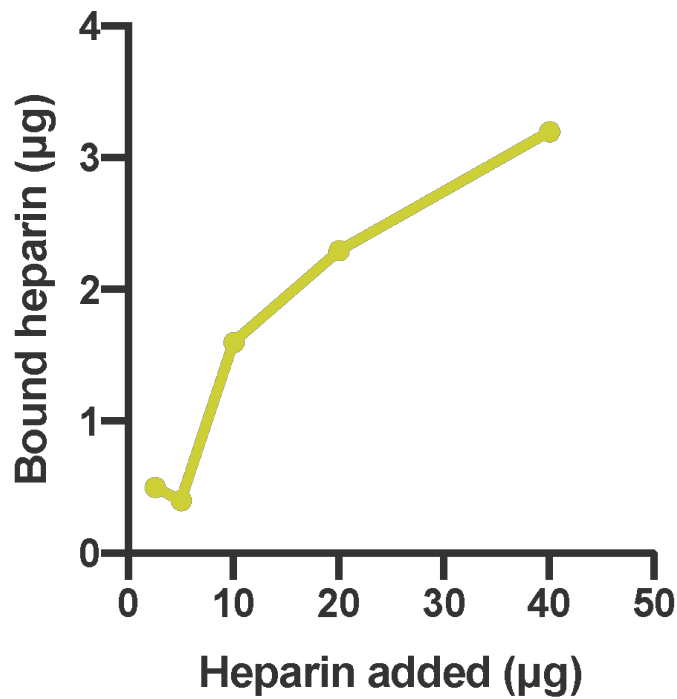


Figure 4.25: different amounts of heparin were added to the plasma-treated scaffolds and plotted against how much was bound out of the total amount after 24 hours at 20 degree C incubation in the dark.

Table 4.4: The percentage of how much heparin bound to the plasma scaffolds.

Amount of heparin added (µg)	Bound heparin %
2.5	19.2
5	7.8
10	16
20	11.6
40	8

4.2.6. Binding of growth factors (TGF- β 1, TGF- β 3 and FGF-2) to heparin-functionalised membranes

The binding of the growth factors was investigated using full length heparin, Low Molecular weight (LMW) heparin and heparan sulphate. The figures below presented the binding of three types of growth factors (TGF- β 1, TGF- β 3 and FGF-2) to glycosaminoglycan functionalised scaffolds. This was to explore how different each type of growth factor binds to GAGs.

For these experiments 96-well plates which had been commercially treated with cold plasma deposition of allylamine were used. The GAGs were incubated in 200 μ l PBS in the wells (10ng/well) overnight. Unbound heparin was removed and the wells washed with PBS followed by incubation with the individual growth factors. After removal of unbound growth factors, the bound growth factors were detected using specific antibodies (see section 3.2.10).

The results indicated that all the growth factor types bond to the heparin, LMW heparin and heparan SO₄ to a different degree.

Figure 4.26 showed TGF- β 1 and FGF-2 bound better with the heparin functionalised surface. While TGF- β 3 binds better to heparan SO₄ than the heparin and LMW heparin.

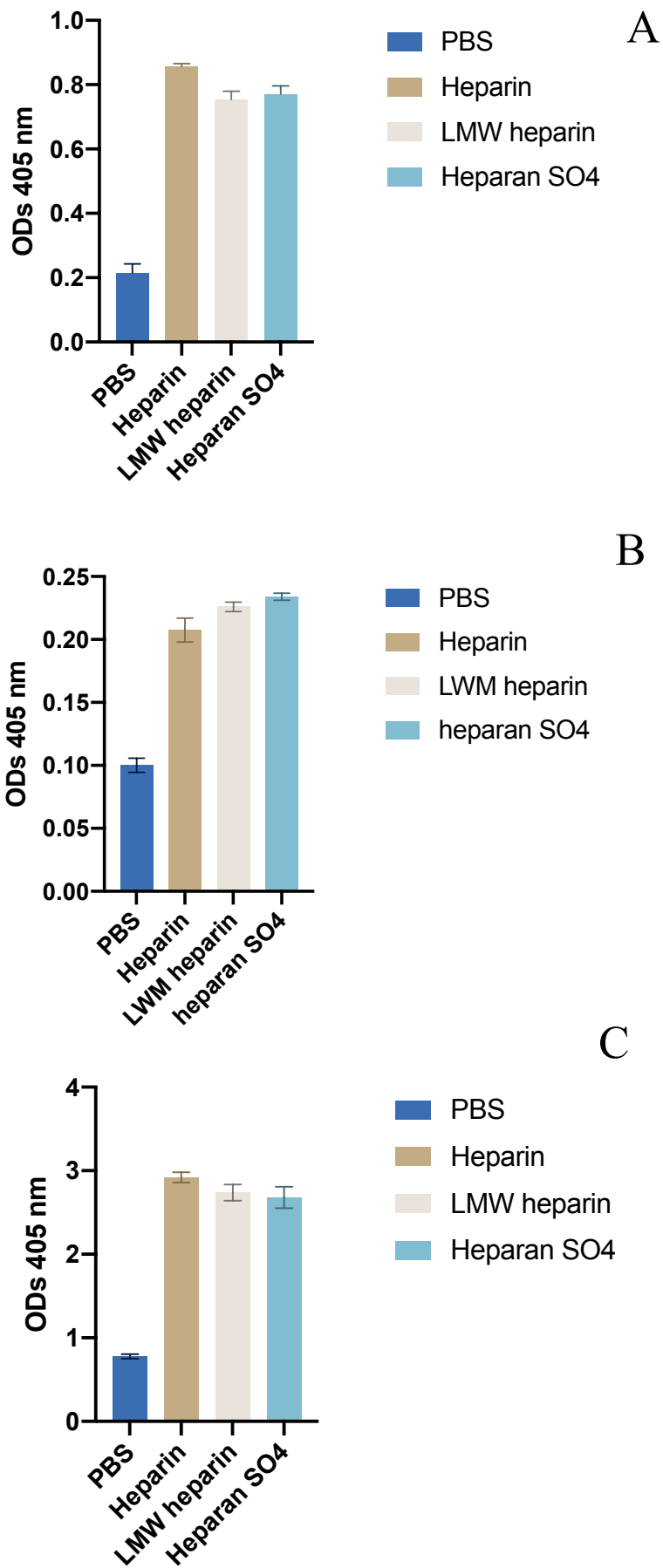


Figure 4.26: different growth factors binding to several example sulphated glycosaminoglycan immobilised on an allylamine functionalised surface. Binding of A: TGF-Beta 1, B: TGF-Beta 3 and C: FGF-2 growth factors. The values are the mean \pm SD of 3 experiments, each is performed in triplicate.

4.2.7. Measurement of binding of the growth factors to plasma treated aligned PCL scaffolds and the elution of the growth factors from the scaffolds

ELISA is a very sensitive test, it is used to detect and quantify substances such as proteins, hormones, antigens, and antibodies. This was achieved by complexing antibodies and antigens to accomplish the result. Each antibody type has a specific region which binds to specific antigens. This interaction between the antibodies and the antigens is applied in ELISA test and let identify specific antibodies and antigens. The total added amount of growth factors to the biofunctionalized membrane are very small, so The ELISA was the best available option to measure the unbound growth factors.

The concentration of all the solutions in the kit was worked out according to the manufacture suggestions then a standard curve was plotted by log of OD against the optical density. Graph pad prism then was used to calculate the concentration by the four-parameter logistic (4-PL) curve fit. Firstly, standard curves for each growth factor (TGF-beta 1, TGF-beta 3 and FGF-2) were prepared to ensure linearity and sensitivity as recommended by the manufacturer. For ELISA, usually, the relationships between optical density (OD) and concentration of the samples are not linear. However, the $\log_{10}OD$ of the standard curves were linearized by plotting the \log_{10} of the OD values of the known standards versus the \log_{10} of the concentration of the known standard. then the analysis was applied to establish the formula for the conversion of OD to growth factor levels.

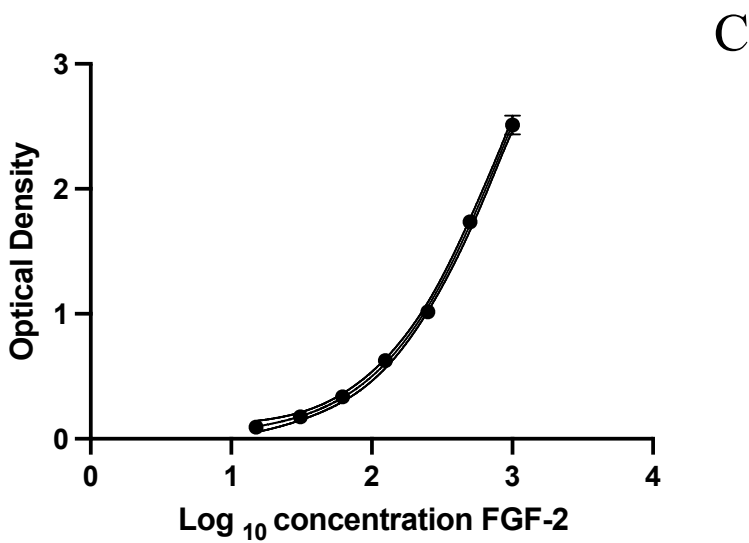
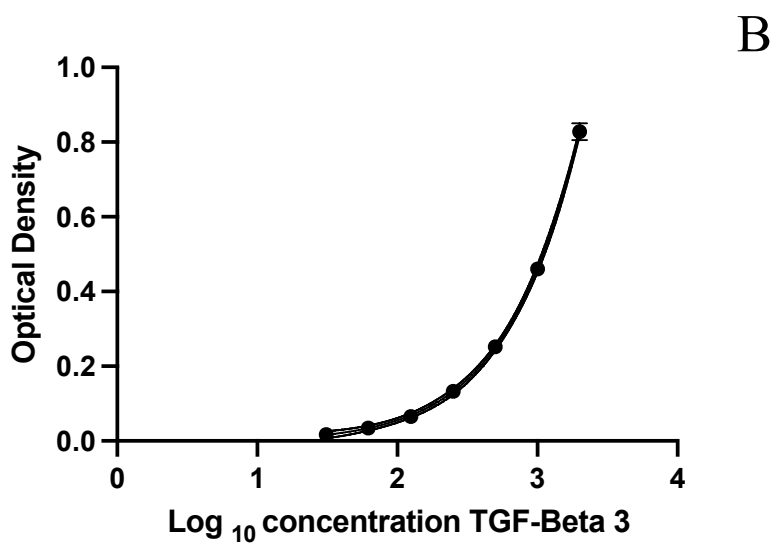
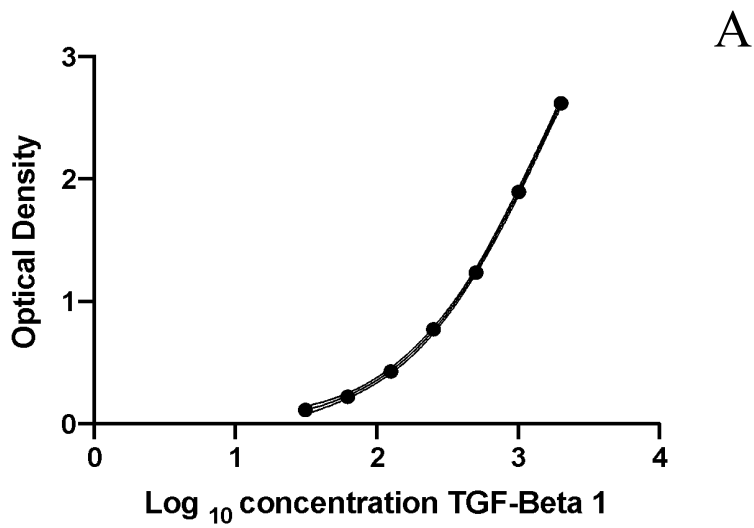


Figure 4.27: sample calibration curve for ELISA A: TGF-Beta-1, B: TGF-Beta-3 and C: FGF-2. The standard curve in between optical density and the different growth factors concentration was linearized by applying logarithmic transformation.

the results showed that all the growth factors were bonded with different levels to the functionalized scaffolds. Elution of the bound growth factors was followed over the following 14 days. TGF- β 3 did not bind as strongly compared to the binding of TGF- β 1 and FGF-2 growth factors. Moreover, about 97% of the TGF- β 1 was bound to the functionalized scaffold which was the strongest bound. Followed by FGF-2 with 90% of the growth factor bound to the functionalized scaffold. Where the lowest bound was recorded with TGF- β 3 with 66% bound.

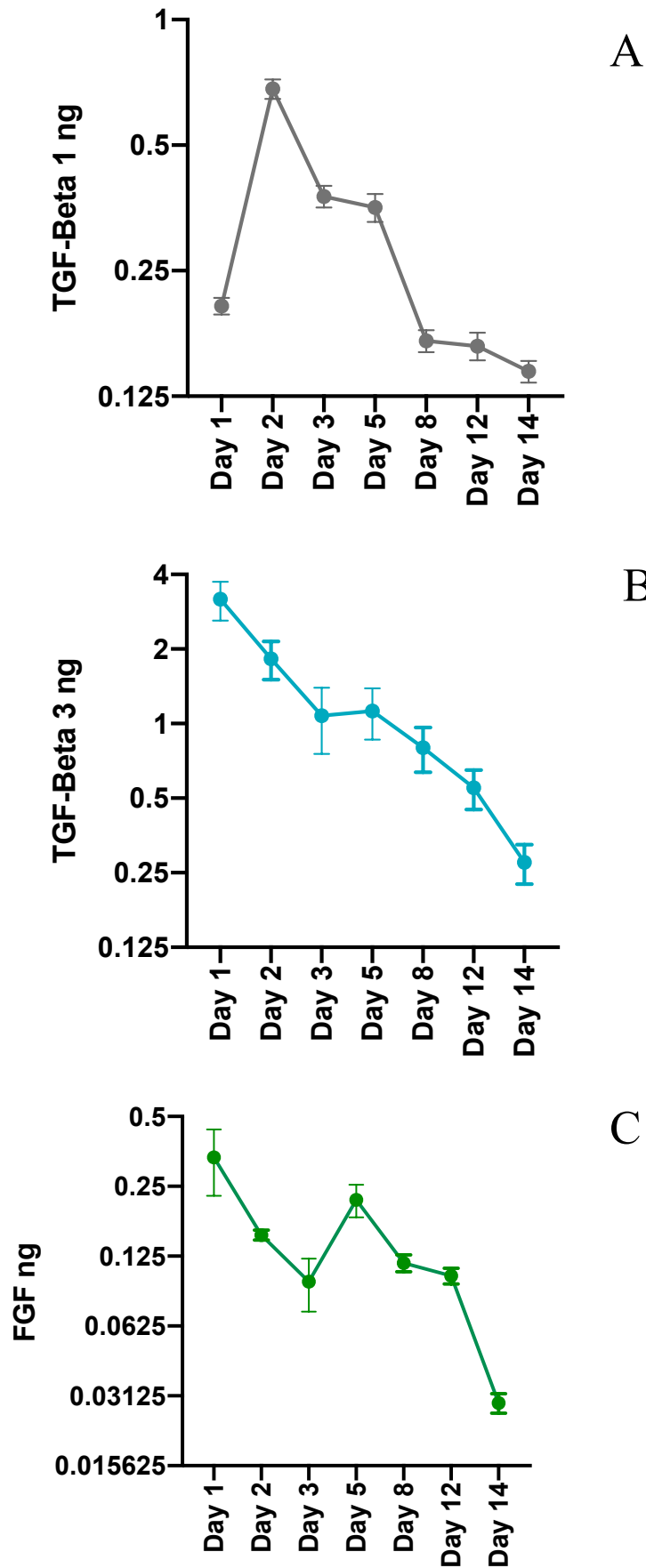


Figure 4.28: shows the release of A: bound TGF-Beta 1, B: bound TFG-Beta 3 and C 3: bound FGF growth factors from the functionalised scaffolds over 14 days. Highest level of release was recorded in day 1 for TGF-Beta 3 and FGF, were for TGF-Beta 1 the highest level was in day 2. All activated membrane demonstrated a release of the growth factors until day 14 but in at deferent rates.

4.3.1. DNA PicoGreen assay

The Quant-iT™ PicoGreen assay was used to quantify the cell number by measuring the DNA content of the cell/scaffold constructs immediately after seeding the scaffolds (after 48 h) with HPDLs cells, after incubating the cell/scaffold constructs for 35 days in culture medium with 1 mg/ml BSA and culture medium containing 5% FCS and after incubating the cell/scaffold constructs for 35 days in culture medium with 1 mg/ml BSA and culture medium without 5% FCS. Three experiments were performed, and the graphs below represent the average of repeats in each group.

The figures of the seeded scaffolds incubated with 5% of foetal calf serum samples presented a significant increase in cell number compared to those incubated without serum samples. Figure 4.30 shows the random fibre PLLA scaffolds incubated in medium with serum where the TGF-beta 3 sample functionalised scaffolds recorded the highest DNA content. Similar results were obtained with the random fibre PCL scaffolds incubated with medium containing 5% serum and aligned fibre PCL scaffolds incubated with medium and 5% serum, as shown in figures B and C, respectively. In figure 4.31, the samples were incubated in medium without serum, the DNA content was higher in the TGF-β3 functionalised random fibre PCL scaffolds, while in the aligned PCL scaffolds, the plasma and heparin functionalised scaffolds recorded high content.

Figure 4.29 the DNA content of scaffolds immediately after 48 hours of seeding. In this figure random fibre PCL scaffolds showed the greatest DNA content in the TGF-β3 functionalised scaffolds while the aligned fibre PCL scaffolds recorded the highest DNA content in allylamine plasma treated scaffolds. The DNA content was highest for all the assays of the allylamine plasma treated scaffolds of the aligned PCL after 48 hours of seeding. Further high DNA

content was observed in the aligned PCL with serum in the TGF- β 3 sample and lowest DNA content in the scaffolds without serum samples. The 48 hours results of aligned PCL functionalised with TGF- β 3 were the highest after the plasma level.

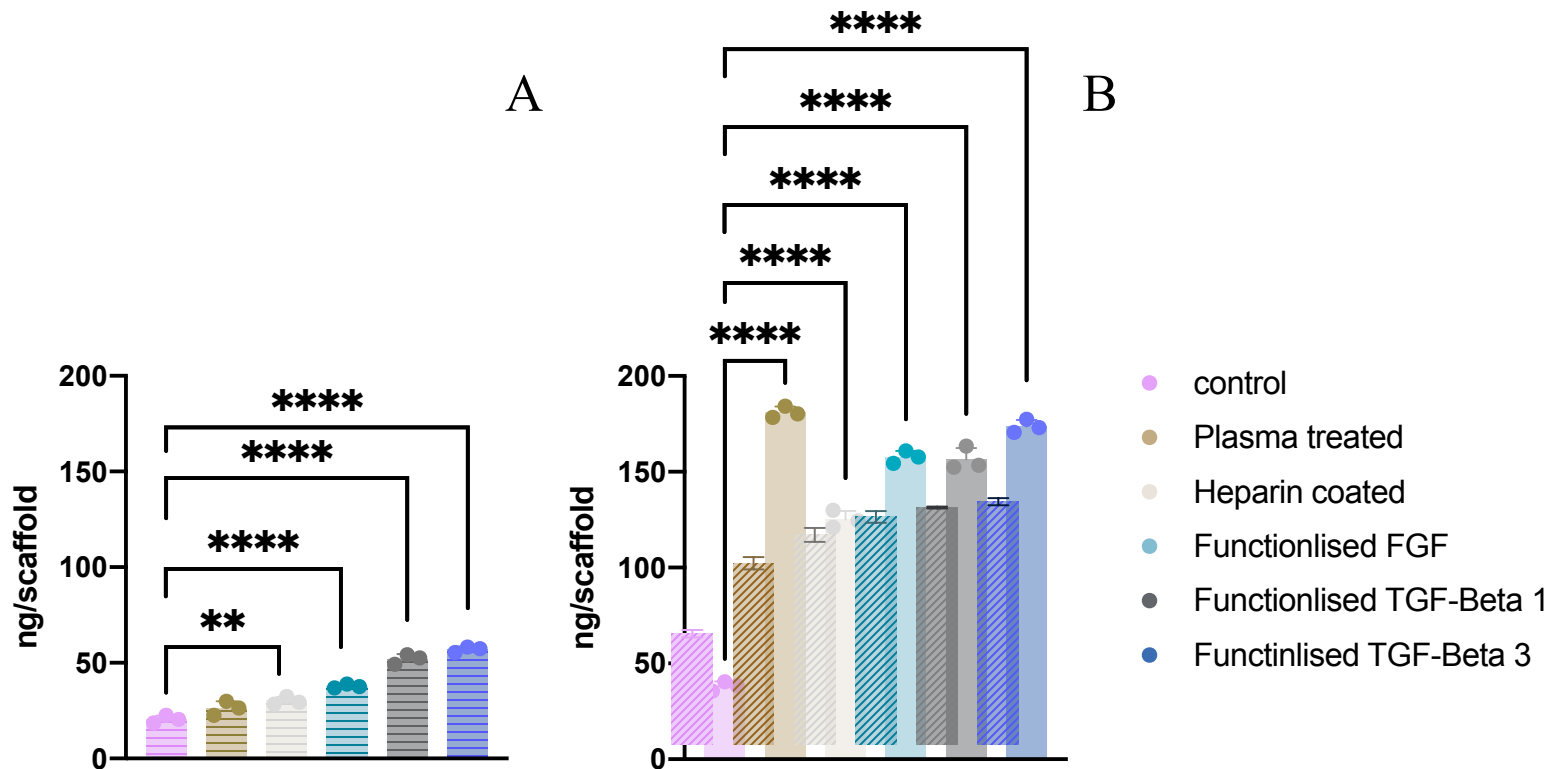


Figure 4.29: shows the DNA quantification using PicoGreen dye 48 hours after seeding. A: Random PCL scaffolds with and without functionalisation and B: Aligned PCL scaffolds with and without functionalisation. The values are the mean \pm SD of 3 experiments, each is performed in triplicate.

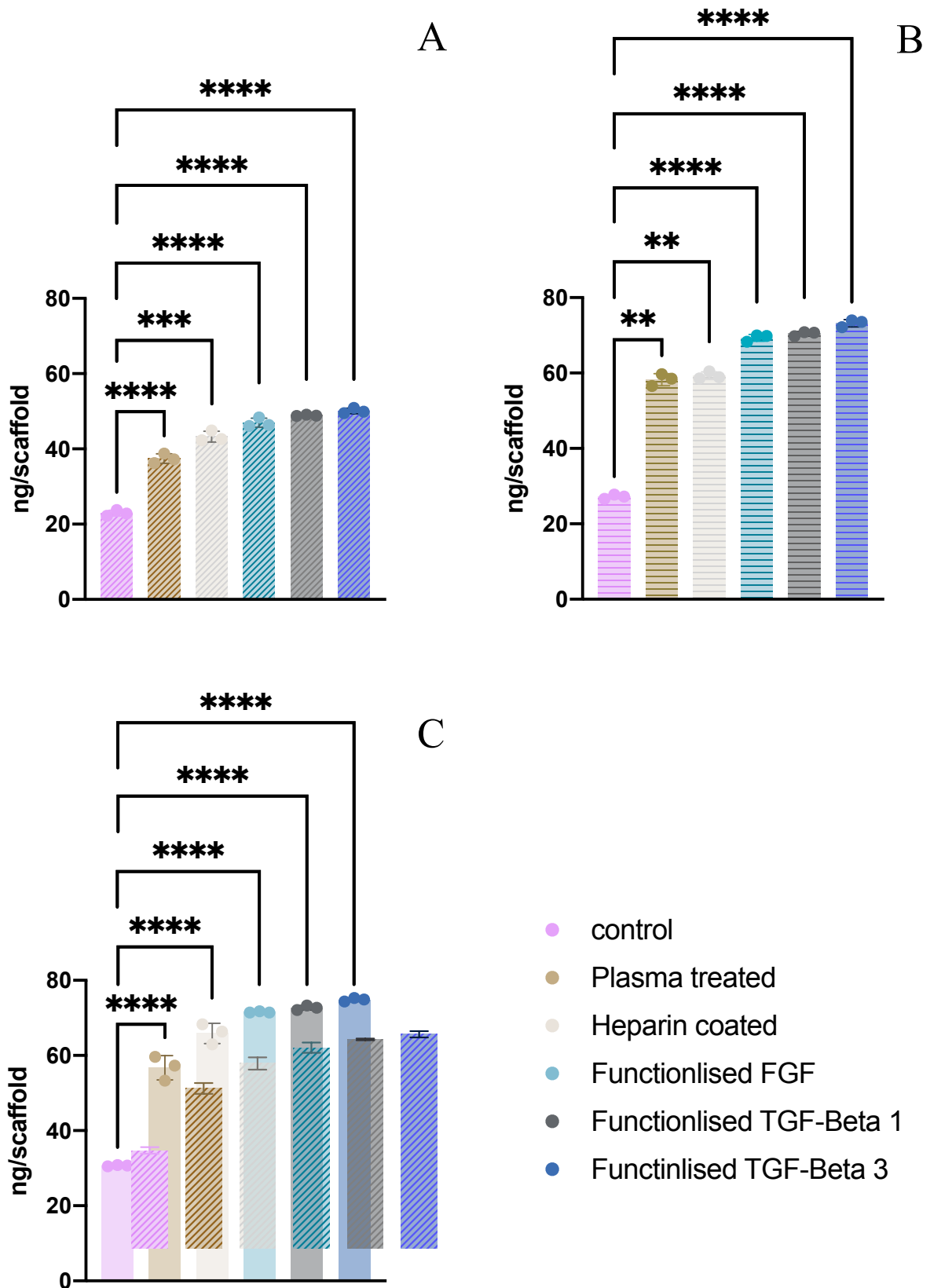


Figure 4.30: shows the DNA quantification by PicoGreen DNA content assay on day 35. A: Random PLLA scaffolds with 5% serum, B: Random PCL scaffolds with 5% serum and C: Aligned PCL scaffolds with 5% serum. The values are the mean \pm SD of 3 experiments, each is performed in triplicate.

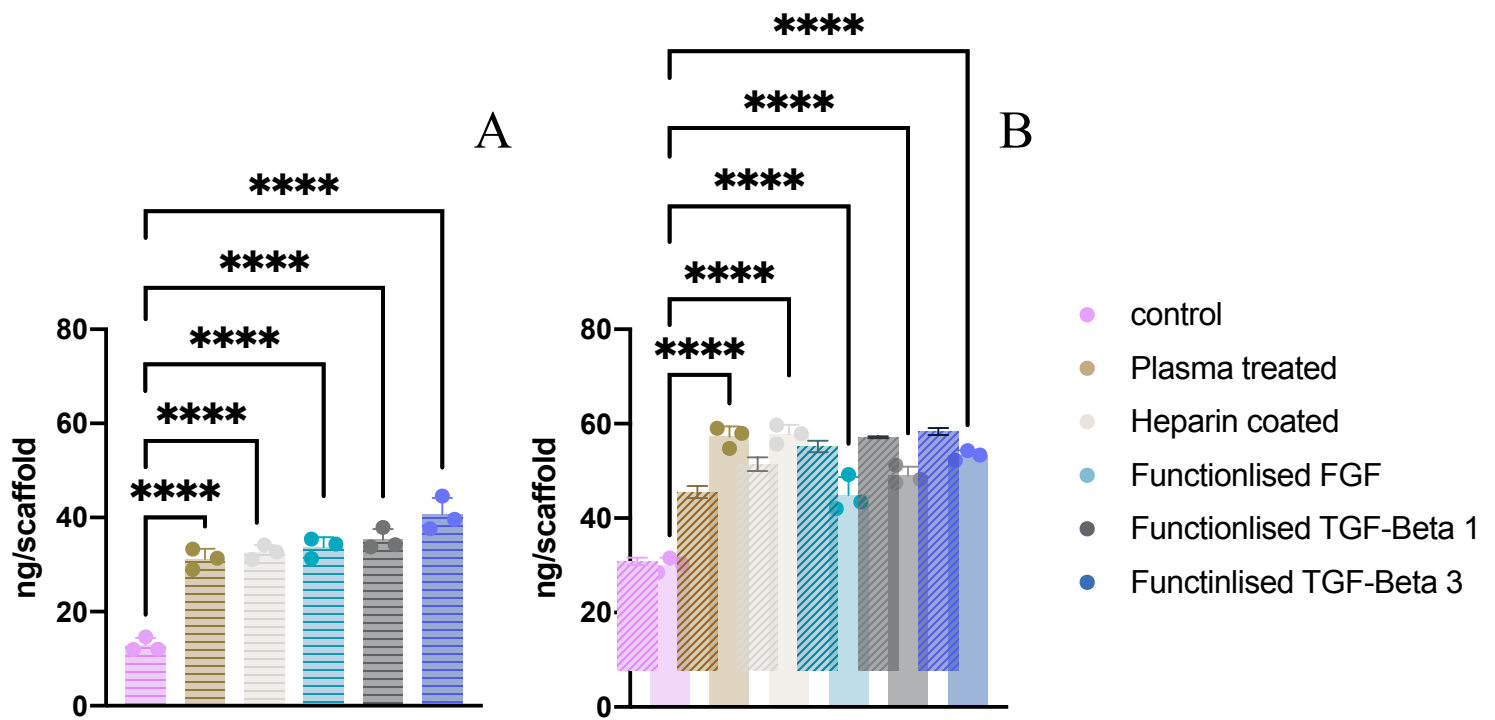


Figure 4.31: shows the DNA quantification by PicoGreen DNA content assay on day 35 without serum. A: Random PCL scaffolds and B: Aligned PCL scaffolds. The values are the mean \pm SD of 3 experiments, each is performed in triplicate.

4.3.2. Total protein assay (BCA)

BCA assay was performed on scaffold samples which had been incubated for up to 35 days in medium with or without serum. The BCA kit from Sigma UK was utilised. The experiments were done in three repeats, each experiment incubated in medium with or without serum. Each graph represents the average of the experimental repeats.

The BCA assay is used to determine the total protein concentration in a material; hence the protein level is directly proportional to the cell proliferation and attachment properties of a scaffold nanofiber. Figure 4.32 indicates results for protein content in the random fibre PLLA scaffolds incubated with 5% serum; the TGF- β 3 functionalised scaffolds showed the highest amounts of total protein. Similar results were obtained with the TGF- β 3 functionalised random fibre PCL scaffolds incubated in the presence of 5% serum, aligned PCL with serum, random PCL without serum, and aligned PCL without serum, as shown in figures 4.33.

However, the without serum assays were significantly higher than those with serum which is opposite to the DNA results.

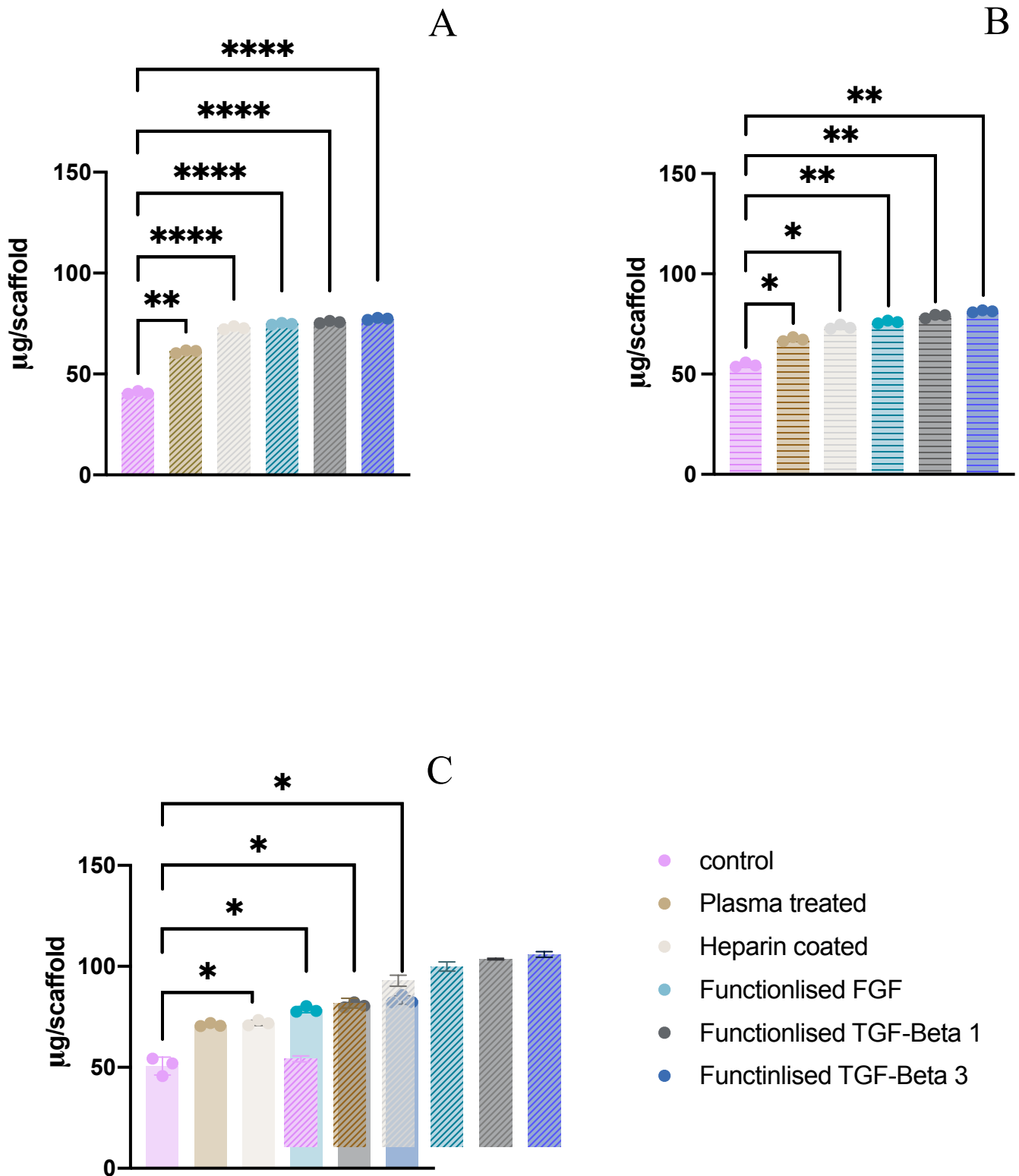


Figure 4.32: shows the total protein of Human Periodontal Ligament cells seeded to A: Random PLLA scaffolds, B: Random PCL scaffolds and C: Aligned PCL scaffolds all with 5% of serum for 35 days. P values were established using ANOVA. Data is presented as mean \pm SDs of 3 experiments, each is performed in triplicate.

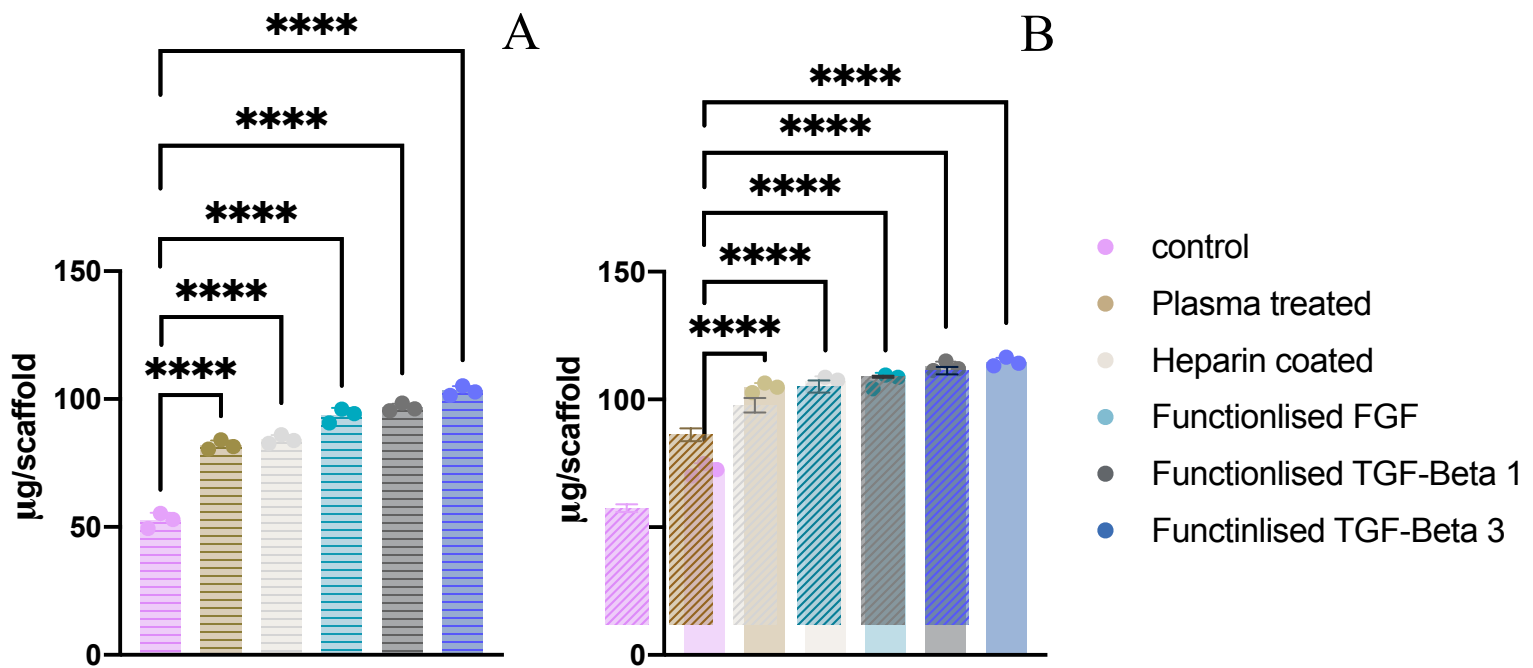


Figure 4.33: shows the total protein of Human Periodontal Ligament cells seeded onto A: Random fibre scaffolds and B: Aligned fibre PCL scaffolds both without serum for 35 days. P values were established using ANOVA. Data is presented as mean \pm SDs of 3 experiments, each is performed in triplicate.

4.3.3. Alkaline phosphatase assay

Alkaline phosphatase (ALP) is a well-characterised accepted marker for osteogenic cells. ALP is a glycoprotein hydrolase found in -the body in different forms depending on the cell origin. In the cell, usually, it is on the cell membranes on its extracellular surface. Alkaline phosphatase activity was measured to find out the ALP activity in the seeded HPDL cells in the scaffolds. By measuring the ALP activities of the cells, the high level of the activities indicates that the periodontal ligament cells are changing to osteogenic cells.

Each graph below represents an average of three repeated experiments. Figure 4.34 below show results for ALP activity on the seeded HPDL cells in scaffolds. The assay measured the differential potential of the cells in the aligned and random PLLA and PLC scaffolds. The results

demonstrated little ALP activity in all the samples, as shown in figure 4.34. which means the cells does not produce high amount of ALP after 35 days of seeding.

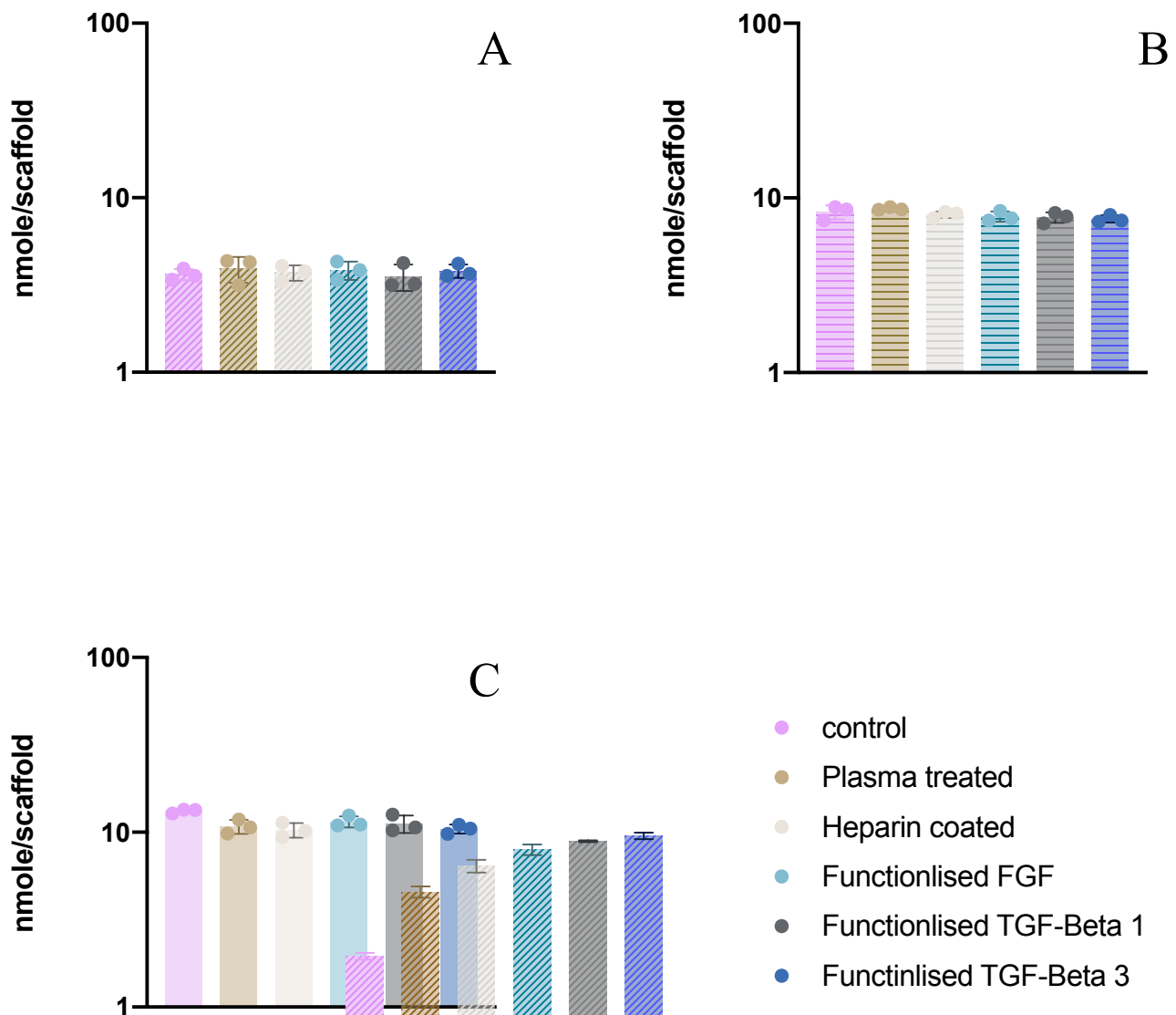


Figure 4.34: shows ALPA expression on the seeded A: Random PLLA scaffolds, B: Random PCL scaffolds and C: Aligned PCL scaffolds all with 5% of serum cultured for 35 days. The ALPA amount in all type of scaffolds are nearly the same which indicated the ALPA activity is very low after 35 days of HPDLs cultured. Data is presented as mean \pm SDs of 3 experiments, each is performed in triplicate.

4.3.4. Total collagen assay

In the periodontal ligament, collagen type I is the major protein abundant in the extracellular matrix. For periodontal ligament regeneration and alveolar bone remodelling, collagen plays an essential role. The total collagen quantity was measured and established by the total collagen assay.

After 35 days of incubation, each scaffold was lysed per Abcam's description of the total collagen kit, and the assay followed the kit's instructions. For each group represented in the graph below (figure 4.35), the experiment was repeated three times and the figures represent their average.

Collagen content was measured in PCL aligned fibre scaffolds and random fibre scaffolds with and without incubation of 5% serum. For both aligned fibre and random fibre scaffolds, the TGF-beta-3 functionalised constructs incubated in medium with serum showed the highest level of collagen contents. Figure 4.35 (A&B) with the aligned fibre scaffold giving the highest values. Similarly, in constructs incubated in the absence of serum, (Figure 4.35 C&D) the random fibre PCL showed the highest collagen content in the TGF-beta 1 and 3 functionalised scaffolds. But these values were lower than those for the plasma treated PCL aligned fibre scaffolds, as illustrated in figures 4.35. The samples of the three types of scaffolds all showed more collagen production with serum compared to the samples without serum.

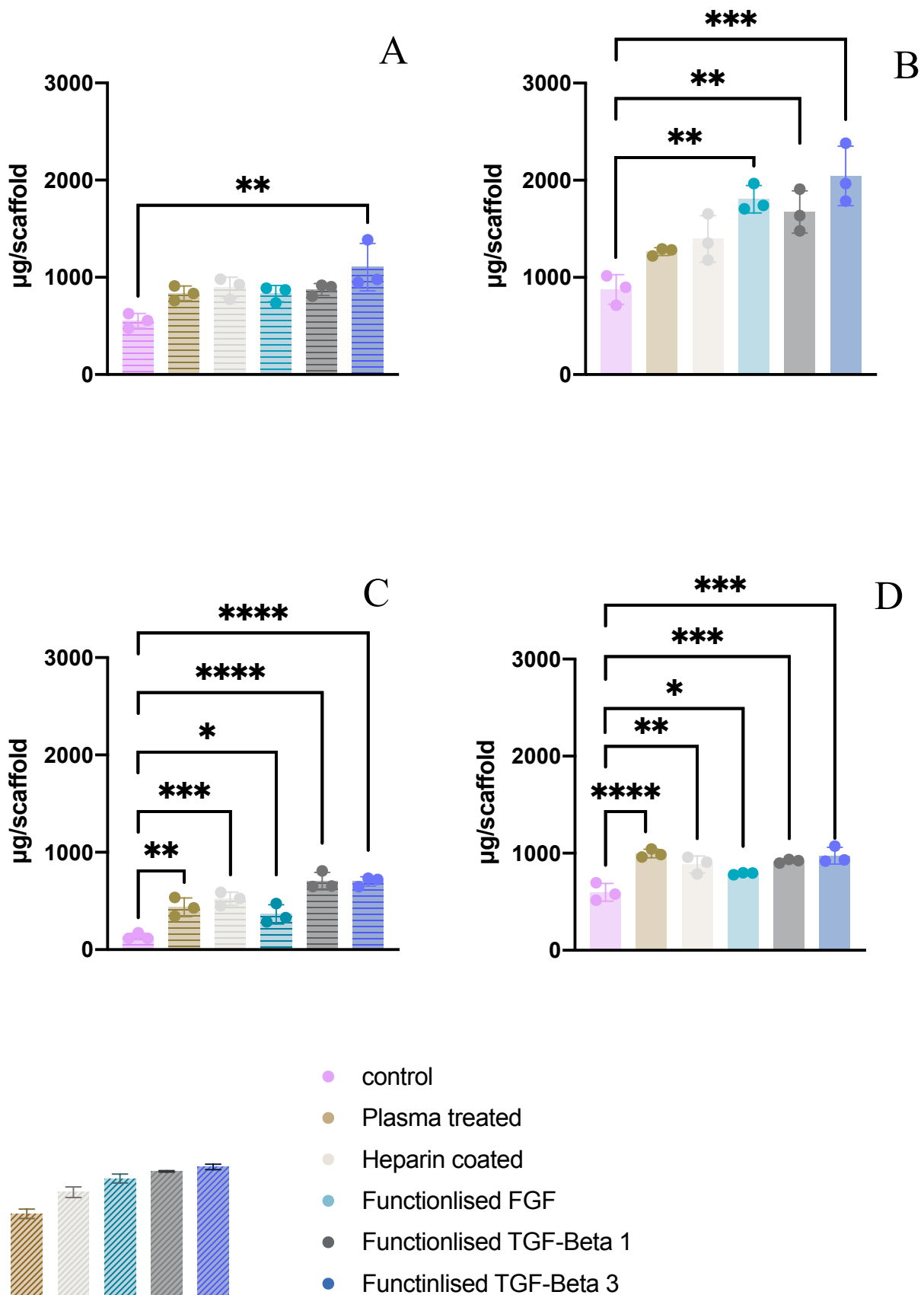


Figure 4.35: shows the total Collagen of HPDL cells seeded to A: Random fibre PCL, B: Aligned fibre PCL incubated in medium with serum and C: Random fibre PCL, D: Aligned fibre PCL without serum all experiment for 35 days. P values were established using ANOVA. Data is presented as mean \pm SDs of 3 experiments, each is performed in triplicate

4.3.5. Hematoxylin and Eosin staining

The figures (4.36, 4.37, 4.38 and 4.39) below represent histology images of seeded functionalised and non-functionalised scaffolds of random fibre and aligned fibre PCL. The HPDL cell/scaffold constructs were incubated with 5% serum or without serum to investigate the architecture of the produced tissue after 5 weeks of incubation. The experiments were to investigate the difference in the extracellular matrix between incubating the cell/scaffold constructs with serum and without serum.

Due to the chemical attraction between the dye and the produced tissue in the scaffolds, the basophilic structures with nucleic acid moieties are stained blue by hematoxylin stain. While the eosin stain is acidic and counterstains the basic parts such as cytoplasm, muscle, and collagen.

Histological imaging for the random and aligned PCL indicated a thin layer of HPDLs covering the outer surface of the scaffolds along with some migration into the depth of the scaffold. Aligned PCL scaffolds incubated with serum demonstrated abundant cells in the heparin sample compared to the control and plasma imaging, as shown in figure 4.36. The random PCL scaffolds with serum show abundance in cells in the TGF- β 1 growth factor compared to TGF- β 3 growth factor and FGF-2 growth factor biofunctionalization (see figure 4.37). The without serum experiment shows the abundance of cells in the aligned and random PCL scaffold in the TGF- β 1 growth factor, as shown in figures 4.38 and 4.39, respectively.

This imaging confirmed that HPDL cells were fully attached and distributed all over the scaffolds.

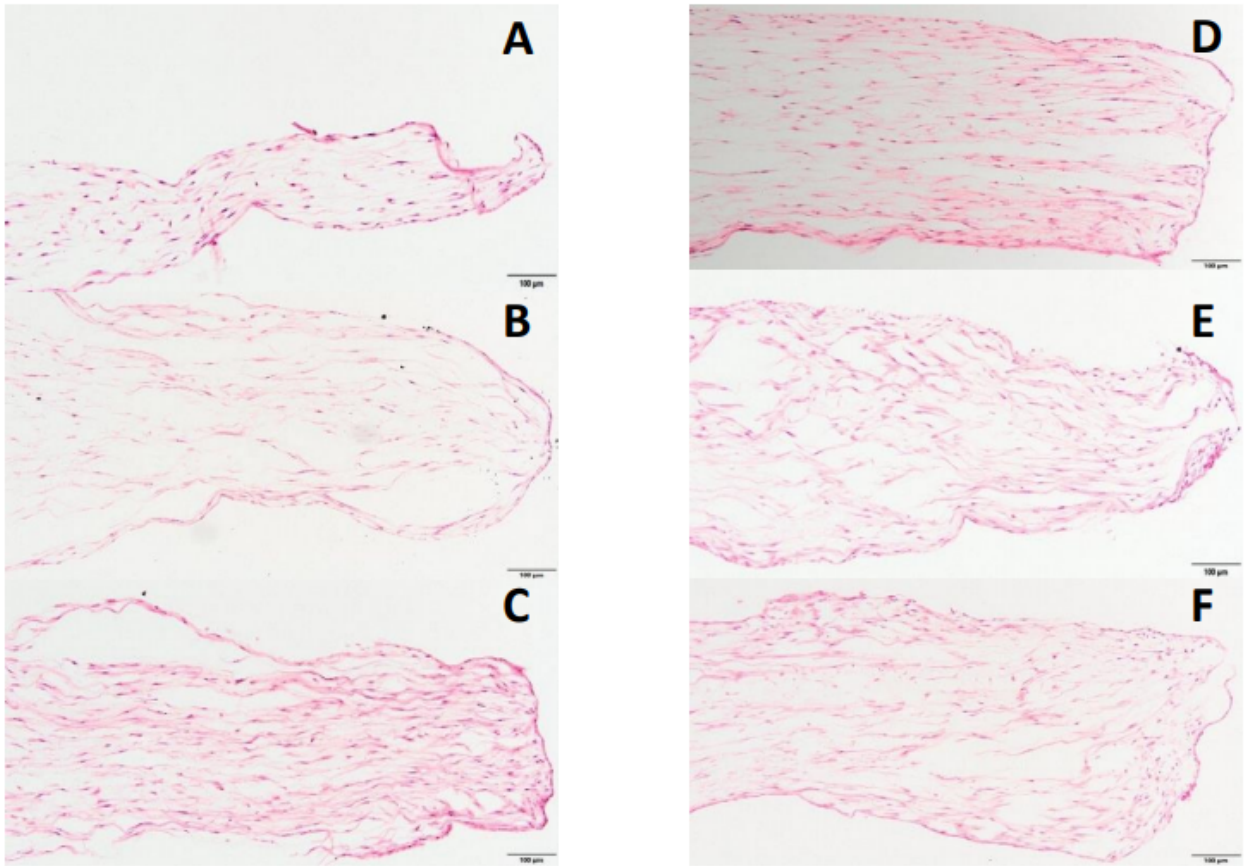


Figure 4.36: shows a light microscope image of H&E stained section of a seeded aligned PCL with 5% serum cultured for 35 days in tissue engineering medium. A: Control, B: Plasma treated, C: Heparin, D: TGF-Beta 1 growth factor, E: TGF-Beta 3 growth factor & F: FGF growth factor. Scale bars = 100 μm .

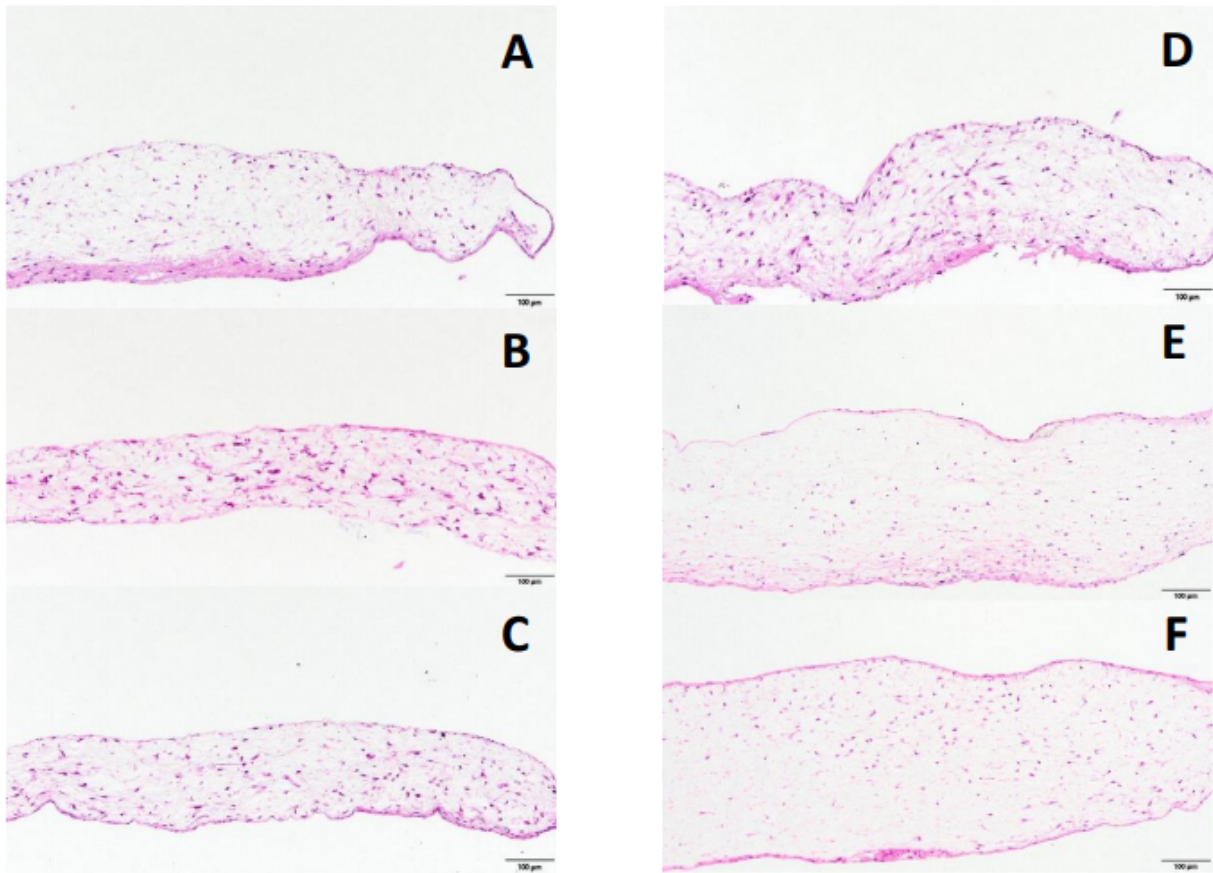


Figure 4.37: shows a light microscope image of H&E stained section of a seeded random PCL with 5% serum cultured for 35 days in tissue engineering medium. A: Control, B: Plasma treated, C: Heparin, D: TGF-Beta 1 growth factor, E: TGF-Beta 3 growth factor & F: FGF growth factor. Scale bars = 100 μm .

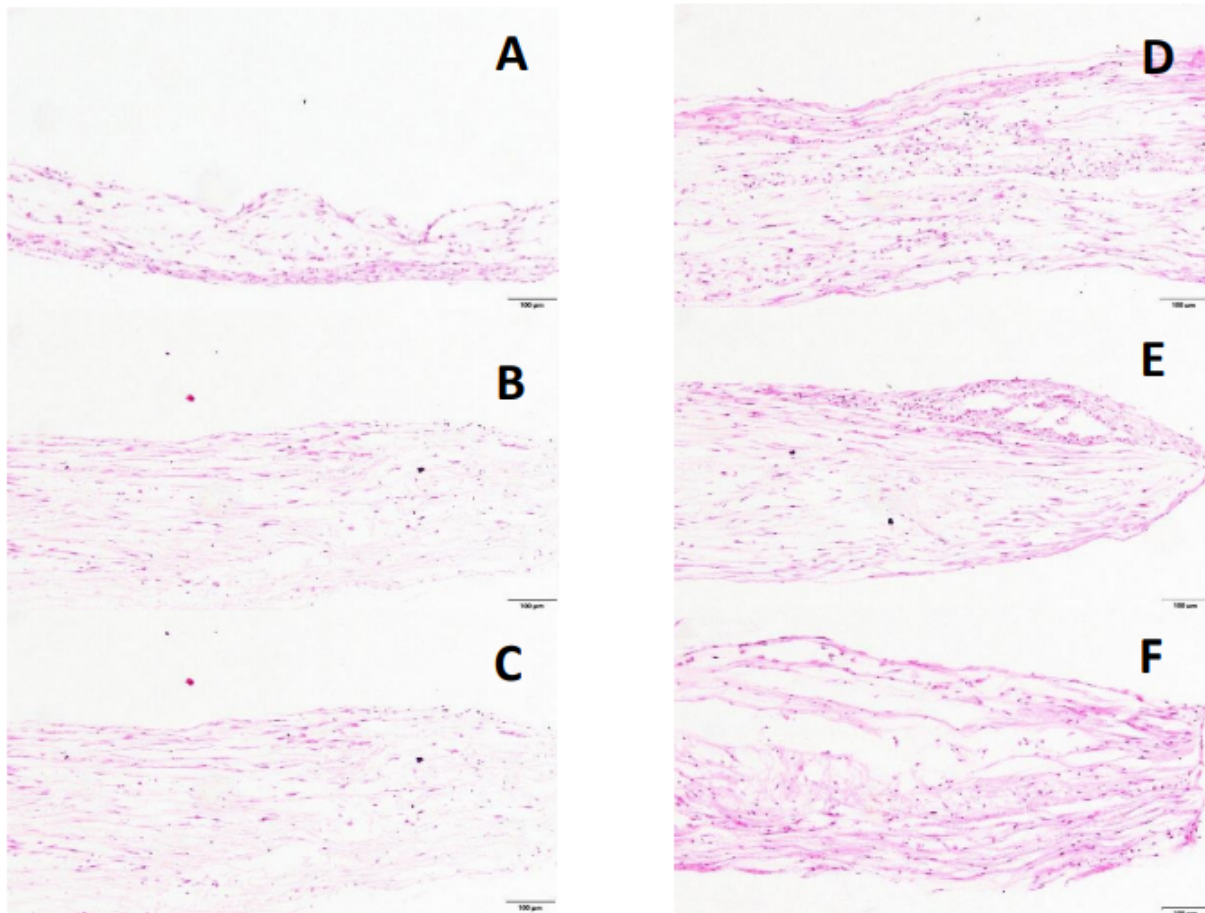


Figure 4.38: shows a light microscope image of H&E stained section of a seeded aligned PCL without serum cultured for 35 days in tissue engineering medium. A: Control, B: Plasma treated, C: Heparin, D: TGF-Beta 1 growth factor, E: TGF-Beta 3 growth factor & F: FGF growth factor. Scale bars = 100 µm.

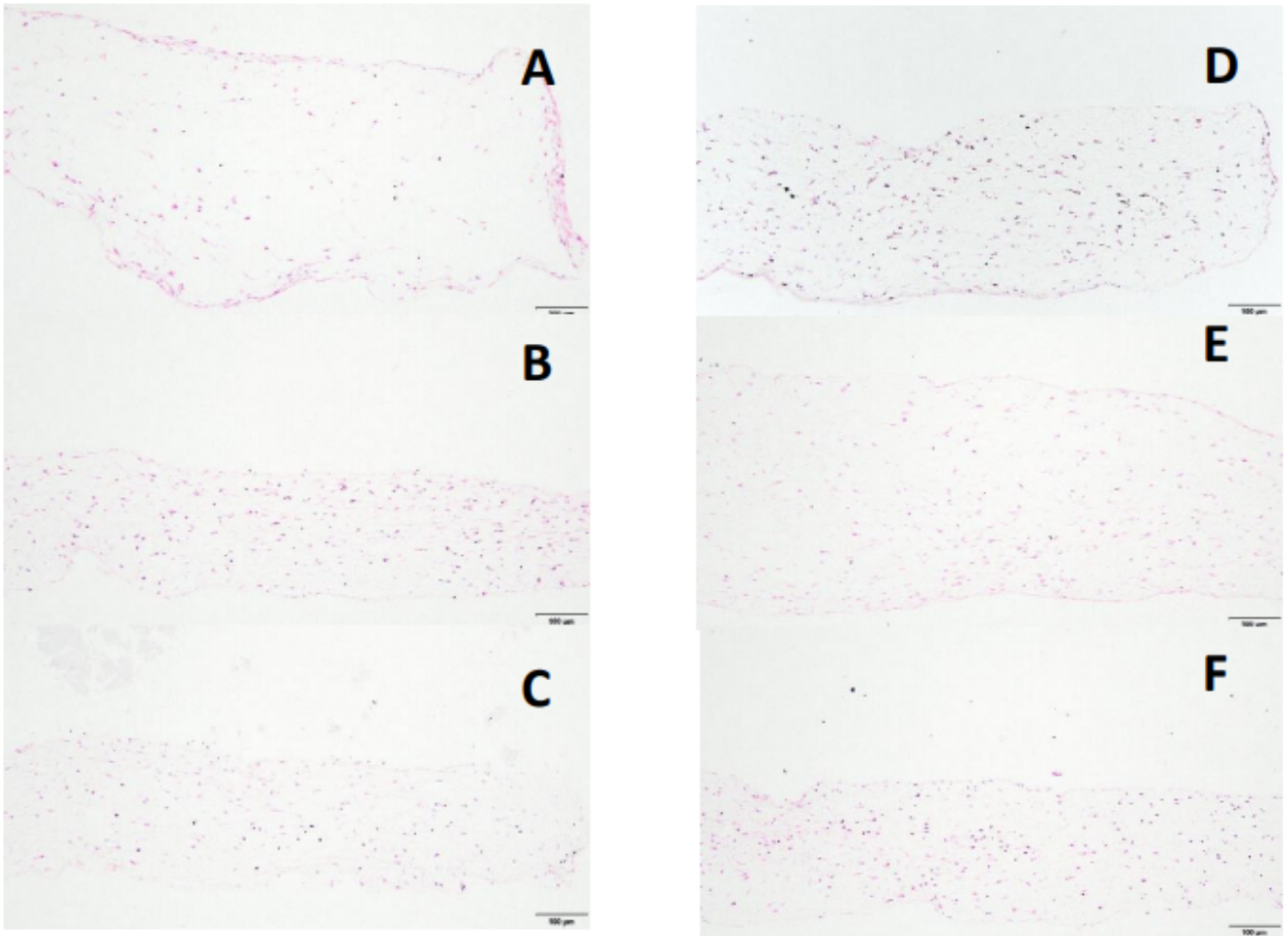


Figure 4.39: shows a light microscope image of H&E stained section of a seeded random PCL without serum cultured for 35 days in tissue engineering medium. A: Control, B: Plasma treated, C: Heparin, D: TGF-Beta 1 growth factor, E: TGF-Beta 3 growth factor & F: FGF growth factor. Scale bars = 100 μ m.

4.3.6. Picro Sirius Red staining (Collagen type I & III)

As mentioned before, collagen type I is the major collagen in periodontal ligament. Followed by collagen type III and others are collagens (V, VI, XII and XIV).

From the imaging, detection of collagen was evident in aligned PCL scaffolds and random PCL scaffolds. Both with and without serum due to the intensity of dark pink staining, as shown below. The samples with serum showed more collagen production from the imaging compared to the without serum samples. However, the aligned PCL seeded scaffold with and without serum indicated more collagen amount compared to the seeded random PCL scaffolds

The image below represents Picro Sirius Red stain stating collagen in aligned PCL scaffolds with serum. Which means the serum helps the HPDLs cells to produce more collagen than without serum.

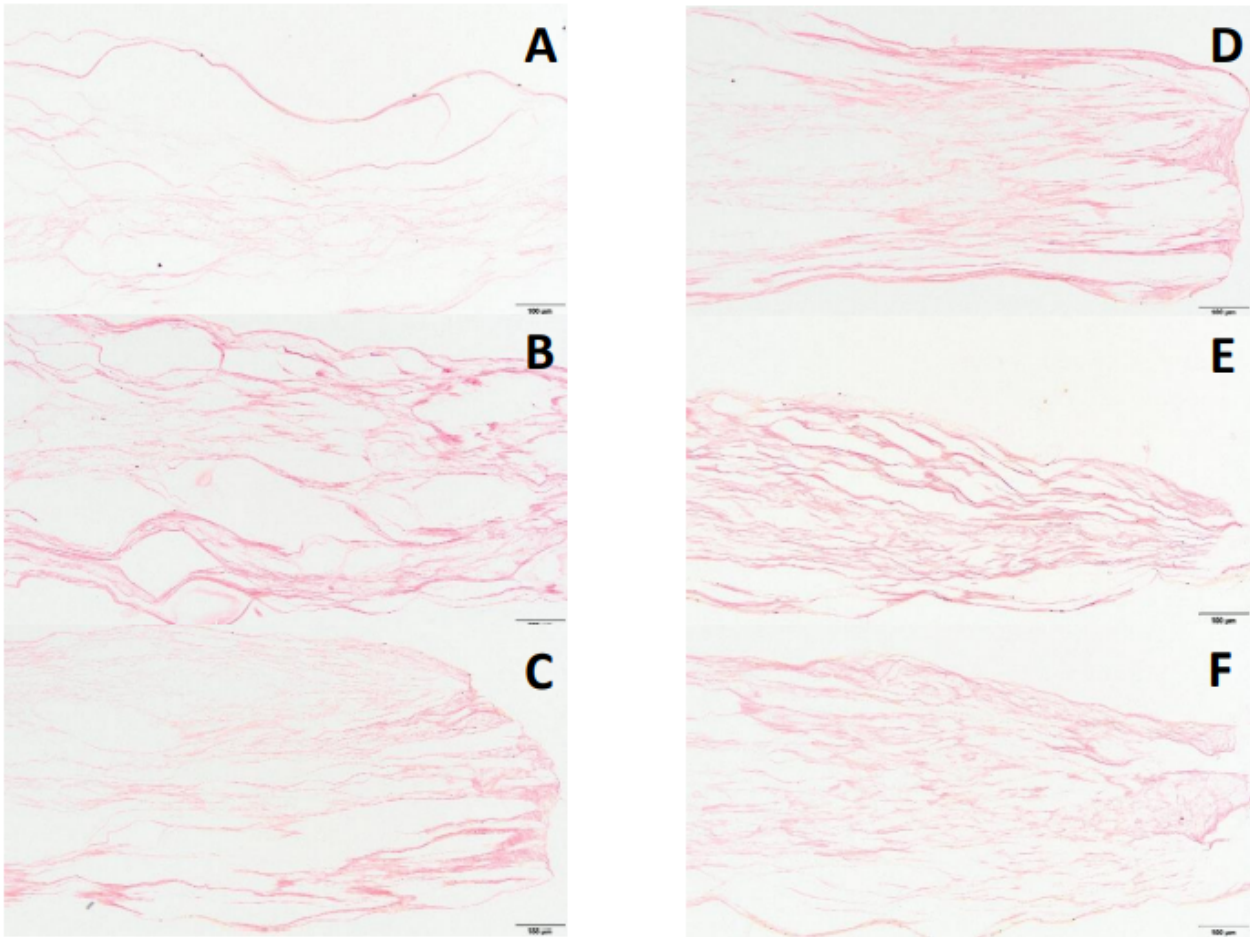


Figure 4.40: shows a light microscope image of Picro Sirius Red stained section of a seeded aligned PCL with 5% serum cultured for 35 days in tissue engineering medium. A: Control, B: Plasma treated, C: Heparin, D: TGF-Beta 1 growth factor, E: TGF-Beta 3 growth factor & F: FGF growth factor. Scale bars = 100 μ m.

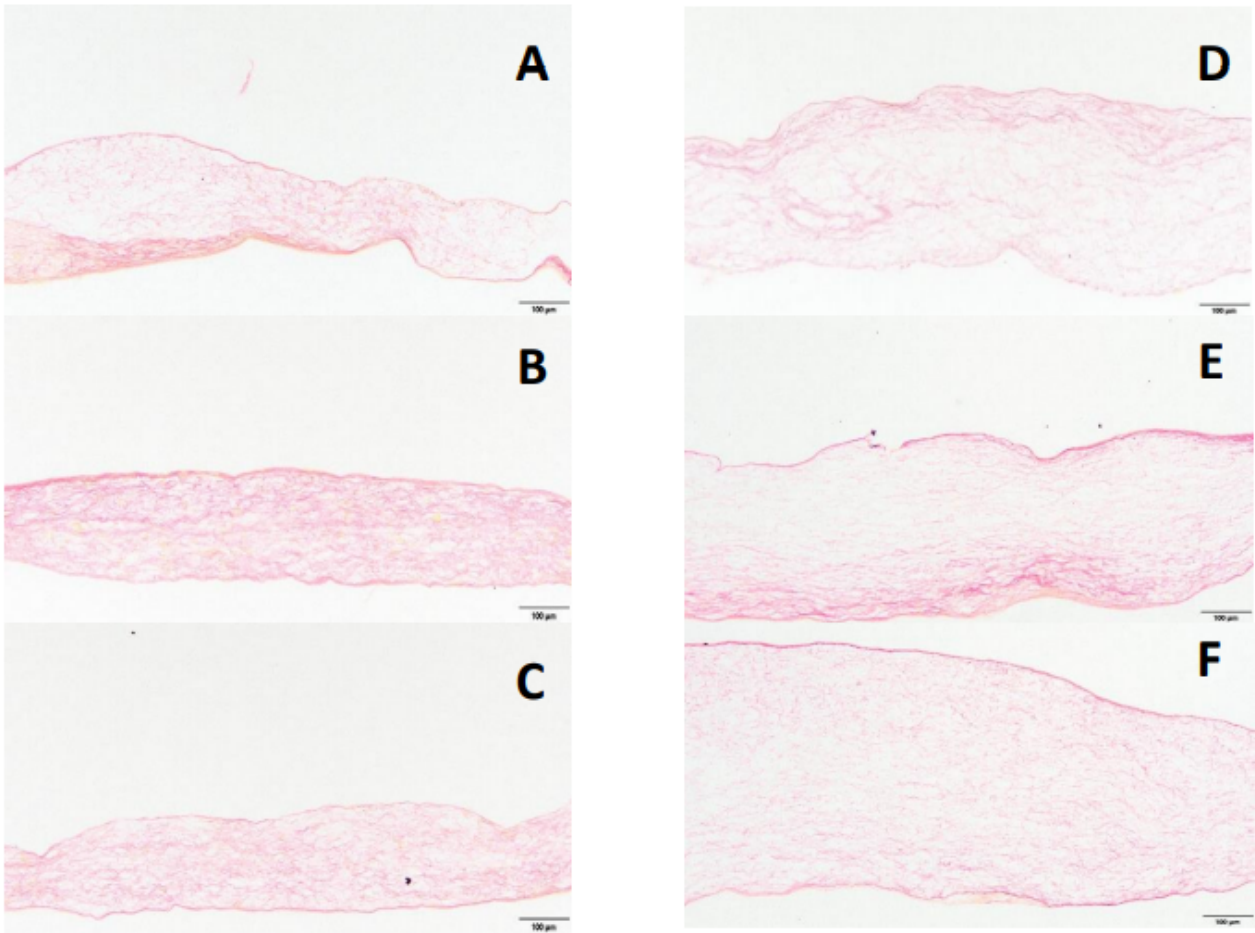


Figure 4.41: shows a light microscope image of Picro Sirius Red stained section of a seeded random PCL with 5% serum cultured for 35 days in tissue engineering medium. A: Control, B: Plasma treated, C: Heparin, D: TGF-Beta 1 growth factor, E: TGF-Beta 3 growth factor & F: FGF growth factor. Scale bars = 100 μm .

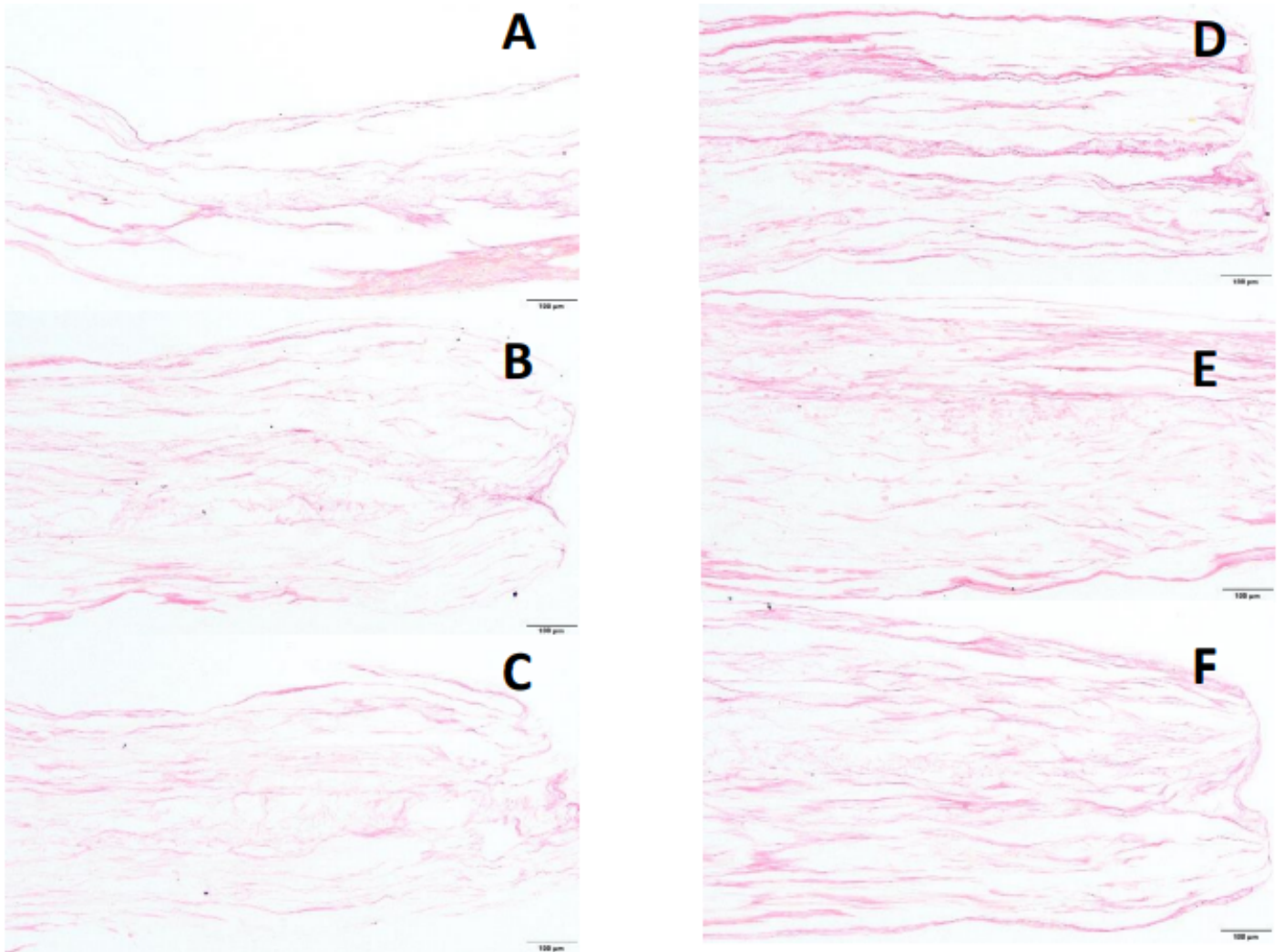


Figure 4.42: shows a light microscope image of Picro Sirius Red stained section of a seeded aligned PCL without serum cultured for 35 days in tissue engineering medium. A: Control, B: Plasma treated, C: Heparin, D: TGF-Beta 1 growth factor, E: TGF-Beta 3 growth factor & F: FGF growth factor. Scale bars = 100 μm .

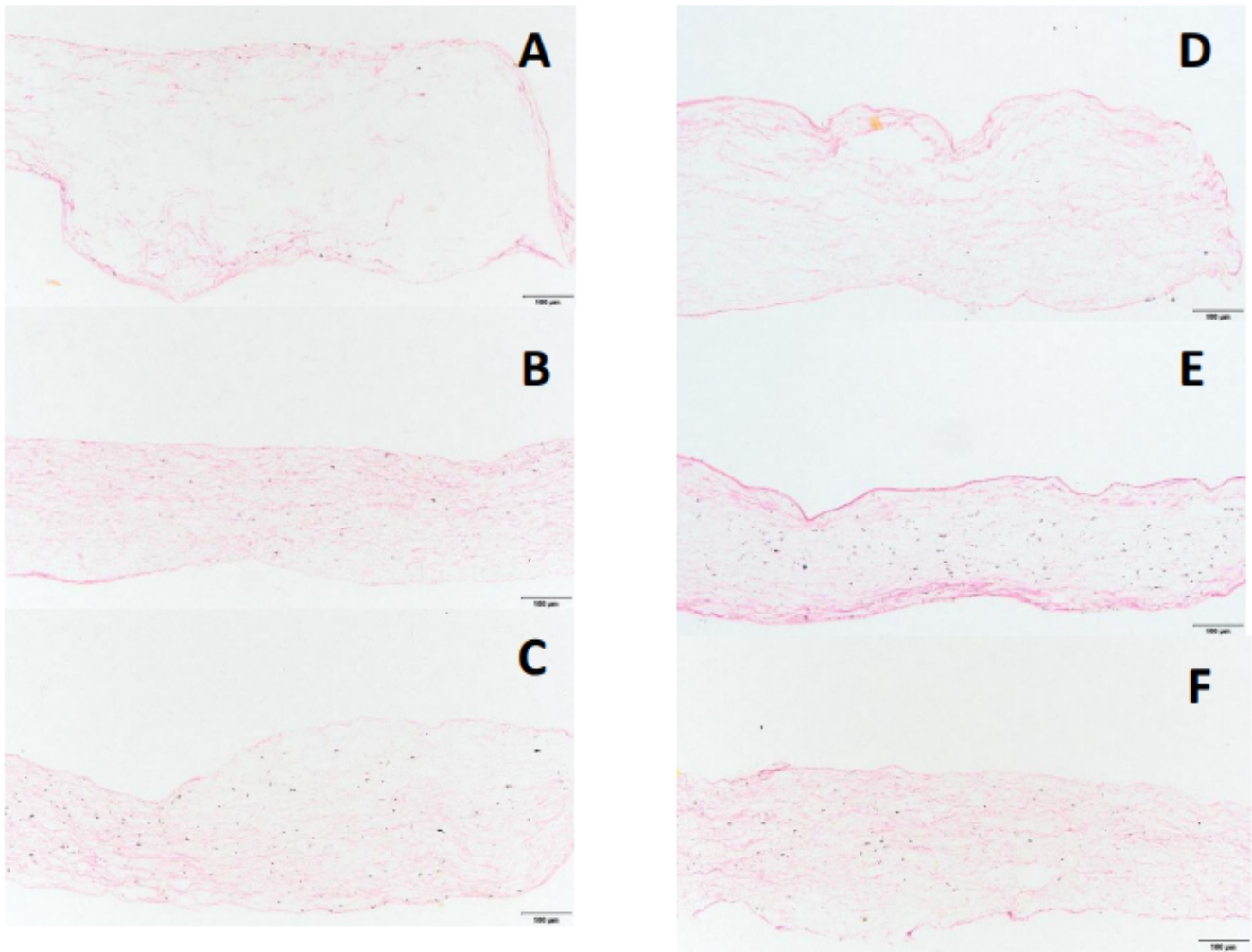


Figure 4.43: shows a light microscope image of Picro Sirius Red stained section of a seeded random PCL without serum cultured for 35 days in tissue engineering medium. A: Control, B: Plasma treated, C: Heparin, D: TGF-Beta 1 growth factor, E: TGF-Beta 3 growth factor & F: FGF growth factor. Scale bars = 100 μ m.

4.3.7. Quantitative PCR

This is a preliminary of the fold change in mRNA expression to indicate the Gene expression for COL1A1 at days 1,4 and 7. It was obtained by qRT-PCR and Human beta-2-microglobulin (β 2M) mRNA was used in this experiment as the 'housekeeping' gene/endogenous control.

The extracellular matrix of the periodontal ligament is comprised primarily of 75% collagen type I. COL1A1 was observed with a high level of expression on day 1 with TGF- β 3 biofunctionalized samples compared to the control scaffolds and the plasma treated scaffolds. Whereas on days 4 and 7 the COL1A1 expression was nearly the same.

This data enhanced the COL1A1 gene expression after seeding the aligned PCL scaffolds for 35 days with HPDL cells.

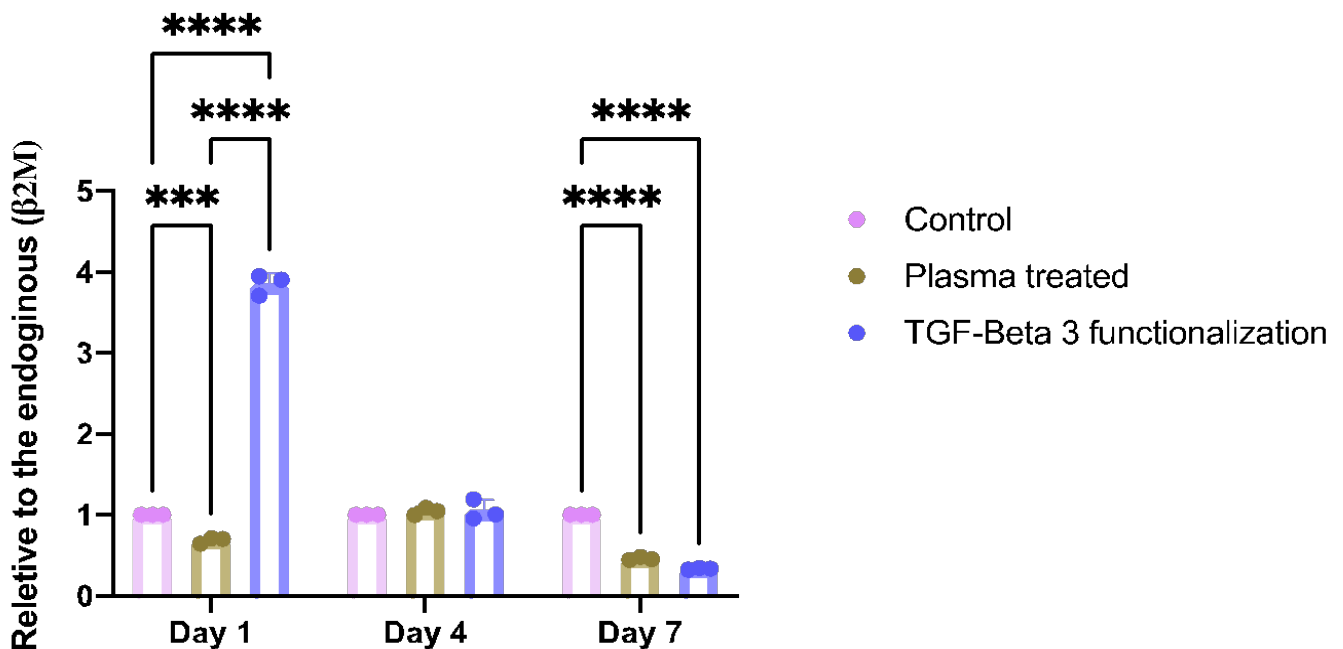


Figure 4.44: Fold change in mRNA expression of COL1A1 gene with time in culture for aligned PCL scaffolds seeded with HPDL cells. Cultured for deferent periods of time points. Data was normalised to the endogenous control (β 2M). P values were calculated using ANOVA. N = 3 separate experiments, each performed in triplicate.

5. Discussion and conclusion

5.1. Discussion

5.1.1. Initial random fibres scaffold selection: PLLA Vs PCL

The methods and conditions to fabricate electrospun random fibre scaffolds were established in this project for both poly-L-Lactic acid (PLLA) and polycaprolactone (PCL). The scaffolds were evaluated by SEM. The SEM images of the PCL random scaffolds showed larger fibre diameters $2.44 \mu\text{m}$, ± 0.45 and less variations in diameter when compared to the fibre diameters of the PLLA random scaffolds $2.69 \mu\text{m}$, ± 1.54 . However, the diameters of the PLLA fibres were more than twice the fibre diameters that were published by Chen et al. (2013), which were reported as $1.06 \pm 0.13 \mu\text{m}$. The fibre size can be controlled by changing the electrospinning conditions. However, the individual properties of the polymer like its viscosity and co-polymer concentration as well as the polymer solution flowrate and the voltage and work distance contribute to the differences in properties of the scaffolds (Seo et al., 2016, Sill et al., 2008, Ki et al., 2005, Haghi et al., 2007, Pham et al., 2006, Zhang et al., 2005). For the aligned scaffolds fabricated in-house, in the early part of the project; the SEM images show partial alignment of the scaffold fibres, but this was expected to improve in further electrospinning experiments with additional process optimisation such as optimising the voltage during electrospinning.

The collagen fibres in the periodontal ligament are perfectly aligned, therefore it is desirable to achieve this feature when electrospinning the scaffold for periodontal ligament tissue engineering experiment. Nowadays, producing aligned fibre scaffolds for periodontal ligament engineering being is an interesting field for some researchers. However, there are no studies focusing on the effect of biofunctionalised aligned scaffold with plasma treatment

then heparin bond and lastly with growth factors on the scaffold biological testing and the extracellular matrix production through the cell culture. In this project, a tissue engineered model system of random fibre scaffold and aligned fibre scaffold was developed in vitro and biofunctionalised with plasma treatment then heparin bond and lastly growth factors to assess the different reaction of HPDL cells behaviour in both random fibre and aligned fibre scaffolds.

Because of Covid restrictions and the associated restricted laboratory access I could not use any electrospinning equipment outside of the Department to fabricate aligned scaffolds and the defective in-house equipment had to be returned to the Spanish manufacturer for repair which was estimated to take several months as mentioned previously. Therefore, a commercial PCL aligned scaffold was ordered from the Electrospinning Company. The commercial PCL aligned scaffold was used for the rest of the project and compared with the in-house fabricated PCL random scaffolds. The fibre diameter of the commercial PCL aligned scaffolds was higher than the random PLLA and PCL scaffolds 3.5-5 μm with a mean fibre diameter of 4.49 μm , \pm 0.43 μm .

The initial biocompatibility of the scaffolds was investigated by seeding bovine ligament cells on the random PLLA and PCL scaffolds to form cell/scaffold constructs and incubating the constructs for up to 3 weeks. To assess the level of biocompatibility, the PLLA and PCL constructs were incubated with the cell viability reagent, PrestoBlue™. These experiments showed that the PLLA and PCL scaffolds did not cause any cell toxicity over the 21-day incubation period. The cellular DNA content showed that the bovine ligament cells were still attached to the PLLA and PCL scaffolds at the end of the 21-day incubation period. Together,

the DNA and Prestoblu[™] data show that the PCL and PLLA scaffolds could support the culture of viable ligament cells for at least 21 days culture period. Moreover, the ability of these scaffolds to allow cell attachment and support cell viability and proliferation was established. It was found that a high density of viable cells attached to the centre of the PLLA random scaffold while the edges of the scaffold had very few cells attached after the cell seeding process. The opposite was observed for PCL random scaffold as the cells were more evenly distributed over the scaffold membrane. This problem with PLLA is thought to be likely due to the scaffold curling up during handling which is a well-known disadvantage of very thin PLLA scaffolds (Chen et al., 2015). Therefore, strategies (to do with the thickness of the membranes) would need to be developed to overcome this issue of curling around the edges if the PLLA scaffolds were used for the rest of this project. The strategies to improve the thickness of PLLA membrane to avoid the curling problem of scaffolds during seeding, incorporate another type of polymer may help solving the problem, applying pressure during the seeding using a steel rings or anchoring devices, and utilising additional support layers during spinning which can provide more stability to the scaffold mat. Utilising anchoring devices such as pins, clips, or adhesive to attach the membrane to the plate could assist in reducing the curling and adding support layers such as a mesh or a non-woven fabric to the membrane to provide extra support reduces curling. More experiments are needed to investigate these strategies to obtain the optimal one to inhibit curling. Grome et al. (2019) found that increasing the thickness of the membrane fosters binding and remodelling and defined diameters. In addition, increasing thickness reduces membrane crystallinity, and improving cellular response as Uygun et al., 2010 mentioned. Adjusting the membrane's thickness is vital for scaffolds to improve cell spreading, proliferation, and attachment. Both PLLA and PCL scaffolds were found to support good cell viability and the scaffolds showed

very minimal cell death. However, PLLA was found to support more live cells than the PCL scaffold using Live-Dead cell staining with CMFDA and PI dyes. The stained cells were then observed using confocal microscopy imaging. A higher cell density in the centre of the PLLA scaffold may facilitate a higher rate of cell proliferation rather than if the cells had been equally distributed across the membrane and which could not only lead to errors in the cell density analysis but can also affect the rate of proliferation and the cell characteristics (Trajkovic et al., 2019). However, analysis of total cell DNA on the scaffolds showed that the PCL random scaffold had significantly higher levels of DNA ($10971.4, \pm 1756.7$ ng/scaffold) compared to PLLA scaffolds ($5760.3, \pm 390.4$ ng/scaffold) indicating that the PCL scaffolds had a higher cell number when compared to the PLLA random scaffolds. Therefore, further work would also need to optimise the cell seeding technique for PLLA to ensure the best cell culture conditions are achieved. This data concludes that there are more cells physically on PCL random fibres scaffolds than PLLA random fibres scaffolds under the same cell seeding conditions. However, the opposite effect appeared in the confocal microscopy imaging (of an apparent larger cell number on the PLLA random scaffolds). This result may have occurred because the PLLA random fibres scaffold tended to curl during the cell seeding. All this indicated that PCL scaffold functioned better than PLLA scaffolds to promote better cell viability and proliferation. PCL was better for cell attachment and it is easy to handle during the experiments so it was chosen for this project.

5.1.2. Aligned fibre PCL scaffold Vs random fibre PCL scaffold

PCL aligned fibre scaffold presented good cell activity and distribution of the HPDL cells on the scaffold although a lower porosity was observed (49.13 m²/g) compared to the PCL

random fibre scaffold (43.68 m²/g) suggesting that the aligned scaffold would favour the periodontal ligament healing process better as it will guide the cells during healing. Therefore, from the results, culturing HPDL cells onto aligned membranes showed better cell production compared to random-fibre membranes. The alignment of the membrane creates an organized environment for the cells which leads to enhanced stability and binding affinity of the cells to the scaffold fibres. Aligning the membrane fibres helps the cells to form the desired ECM, which offers an efficient and higher yield product of ECM (Yin et al., 2010, Shang et al., 2010). Fibre alignment in scaffolds has been shown to enhance cell proliferation and upregulate gene expression (Chen et al., 2021; Han et al., 2021; Huang et al., 2021; Xie et al., 2021). Further, fibre alignment has been found to improve the expression of growth factors in the scaffolds and cell migration (Olvera et al., 2017; Huynh and Holsinger, 2023). However, when the fibres are fully aligned, it is easier for cell attachment PDLs and spreading, leading to higher seeding efficiency. Ghollasi and Poormoghadam (2022) found that scaffold fibre alignment improved the scaffold hydrophilicity and biocompatibility, which also resulted in better adhesion and differentiation. In conclusion, aligned fibre scaffolds have improved cell growth, attachment, proliferation and differentiation compared to random fibre scaffolds. Which giving them a great potential in periodontal ligament tissue engineering.

5.1.3. Effect of surface modification and biofunctionalization of scaffold's mats

In periodontal ligament tissue engineering, scaffolds usually act as a framework supporting the cell's tissue formation, but they don't aid tissue formation. Therefore, biofunctionalisation is a promising method that can help stimulate tissue formation. To the best of my knowledge, this has been done in various ways; and one of these ways is

biofunctionalisation. In this study, we tried to mimic the way that has been presented in our body. Where, plasma polymerisation using allylamine has been utilised in this project to give the scaffold surfaces a positive charge to enable biofunctionalization with heparin which is negatively charged and provide a strong ionic bond between them. Moreover, another major benefit of using allylamine plasma-treatment in this study, was that the membranes can be biofunctionalised with heparin. Then the heparin can bind heparin-binding proteins (Freeman et al., 2008) for example, growth factors such as TGF- β 1, TGF- β 3 and FGF-2.

Heparin is a linear polysaccharide composed of sulphated glycosaminoglycans. It has been used in various studies as a mimic for heparan sulphate-containing glycosaminoglycans which are found in proteins of the extracellular matrix and cell membranes in our body. The heparan sulphate-containing glycosaminoglycans are necessary for the binding and regulation of activity of many proteins such growth factors, cytokines and chemokines (Sakiyama-Elbert, 2014). The main advantage of this method is to protect the growth factors of being degraded as the heparin is an extremely sulphated GAG responsible for releasing and restoring the growth factors (You et al., 2014)

Barry et al. (2005) suggested that PLLA scaffolds need to be modified to enhance their ability to support cell activity and attachment. It has been reported that plasma surface modification of the scaffold with amine groups, increased the hydrophilicity and cell attachment (Cipiria et al., 2011). Allylamine polymerisation provides excellent coating uniformity, and aligned scaffolds present raised proliferation, osteogenic differentiation, and adhesion (Cheng et al., 2020; Yang et al., 2020; Liu et al., 2019). Allylamine plasma-treated scaffolds increase cell adhesion and spreading when utilised compared to non-treated membranes. Therefore Barry

(2005) compared a virgin P_{DL}LA scaffold with an allylamine plasma treated P_{DL}LA scaffold. XPS analyses showed the presence of nitrogen groups on the surface of the allylamine treated scaffolds which is the same observation of this project allylamine plasma treated scaffolds. This confirmed the deposition of amine groups, where this indication gives prospect of better cell attachment and activity on the allylamine treated scaffolds. Better cell attachment and effect on cell phenotype has been observed with surfaces enriched in nitrogen groups. There are several studies suggesting this (Yang et al., 2002; France et al., 1998; Harsch et al., 2000). Therefore, further work and improving the experimental conditions needed for the allylamine-plasma polymerization to optimise the surface modification and cell signalling characteristics of both scaffolds are needed to further improved cell attachment and proliferation (Mahoney et al., 2004; Robinson et al., 2010; Barry et al., 2005; Harding et al., 2012;).

There are various studies using heparin addition to the scaffold which supported an increase in the biocompatibility of the scaffolds (Tsai et al., 2001). Heparin can be incorporated into the scaffolds by either layer by layer (LbL) method (Ferreira AM et al., 2016) or absorbed onto the scaffold surface method (Zhou et al., 2020).

In this study, the results showed that the heparin-aligned fibre PCL scaffold had a higher DNA content than the random fibre PCL scaffold. These results show that the addition of heparin stimulated binding of the hPDL cells to the aligned scaffolds and promoted cell proliferation. Heparin is a naturally occurring anticoagulant that helps to prevent blood clotting in the blood vessels of the circulatory system. Heparin-coated scaffolds have been shown to enhance blood supply and support other cell functions, such as insulin-secreting cells (Xu et al., 2018).

The effectiveness of heparin in promoting growth factor binding to scaffolds provides a potential for its application in tissue engineering. Heparin surfaces have been shown to have endothelial cell-stimulating ability, when used with growth factors, it is significant as a pre-vascularized site (Leijon et al., 2013). The site is essential for cell and tissue implantation, especially inflammation sensitive. The heparin surface is crucial and fosters angiogenesis (Wu et al., 2016). The results in this study shown that the use of a scaffold biofunctionalised with heparin and a growth factor (TGF- β 1, TGF- β 3 or FGF-2) increased the cell attachment and proliferation of HPDL cells as well as their total protein and collagen production in the extracellular matrix.

Heparin was confirmed to bind to the allylamine plasma-treated membranes by investigating the binding of a fluorescent-labelled. The attachment of the heparin to the allylamine plasma treated membranes was determined by measuring the fluorescence of the heparin in the unbound fraction (3.2.5.4). The results showed that the more heparin was added to the membranes (over a concentration range of 2.5. to 40 μ g) the more heparin was bound to the membranes. When a fluorescent heparin solution containing 2.5 μ g of fluorescent heparin was added to the plasma-treated membrane a 19.2 % of the heparin was bound. whereas, when a 40 μ g of heparin was added to the plasma treated membrane an 8% of the heparin was bound to the membrane. However, it is possible this is because of the hydrophobicity of the fluorescein. The fluorescein-heparin that have been used in this experiment may have had different binding characteristics in the heparin allylamine-functionalised membranes compared to the heparin used in this project.

Growth factors are proteins that act as chemical messengers to stimulate cell growth, proliferation, and differentiation. TGF- β 1, TGF- β 3, and FGF-2 are three growth factors that bind to different receptors on cell surfaces. From the dissertation, TGF- β 1 showed high cell differentiation and proliferation. Using different types of growth factors enables studying cell functioning effects. TGF- β 1 growth factor binding is the process by which proteins containing a TGF- β 1 binding domain recognize and bind to TGF- β 1. This binding regulates the activity of TGF- β 1 and its downstream targets. TGF- β 1 functions in cellular processes, such as inflammation, immune response, and cell cycle control and is utilized in therapeutic strategies development to target various diseases, including cancer, autoimmune diseases, and fibrosis. From the results presented in section (4.3.2) of the scaffolds biofunctionalised with heparin and either TGF- β 1 or TGF- β 3 or FGF-2, the highest content or total protein in the aligned PCL fibre scaffold constructs was found with scaffolds biofunctionalized with TGF- β 3. Moreover, TGF- β 3 growth factor binding is used to promote cell growth and development and applied in tissue engineering and regenerative medicine to stimulate the growth of new tissue and organs (Voleti et al., 2012; Sasaki et al., 2018). TGF- β 3 regulates inflammation and the immune system, fosters wound healing, and modulates stem cell differentiation (Xu, Zheng et al., 2018; Cetik et al., 2022; Roth et al., 2019). FGF-2 growth factor is used to study the role in regulating cellular processes such as growth, differentiation, and cell motility (Yamaguchi and Rossant, 1995).

TGF- β 1, TGF- β 3, and FGF-2 are growth factors which enable cell differentiation, growth, and division (Li et al., 2019; Janssens et al., 2005; Xu et al., 2020; Yamaguchi and Rossant, 1995). TGF- β 1 and TGF- β 3 are cytokines involved in numerous biological processes, including

inflammation, cell proliferation and differentiation, and extracellular matrix formation. They are involved in regulating cell growth, migration, and differentiation. FGF-2 enables cell proliferation, migration, healing, and differentiation and acts as a chemoattractant, stimulating cell migration and binding to specific receptors on the cell surface (Apriasari et al., 2019). All these growth factors affect cell binding to the extracellular matrix and angiogenesis.

The binding of growth factors to immobilised GAGs was examined and the result established the significant binding of the all growth factors (TGF- β 1, TGF- β 3 and FGF-2) to scaffolds functionalised with heparin, LMW heparin and heparan SO₄. There was a different level of binding during the ELISA assay. Each of the growth factors were used to follow the binding and elution of the growth factors from the biofunctionalized membranes for a period of 14 days after binding. The data presented that TGF- β 3 showed the lowest binding to the heparin-functionalised assays with 66% binding of the total growth factor added. Whereas TGF- β 1 and FGF-2 showed much stronger binding with the amounts of 97% binding and 90% binding, respectively. TGF- β 1 and FGF-2 eluted much more slowly compared to TGF- β 3. The three of the growth factors were eluted from the biofunctionalized membrane over the period of 14 days. Although, TGF- β 1 and FGF-2 bound much more to the heparin functionalised membranes with higher amounts of bound growth factor, they had slower elution rate compared to TGF- β 3 (4.2.7). All the biological testing suggested that the TGF- β 3 biofunctionalized membranes showed greater biological activity than the TGF- β 1 and FGF-2 biofunctionalised membranes. The project outcomes suggested that the higher amount of growth factor binding observed with TGF- β 1 and FGF-2 to the biofunctionalized membrane did not result in a better stimulation in cell growth, proliferation, and differentiation.

Cheng, Shie et al. (2021) showed that TGF- β 1 improved cell adhesion after a 6-hour cell culture. About TGF- β 3, it promotes cell shape elongation, contraction of the scaffolds, and upregulation of the expression of genes (Roth et al., 2019). Thus, this growth factor has been suggested to be vital for enhancing the bioactivity of scaffolds (Roth et al., 2019). FGF-2 is vital for cell proliferation, migration, and wound healing. It reduces scars and enhances the neovascularization and arrangement of collagen (Chen et al., 2022). Therefore, FGF-2 is recommended as an application for wound repair (Yamaguchi and Rossant, 1995).

Experiments were done to test the mechanical properties of the PCL random fibre and aligned fibre scaffolds (4.2.2). The experiment produced showed typical non-linear stress-strain curves. The non-treated aligned fibre PCL scaffold had the higher Young's modulus value (41.58 ± 7.04 MPa) compared to the PLLA non-treated random fibre (0.86 ± 0.24 MPa) and PCL non-treated random fibre (0.32 ± 0.04 MPa). The alignment of the scaffolds affected the tensile stress and the Young's modulus of the scaffold. Shang et al., 2010; Gauthier et al., 2021 were reported that the aligned fibre scaffolds resulted in higher tensile stress and Young's modulus compared to random scaffolds. The same was observed in this study, where the aligned fibre scaffold reported the highest tensile stress and Young's modulus.

Plasma treatment increased the Young's modulus for PCL aligned fibre value (47.21 ± 3.81 MPa) with no significant effect on the, increased the PCL random fibre value (0.78 ± 0.03 MPa) and decreased it value for the PLLA random fibre value (0.34 ± 0.28 MPa). Joseph et al., 2021 reported that the allylamine plasma treatment on his PCL scaffolds did not effect their mechanical properties. The Plasma treatment effects the hydrophilicity properties of the scaffold especially which will affect their mechanical testing properties (Jahani et al., 2012). Allylamine plasma treatment resulted in addition of amine group to the scaffold surface,

(which was confirmed by XPS) this could have led to change in the chemical surface compositions and the process of plasma polymerisation or the added surface amine groups may have caused the decreases in the mechanical properties of the scaffold.

The mechanical force exerted on scaffolds differs significantly depending on the direction and magnitude of the force, which can be sporadic, repetitive, or sustained over time. In recent years, the mechanical strengths of biomaterial microfiber scaffolds have been studied and become a trending topic in the field of bone and tissue engineering. The microfiber scaffolds have been utilised in regenerative treatments and have demonstrated enhanced cell growth, tissue, and bone formation and have greatly improved, regeneration of tissues, and biomaterial developments (Sakar et al., 2006). Recently, there have been efforts to ensure that the microfibers mimic the mechanical properties of the native tissue (Guimarães et al., 2020). Mechanical properties, low cost, biocompatibility, slow bioresorption and pore size are among the essential characteristics of scaffold materials, hence the broad application of PCL and PLLA in the field of regenerative medicine. These properties are vital so they can provide a 3D structure for nutrient diffusion and tissue formation and maintain the structure during implantation (Wiwatwongwana and Promma, 2020). PLLA and PCL scaffolds have been extensively used due to their ability to mimic the fibres of the ECM. For instance, these scaffolds are able to take up properties of collagen barriers and perform the same functions in tissue regeneration (Gonzalez-Fernandez et al., 2016).

The extension of the scaffold is their response to strain shown by the scaffolds measured by applying force, which is the stress; this produces the stress-strain curve, from which physical properties of a material can be determined. Tensile strain, which is the stretching of the

materials, was the applied force utilised (Muiznieks and Keeley, 2012). The stress and strain at the rupture point are directly proportional to the maximum extensibility of a scaffold type and strength. From the results, it is deduced that plasma treatment increases the hydrophilicity of scaffolds (shown by the decreased WCA) and decreases their tensile stress. This could be because the actual process of the plasma treatment can damage the scaffold fibres and change their mechanical properties as found in this project. Further, the chemical reaction caused during the plasma treatment may also contribute to damage of the scaffold fibres.

The findings are similar to those which Jahani et al. (2012) found in PCL O₂ plasma treated. Therefore, plasma treatment, as discovered in this study, is significant as it will enhance the tissue formation, which will be critical during guided tissue regeneration (Hughes, 2015). The scaffolds have been shown to prevent wound tension and support the healing tissues due to their excellent mechanical properties (Bhavsar et al. 2018). However, the mechanical characteristics decline quickly; hence the promotion of osteoblast and bone formation is required to be commenced soon after placement of the scaffold to the wound (Schofer et al., 2011).

From the findings in this thesis, PLLA random fibre scaffolds showed the largest average pore size (63.16 m²/g), which means that its porosity level is high, while PCL random has the lowest pore size (43.68 m²/g) hence lower porosity (Section 4.2.3). Therefore, these data showed that PLLA exhibited better characteristics than PCL in terms of cell porosity, and they are better in tissue growth, targeted cell delivery and other biomolecules (Loh and Choong, 2013). The pore size affects the material's biological and mechanical properties. Since the PLLA random depicted macroporosity as their pore sizes were >50 µm, that determines cell

colonisation making them promote the growth of vascular and bone tissue (Loh and Choong, 2013). On the other hand, PCL scaffolds pore size was found to be <50um, are critical in the adsorption of protein and influence the fate of the cell as they dictate cell adhesion. Protein adsorption properties enhance bone formation and trigger osteogenic differentiation (Perez and Mestres, 2016).

The hydrophobicity of PLLA and PCL is a significant drawback in tissue engineering and regenerative medicine as it hinders the achievement of enough mass of seeded cells required for the process (Wan et al., 2006). As depicted in the results on scaffold hydrophobicity, plasma treatment enhances the hydrophilic properties of the microfibers (section (4.2.4)/figure 4.22). It improved the wettability of the scaffold fibres since the WCA angles of plasma-treated scaffolds were lower than those of the non-treated nanofibers. Plasma treatment is a valuable method in improving the hydrophilicity of scaffold materials, and another method is introducing functional groups on their surfaces. The process is rapid and a non-solvent surface modification which creates active sites on polymeric material surfaces (Morent et al., 2011). WCA reveals the microfiber scaffolds' hydrophilic surface properties and enables better cell adhesion and proliferation compared to hydrophobic surfaces. Cell adhesion and proliferation on biomaterial surfaces are directly proportional to the increased hydrophilicity of the biomaterial surfaces. The high degree of WCA among the non-treated scaffolds affirms that plasma treatment aids in the improvement of hydrophilicity in nanofibers. PCL and PLLA have been highly used in tissue engineering because of their biodegradability, high tensile strength, and non-toxic aspects. However, their hydrophobicity is not desirable in vitro cell culture. Changing the biomaterial properties to yield hydrophilic scaffolds enables them to have better cell growth and adhesion (Jahani et al., 2012).

Therefore, from the results obtained in this thesis, it is sufficient to say that plasma treatment is a convenient method and effective in improving the hydrophobic nature of the PLLA and PCL microfiber.

From the results of the PicoGreen assay for DNA quantification (to indicate the number of cells) and that of the Picro Sirius red to stain collagen fibres (collagen types 1&3), PCL-aligned scaffolds show the presence of collagen type 1 and 3 and a high level of DNA content in the scaffold. Furthermore, the DNA quantity was recorded highest in the aligned PCL after 48 hours, suggesting that high cell proliferation and viability levels are high and are competent for tissue regeneration a few hours from the seeding time. A delay reduces cell adherence and affinity. The heparin-aligned PCL sample scaffold has higher DNA cell than the random PCL. The scaffold enhanced cell binding to the scaffold and/or stimulated cell proliferation, which mean that the total DNA on the scaffold will also increase.

Protein delivery to cells is complex and various growth factors are required to optimise cell proliferation and ECM formation. Tissue culture techniques often use foetal calf serum to support cell proliferation and ECM formation. The Foetal calf serum is an essential component of cell culture medium as it provides various growth-promoting factors and nutrients for cell health, function and proliferation (Pilgrim et al., 2022). In the absence of serum, the individual growth factors must be added to maintain cell viability and proliferation during the cell culturing.

In this project, growth factors (TGF- β 1, TGF- β 3 and FGF-2) were bound to scaffolds via binding to heparin which itself was non-covalently, tightly bound to surface amine groups deposited

by plasma polymerisation on PLLA and PCL scaffolds. ensuring a medium that provides favourable growth for cell differentiation and proliferation during tissue culture. Delivery of growth factors is vital because it ensures more extended support for adherent cell proliferation. This research project found that the TGF- β 3 functionalised scaffold had a higher amount of cells protein concentration than the heparin only biofunctionalised scaffold. This outcome, suggesting that the growth factor can be applied in tissue regeneration to support adherence to cell proliferation (Ito et al., 1998).

ALP activity (the recognised marker of osteogenic cells) (Trivedi et al., 2020) was used to measure potential osteogenic differentiation of HPDL-seeded cells in the PCL aligned and random fibre scaffolds and PLLA random fibre. ALP plays a significant function in hard tissue mineralisation and measuring the activity of this enzyme in HPDL seeded functionalised scaffolds. The ALP activity showed no significant difference in the PLLA random fibre scaffolds, PCL random fibre scaffolds and PCL aligned fibre scaffold samples as they demonstrated the same results which is a very low activity level. That means the cells did not show significant differentiation into osteoblastic cells after five weeks of Incubation. Lack of ALP expression is suggestive that osteocalcin a late marker of osteoblast differentiation also was not expressed in this project (Alotaibi, 2014).

The results from the quantification of total collagen content obtained were similar to that of the BCA assay. In that membranes biofunctionalised with TGF- β 3 was found to contain higher levels of collagen for both random fibre and aligned fibre PCL scaffold (figure 4.35). The aligned fibre PCL scaffold/HPDL construct incubated with serum finding showed a significant difference between the control and the three biofunctionalized groups with growth factors

(TGF- β 1, TGF- β 3 and FGF-2). While the random fibre PCL scaffold with serum resulted in a significant difference only between the control and the biofunctionalized membrane with TGF- β 3. These findings further promote the importance of investigating TGF- β 3 in future studies of promoting protein delivery to HPDLs via biofunctionalised membranes. A further advantage of delivering growth factors on biofunctionalised membranes is that the membranes increase the half-life of the growth factors compared to if they were circulating in the blood or added as a soluble growth factor to an incubation. The study is also backed up by that of Gonzalez-Fernandez et al. (2016), where it was found that cell delivery of the TGF- β 3 gene enhanced the production of hyaline cartilage in tissues. However, for the collagen content experiment is seen that the effect of the TGF- β 3 was further enhanced by incubating the seeded biofunctionalised membranes with 5% serum-containing culture medium as shown in this thesis and by (Yamamoto et al., 2016). Due to the high turnover of collagen on the periodontal ligament, the findings of the TGF- β 3 growth factor can be used to enhance collagen content in HPDL (Lindhe, 2003).

Cell abundance and differentiation are promoted by providing cell proliferation and adherence factors. The H&E histology results showed that random fibre PCL scaffold incubated without serum showed low cell abundance, as indicated the lighter staining. Aligned fibre PCL scaffold has also been shown to promote cell attachment and proliferation. Regenerative medicine and tissue engineering rely on biomaterials for cell adherence, proliferation, and differentiation; hence such findings improve the process and are used as a foundation for further research. TGF- β 1 is associated with improved cell proliferation and early differentiation as known in literature (Li et al., 2019). Therefore, TGF- β 1 growth factors can be used to promote cell differentiation and proliferation earlier during periodontal tissue

regeneration. From the results presented in this thesis, the study by Salehi-Nik et al., 2017, supports that PCL scaffolds needs to be incorporated with other biomolecules and the scaffold fibres should be aligned so they would promote better differentiation in HPDL.

Picro Sirius red histological dye will stain fibres of collagen type 1 and 3 in red. Staining the wax-mounted sections of the aligned fibre PCL-HPDL cell constructs incubated with and without serum with Picro Sirius red stained in the scaffold sections. Evidence of collagen production was found with all the experimental groups of scaffolds after 35 days of incubation. Figures 4.40 showed that the alignment of fibres enhanced the cell differentiation and proliferation of the HPDL cells. Therefore, PCL aligned fibre scaffolds were mimicked the collagen fibres alignment, which enabled them to support the regeneration of tissues and to be colonised by directing and hosting cells (Schoferet al., 2011). Control sections of the aligned fibre scaffold (not seeded with HPDLs) were also stained with Pico Sirius Red to check for non-specific scaffold staining and no staining was observed.

The preliminary data spotted the advantage of functionalisation of scaffold with TGF- β 3 to aid cell-cell or cell-matrix interaction which is important in developing 3D periodontal ligament tissue engineered in *vitro*. The results showed a significant elevation in the amount produced of COL1A1 at the start specially in TGF- β 3. Chan et al., 2008 found that TGF- β 3 exposed the highest stimulation of COL1A1 and COL3A1 compared to TGF- β 1&2. This suggests that the biofunctionalization method with TGF beta 3 produced more collagen immediately after seeding than the control and plasma treated scaffolds. TGF- β 3 cell stimulation dropped at day 4 and 7 this is maybe because the cells stopped proliferation and they were started producing protein forming the extracellular matrix. It is suggested that TGF- β 1 may have a

dual effect on PDLF proliferation, either inhibitory or stimulatory, depending on the stage of cell differentiation (Fujii et al., 2010). The hydrophobicity of the plasma treated scaffold may have affected the cell stimulation of COL1A1 gene expression which explains the difference with the TGF- β 3 biofunctionalised scaffolds. This finding supports the Picro Sirius red staining results where there was an evidence of collagen production was found in all of the experimental groups. The result suggests that TGF- β 3 biofunctionalised scaffold is a good method stimulating COL1A1 compared to the control and plasma treated scaffolds for the periodontal ligament regeneration application.

5.2. Conclusion

This data showed that electrospun random fibre PLLA and PCL scaffolds were fully compatible when bovine cells and HPDL cells were cultured on them. There were more cells physically on the PCL random fibre scaffolds than the PLLA random fibres scaffolds under the same cell seeding conditions. However, the opposite effect appeared in the confocal microscopy imaging (of an apparent larger cell number on the PLLA random fibre scaffolds). This result may have occurred because the PLLA random fibres scaffold tended to curl during the cell seeding. Which concludes that the PCL random fibre scaffolds yield to a better cell attachment and cell activity compared to the random fibre PLLA scaffolds. Fabricating aligned fibre scaffolds failed in-house and therefore, aligned fibre scaffolds were purchased from the Electrospinning Company to continue the research.

XPS analyses of allylamine-treated scaffolds indicated a substantial increase in nitrogen groups at the surface of the allylamine treated scaffolds. The intention was to biofunctionalise the GTR scaffolds to stimulate both cell proliferation and tissue formation of the periodontal ligament to aid the regeneration. This improvement of scaffold bio-functionality and activity would allow production of smart bioactive membranes that promoted periodontal ligament regeneration.

Allylamine treatment on PCL and PLLA scaffolds improved their hydrophobic properties and reduced their mechanical strength. Plasma treatment is an effective and efficient method for enhancing the hydrophilicity of scaffold biomaterials which can be used in PDL to enhance cell adhesion and proliferation. The increase in hydrophilicity among scaffolds is directly proportional to an increase in wettability which improves their attachment to HPDL cells,

combined with their reduction in tensile stress, which promotes their viability and hence is critical in tissue regeneration. Therefore, PCL and PLLA scaffolds could be suitable polymers for use in PDL treatments after they have been subjected to plasma treatment to improve their hydrophobicity, although it lowered their mechanical strength properties.

PLLA random fibre scaffolds were found to have higher porosity levels than the PCL random fibre scaffolds, showing that they had better wettability due to their low WCA and better cell proliferation, attachment, and viability properties. Tissue engineering aims at producing porous scaffolds for tissue regeneration and 3D formation of tissues, and the study produces a founding point for the examination of PLLA random fibre scaffolds due to its microporosity characteristics. Furthermore, the microporosity nature of PCL random fibre scaffolds showed that they had better mechanical strength, which increased with an increase in the fibre diameter compared to aligned fibre as seen in the results (section 4.2.2). The alignment of scaffold fibres is crucial to enhance the mechanical strength of scaffolds as shown in section (4.2.2). The high WCA of the aligned fibre PCL scaffold further confirmed their higher mechanical strength, which aids in tissue engineering. The low porosity observed in the aligned fibre PCL scaffold showed that they could favour the periodontal ligament healing process as they would guide the cell during healing.

This study found that HPDL seeded on TGF- β 3 biofunctionalised scaffolds produced more total protein and collagen. That is a vital element due to the difficulty experienced in protein delivery in tissue engineering which provides the foundation for more studies on the TGF- β 3 and biomaterials to solve the challenges experienced. Further, due to the advancement of the

growth factors in bone formation and tissue engineering, it is essential to come up with more studies on the growth factors due to their ability to be fast degraded and inactivated. The experiments show that aligned fibre PCL scaffolds are an essential biomaterial due to their interaction with various biomolecules, especially the TGF- β 3 growth factor, to enhance tissue regeneration. They provide significant advancements in PDL-guided tissue regeneration as they have been found in the study. TGF- β 1, TGF- β 3 and FGF-2 also have been evidenced as vital in cell proliferation and differentiation, which supports existing literature from the study's findings.

6. Future work

The following research experiments are suggested to be carried out in the future based on the findings and difficulties observed during this project:

- Further optimisation of fabrication electrospun aligned fibre PCL scaffolds.
- Compare the performance of different surface treatment and growth factors biofunctionalization of aligned fibre scaffolds and their roles in the periodontal ligament regeneration.
- Further evaluate the added amount of growth factors to biofunctionalised the scaffolds and their elution period.
- Study the combination of multiple growth factors to biofunctionalised scaffold and their effect in the periodontal ligament regeneration.
- In depth valuation of the effect of different type of growth factors in COL1A1 expression.

7. References

- Abedalwafa, M., Wang, F., Wang, L., Li, C. (2013). Biodegradable poly-epsilon-caprolactone (PCL) for tissue engineering applications: A review. *Rev. Adv. Mater. Sci.* 34, 123–140.
- Ahmadi M, Seyedjafari E, Zargar SJ, Birhanu G, Zandi-Karimi A, Beiki B, Tuzlakoglu K (2017) Osteogenic differentiation of mesenchymal stem cells cultured on PLLA scaffold coated with Wharton's jelly. *EXCLI Journal* 16, 785 - 794.
- Agerbæk, M.R., Haubek, D., Birkelund, S. and Kilian, M., 2006. *Identification of dominant immunogenic bacteria and bacterial proteins in periodontitis.*
- Ahmad, S.S., Ahmad, K., Lee, E.J., Lee, Y.H. and Choi, I., 2020. Implications of insulin-like growth factor-1 in skeletal muscle and various diseases. *Cells*, 9(8), p.1773.
- Akbarian, M., Bertassoni, L.E. and Tayebi, L., 2022. Biological aspects in controlling angiogenesis: current progress. *Cellular and Molecular Life Sciences*, 79(7), p.349.
- Alotaibi, D., 2013. *Aligned polymer scaffolds in periodontal tissue engineering.* Doctoral dissertation, University of Sheffield.
- American Dental Association., 2005. Treating periodontal diseases. *JADA*, 136, p.127.
- Anjum, S., Rahman, F., Pandey, P., Arya, D.K., Alam, M., Rajinikanth, P.S. and Ao, Q., 2022. Electrospun biomimetic nanofibrous scaffolds: a promising prospect for bone tissue engineering and regenerative medicine. *International Journal of Molecular Sciences*, 23(16), p.9206.
- Apriasari, M.L., Pramitha, S.R., Puspitasari, D. and Ernawati, D.S., 2019. Expression of fibroblast growth factor- β and transforming growth factor- β in mauli banana stem (*Musa Acuminata*) extract gel-treated traumatic ulcer. *Tropical Journal of Pharmaceutical Research*, 18(3), pp.527-531).

- Archana A, Srikanth V, Sasireka, Kurien B, Ebenezer (2016) Fibroblast heterogeneity in periodontium - a review. *International Journal of Dental Sciences and Research* **2**(3), 50 - 54.
- Asadian, M., Chan, K.V., Norouzi, M., Grande, S., Cools, P., Morent, R. and De Geyter, N., 2020. Fabrication and plasma modification of nanofibrous tissue engineering scaffolds. *Nanomaterials*, **10**(1), p.119.
- Asadian, M., Onyshchenko, I., Thiry, D., Cools, P., Declercq, H., Snyders, R., Morent, R. and De Geyter, N., 2019. Thiolation of polycaprolactone (PCL) nanofibers by inductively coupled plasma (ICP) polymerization: Physical, chemical and biological properties. *Applied Surface Science*, **479**, pp.942-952.
- Aswin, S.K., Jothishwar, S., Nayagam, P. and Priya, G., 2018. Scaffolds for biomolecule delivery and controlled release-A Review. *Research Journal of Pharmacy and Technology*, **11**(10), pp.4719-4730.
- Armitage, G. 2004. Periodontal diagnoses and classification of periodontal diseases. *Periodontology* 2000, **34**, 9-21.
- Aziz, G., Ghobeira, R., Morent, R. and De Geyter, N., 2018. Plasma polymerization for tissue engineering purposes. *Recent Research in Polymerization*, p.69. DOI: 10.5772/intechopen.72293
- Azizah, A. (2020). "A Review of Bandotan Leaf Extract (*Ageratum conyzoides* L.) in Inhibition Test to the Growth of Bacteria (*Porphyromonas gingivalis*) Case of Periodontitis Disease". *Systematic Reviews in Pharmacy*.

- Baranowska-Korczyk A, Warowicka A, Jasiurkowska-Delaporte M (2016) Antimicrobial electrospun poly(ϵ -caprolactone) scaffolds for gingival fibroblast growth. *RSC Advances* **6**, 19647– 19656.
- Barhoum, A., Bechelany, M. and Makhoul, A.S.H. eds., 2019. *Handbook of nanofibers*. Cham: Springer International Publishing.
- Barry, J.J.A., Silva, M.M.C.G., Shakesheff, K.M., Howdle, S.M., & Alexander, M.R. (2005). Using plasma deposits to promote cell population of the porous interior of three-dimensional poly (D, L -Lactic acid) tissue-engineering scaffolds. *Advanced Functional Materials* **15**, 1134 - 1140.
- Bazaka, K., Jacob, M.V. and Ostrikov, K., 2016. Sustainable life cycles of natural-precursor-derived nanocarbons. *Chemical Reviews*, **116**(1), pp.163-214.
- Bazaka, K., Jacob, M.V., Crawford, R.J. and Ivanova, E.P., 2011. Plasma-assisted surface modification of organic biopolymers to prevent bacterial attachment. *Acta Biomaterialia*, **7**(5), pp.2015-2028.
- Bazgir, M., Zhang, W., Zhang, X., Elies, J., Saeinasab, M., Coates, P., Youseffi, M. and Sefat, F., 2021. Degradation and characterisation of electrospun polycaprolactone (PCL) and poly (lactic-co-glycolic acid) (PLGA) scaffolds for vascular tissue engineering. *Materials*, **14**(17), p.4773.
- Benatti, B.B., Silvério, K.G., Casati, M.Z., Sallum, E.A. and Nociti Jr, F.H., 2007. Physiological features of periodontal regeneration and approaches for periodontal tissue engineering utilizing periodontal ligament cells. *Journal of Bioscience and Bioengineering*, **103**(1), pp.1-6.
- Bermejo-Fenoll A, Sanchez-Perez A (2004) Necrotising disease. *Med Oral Patol Oral Cir Bucal* **9**(Suppl), 114 - 119.

- Bernabe E, Marcenes W, Hernandez CR, Bailey J, Abreu LG, Alipour V and others. Global, Regional, and National Levels and Trends in Burden of Oral Conditions from 1990 to 2017: A Systematic Analysis for the Global Burden of Disease 2017 Study. *Journal of Dental Research*. 2020;99(4):362-73.
- Bhavsar AK, Parween S, Varadhan KB, Prabhuji MLV (2018) Critical Issues in Periodontal Regeneration - A Review. *Journal of Oral Health and Dentistry* **2**, 204.
- Bosshardt DD, Nanci A. 2004. Hertwig's epithelial root sheath, enamel matrix proteins, and initiation of cementogenesis in porcine teeth. *J Clin Periodontol*. 31:184–192
- Bosshardt DD, Schroeder HE (1991) Establishment of acellular extrinsic fiber cementum on human teeth. A light- and electron-microscopic study. *Cell Tissue Research* **263**, 325-36.
- Bosshardt DD, Selvig KA (1997) Dental cementum: the dynamic tissue covering of the root. *Periodontology 2000* **13**, 41-75.
- Bousnaki, M., Beketova, A. and Kontonasaki, E., 2022. A review of in vivo and clinical studies applying scaffolds and cell sheet technology for periodontal ligament regeneration. *Biomolecules*, **12**(3), p.435.
- Brahmkhatri, V.P., Prasanna, C. and Atreya, H.S., 2015. Insulin-like growth factor system in cancer: novel targeted therapies. *BioMed Research International*.
- Caffesse, R.G., Sweeney, P.L. and Smith, B.A., 1986. Scaling and root planing with and without periodontal flap surgery. *Journal of Clinical Periodontology*, **13**(3), pp.205-210.
- Capodiferro, S., Tempesta, A., Limongelli, L., Maiorano, E., Benedicenti, S. and Favia, G., 2019. Nonsurgical periodontal treatment by erbium: YAG laser promotes regression

- of gingival overgrowth in patient taking cyclosporine A: a case report. *Photobiomodulation, Photomedicine, and Laser Surgery*, **37**(1), pp.53-56.
- Casale, J. and Crane, J.S., 2019. Biochemistry, glycosaminoglycans. StatPearls Publishing.
- Cetik, R.M., Yabanoglu Ciftci, S., Arica, B., Baysal, I., Akarca Dizakar, S.O., Erbay Elibol, F.K., Gencer, A., Demir, T. and Ayvaz, M., 2022. Evaluation of the effects of transforming growth factor–beta 3 (TGF- β 3) loaded nanoparticles on healing in a rat achilles tendon injury model. *The American Journal of Sports Medicine*, **50**(4), pp.1066-1077.
- Chai YC, Carlier A, Bolander J, Roberts SJ, Geris L, Schrooten J (2012) Current views on calcium phosphate osteogenicity and the translation into effective bone regeneration strategies. *Acta Biomaterials* **8**, 3876 - 3887.
- Chan KM, Fu SC, Wong YP, Hui WC, Cheuk YC, Wong MW. Expression of transforming growth factor beta isoforms and their roles in tendon healing. *Wound Repair Regen*. 2008 May-Jun;16(3):399-407.
- Chen, C.H., Li, D.L., Chuang, A.D.C., Dash, B.S. and Chen, J.P., 2021. Tension stimulation of tenocytes in aligned hyaluronic acid/platelet-rich plasma-polycaprolactone core-sheath nanofiber membrane scaffold for tendon tissue engineering. *International Journal of Molecular Sciences*, **22**(20), p.11215.
- Chen, L., Ma, J., Chen, Y., Huang, C., Zheng, Z., Gao, Y., Jiang, Z., Wei, X., Peng, Y., Yu, S. and Yang, L., 2022. Polydopamine modified acellular dermal matrix sponge scaffold loaded with a-FGF: Promoting wound healing of autologous skin grafts. *Biomaterials Advances*, **136**, p.212790.
- Chen, P.C. and Xu, Z.K., 2013. Mineral-coated polymer membranes with superhydrophilicity and underwater superoleophobicity for effective oil/water separation. *Scientific reports*, **3**(1), p.2776.

Chen S, Hao Y, Cui W, Chang J, Zhou Y (2013) Biodegradable electrospun PLLA/chitosan membrane as guided tissue regeneration membrane for treating periodontitis. *Journal of Material Science* **48**, 6567 - 6577.

Chen, F.M. and Jin, Y., 2010. Periodontal tissue engineering and regeneration: current approaches and expanding opportunities. *Tissue Engineering Part B: Reviews*, **16**(2), pp.219-255.

Cheng, C.H., Shie, M.Y., Lai, Y.H., Foo, N.P., Lee, M.J. and Yao, C.H., 2021. Fabrication of 3D printed poly (lactic acid)/polycaprolactone scaffolds using TGF- β 1 for promoting bone regeneration. *Polymers*, **13**(21), p.3731.

Cheng, L., Ghobeira, R., Cools, P., Liu, Z., Yan, K., De Geyter, N. and Morent, R., 2020. Comparative study of different nitrogen-containing plasma modifications applied on 3D porous PCL scaffolds and 2D PCL films. *Applied Surface Science*, **516**, p.146067.

Choi, S., Cho, T.J., Kwon, S.K., Lee, G. and Cho, J., 2013. Chondrogenesis of periodontal ligament stem cells by transforming growth factor- β 3 and bone morphogenetic protein-6 in a normal healthy impacted third molar. *International journal of oral science*, **5**(1), pp.7-13.

Chapter 5: Periodontal diseases. (2022, October 17).

GOV.UK. <https://www.gov.uk/government/publications/delivering-better-oral-health-an-evidence-based-toolkit-for-prevention/chapter-5-periodontal-diseases#fn:5>

Cionca, N., Giannopouloul, C., Ugolotti, G. & Mombelli, A. 2010.

Microbiologic Testing and Outcomes of Full-Mouth Scaling and Root Planing With or Without Amoxicillin/Metronidazole in Chronic Periodontitis. *Journal of Periodontology*, **81**, 15-23.

- Cipitria, A., Skelton, A., Dargaville, T. R., Dalton, P. D. and Hutmacher, D. W. (2011), Design, Fabrication and Characterization of PCL Electrospun Scaffolds - A Review. *Journal of Materials Chemistry*, 21(26): 9419–9453.
- Chuenjitkuntaworn B, Osathanon T, Nowwarote N (2016) The efficacy of polycaprolactone/hydroxyapatite scaffold in combination with mesenchymal stem cells for bone tissue engineering. *Journal of Biomedical Material Research Part A* **104**, 264–271.
- Coad, B.R., Favia, P., Vasilev, K. and Griesser, H.J., 2022. Plasma polymerization for biomedical applications: A review. *Plasma Processes and Polymers*, p.e2200121.
- Conte R, Di Salle A, Riccitiello F, Petillo O, Peluso G, Calarco A (2018) Biodegradable polymers in dental tissue engineering and regeneration. *Materials Science* **5**(6), 1073 - 1101.
- Cortellini, P., Buti, J., Pini Prato, G. and Tonetti, M.S., 2017. Periodontal regeneration compared with access flap surgery in human intra-bony defects 20-year follow-up of a randomized clinical trial: Tooth retention, periodontitis recurrence and costs. *Journal of Clinical Periodontology*, **44**(1), pp.58-66.
- Croisier F, Jérôme C (2013) Chitosan-based biomaterials for tissue engineering. *European Polymer Journal* **49**. 780-792.
- Da Silva D, Kaduri M, Poley M, Adir O, Krinsky N, Shainsky-Roitman J, Schroeder A (2018) Biocompatibility, biodegradation and excretion of polylactic acid (PLA) in medical implants and theranostic systems. *Chemical Engineering Journal*
- Dabra S, China K, Soni N, Bhatnagar R (2012) Tissue engineering in periodontal regeneration: A brief review. *Dental Research Journal* **9**(6), 671 - 680.

- Dai, S., Zhou, Z., Chen, Z., Xu, G. and Chen, Y., 2019. Fibroblast growth factor receptors (FGFRs): structures and small molecule inhibitors. *Cells*, **8**(6), p.614.
- Damanik, F.F., Brunelli, M., Pastorino, L., Ruggiero, C., Van Blitterswijk, C., Rotmans, J. and Moroni, L., 2020. Sustained delivery of growth factors with high loading efficiency in a layer by layer assembly. *Biomaterials Science*, **8**(1), pp.174-188.
- Dean R (2017) The periodontal ligament: development, anatomy and function. *OHDM* **16**, 1-7.
- De Jong T, Bakker AD, Everts V, Smit TH (2017) The intricate anatomy of the periodontal ligament and its development: Lessons for periodontal regeneration. *Journal of Periodontal Research* **52**(6), 965 - 974.
- Delima AJ, Karatzas S, Amar S, Graves DT (2002) Inflammation and tissue loss caused by periodontal pathogens is reduced by Interleukin-1 antagonists. *Journal of Infectious Diseases* **186**, 511 - 516.
- Diomede, F., D'Aurora, M., Gugliandolo, A., Merciaro, I., Orsini, T., Gatta, V., Piattelli, A., Trubiani, O. and Mazzon, E., 2018. Biofunctionalized scaffold in bone tissue repair. *International Journal of Molecular Sciences*, **19**(4), p.1022.
- Fan, C., Ji, Q., Zhang, C., Xu, S., Sun, H., & Li, Z. (2019). TGF β induces periodontal ligament stem cell senescence through increase of ROS production. *Molecular Medicine Reports*, **20**(4), [3123–3130](#).
- Farooq, M., Khan, A.W., Kim, M.S. and Choi, S., 2021. The role of fibroblast growth factor (FGF) signaling in tissue repair and regeneration. *Cells*, **10**(11), p.3242.
- Forciniti, L., 2011. *Directing neuronal behavior via polypyrrole-based conductive biomaterials*. Doctoral dissertation, The University of Texas.

- Ferreira AM, Gentile P, Toumpaniari S, Ciardelli G, Birch MA. (2016). Impact of collagen/heparin multi-layers for regulating bone cellular functions. *ACS Applied Materials & Interfaces*, **8**(44), 29923-29932.
- Fraser, S., Short, R.D., Barton, D. and Bradley, J.W., 2002. A multi-technique investigation of the pulsed plasma and plasma polymers of acrylic acid: Millisecond pulse regime. *The Journal of Physical Chemistry B*, 106(22), pp.5596-5603.
- France R, Sort R, Dawson R, MacNeil S. (1998). Attachment of human keratinocytes to plasma co-polymers of acrylic acid/octa-1,7-diene and allylamine/octa-1,7-diene. *Journal of material chemistry* **8**. 37.
- Freeman, I., Kedem, A. and Cohen, S. (2008) "The effect of sulfation of alginate hydrogels on the specific binding and controlled release of heparin-binding proteins," *Biomaterials*, 29(22), pp. 3260–3268.
- FUJII, S., MAEDA, H., TOMOKIYO, A., MONNOUCHI, S., HORI, K., WADA, N. & AKAMINE, A. 2010. Effects of TGF- β 1 on the proliferation and differentiation of human periodontal ligament cells and a human periodontal ligament stem/progenitor cell line. *Cell and Tissue Research*, 342, 233-242.
- Gandhi, N.S. and Mancera, R.L., 2008. The structure of glycosaminoglycans and their interactions with proteins. *Chemical Biology & Drug Design*, 72(6), pp.455-482.
- Gauthier, R., Jeannin, C., Attik, N., Trunfio-Sfarghiu, A.M., Gritsch, K. and Grosgeat, B. (2021) "Tissue Engineering for Periodontal Ligament Regeneration: Biomechanical Specifications," *Journal of Biomechanical Engineering*, 143(3).
- Ghollasi, M. and Poormoghadam, D., 2022. Enhanced neural differentiation of human-induced pluripotent stem cells on aligned laminin-functionalized polyethersulfone

- nanofibers; a comparison between aligned and random fibers on neurogenesis. *Journal of Biomedical Materials Research Part A*, **110**(3), pp.672-683.
- Ghorbani, F., Zamanian, A. and Aidun, A., 2020. Conductive electrospun polyurethane-polyaniline scaffolds coated with poly (vinyl alcohol)-GPTMS under oxygen plasma surface modification. *Materials Today Communications*, **22**, p.100752.
- Goel, A., Ncho, C.M. and Choi, Y.H., 2021. Regulation of gene expression in chickens by heat stress. *Journal of Animal Science and Biotechnology*, **12**(1), pp.1-13.
- Goldberg, M., 2020. Scaffolds Combined with Stem Cells have Synergistic Effect in Regenerative Dentistry. *Journal of Clinical Medical Research*, **1**(3), pp.1-11.
- Gomez-Sosa, J.F., Cardier, J.E. and Caviedes-Bucheli, J., 2022. The hypoxia-dependent angiogenic process in dental pulp. *Journal of Oral Biosciences*, **64**(4).
- Gonclaves PF, Sallum EA, Sallum AW, Casati MZ, de Toledo S, Nociti Junior FH (2005) Dental cementum reviewed: development, structure, composition, regeneration and potential functions. *Brazilian Journal of Oral Science* **4**(12), 651 - 658.
- Gonclaves F, de Moraes MS, Ferreira LB, Carreira ACO, Kossugue PM, Boaro LCC, Bentini R, da Silva Garcia CR, Sogayar MC, Arana-Chavez VE, Catalani LH (2016) Combination of bioactive polymeric membranes and stem cells for periodontal regeneration: in vitro and in vivo analyses. *PLoS ONE* **11**(3), e0152412.
- Gonzalez-Fernandez, T., Tierney, E.G., Cunniffe, G.M., O'Brien, F.J. and Kelly, D.J., 2016. Gene delivery of TGF- β 3 and BMP2 in an MSC-laden alginate hydrogel for articular cartilage and endochondral bone tissue engineering. *Tissue Engineering Part A*, **22**(9-10), pp.776-787.

- Grome, M.W., Zhang, Z. and Lin, C., 2019. Stiffness and membrane anchor density modulate DNA-nanospring-induced vesicle tubulation. *ACS Applied Materials & Interfaces*, 11(26), pp.22987-22992.
- Guimarães, C.F., Gasperini, L., Marques, A.P. and Reis, R.L., 2020. The stiffness of living tissues and its implications for tissue engineering. *Nature Reviews Materials*, 5(5), pp.351-370.
- Gürkan, A., Emingil, G., Cinarcik, S., and Berdeli, A., 2006. Gingival crevicular fluid transforming growth factor-beta1 in several forms of periodontal disease. *Archives of Oral Biology*, 51(10), pp.906–912. <https://doi.org/10.1016/j.archoralbio.2006.04.008>
- Guo, X., Hutcheon, A.E. and Zieske, J.D., 2016. Molecular insights on the effect of TGF- β 1/- β 3 in human corneal fibroblasts. *Experimental eye research*, 146, pp.233-241.
- Hadj-Ahmed, M., Ghali, R.M., Bouaziz, H., Habel, A., Stayoussef, M., Ayedi, M., Hachiche, M., Rahal, K., Yacoubi-Loueslati, B. and Almawi, W.Y., 2019. Transforming growth factor beta 1 polymorphisms and haplotypes associated with breast cancer susceptibility: A case-control study in Tunisian women. *Tumor Biology*, 41(8), p.1010428319869096.
- Haghi, A. K. and Akbari, M. (2007), Trends in Electrospinning of Natural Nanofibers. *Physica Status Solidi (A) Applications and Materials Science*, 204(6): 1830– 1834.
- Hall-Glenn, F., De Young, R.A., Huang, B.L., van Handel, B., Hofmann, J.J., Chen, T.T., Choi, A., Ong, J.R., Benya, P.D., Mikkola, H. and Iruela-Arispe, M.L., 2012. CCN2/connective tissue growth factor is essential for pericyte adhesion and endothelial basement membrane formation during angiogenesis. *PLoS One*, 7(2), p.e30562.

- Han, P., Vaquette, C., Abdal-Hay, A. and Ivanovski, S., 2021. The mechanosensing and global DNA methylation of human osteoblasts on MEW fibers. *Nanomaterials*, **11**(11), p.2943.
- Harding, F. J., Clements, L. R., Short, R. D., Thissen, H., & Voelcker, N. H. (2012). Assessing embryonic stem cell response to surface chemistry using plasma polymer gradients. *Acta biomaterialia*, **8**(5), 1739–1748.
- Harsch A, Calderon J, Timmons R, Gross G. (2000). Polymer Surface modification relevance to adhesion. Tylor & Francis Group.
- Hasan, A. and Palmer, R.M., 2014. A clinical guide to periodontology: Pathology of periodontal disease. *British dental journal*, **216**(8), pp.457-461.
- Haug RH, Abdul-Majid J, Blakey GH, White RP. (2009). “Evidenced-Based Decision Making: The Third Molar,” *Dental Clinics of North America*, **53**(1), pp. 77–96
- Holderegger C, Schmidlin PR, Weber FE, Mohn D (2015) Preclinical in vivo performance of novel biodegradable, electrospun poly (lactic acid) and poly (lactic-co-glycolic acid) nanocomposites: a review. *Materials* **8**, 4912 - 4931.
- Hu J, Sun X, Ma H, Xie C, Chen YE, Ma PX (2010). Porous nanofibrous PLLA scaffolds for vascular tissue engineering. *Biomaterials* **31**(31), 7971 - 7977.
- Hu L, Liu Y, Wang S (2017) Stem cell-based tooth and periodontal regeneration. *Oral Diseases* **24**, 696 - 705.
- Huang, Z., Sun, M., Li, Y., Guo, Z. and Li, H., 2021. Reduced graphene oxide-coated electrospun fibre: effect of orientation, coverage and electrical stimulation on Schwann cells behavior. *Journal of Materials Chemistry B*, **9**(11), pp.2656-2665.

- Hub, E. and Rot, A., 1998. Binding of RANTES, MCP-1, MCP-3, and MIP-1alpha to cells in human skin. *The American Journal of Pathology*, 152(3), p.749.
- Hughes FJ (2015) Periodontium and Periodontal Disease. In: *Stem Cell Biology and Tissue Engineering in Dental Sciences*. Academic Press.
- Huynh, Q.-S. and Holsinger, R.M.D. (2023) "Fiber and Electrical Field Alignment Increases BDNF Expression in SH-SY5Y Cells following Electrical Stimulation," *Pharmaceuticals*, 16(2), p. 138.
- Ibrahimi, O.A., Zhang, F., Lang Hrstka, S.C., Mohammadi, M. and Linhardt, R.J., 2004. Kinetic model for FGF, FGFR, and proteoglycan signal transduction complex assembly. *Biochemistry*, 43(16), pp.4724-4730.
- Ichioka, H., Yamamoto, T., Yamamoto, K., Honjo, K.I., Adachi, T., Oseko, F., Mazda, O., Kanamura, N. and Kita, M., 2016. Biomechanical force induces the growth factor production in human periodontal ligament-derived cells. *Odontology*, **104**, pp.27-34.
- Ishikawa I, Iwata T, Washio K, Okano T, Nagasawa T, Iwasaki K (2009) Cell sheet engineering and other novel cell-based approaches to periodontal regeneration. *Periodontology* 2000 **51**, 220–238.
- Ito, Y., Aten, J., Bende, R.J., Oemar, B.S., Rabelink, T.J., Weening, J.J. and Goldschmeding, R., 1998. Expression of connective tissue growth factor in human renal fibrosis. *Kidney international*, 53(4), pp.853-861.
- Jahani, H., Kaviani, S., Hassanpour-Ezatti, M., Soleimani, M., Kaviani, Z. and Zonoubi, Z., 2012. The effect of aligned and random electrospun fibrous scaffolds on rat mesenchymal stem cell proliferation. *Cell Journal (Yakhteh)*, 14(1), p.31.

- Jameson, J.M., Sharp, L.L., Witherden, D.A. and Havran, W.L., 2004. Regulation of skin cell homeostasis by gamma delta T cells. *Frontiers in Bioscience-Landmark*, **9**(4), pp.2640-2651.
- Janssens, K., Ten Dijke, P., Janssens, S. and Van Hul, W., 2005. Transforming growth factor- β 1 to the bone. *Endocrine reviews*, **26**(6), pp.743-774.
- Jeong, S.I., Kwon, J.H., Lim, J.I., Cho, S.W., Jung, Y., Sung, W.J., Kim, S.H., Kim, Y.H., Lee, Y.M., Kim, B.S. and Choi, C.Y., 2005. Mechano-active tissue engineering of vascular smooth muscle using pulsatile perfusion bioreactors and elastic PLCL scaffolds. *Biomaterials*, **26**(12), pp.1405-1411.
- Joseph, B., Ninan, N., Visalakshan, R.M., Denoual, C., Bright, R., Kalarikkal, N., Grohens, Y., Vasilev, K. and Thomas, S., 2021. Insights into the biomechanical properties of plasma treated 3D printed PCL scaffolds decorated with gold nanoparticles. *Composites Science and Technology*, **202**, p.108544.
- Jönsson, B. and Abrahamsson, K.H., 2020. Overcoming behavioral obstacles to prevent periodontal disease: Behavioral change techniques and self-performed periodontal infection control. *Periodontology 2000*, **84**(1), pp.134-144.
- Jönsson D, Nebel D, Bratthall G, Nilsson B (2011). The human periodontal ligament cell: a fibroblast-like cell acting as an immune cell. *Journal of Periodontal Research* **46**(2), 153-157.
- Karamichos, D., Hutcheon, A.E.K. and Zieske, J.D., 2014. Reversal of fibrosis by TGF- β 3 in a 3D in vitro model. *Experimental eye research*, **124**, pp.31-36.

- Ki, Chang Seok, Baek, Doo Hyun, Gang, Kyung Don, Lee, Ki Hoon, Um, In Chul and Park, Young Hwan (2005), Characterization of Gelatin Nanofiber Prepared from Gelatin-Formic Acid Solution. *Polymer*, 46(14): 5094–5102.
- Kim, H.Y., Kim, B.H. and Kim, M.S., 2022. Amine Plasma-Polymerization of 3D Polycaprolactone/ β -Tricalcium Phosphate Scaffold to Improving Osteogenic Differentiation In Vitro. *Materials*, 15(1), p.366.
- Kim J, Amar S (2006). Periodontal disease and systemic conditions: a bidirectional relationship. *Odontology* **94**(1), 10 - 21.
- Kim J-H, Moon H-J, Kim T-H (2013) A novel in vivo platform for studying alveolar bone regeneration in rat," *Journal of Tissue Engineering* **4**.
- Ko, H.M., Moon, J.S., Shim, H.K., Lee, S.Y., Kang, J.H., Kim, M.S., Chung, H.J. and Kim, S.H., 2020. Inhibitory effect of CXC motif chemokine ligand 14 on the osteogenic differentiation of human periodontal ligament cells through transforming growth factor-beta1. *Archives of Oral Biology*, **115**, p.104733.
- Koba, T., Watanabe, K., Goda, S., Kitagawa, M., Mutoh, N., Hamada, N. and Tani-Ishii, N., 2021. The Effect of Transforming Growth Factor Beta 1 on the Mineralization of Human Cementoblasts. *Journal of endodontics*, 47(4), pp.606-611.
- Krook, M.A., Reeser, J.W., Ernst, G., Barker, H., Wilberding, M., Li, G., Chen, H.Z. and Roychowdhury, S., 2021. Fibroblast growth factor receptors in cancer: genetic alterations, diagnostics, therapeutic targets and mechanisms of resistance. *British Journal of Cancer*, 124(5), pp.880-892.

- KURU, L., PARKAR, M. H., GRIFFITHS, G. S., NEWMAN, H. N. & OLSEN, I. 1998. Flow Cytometry Analysis of Gingival and Periodontal Ligament Cells. *Journal of Dental Research*, **77**, 555-564.
- Laestander, C. and Engström, W., 2014. Role of fibroblast growth factors in elicitation of cell responses. *Cell Proliferation*, **47**(1), pp.3-11.
- Lanzalaco, S., Del Valle, L.J., Turon, P., Weis, C., Estrany, F., Alemán, C. and Armelin, E., 2020. Polypropylene mesh for hernia repair with controllable cell adhesion/de-adhesion properties. *Journal of Materials Chemistry B*, **8**(5), pp.1049-1059.
- Lee, S.H. and Shin, H., 2007. Matrices and scaffolds for delivery of bioactive molecules in bone and cartilage tissue engineering. *Advanced drug delivery reviews*, **59**(4-5), pp.339-359.
- Leijon, J., Carlsson, F., Brännström, J., Sanchez, J., Larsson, R., Nilsson, B., Magnusson, P.U. and Rosenquist, M., 2013. Attachment of flexible heparin chains to gelatin scaffolds improves endothelial cell infiltration. *Tissue Engineering Part A*, **19**(11-12), pp.1336-1348.
- Lekic P, McCulloch C (1996) Periodontal ligament cell population: the central role of fibroblasts in creating a unique tissue. *Anatomy Records* **245**, 327 - 341.
- Levenberg S, Langer R (2004) Advances in tissue engineering. *Current Topics in Developmental Biology* **61**, 113 - 134.
- Li, G., Fan, Y., Lai, Y., Han, T., Li, Z., Zhou, P., Pan, P., Wang, W., Hu, D., Liu, X. and Zhang, Q., 2020. Coronavirus infections and immune responses. *Journal of Medical Virology*, **92**(4), pp.424-432.

- Li M, Feng C, Gu X, He Q, Wei F (2017) Effect of cryopreservation on proliferation and differentiation of periodontal ligament stem cell sheets. *Stem Cell Research Therapy* **8**, 77.
- Li, Y., Qiao, Z., Yu, F., Hu, H., Huang, Y., Xiang, Q., Zhang, Q., Yang, Y., and Zhao, Y., 2019. Transforming Growth Factor- β 3/Chitosan Sponge (TGF- β 3/CS) Facilitates Osteogenic Differentiation of Human Periodontal Ligament Stem Cells. *International Journal of Molecular Sciences*, **20**(20), 4982.
- Lin JD, Ozcoban H, Greene J, Jang AT, Djomehri S, Fahey K, Hunter L, Schneider GA, Ho SP (2013) Biomechanics of a Bone-Periodontal Ligament-Tooth Fibrous Joint. *Journal of Mechanics* **46**(3), 443 - 449.
- Lin, Y., Lin, H., Ramamoorthi, M. and Wu, D.T., 2019. *Handbook of Tissue Engineering Scaffolds*, Volume One., Duxford: United Kingdom.
- Lindhe J, Thorkild K, Bosshardt DD, Araujo M (2003) The anatomy of periodontal tissues. In: Lindhe J (Ed.) *Clinical Periodontology and Implant Dentistry*. Oxford, UK: Blackwell Publishing Ltd.
- Liu, E., Gao, H., Zhao, Y., Pang, Y., Yao, Y., Yang, Z., Zhang, X., Wang, Y., Yang, S., Ma, X. and Zeng, J., 2022. The potential application of natural products in cutaneous wound healing: a review of preclinical evidence. *Frontiers in Pharmacology*, **13**.
- Liu, J., Jin, J., Liang, T. and Feng, X.H., 2022. To Ub or not to Ub: a regulatory question in TGF- β signaling. *Trends in Biochemical Sciences*, **47**(12).
- Liu J, Ruan J, Weir MD, Ren K, Schneider A, Wang P, Oates TW, Chang X, Xu HHK (2019) Periodontal bone-ligament-cementum regeneration via scaffolds and stem cells. *Cells* **8**, 537.

- Liu, J., Zou, Q., Wang, C., Lin, M., Li, Y., Zhang, R. and Li, Y., 2021. Electrospinning and 3D printed hybrid bi-layer scaffold for guided bone regeneration. *Materials & Design*, 210, p.110047.
- Liu, J., Zou, Q., Cai, B., Wei, J., Yuan, C. and Li, Y., 2020. Heparin conjugated PCL/Gel–PCL/Gel/n-HA bilayer fibrous membrane for potential regeneration of soft and hard tissues. *Journal of Biomaterials Science, Polymer Edition*, 31(11), pp.1421-1436.
- Liu, X., Xie, Y., Shi, S., Feng, Q., Bachhuka, A., Guo, X., She, Z., Tan, R., Cai, Q. and Vasilev, K., 2019. The co-effect of surface topography gradient fabricated via immobilization of gold nanoparticles and surface chemistry via deposition of plasma polymerized film of allylamine/acrylic acid on osteoblast-like cell behavior. *Applied Surface Science*, 473, pp.838-847.
- Liu, X., Feng, Q., Bachhuka, A., and Vasilev, K., 2014. Surface modification by allylamine plasma polymerization promotes osteogenic differentiation of human adipose-derived stem cells. *ACS applied materials & interfaces*, 6(12), 9733–9741.
- López, G.P., Ratner, B.D., Tidwell, C.D., Haycox, C.L., Rapoza, R.J. and Horbett, T.A., 1992. Glow discharge plasma deposition of tetraethylene glycol dimethyl ether for fouling-resistant biomaterial surfaces. *Journal of Biomedical Materials Research*, 26(4), pp.415-439.
- Loh, Q.L. and Choong, C. (2013) “Three-Dimensional Scaffolds for Tissue Engineering Applications: Role of Porosity and Pore Size,” *Tissue Engineering Part B-reviews*, 19(6), pp. 485–502.
- Louvrier A, Euvrard E, Nicod L (2017) Odontoblastic differentiation of dental pulp stem cells from healthy and carious teeth on an original PCL-based 3D scaffold. *International Endodontic Journal* 51, e252–e263.

- Ma, S.N., Mao, Z.X., Wu, Y., Liang, M.X., Wang, D.D., Chen, X., Chang, P.A., Zhang, W. and Tang, J.H., 2020. The anti-cancer properties of heparin and its derivatives: A review and prospect. *Cell Adhesion & Migration*, 14(1), pp.118-128.
- Macri, L., Silverstein, D. and Clark, R.A., 2007. Growth factor binding to the pericellular matrix and its importance in tissue engineering. *Advanced drug delivery reviews*, 59(13), pp.1366-1381.
- Mahoney, D. J., Whittle, J. D., Milner, C. M., Clark, S. J., Mulloy, B., Buttle, D. J., Jones, G. C., Day, A. J., & Short, R. D. (2004). A method for the non-covalent immobilization of heparin to surfaces. *Analytical biochemistry*, 330(1), 123–129.
- Mamidi, N., García, R.G., Martínez, J.D.H., Briones, C.M., Martínez Ramos, A.M., Tamez, M.F.L., Del Valle, B.G. and Segura, F.J.M., 2022. Recent advances in designing fibrous biomaterials for the domain of biomedical, clinical, and environmental applications. *ACS Biomaterials Science & Engineering*, 8(9), pp.3690-3716.
- Manakhov, A., Nečas, D., Čechal, J., Pavliňák, D., Eliáš, M. and Zajíčková, L., 2015. Deposition of stable amine coating onto polycaprolactone nanofibers by low pressure cyclopropylamine plasma polymerization. *Thin Solid Films*, 581, pp.7-13.
- Mancuso, E., Tonda-Turo, C., Ceresa, C., Pensabene, V., Connell, S.D., Fracchia, L. and Gentile, P., 2019. Potential of manuka honey as a natural polyelectrolyte to develop biomimetic nanostructured meshes with antimicrobial properties. *Frontiers in bioengineering and biotechnology*, 7, p.344.
- Mariz, B.A., Soares, C.D., de Carvalho, M.G. and Jorge-Júnior, J., 2019. FGF-2 and FGFR-1 might be independent prognostic factors in oral tongue squamous cell carcinoma. *Histopathology*, 74(2), pp.311-320.

- Martino A, Liverani L, Rainer A, Salvatore G, Trombetta M, Denaro V. 2011) "Electrospun scaffolds for bone tissue engineering," *Musculoskeletal Surgery*, 95(2), pp. 69–80.
- Martino S, D'Angelo F, Armentano I, Kenny JM, Orlacchio A (2012) Stem cell - cell biomaterial interactions for regenerative medicine. *Biotechnological Advances* **30**, 338 - 351.
- McCaffrey, T.A., Falcone, D.J. and Du, B., 1992. Transforming growth factor- β 1 is a heparin-binding protein: identification of putative heparin-binding regions and isolation of heparins with varying affinity for TGF- β 1. *Journal of cellular physiology*, 152(2), pp.430-440.
- McCulloch CA, Lecki P, McKee MD (2000) Role of physical forces in regulating the form and function of the periodontal ligament. *Periodontology 2000* **24**, 56 - 72.
- Metavarayuth, K., Sitasuwan, P., Zhao, X., Lin, Y., & Wang, Q. (2016). Influence of Surface Topographical Cues on the Differentiation of Mesenchymal Stem Cells in Vitro. *ACS biomaterials science & engineering*, 2(2), 142–151.
- Mirzaeei, S., Ezzati, A., Mehrandish, S., Asare-Addo, K. and Nokhodchi, A., 2022. An overview of guided tissue regeneration (GTR) systems designed and developed as drug carriers for management of periodontitis. *Journal of Drug Delivery Science and Technology*, **71**, p.103341.
- Mitchell, A.C., Briquez, P.S., Hubbell, J.A. and Cochran, J.R., 2016. Engineering growth factors for regenerative medicine applications. *Acta Biomaterialia*, **30**, pp.1-12.
- Milosavljevic, A., 2018. *Periodontal treatment strategies in general dentistry*, Doctoral dissertation, Malmö University, Faculty of Odontology.

- Morent, Rino, De Geyter, Nathalie, Desmet, Tim, Dubrueel, Peter and Leys, Christophe (2011), Plasma Surface Modification of Biodegradable Polymers: A Review. *Plasma Processes and Polymers*, 8(3): 171–190.
- Muiznieks LD, Keeley FW (2012) Molecular assembly and mechanical properties of the extracellular matrix: a fibrous protein perspective. *Biochim Biophys Acta* S0925-4439(12)00283-289.
- Nagayasu-Tanaka, T., Anzai, J., Takedachi, M., Kitamura, M., Harada, T. and Murakami, S., 2023. Effects of combined application of fibroblast growth factor (FGF)-2 and carbonate appetite for tissue regeneration in a beagle dog model of one-wall periodontal defect. *Regenerative Therapy*, 23, pp.84-93.
- NANCI, A. 2008. Ten Cate's Oral Histology: development, structure, and function, Missouri, Mosby.
- Nanci A, Bosshardt DD (2006) Structure of periodontal tissues in health and disease. *Periodontology 2000* 40, 11 - 28.
- Nathan, J., Shameera, R. and Palanivel, G., 2022. Studying molecular signaling in major angiogenic diseases. *Molecular and Cellular Biochemistry*, 477(10), pp.2433-2450.
- Negreros, M., Hagood, J.S., Espinoza, C.R., Balderas-Martínez, Y.I., Selman, M. and Pardo, A., 2019. Transforming growth factor beta 1 induces methylation changes in lung fibroblasts. *PloS one*, 14(10), p.e0223512.
- Nemesh OM, Honta ZM, Slaba OM, Shylyivskiy IV (2021) PATHOGENETIC MECHANISMS OF COMORBIDITY OF SYSTEMIC DISEASES AND PERIODONTAL PATHOLOGY. *Wiadomości Lekarskie (Warsaw Poland)*, 74(5), pp. 1262–1267.

- Newman, M.G., Takei, H., Klokkevold, P.R. and Carranza, F.A., 2011. Carranza's clinical periodontology. Elsevier health sciences.
- Nobile MR, Lucia G, Santella M (2015) Biodegradable compounds: Rheological, mechanical and thermal properties. *AIP Conference Proceedings* **1695**, 020058.
- Nosrati, H., Khodaei, M., Alizadeh, Z. and Banitalebi-Dehkordi, M., 2021. Cationic, anionic and neutral polysaccharides for skin tissue engineering and wound healing applications. *International Journal of Biological Macromolecules*, **192**, pp.298-322.
- Nyvad, B. and Takahashi, N. (2020) "Integrated hypothesis of dental caries and periodontal diseases," *Journal of Oral Microbiology*, 12(1), p. 1710953.
- O'Brien FJ (2011) Biomaterials and scaffolds for tissue engineering. *Materials Today* **14**(3), 88 – 95.
- Oh SH, Kang SG, Kim ES, Cho SH, Lee JH (2003) Fabrication and characterization of hydrophilic poly(lactic-co-glycolic acid)/poly(vinyl alcohol) blend cell scaffolds by melt-molding particulate-leaching method. *Biomaterials* **24**(22), 4011–4021.
- Olvera, D. Sathy, B.N., Carroll, S.F. and Kelly, D.J. (2017) "Modulating microfibrillar alignment and growth factor stimulation to regulate mesenchymal stem cell differentiation," *Acta Biomaterialia*, 64, pp. 148–160.
- Onisor, F., Bran, S., Mitre, I., Mester, A., Voina-Tonea, A., Armencea, G., & Baciut, M., 2021. Polymer-Based Bone Substitutes in Periodontal Infrabony Defects: A Systematic Evaluation of Clinical Studies. *Polymers*, 13(24), 4445.
- Ornitz, D.M. and Marie, P.J., 2015. Fibroblast growth factor signaling in skeletal development and disease. *Genes & Development*, **29**(14), pp.1463-1486.
- Paolantonio M, Femminella B, Coppolino E, Sammartino G, D'Arcangelo C, Perfetti G, Perinetti G (2010) Autogenous periosteal barrier membranes and bone grafts in the treatment

- of periodontal intrabony defects of single-rooted teeth: a 12-month reentry randomized controlled clinical trial. *Journal of Periodontology* **81**(11), 1587 - 1595.
- Park, J., Park, S., Kim, J.E., Jang, K.J., Seonwoo, H. and Chung, J.H., 2021. Enhanced osteogenic differentiation of periodontal ligament stem cells using a graphene oxide-coated poly (ϵ -caprolactone) scaffold. *Polymers*, **13**(5), p.797.
- Park, J.S., Woo, D.G., Yang, H.N., Lim, H.J., Chung, H.M. and Park, K.H., 2008. Heparin-bound transforming growth factor- β 3 enhances neocartilage formation by rabbit mesenchymal stem cells. *Transplantation*, **85**(4), pp.589-596.
- Patel PV, Kumar S, Patel A (2011) Periodontal abscess: a review. *Journal of Clinical & Diagnostic Research* **5**(2), 404 - 409.
- Paterson TE, Beal SN, Santocildes-Romero ME, Sidambe AT, Hatton PV, Asencio IO (2017). "Selective laser melting-enabled electrospinning: Introducing complexity within electrospun membranes," Proceedings of the Institution of Mechanical Engineers, Part H: Journal of Engineering in Medicine.
- Patrício T, Domingos M, Gloria A, Bártolo P (2013) Characterisation of PCL and PCL/PLA scaffolds for tissue engineering. *Procedia CIRP* **5**, 110-114.
- Petisco-Ferrero, S., Álvarez, L.P., Ruiz-Rubio, L., Vilela, J.V. and Sarasua, J.R., 2018. Plasma poly (acrylic acid) compatibilized hydroxyapatite-poly lactide biocomposites for their use as body-absorbable osteosynthesis devices. *Composites Science and Technology*, **161**, pp.1-23.
- Pham, Quynh P., Sharma, Upma and Mikos, Antonios G. (2006), Electrospinning of Polymeric Nanofibers for Tissue Engineering Applications: A Review. *Tissue Engineering*, **12**(5): 1197–1211.

- Pius-Sadowska, E. and Machaliński, B., 2021. Pleiotropic activity of nerve growth factor in regulating cardiac functions and counteracting pathogenesis. *ESC Heart Failure*, **8**(2), pp.974-987.
- Pilgrim, C.R. McCahill, K.A., Rops, J.G., Dufour, J.M., Russell, K.A. and Koch, T.G., (2022) "A Review of Fetal Bovine Serum in the Culture of Mesenchymal Stromal Cells and Potential Alternatives for Veterinary Medicine," *Frontiers in Veterinary Science*, **9**.
- Polimeni G, Xiropaidis AV, Wikesjo UME (2006) Biology and principles of periodontal wound healing/regeneration. *Periodontology 2000* **41**, 30 - 47.
- Pomin, V. H., & Mulloy, B. (2018). Glycosaminoglycans and Proteoglycans. *Pharmaceuticals (Basel, Switzerland)*, **11**(1), 27.
- Pomin, V.H. and Mulloy, B., 2015. Current structural biology of the heparin interactome. *Current Opinion in Structural Biology*, **34**, pp.17-25.
- Queiroz, A., Pelissari, C., Paris, A.F.C., Rodrigues, M.F.S.D. and Trierweiler, M., 2023. Periodontal ligament cells mobilised by transforming growth factor-beta 1 and migrated without stimuli showed enhanced osteogenic differentiation. *Archives of Oral Biology*, **147**, p.105636.
- Raman, R., Sasisekharan, V. and Sasisekharan, R., 2005. Structural insights into biological roles of protein-glycosaminoglycan interactions. *Chemistry & Biology*, **12**(3), pp.267-277.
- Ramos-Rodriguez DH, MacNeil S, Claeysens F, Ortega Asencio I. (2021) "Fabrication of Topographically Controlled Electrospun Scaffolds to Mimic the Stem Cell Microenvironment in the Dermal-Epidermal Junction," *ACS Biomaterials Science & Engineering*, **7**(6), pp. 2803–2813.

- Rapraeger, A.C., Guimond, S., Krufka, A. and Olwin, B.B., 1994. [11] Regulation by heparan sulfate in fibroblast growth factor signaling. In *Methods in enzymology* (Vol. 245, pp. 219-240). Academic Press.
- RASAL, R., JANORKAR, A. & HIRT, D. 2010. Poly (lactic acid) modifications. *Progress in Polymer Science*, 35, 338-356.
- Retrouvey J-M, Goldberg M, Schwartz S (2012) Dental development and maturation, from the dental crypt to the final occlusion. In: *Paediatric Bone*. 2nd Ed. Academic Press.
- Rawtani, D. and Agrawal, Y.K. (2014) "Emerging Strategies and Applications of Layer-by-Layer Self-Assembly," *Nanobiomedicine*, 1, p. 8.
- Richbourg, N.R., Peppas, N.A. and Sikavitsas, V.I., 2019. Tuning the biomimetic behavior of scaffolds for regenerative medicine through surface modifications. *Journal of tissue engineering and regenerative medicine*, 13(8), pp.1275-1293.
- Richardson SM, Curran JM, Chen R, Vaughan-Thomas A, Hunt JA, Freemont A J, Hoyland JA (2006) The differentiation of bone marrow mesenchymal stem cells into chondrocyte-like cells on poly-L-lactic acid (PLLA) scaffolds. *Biomaterials* **27**, 4069-4078.
- Roach, P., Farrar, D. and Perry, C.C., 2005. Interpretation of protein adsorption: surface-induced conformational changes. *Journal of the American Chemical Society*, 127(22), pp.8168-8173.
- Robinson, D.E., Buttle, D.J., Whittle, J.D., Short, R.D., & Steele, D.A. (2010). The Substrate and Composition Dependence of Plasma Polymer Stability. *Plams Processes and Polymers* 7(2), 102 - 106.

- Roth, S.P., Brehm, W., Groß, C., Scheibe, P., Schubert, S. and Burk, J., 2019. Transforming growth factor beta 3-loaded decellularized equine tendon matrix for orthopedic tissue engineering. *International Journal of Molecular Sciences*, **20**(21), p.5474.
- Roy, S. and Rhim, J.W., 2020. Carboxymethyl cellulose-based antioxidant and antimicrobial active packaging film incorporated with curcumin and zinc oxide. *International journal of biological macromolecules*, **148**, pp.666-676.
- Richbourg, N.R., Peppas, N.A. and Sikavitsas, V.I., 2019. Tuning the biomimetic behaviour of scaffolds for regenerative medicine through surface modifications.
- Safi, I.N., Al-Shammari, A.M., Ul-Jabbar, M.A. and Hussein, B.M., 2020. Preparing polycaprolactone scaffolds using electrospinning technique for construction of artificial periodontal ligament tissue. *Journal of Taibah University Medical Sciences*, **15**(5), pp.363-373.
- Sahni, A., Odrliin, T. and Francis, C.W., 1998. Binding of basic fibroblast growth factor to fibrinogen and fibrin. *Journal of Biological Chemistry*, **273**(13), pp.7554-7559.
- Sarkar, Sumona, Lee, George Y., Wong, Joyce Y. and Desai, Tejal A. (2006), Development and Characterization of a Porous Micro-Patterned Scaffold for Vascular Tissue Engineering Applications. *Biomaterials*, **27**(27): 4775–4782.
- Sakiyama-Elbert, Shelly E. (2014), Incorporation of Heparin into Biomaterials. *Acta Biomaterialia*, **10**(4): 1581–1587.
- Salehi-Nik N, Rezai Rad M, Nazeman P, Khojasteh A (2017) Polymers for oral and dental tissue engineering. In: *Biomaterials for Oral and Dental Tissue Engineering*. Elsevier.

- Sano, M., Hirakawa, S., Suzuki, M., Sakabe, J.I., Ogawa, M., Yamamoto, S., Hiraide, T., Sasaki, T., Yamamoto, N., Inuzuka, K. and Tanaka, H., 2020. Potential role of transforming growth factor-beta 1/Smad signaling in secondary lymphedema after cancer surgery. *Cancer science*, 111(7), pp.2620-2634.
- Sardella, E., Salama, R.A., Waly, G.H., Habib, A.N., Favia, P. and Gristina, R., 2017. Improving internal cell colonization of porous scaffolds with chemical gradients produced by plasma assisted approaches. *ACS Applied Materials & Interfaces*, 9(5), pp.4966-4975.
- Sarment DP, Cooke JW, Miller SE, Jin Q, McGuire MK, Kao RT (2006) Effect of rhPDGF-BB on bone turn over during periodontal repair. *Journal of Clinical Periodontology* **33**, 135—40.
- Sasaki, H., Rothrauff, B.B., Alexander, P.G., Lin, H., Gottardi, R., Fu, F.H. and Tuan, R.S., 2018. In vitro repair of meniscal radial tear with hydrogels seeded with adipose stem cells and TGF- β 3. *The American journal of sports medicine*, 46(10), pp.2402-2413.
- Saygin NE, Giannobile WV, Somerman MJ (2000) Molecular and cell biology of cementum. *Periodontol 2000* **24**, 73-98.
- Schroeder HE (1986) *Handbook of microscopic anatomy*. Vol. 5. Berlin: Springer.
- Scantlebury T (1993) 1982 - 1992: a decade of technology development for guided tissue regeneration. *Journal of Periodontology* **64**, 1129 - 1137.
- Schander, K., Arvidson, K., Mustafa, K., Hellem, E., Bolstad, A.I., Finne-Wistrand, A. and Albertsson, A.C., 2010. Response of bone and periodontal ligament cells to biodegradable polymer scaffolds in vitro. *Journal of bioactive and compatible polymers*, 25(6), pp.584-602.

- Schofer MD, Roessler PP, Theisen C, Schlimme S, Heverhagen JT, Voelker M, Dersch R, Agarwal S, Fuchs-Winkelmann S, Paletta JRJ (2011) Electrospun PLLA nanofiber scaffolds and their use in combination with BMP-2 for reconstruction of bone defects. *PLoS ONE* **6(9)**, e25462.
- Seo S-J, Kim H-W, Lee J-H (2016) Electrospun nanofibers applications in dentistry. *Journal of Nanomaterials* **5931949**.
- Shah, P., Keppler, L. and Rutkowski, J., 2014. A review of platelet derived growth factor playing pivotal role in bone regeneration. *Journal of Oral Implantology*, **40(3)**, pp.330-340.
- Shang, S. Yang, F., Cheng, X., Walboomers, X.F. and Jansen, J.A. (2010) "The effect of electrospun fibre alignment on the behaviour of rat periodontal ligament cells," *European Cells and Materials*, 19, pp. 180–192.
- Shi H, Zong W, Xu X, Chen J (2018) Improved biphasic calcium phosphate combined with periodontal ligament stem cells may serve as a promising method for periodontal regeneration. *American Journal of Translational Research* **10**, 4030.
- Shi, Y., Jones, W., Beatty, W., Tan, Q., Mecham, R.P., Kumra, H., Reinhardt, D.P., Gibson, M.A., Reilly, M.A., Rodriguez, J. and Bassnett, S., 2021. Latent-transforming growth factor beta-binding protein-2 (LTBP-2) is required for longevity but not for development of zonular fibers. *Matrix Biology*, 95, pp.15-31.
- Shimauchi H, Nemoto E, Ishihata H, Shimomura M (2013) Possible functional scaffolds for periodontal regeneration. *Japanese Dental Science Review* **49**, 118 - 130.
- Shie, M.Y., Lai, Y.H., Foo, N.P., Lee, M.J. and Yao, C.H., 2021. Fabrication of 3D printed poly (lactic acid)/polycaprolactone scaffolds using tgf- β 1 for promoting bone regeneration. *Polymers*, 13(21), p.3731.

- Shin SH, Purevdorj O, Castano O, Pianell JA, Kim H-W (2012) A short review: recent advances in electrospinning for bone tissue regeneration. *Journal of Tissue Engineering* **3**(1), 2041731412443530.
- Short, R., Buttle, D., and Day, A., 2009. Sugar binding surface. PCT/GB2003/004653(WO/2004/040308).
- Siaili M, Chatzopoulou D, Gillam DG (2018) An overview of periodontal regenerative procedures for the general dental practitioner. *Saudi Dental Journal* **30**, 26 - 37.
- Sill, T.J. and Von Recum, H.A., 2008. Electrospinning: applications in drug delivery and tissue engineering. *Biomaterials*, 29(13), pp.1989-2006.
- Singh P (2011) Endo-perio dilemma: a brief review. *Dental Research Journal* **8**(1), 39 - 47
- Sodek J, McKee MD (2000) Molecular and cellular biology of alveolar bone. *Periodontology* 2000 **24**(1), 99 - 126.
- Somerman, M. J., Archer, S. Y., IMM, G. R. & Foster, R. A. 1988. A comparative study of human periodontal ligament cells and gingival fibroblasts in vitro. *Journal of Dental Research*, 67, 66-70.
- Speight, J. G. (2011). Monomers, polymers, and plastics. In Elsevier eBooks (pp. 499–537).
- Subramanian A, Krishnan UM, Sethuraman S (2011) Fabrication of uniaxially aligned 3D electrospun scaffolds for neural regeneration. *Biomedical Materials* **6**, 1–10.
- Sylvester, M.A., Amini, F. and Tan, C.K., 2020. Electrospun nanofibers in wound healing. *Materials Today: Proceedings*, 29, pp.1-6.
- Tatakis DN, Promsudthi A, Wikesjo UM (2000) Devices for periodontal regeneration. *Periodontology* **19**, 59 - 73.

- Sun, C., Tian, X., Jia, Y., Yang, M., Li, Y. and Fernig, D.G., 2022. Functions of exogenous FGF signals in regulation of fibroblast to myofibroblast differentiation and extracellular matrix protein expression. *Open Biology*, **12**(9), p.210356.
- Sylvester, M.A., Amini, F. and Tan, C.K., 2020. Electrospun nanofibers in wound healing. *Materials Today: Proceedings*, **29**, pp.1-6.
- Tacias-Pascacio, V.G., Ortiz, C., Rueda, N., Berenguer-Murcia, Á., Acosta, N., Aranaz, I., Civera, C., Fernandez-Lafuente, R. and Alcántara, A.R., 2019. Dextran aldehyde in biocatalysis: More than a mere immobilisation system. *Catalysts*, **9**(7), p.622.
- Taipale, J. and Keski-Oja, J., 1997. Growth factors in the extracellular matrix. *The FASEB Journal*, **11**(1), pp.51-59.
- Tanaka, T., Narazaki, M. and Kishimoto, T., 2014. IL-6 in inflammation, immunity, and disease. *Cold Spring Harbor Perspectives in Biology*, **6**(10), p.a016295.
- Tatakis, D.N., Promsudthi, A. and Wikesjö, U.M.E. (1999) "Devices for periodontal regeneration," *Periodontology 2000*, **19**(1), pp. 59–73.
- Tran, T. T., Hamid, Z. a. A., & Cheong, K. Y. (2018). A review of mechanical properties of scaffold in tissue engineering: Aloe vera composites. *Journal of Physics*, **1082**, 012080.
- Trejo PM, Weltman R, Caffesse RG (1998) Effects of expanded polytetrafluoroethylene and polylactic acid barriers on healthy sites. *Journal of Periodontology* **69**(1), 14.
- Trivedi, S. Srivastava, K., Gupta, A., Saluja, T.S., Kumar, S., Mehrotra, D. and Singh, S.K., (2020) "A quantitative method to determine osteogenic differentiation aptness of scaffold.," *Journal of Oral Biology and Craniofacial Research*, **10**(2), pp. 158–160.
- Tomokiyo A, Wada N, Maeda H (2019) Periodontal Ligament Stem Cells: Regenerative Potency in Periodontium. *Stem Cells Development* **28**(15), 974 - 985.

- Tsai, Chen-Chi, Chang, Yen, Sung, Hsing-Wen, Hsu, Jer-Chen and Chen, Chiun- Nan (2001), Effects of Heparin Immobilization on the Surface Characteristics of a Biological Tissue Fixed with a Naturally Occurring Crosslinking Agent (Genipin): An in Vitro Study. *Biomaterials*, 22(6): 523–533.
- Uygun, B.E., Bou-Akl, T., Albanna, M. and Matthew, H.W., 2010. Membrane thickness is an important variable in membrane scaffolds: Influence of chitosan membrane structure on the behavior of cells. *Acta Biomaterialia*, 6(6), pp.2126-2131.
- Vaidyanathan, L., 2021. Growth factors in wound healing—a review. *Biomed. Pharmacol. J*, 14, pp.1469-1481.
- Veith, A.P., Henderson, K., Spencer, A., Sligar, A.D. and Baker, A.B., 2019. Therapeutic strategies for enhancing angiogenesis in wound healing. *Advanced Drug Delivery Reviews*, 146, pp.97-125.
- Voleti, P.B., Buckley, M.R. and Soslowsky, L.J., 2012. Tendon healing: repair and regeneration. *Annual Review of Biomedical Engineering*, 14, pp.47-71.
- Wagoner-Johnson AJ, Helsheler AJ (2011) A review of the mechanical behavior of CaP and CaP/polymer composites for applications in bone replacement and repair. *Acta Biomaterials* 7, 16 - 30.
- Walmsley AD, Walsh TF, Lunsley PJ, Burke FJT, Shortall AC, Hayes-Hall R, Pretty IA (2007) *Restorative Dentistry*. 2nd Ed. Elsevier.
- Wan, A.C., Le Visage, C., Liao, I.C. and Leong, K.W., 2006. Proliferation and differentiation of human mesenchymal stem cell encapsulated in polyelectrolyte complexation fibrous scaffold. *Biomaterials*, 27(36), pp.6111-6122.

- Weltmann, K.D. and Von Woedtke, T., 2016. Plasma medicine—current state of research and medical application. *Plasma Physics and Controlled Fusion*, 59(1), p.014031.
- Wilson, S.E., 2021. TGF Beta- 1,- 2 and- 3 in the Modulation of Fibrosis in the Cornea and Other Organs. *Experimental eye research*, 207, p.108594.
- Wiwatwongwana, F. and Promma, N., 2020. *Mechanical Properties Analysis of Scaffold Material Using Nonlinear Least Squares Fitting by Hyperelastic Model. International Journal of Materials, Mechanics and Manufacturing*, 8(3), pp.84-88.
- Woo KM, Chen VJ, Jung HM, Kim TI, Shin HI, et al. (2009) Comparative evaluation of nanofibrous scaffolding for bone regeneration in critical-size calvarial defects. *Tissue Engineering* **15**, 2155–2162.
- Wu, Q., Li, Y., Wang, Y., Li, L., Jiang, X., Tang, J., Yang, H., Zhang, J., Bao, J. and Bu, H., 2016. The effect of heparinized decellularized scaffolds on angiogenic capability. *Journal of Biomedical Materials Research Part A*, 104(12), pp.3021-3030.
- Xie, J., Shen, H., Yuan, G., Lin, K. and Su, J., 2021. The effects of alignment and diameter of electrospun fibers on the cellular behaviors and osteogenesis of BMSCs. *Materials Science and Engineering: C*, 120, p.111787.
- Xu, L., Guo, Y., Huang, Y., Xiong, Y., Xu, Y., Li, X., Lu, J., Wang, L., Wang, Y., Lu, Y. and Wang, Z., 2018. Constructing heparin-modified pancreatic decellularized scaffold to improve its re-endothelialization. *Journal of Biomaterials Applications*, 32(8), pp.1063-1070.
- Xu Q, Li B, Yuan L, Dong Z, Zhang H, Wang H (2017) Combination of platelet-rich plasma within periodontal ligament stem cell sheets enhances cell differentiation and matrix production. *Journal of Tissue Engineering and Regenerative Medicine* **11**, 627–636.

- Xu, X., Zheng, L., Yuan, Q., Zhen, G., Crane, J.L., Zhou, X. and Cao, X., 2018. Transforming growth factor- β in stem cells and tissue homeostasis. *Bone Research*, 6(1), p.2).
- Xu, Z., Feng, Z., Guo, L., Ye, L., Tong, Z., Geng, X., Wang, C., Jin, X., Hui, X. and Gu, Y., 2020. Biocompatibility evaluation of heparin-conjugated poly (ϵ -caprolactone) scaffolds in a rat subcutaneous implantation model. *Journal of Materials Science: Materials in Medicine*, 31, pp.1-13.
- Xue, K., Zhang, J., Li, C., Li, J., Wang, C., Zhang, Q., Chen, X., Yu, X., Sun, L. and Yu, X., 2019. The role and mechanism of transforming growth factor beta 3 in human myocardial infarction-induced myocardial fibrosis. *Journal of cellular and molecular medicine*, 23(6), pp.4229-4243.
- Yamaguchi, T.P. and Rossant, J., 1995. Fibroblast growth factors in mammalian development. *Current opinion in genetics & development*, 5(4), pp.485-491.
- Yamamoto T, Hasegawa T, Yamamoto T, Hongo H, Amizuka N (2016) Histology of human cementum: Its structure, function, and development. *Japanese Dental Science Review* 52, 63 - 74.
- Yamawaki, K., Matsuzaka, K., Kokubu, E. and Inoue, T., 2010. Effects of epidermal growth factor and/or nerve growth factor on Malassez's epithelial rest cells in vitro: expression of mRNA for osteopontin, bone morphogenetic protein 2 and vascular endothelial growth factor. *Journal of periodontal research*, 45(3), pp.421-427.
- Yang, D.H., Heo, G.M., Park, H.J., Oh, H.K. and Kook, M.S., 2020. Comparative effectiveness of surface functionalized poly- ϵ -caprolactone scaffold and β -TCP mixed PCL scaffold for bone regeneration. *Journal of Nanoscience and Nanotechnology*, 20(9), pp.5349-5355.

- Yang F, Murugan R, Ramakrishna S, Wang X, Ma YX, Wnag S (2004) Fabrication of nano-structured porous PLLA scaffold intended for nerve tissue engineering. *Biomaterials* **25**(10), 1891 - 1900.
- Yang J, Shi G, Bei J, Wang S, Cao Y, Shang Q, Yang G, Wang w (2002) fabrication and surface modification of macroporous poly(L-lactic acid) poly (L-lactic - c – glycolic acid) (70/30) cell scaffolds for human skin fibroblast cell culture. *Biomedical material* **62**, 438.
- Yasuda, H.K., 1985. General characteristics of plasma polymers. Plasma Polymerization, Academic Press, London, p.355.
- Yasuda, H. and Gazicki, M., 1982. Biomedical applications of plasma polymerization and plasma treatment of polymer surfaces. *Biomaterials*, **3**(2), pp.68-77.
- Yao, Q., Cosme, J.G., Xu, T., Miszuk, J.M., Picciani, P.H., Fong, H. and Sun, H., 2017. Three dimensional electrospun PCL/PLA blend nanofibrous scaffolds with significantly improved stem cells osteogenic differentiation and cranial bone formation. *Biomaterials*, **115**, pp.115-127.
- Yasuda, H. and Gazicki, M., 1982. Biomedical applications of plasma polymerization and plasma treatment of polymer surfaces. *Biomaterials*, **3**(2), pp.68-77.
- YIN, Z., CHEN, X., CHEN, J., SHEN, W., HIEU NGUYEN, T., GAO, L. & OUYANG, H. 2010. The regulation of tendon stem cell differentiation by the alignment of nanofibers. *Biomaterials*, **31**, 2163-2175.
- You, J.; Raghunathan, V. K.; Son, K. J.; Patel, D.; Haque, A.; Murphy, C. J.; Revzin, A.,(2014). Impact of nanotopography, heparin hydrogel microstructures, and encapsulated fibroblasts on phenotype of primary hepatocytes. *ACS Appl. Mater. Interfaces*, **7** (23), 12299-12308.

- Zafar M, Najeeb S, Khursid Z, Vazirzadeh M, Zohaib S, Najeeb B, Sefat F (2016) Potential of electrospun nanofibers for biomedical and dental applications. *Materials* **9**(2), 73.
- Zhang, C., Wang, J., Xie, Y., Wang, L., Yang, L., Yu, J., Miyamoto, A. and Sun, F., 2021. Development of FGF-2-loaded electrospun waterborne polyurethane fibrous membranes for bone regeneration. *Regenerative Biomaterials*, *8*(1), p.rbaa046.
- Zhang, C., Liu, J., Wang, J., Hu, W. and Feng, Z., 2021. The emerging role of leukemia inhibitory factor in cancer and therapy. *Pharmacology & Therapeutics*, **221**, p.107754.
- Zhao, P., Chen, W., Feng, Z., Liu, Y., Liu, P., Xie, Y. and Yu, D.G., 2022. Electrospun nanofibers for periodontal treatment: a recent progress. *International Journal of Nanomedicine*, **17**, pp.4137-4162.
- Zhou, J., Xiong, Z., Liu, M., Yang, L., Yao, S., Chen, K., et al. (2020). Creation of Bony Microenvironment with Extracellular Matrix Doped-Bioactive Ceramics to Enhance Osteoblast Behavior and Delivery of Aspartic Acid-Modified BMP-2 Peptides. *Ijn* *15*, 8465–8478.
- Zhuang, Y., Lin, K. and Yu, H., 2019. Advance of nano-composite electrospun fibers in periodontal regeneration. *Frontiers in Chemistry*, **7**, p.495.